Integrated Optimal Design and Operation of Compressed Air Energy Storage for Decentralized Applications

Elaheh Bazdar

A Thesis in the Department of

Building, Civil, and Environmental Engineering (BCEE)

Presented in Partial Fulfillment of the Requirements
For the Degree of
Doctor of Philosophy in Civil Engineering
at Concordia University
Montreal, Quebec, Canada

August 2024

CONCORDIA UNIVERSITY
SCHOOL OF GRADUATESTUDIES

This is to certify that the Ph.D. thesis prepared

By: Elaheh Bazdar

Entitled: Integrated Optimal Design and Operation of Compressed Air Energy Storage for Decentralized Applications

And submitted in partial fulfillment of the requirements for the degree of

Doctor of Philosophy (Civil Engineering)

complies with the regulations of this University and meets the accepted standards with respect to originality and quality.

Signed by the final examining committee:

_____Chair
Dr. Govind Gopakumar

_____External Examiner
Dr. Ibrahim Dincer

_____Arms-Length Examiner
Dr. Khashayar Khorasani

_____Examiner
Dr. Liangzhu Wang

_____Examiner
Dr. Radu Grigore Zmeureanu

_____Thesis Supervisor
Dr. Fariborz Haghighat

_____Thesis Supervisor
Dr. Fuzhan Nasiri

Approved by. _____
Dr. Chunjiang An, Graduate Program Director

_____
Dr. Mourad Debbabi, Dean, Gina Cody School of Engineering and Computer Science

Abstract

Integrated Optimal Design and Operation of Compressed Air Energy Storage for Decentralized Applications

Elaheh Bazdar, Ph.D., Concordia University, 2024

This thesis aims to investigate the integration of compressed air energy storage (CAES) technology into decentralized energy systems, addressing associated technological and integration challenges within the dynamic energy system environment. A multi-layer simulation-optimization framework is developed to comprehensively evaluate the feasibility of integrating decentralized CAES into local hybrid energy systems (HES) through optimal sizing and operation. In the first layer, an improved energy management operation strategy (I-EMOS) is designed to enhance the integration of adiabatic-CAES (A-CAES) systems into decentralized applications. In doing so, the interaction and limitations of A-CAES subsystems, including power conversion units, air storage tank, and thermal energy storage, are considered to evaluate the long-term performance and dynamic behavior of A-CAES systems, especially when connected to intermittent renewable energy sources and end-user load demand. Subsequently, the second layer develops a holistic sizing-planning framework, including a generic A-CAES model and various alternative power dispatch strategies (PDS), based on the application potentials of A-CAES. This module aims to enhance A-CAES contribution while minimizing the levelized cost of energy and achieving the optimal configuration for the corresponding applications. Eventually, the final layer focuses on improving the resilience of the energy system, incorporating A-CAES technology, within scenarios involving limited energy sources and hybrid energy storage solutions. Therefore, an operational unit-commitment optimization model is developed, considering the A-CAES system's response and charging-discharging transition times. This model is integrated into the sizing-planning module to co-optimize the economic performance and system resilience through two-stage optimization, involving long-term planning and short-term scheduling. The methodology is applied to Concordia University buildings in Montreal, Canada. Validation against data from an existing A-CAES pilot plant shows a 42.5% improvement using I-EMOS compared to traditional EMOS.

Optimal configurations under various PDSs demonstrate energy cost savings between $0.015 and $0.021 per kWh, with significant improvements in electrical load management (52%) and carbon emission reduction (65%) for the system in which A-CAES is planned for both solar

energy integration and seasonal load shifting. Furthermore, under the worst-case scenario (zero selling back), the HES achieves a PV self-consumption rate of around 92% and a payback time of 15.5 years. In scenarios of limited grid dependency, a substantial annual resiliency improvement of approximately 41.1% is achieved by integrating the energy storage system. Additionally, despite the superior cost performance of the PV/A-CAES system, the PV-based HES featuring hybrid A-CAES, and battery storage achieves a 47.3% electrical load management ratio and a 96% self-consumption rate, improving by about 6% over HES with only A-CAES system. Furthermore, findings indicate that under optimal operational conditions, even with the highest PV power availability during grid interruptions, the HES could meet 94% of load demand using individual A-CAES, increasing to 100% by integrating fast-response batteries. In conclusion, the proposed framework offers a reliable approach for integrating and customizing decentralized A-CAES systems, considering specific service requirements and constraints. It identifies critical times of loss of power probability, enhances understanding of local energy system design, and facilitates better integration with renewable energy sources and storage systems. The findings provide valuable insights for decision-makers, helping select suitable systems and scenarios based on key performance indicators. The framework also is adaptable to various scale scenarios, accommodating both local and regional generation considerations.

Keywords: Decentralized hybrid energy system, Adiabatic-compressed air energy storage, Optimal design, Optimal operation, Cost-effectiveness, Resilience, Dynamic modeling

Acknowledgment

I would like to express my deepest gratitude to my supervisors, Dr. Fariborz Haghighat and Dr. Fuzhan Nasiri for their support, invaluable guidance, and constant encouragement throughout the PhD journey. Their expertise and constructive feedback have been instrumental in shaping the quality of my work.

I also would like to express my sincere appreciation to the members of my examination committee Dr. Govind Gopakumar, Dr. Ibrahim Dincer, Dr. Khashayar Khorasani, Dr. Radu Grigore Zmeureanu, and Dr. Liangzhu Wang for their insightful comments and valuable suggestions throughout my defense exam, comprehensive exam and proposal.

I would like to thank Mr. Daniel Gauthier (facility management of Concordia University) for providing some part of the data used in this study.

A heartfelt thanks goes out to my friends, whose unwavering support sustained me during the highs and lows of this academic endeavor. Their encouragement and support have been a constant source of motivation, making this journey more meaningful and enjoyable.

To my family, my mother Masoumeh, my father Shahryar, my lovely sister Bahareh, and my family-in-law, I owe an immeasurable debt of gratitude. Their unwavering belief in my abilities and unconditional love sustained me through the challenges, and I am forever thankful for that.

Lastly, I would like to express my deepest gratitude to my wonderful husband, Navid, whose endless support, love, patience, and encouragement have been my anchor. His belief in my potential has fueled my determination, and I am grateful for the strength he has provided.

This thesis would not have been possible without the collective support and encouragement of all those mentioned above. I am truly grateful for their contributions to this academic achievement.

I would like to dedicate this thesis to

My cherished ones who fill my life with love, warmth, and purpose: my mother, Masoumeh, my father, Shahryar, my sister Bahareh, and my husband Navid.

Thank you for being the heartbeat of my existence.

Table of content

List of Figures

List of Tables

Nomenclature

Abbreviations

A-CAES	Adiabatic compressed air energy storage
AC	Alternating current
AMFR	Air mass flow rate
AST	Air storage tank
BTM	Behind-the-meter
CAES	Compressed air energy storage
CAPEX	Capital expenditure
CE	Carbon emission
CER	Carbon emission reduction
CF	Cash flow
CRF	Capital recovery factor
D-CAES	Diabatic compressed air energy storage
DC	direct current
DIG	Diesel generator
DPBP	Discounted payback period
DRP	Demand response program
e-Boiler	Electric Boiler
EESS	Electric energy storage system
ELMR	Electrical load management ratio
EMOS	Energy management operation strategy
ERF	Energy Retention Factor
ESS	Energy storage system
GA	Genetic algorithm
GT	Gas turbine
HD	High demand
HES	Hybrid energy system
HESS	Hybrid energy storage system
HEX	Heat exchanger
HP	High power
HRR	Heat recovery ratio
I-EMOS	Improved energy management operation strategy
KPI	Key performance indicator
LCC	Life cycle cost
LCOE	Levelized cost of energy
LCR	Load coverage ratio
LD	Low demand
LP	Low power
LPS	loss of power supply
LPSP	Loss of power supply probability
LS	Large-scale
MCFC	Molten carbonate fuel cell
MG	Microgrid
OPEX	Operational expenditure
PAST	Air pressure in the tank
PBP	Payback period
PCS	Power conversion system
PDS	Power dispatch strategy
PSO	Particle swarm optimization
PV	Photovoltaic
REPEX	Replacement expenditure
RES	Renewable energy source
RTE	Round trip efficiency
SCR	Self-consumption rate
SOC	State of the charge
SPBP	Simple payback period
SPPWF	Single payment present worth
SR	Storage ratio
SS	Small-Scale
t	Time
T-EMOS	Traditional energy management operation strategy
TCER	Total Carbon emission reduction
TES	Thermal energy storage
TOU	Time of use
WT	Wind turbine
Yr.	Year

Parameters

M	Air mass in the tank
P	Air pressure
ϑ, δ, ν	binary variable
C	Cost
dod	Depth of charge
x	Design variable
WGAP	Difference between the load demand and power generation
n	Efficiency
λ_e	Emission factor per electricity
EF	Emission factor per unit of mass
E	Energy capacity
R	Gas constant
Ca,p	Heat capacity of air
A	Heat exchanger area
e	Heat exchanger effectiveness
If	Inflation rate
I	Irradiance
n	Lifetime
m	Mass flow rate

In	Nominal interest rate
N	Number
W	Power
Ir	Real interest rate
T	Temprature
Q	Thermal power
t	Time
X	Vector of design variable
V	Volume
γ	Isentropic coefficient

Subscripts

a	Air
AC	Alternating current
am	Ambient
AST	Air storage tank
B	Battery
c	Compressor
CAES	Compressed air energy storage
conv.	Converter
crg	Charging
cur	Curtailment
DC	Direct current
dcrg	Discharging
e	Emission
eboiler	Electric boiler
exc	Excess electricity
exp	Export
f	Inflation
flex	Flexible load
G	Power Generation
g	Grid
gboiler	Gas boiler
Gen	Generator
HEX	Heat exchanger
i,j	Number of stages
id	Idle mode
imp	Import
in	Input
inv	inverter
L	Load demand
ist	Isothermal
j,i	Number of stages
k	Iteration number
L	Load demand
lps	Loss of power
M	Motor
max	Maximum
min	Minimum
mis	Mismatch
n	Nominal
NG	Natural gas
npv	Net present value
p	Pressure
per	Purchased power
PV	photovoltaic
r	Real
ref	References
ren	Renewable
sell	Sell
TES	Thermal energy storage
tr	Turbine
v	Number of design variable
w	Water
yr	Year
z	Particle number

Superscripts

bps	Basic power system
bs	Basic scenario
cs	Current scenario
ex	Heat exchanger
in	Input
is	Isentropic
max	Maximum
min	Minimum
out	Output
r	Rated
w	Water

Chapter 1: Introduction

Concerns for global warming and energy security arising from population and urbanization growth have led to a worldwide transition from a centralized (fossil-fuel-based) large-scale power generation toward small-scale decentralized power generation practices involving renewable energy sources (RES) to meet the ever-increasing load demand using more sustainable sources [1,2]. Incorporating a local hybrid energy system (HES) close to the energy consumer could be one way to tackle this issue and an essential step towards a smart grid, smart city, and decarbonization by adopting renewables [3,4]. This approach also allows for on-site energy generation and consumption, reducing transmission losses and contingency challenges as well as increasing resilience to power outages.

Although RESs offer an environmentally friendly performance, their intermittency nature is a significant problem that can create operational issues such as supply and demand mismatch [5]. Thus, incorporating energy storage systems (ESS) is an indispensable solution to promote supply reliability and exploitation of RES in an efficient and economical way [6,7]. ESSs have diverse variations and configurations, processing distinct attributes that make them appropriate for particular uses [8]. Therefore, they can be categorized according to different characteristics such as energy/power density and capacity (scale), duration of storage, discharge time, response time, lifetime, storage cost, function, and environmental aspects [9,10]. This classification can help identify the most appropriate ESS for a specific application [11]. Currently, as standard systems, batteries are the most used and preferred storage that can work perfectly and easily be installed on-site [12,13]. The battery stands out as a widely used energy storage technology, characterized by its high efficiency, fast responsiveness, and substantial energy density, playing a crucial role in smoothing renewable output and enhancing overall system reliability [14]. However, their limited capacity and lifetime can limit their effectiveness for larger buildings or communities with high energy demands while being costly due to periodic replacement [11,15]. In addition, they face environmental problems at the end of their lifetime due to toxic material, waste disposal, and recycling issues, which are costly compared to their limited lifecycle [7]. These challenges have raised attention to alternative ESSs with a lower energy cost, less environmental impact, and longer lifetime [16].

Among all ESS, compressed air energy storage (CAES) as mechanical energy storage is a promising bulk-energy storage that can be an alternative solution with more flexibility than batteries due to the decoupled power rating and energy capacity [12]. The most attractive

advantages of CAES technology include the ability to be scaled up/down, high energy capacity, long lifetime, high durability, as well as capability of discharging energy for an extended period of time. These characteristics facilitate its utilization as a decentralized ESS, functioning not only to integrate renewable resources but also to manage and shift the electric load demand. Decentralized CAES can also interact with the power grid during off-peak hours for more efficient energy management. Considering their broad applicability, varied efficiency, and emission elimination potentials, CAES systems can be categorized into different types based on their design characteristics, heat management process, fossil fuel utilization, air reservoir form, etc. [11]. Diabatic_CAES (D-CAES), adiabatic-CAES (A-CAES), and isothermal-CAES (I-CAES) are the most popular types of CAES distinguished by their heat management process [11]. Among all, adiabatic-CAES (A-CAES) has been put forward based on a combination of conventional CAES known as diabatic CAES (D-CAES) and thermal energy storage (TES) unit. A-CAES is an emission-free system that adopts a regenerative heat unit into the D-CAES to recycle heat generated from the compression process for preheating the high-pressure air in the expansion process. Such configuration has brought about significant efficiency improvement, up to 70% of theoretical cycle efficiency, while eliminating the need to burn a huge amount of fossil fuels [17].

A-CAES has recently captured a growing attention for decentralized and behind-the-meter applications and customer-sited stationary storage systems by contributing to improve renewable energy integration and load shifting [18]. It also can be used as an alternative to battery storage systems. Compared to the battery, CAES also has a lower ecological footprint; a clean storage medium and the non-toxic materials utilized in manufacturing are abundant and ubiquitous, and components can be easily recycled and replaced. To date, there are several A-CAES projects under construction or in the early stage of planning and experimentation around the world. Although most have resulted in increasing renewable energy penetration in the power system, they are mainly used in grid-scale applications and not in behind-the-meter usage [7,19]. Integrating A-CAES with RESs in the form of decentralized energy storage brings about new challenges [20], which will be elaborated in the subsequent section.

1.1. Problem statement and research questions

In summary, despite the attractive advantages of CAES, the successful implementation of this technology for decentralized applications is hindered by various challenges led from both

its inherent complexities and integration into diverse energy systems. These challenges can be categorized into two distinct perspectives: technological challenges and integration obstacles.

Unlike conventional energy storages, CAES is a complex system due to combining mechanical, electrical, and thermal engineering aspects that causes relatively low efficiency due to multi-step energy conversion and losses. Energy in CAES is partly stored in the form of high-pressure air and partially converted into thermal energy. One way to improve the CAES cycle efficiency and reduce its carbon footprint is recycling the thermal energy by integrating regenerative heat units into CAES [21].

In CAES system, the energy storage unit (air reservoir) and power conversion systems (PCS) such as compressor and turbine trains are decoupled, and the charging/discharging process occurs in a different path. Although these features add more power flexibility to the decentralized HES close to the end-user, it also poses new challenges because CAES must absorb intermittent renewable energies and supply fluctuated energy demand. That means compressor and turbine operation must be tuned by output power from renewable [22–24] and end-user energy demand [23,25,26], respectively. The operation of CAES under this condition often causes it to work unsteadily and over/under a range of operating conditions [22,26] which causes choke/surge and failure problems in the mechanical sub-system and eventually CAES shut-down, which decreases HES reliability. Therefore, it is necessary to avoid this issue by controlling the operation of the turbomachinery from low flows close to the surge point to very high flows near the choke point [20].

Moreover, some issues arise for decentralized CAES concerning the system performance and configuration as it combines several interconnected sub-systems [27]. These challenges are driven by factors such as the trade-off between storage capacity and efficiency, the limited space, and the need for system-level optimization, affecting CAES feasibility for small-scale and behind the meter applications [11]. For example, inadequate space in the urban-integrated system (or buildings) limit the installation of a sizable storage tanks, while relatively low storage efficiency would necessitate larger renewable power plants (i.e., photovoltaic (PV), wind turbine (WT), etc.) to compensate for the energy shortage [18,28]. This would result in increased expenses and decreased sustainability of the system. Hence, the system's design and operational flexibility are the two main factors that influence the feasibility of the CAES system for specific applications [29]. Despite being technologically mature, there is still no unique configuration for the CAES system, especially for the decentralized applications (behind-the-meter applications) where the system needs to handle intermittent renewables and supply

fluctuating end-user demand. Up to now, most of the small-scale D-CAES and A-CAES facilities have been built and put into operation with the role of peaking capacity for front-of-the-meter applications [19,30].

The optimal sizing and planning of a CAES system is not straightforward, as it involves several interconnected subsystems with varying characteristics and functions. The configuration of CAES can significantly affect its operation and contribution to storing and delivering energy. In the CAES system, the volume and pressure range of the air reservoir define the amount of energy that can be stored in the form of high-pressure air, while the power PCSs (compressors and turbines) determine the rate of input and output power [31]. So, the compressors' number and power nominal capacity set the charging time duration/rate at which energy in the form of high-pressure air can be absorbed from the grid or renewable generation systems. Similarly, the turbines' number and size determine the discharging time duration/rate at which energy can be supplied to meet the energy demand [29][30].

On the other hand, the feasibility of the CAES system is also influenced by the range and type of services it provides [11]. Hence, the sizing of the CAES system should be based on its highest possible contribution within a specific energy environment. This is particularly important when CAES is interacting with other sources of energy. That implies a trade-off between nominal power and energy capacities, charging and discharging times, and the cycle efficiency of the CAES system [31]. While optimizing the individual component of CAES is essential, it does not imply process optimization and is not enough to ensure the system's effectiveness. Efficient, reliable, and cost-effective ways while minimizing the environmental impact can be achieved by implementing a system-level management and optimization for CAES technology. Such an approach is critical to ensure that the hybrid system can meet the energy demands of end-users while maximizing renewable energy penetration. It would also ensure long-term efficient operation and maintenance of the system [32][30].

Furthermore, CAES falls short in terms of energy density and responsiveness compared to batteries [11], which can affect the resiliency of the implemented local energy system, especially when a sudden outage happens, and the storage is responsible for compensating for most of it. There are several ways to improve the resiliency of HES. Adopting hybrid energy storage presents an appealing option to mitigate the drawbacks of individual technologies. It could enhance the reliability and resilience of HES, especially the one that involves only one renewable energy resource, like a PV-based energy system and a limited source of convectional

energy as a backup [33]. On the other hand, the resilience of energy systems can be analyzed and improved by employing a combination of long-term and short-term strategies [34].

Addressing these combined technological and integration challenges is essential for unlocking the full potential of A-CAES systems in decentralized applications. This research aims to contribute to the optimal sizing and operation of A-CAES systems, offering solutions that enhance A-CAES contribution, overcome space limitations, and ensure reliable performance in the face of dynamic renewable energy and load demand scenarios and grid disruptions.

Therefore, based on the mentioned limitation, the main research question arises: "*How can A-CAES utilization for decentralized applications be improved?"*

Hence, the thesis tries to answer several sub-research questions as follows:

1) How could we improve the operation strategy of the A-CAES system in terms of energy management to systematically analyze it for decentralized applications?
2) How could A-CAES be efficiently customized and planned to meet the specific user needs in the decentralized applications?
3) Is it feasible to incorporate decentralized A-CAES close to the end-user in urban areas? And under what conditions and configurations can A-CAES become an efficient and economically viable option to manage the urban users' electrical load demand while improving the renewable self-consumption for on-site generation?
4) How do space availability, grid dynamic pricing, and trade-off restrictions affect the A-CAES design and operation in urban-integrated hybrid energy systems (Microgrids)?
5) How could we optimize the operational schedule while having high renewable penetration and low grid dependency, especially during peak grid hours and grid failure situations?
6) How do the A-CAES response time (charging/discharging transition) and its integration with the battery influence the reliability and resiliency of the urban-integrated hybrid energy system, especially under grid outage conditions?

1.2. Research objectives

Accordingly, the main objective of this thesis is to develop a holistic customizable approach for the feasibility assessment of integrating CAES in decentralized applications through optimal design and schedule operation considering techno-economic, environmental, and resilience aspects. To reach that goal, the main sub-objectives of this study can be summarized as follows:

1. Improving A-CAES's energy management operation strategy (EMOS) via an accurate simulation model considering TES unit, PCSs, and AST characteristics and interactions.
2. Presenting several alternative power dispatch strategies (PDS) for feasibility assessment of A-CAES system towards its application potentials such as load shifting, renewable integration, or joint application for decentralized integrations.
3. Developing a comprehensive sizing-planning framework for customizing decentralized A-CAES based on user-specific requirements and long-term real-time data, considering techno-economic and environmental aspects.
4. Structuring an optimal dynamic unit-commitment model for short-term operational scheduling of a hybrid system considering A-CAES response time and charging-discharging transition time
5. Presenting a two-layer resilience-centric approach for improving the reliability and resiliency of the entire hybrid system by hybridizing A-CAES with fast-response energy storage such as the battery, especially under scenarios of the grid failure situation.
6. Evaluating the performance of the A-CAES system in terms of energy, financial profitability, and resiliency in local energy systems through long-term and short-term analysis under various scenarios.

1.3. Organization of the thesis

The subsequent sections of this dissertation are organized as follows: Chapter 2 presents a comprehensive literature review covering the prior research on the technological development, design, and operation of CAES systems within integrated energy systems. It provides an in-depth discussion of design and operation methodologies, delves into their limitations, and proposes potential research directions in this domain. Chapter 3 focuses on the methodology developed at each stage of this work. Firstly, in section 3.2. an improved energy management operation strategy (I-EMOS) is developed for integrating A-CAES systems into decentralized

energy systems. The developed strategy is compared with traditional operation strategies to validate and assess the accuracy of the proposed model, utilizing real data from an existing A-CAES pilot plant. Furthermore, the influence of key design parameters on system performance indicators is investigated.

Then, in section 3.3, we specifically explore the impact of the presence of a low-temperature TES system on the performance of A-CAES, comparing it with a diabatic-CAES system featuring a combustion chamber for preheating the high-pressure air before expansion. Section 3.4. introduces a holistic sizing and planning approach to customize and optimize A-CAES systems for decentralized applications based on specific requirements. Several power dispatch strategies (PDS) are proposed, aligning with the potential of A-CAES systems for load-shifting and renewable integration. This part also explores the potential profitability of incorporating A-CAES systems in urban building applications through a comprehensive techno-economic and environmental evaluation. Additionally, it investigates the effects of critical parameters, such as the size of energy generation systems and available space area, on the optimal configuration and cost of A-CAES systems to verify their applicability across different case studies with various characteristics. In section 3.5. a sizing-planning strategy is integrated into an operation-scheduling approach. Accordingly, a resilience-oriented sizing-scheduling approach is proposed to determine the optimal configuration and operation of the entire hybrid energy system, including A-CAES technology. Economic and resiliency aspects for both short-term and long-term system operations are considered. This section also explores the potential of a hybrid A-CAES and battery system and its influence on the resiliency of the optimal hybrid energy system, particularly during power generation disruptions. Finally, Chapter 4 provides a comprehensive summary, conclusions, and discussions on the limitations of the current work. It serves to guide future research directions.

The present dissertation mostly follows a manuscript-based structure, wherein the subsequent chapters mostly consist of scientific paper manuscripts. The manuscripts included in this dissertation have either been published or submitted to scientific journals and conferences:

Chapter 2: Literature review

E. Bazdar, M. Sameti, F. Nasiri, F. Haghighat, Compressed air energy storage in integrated energy systems : A review, Renew. Sustain. Energy Rev. 167 (2022) 112701. https://doi.org/10.1016/j.rser.2022.112701.

Chapter 3: Methodology and Results

Section 3.2. E. Bazdar, F. Nasiri, F. Haghighat, An improved energy management operation strategy for integrating adiabatic compressed air energy storage with renewables in decentralized applications, Energy Convers. Manag. 286 (2023) 117027. https://doi.org/10.1016/j.enconman.2023.117027.

Section 3.3. E. Bazdar, F. Nasiri, F. Haghighat, Effect of Low-Temperature Thermal Energy Storage on the Hybrid PV-compressed Air Energy Storage Operation, in: (2022): pp. 1609–1616. https://doi.org/10.4229/WCPEC-82022-5DV.2.19.

Section 3.4. E. Bazdar, F. Nasiri, F. Haghighat, Optimal planning and configuration of adiabatic compressed air energy storage for urban buildings application : Techno-economic and environmental assessment, J. Energy Storage. 76 (2024) 109720. https://doi.org/10.1016/j.est.2023.109720.

Section 3.5. E. Bazdar, F. Nasiri, F. Haghighat, Resilience-Centered Optimal Sizing and Scheduling of a Building- Integrated PV-based Energy System with Hybrid Adiabatic-Compressed Air Energy Storage and Battery Systems, Energy. 308 (2024) 132836. https://doi.org/10.1016/j.energy.2024.132836.

Chapter 2: Literature review

Over the past decades, rising urbanization and industrialization levels due to the fast population growth and technology development have significantly increased worldwide energy consumption, particularly in the electricity sector [35,36]. In 2020, the international energy agency (IEA) projected that the world energy demand is expected to increase by 19% until 2040 due to population growth from 7.7 billion in 2019 to 9 billion in 2040 [3]. Therefore, if it were not for frequent energy efficiency upgrades, the world would require energy two times more than it generates today [4]. Nowadays, a significant part of the world's energy demand (around 90%) is supplied by fossil fuels such as coal (27%), oil (31%), and natural gas (23%) [5–7]. The remaining energy demand is fulfilled by nuclear power (5%), biofuels (9%), hydro (3%), and other renewable sources (2%) such as wind, solar, and geothermal energy [41]. Using conventional energy sources to generate energy is associated with economic problems such as growth in fuel prices due to their limitation, scarcity, and environmental issues such as greenhouse gases [42]. Concern for climate change and global warming necessitates reducing dependency on fossil fuel power plants to fulfill the world energy requirements [1,43]. Using RESs has become a promising alternative to fossil fuel sources [39,44] to tackle environmental challenges by decarbonizing the energy generation process [45]. Although RES offers an environmental-friendly performance, these sources' intermittency nature is a significant problem that can create operational problems and severe issues to the grid stability and load balance that cause the supply and demand mismatch [5]. Therefore, applying the ESS could effectively solve these issues because it enhances reliability and provides technical, financial, and environmental advantages to the energy system network [6]. According to the report published by the international renewable energy agency [46], with increasing the share of renewable energies in the world’s energy generation, the total capacity of ESS will be enhanced three times by 2030. Besides, adopting ESSs in the energy system has brought many vital benefits [46–48], such as adding flexibility and reliability to the grid, shifting energy availability, grid system balancing, decreasing the need for constructing the additional energy generation capacity, and consequently diminishing significant infrastructure investment and allowing decarbonization. Enhancing safety, increasing the availability of renewable energy, distributed generation, and the smart grid, using a more comprehensive range and type of energy sources, and providing many useful services are also the other merits of ESSs. The services provided by ESSs can be categorized into three classes 1) Front-of-the-meter applications (e.g.,

black start, fast frequency regulation, voltage support, capacity reserve, energy shifting, peak shaving, etc.), 2) behind-the-meter applications (e.g., self-consumption, community storage, power quality, load shifting, peak-shaving, Time-of-use, etc.), and 3) off-grid applications (e.g., nano off-grid, village electrification, island grid, remote area, etc.).

Among all energy storage systems, the CAES as mechanical energy storage has shown its unique eligibility in terms of clean storage medium, scalability, high lifetime, long discharge time, low self-discharge, high durability, and relatively low capital cost per unit of stored energy. In contrast, low roundtrip efficiency (RTE), low depth of discharge, and high response time are considered its main drawbacks. This chapter presents a comprehensive review of technological developments in CAES systems, including its design criteria and emerging application potentials. Furthermore, a detailed review of the most recent research progress on CAES technology and its challenges is presented from the point of view of the different integration potential of CAES, optimal designing, and scheduling with the role of CAES towards micro-grid, distribution energy network, and energy market environment. Finally, the limitations and future perspectives of CAES are described and summarized. The present chapter provides a comprehensive reference for integrating and planning different types of CAES in integrated energy systems for various applications. The structure of the present chapter and its subsections are as follows:

- The applications and characteristics of CAES technology and its comparison to other EES systems are explained in Sections 2.2.
- Section 2.3 provides details on the technology developments in the CAES domain with an overview of their advantages and challenges.
- Section 2.4 elaborates on the benefits and challenges of integrating CAES into energy conversion and renewable energy systems.
- In addition, various approaches for the sizing of CAES when integrated into renewables are investigated. CAES's optimal operation and scheduling at different levels of energy systems such as microgrids, distribution networks, and energy markets are discussed in Sections 2.5, 2.6 and 2.7.
- Finally, section 2.8 highlights the existing limitations and gaps of previous research.

2.1. CAES versus other energy storage systems

There are different types of ESSs that can be appropriate for specific applications based on their unique characteristics. Therefore, ESS can be classified based on their characteristics and several methods proposed in the literature [20–23]. For instance, in terms of their energy and power density, size (energy/power rating capacity), discharge time, storage duration, self-discharge rate, depth of discharge, response time, lifetime, application, storage cost (capital, operation, and maintenance cost), environmental aspect, etc. The most common methods for classification of ESSs are based on energy usage in a specific form, including electrical energy storage (EES) and thermal energy storage (TES), or based on the types of energy stored in the system (kinetic or potential; thermal, electrical, mechanical, chemical, etc.) [44,49,54]. Fig. 2.2. demonstrates a comparison of different EES systems based on their power rating, rated energy capacity, discharge time, and the grid-scale services.

As it can be seen, among all EESs, only CAES and pumped hydro energy storage (PHES) can be utilized for large-scale applications due to their advantage of long discharge times (hours to days) [1,55]. PHES system with a maximum power rate of 5,000 MW is the first large-scale commercially mature EES. According to the IEA [46], PHES has dominated 96% of total power storage capacities installed worldwide. The other ESSs, including thermal storage, batteries, and other mechanical energy storages in significant use, have a portion of 3.3 GW (1.9%),1.9 GW (1.1%), and 1.6 GW (0.9%), respectively.

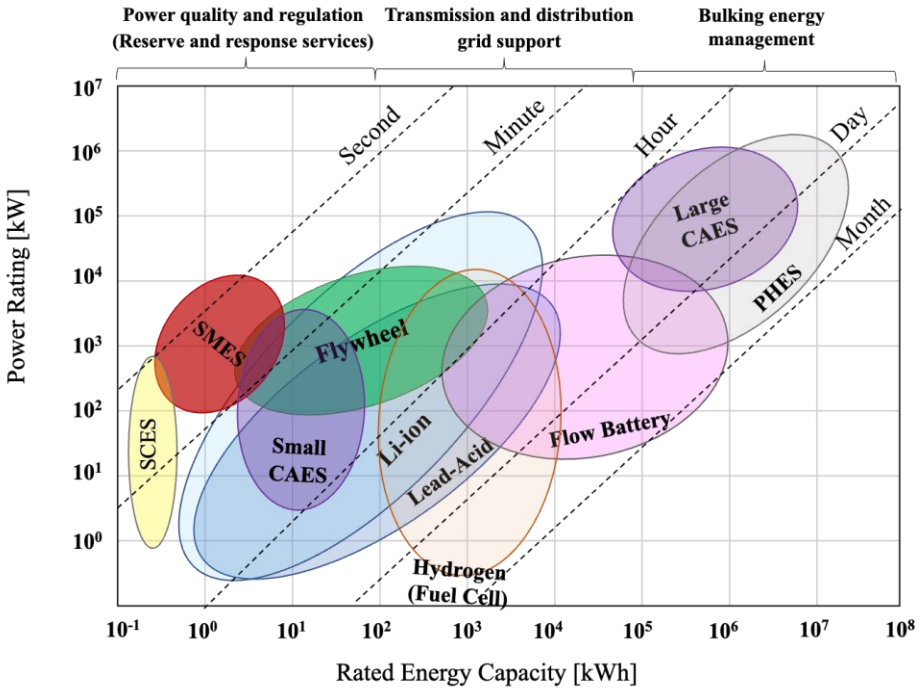

Fig. 2. 1. Comparison of EES systems based on their power rating, rated energy capacity, discharge time, and grid-scale services based on Refs. [56–59].

However, PHES requires a particular geographical condition with appropriate hydrology, including water resources and raised-high water storage. Therefore, geological constraints to provide adequate and massive rooms for reservoir constructions, as well as environmental concerns, are the crucial obstacles that make the new and further development of such a system complicated [1,6]. On the contrary, CAES can store energy in an above-ground container or high-pressure vessels, underground or underwater reservoirs. Large-scale CAES stores compressed air in the reservoirs, typically in forms of underground geology such as abandoned mines, depleted gas fields, rock caverns, and aquifers with sufficient porosity and permeability [1,60]. Therefore, CAES not only has easier installation [61] but also offers a few geological restrictions compared to PHES that significantly reduce its capital and maintenance cost [55].

To date, PHES and large-scale CAES have been employed for grid-scale storage applications, while batteries have been applied at smaller scales [62]. However, electrochemical storage technologies like batteries are considered mature and, in some cases, immature storage technologies utilized for small-scale applications (e.g., residential, smart grid, etc.). Therefore, the cost of this EES is prohibitively expensive compared to their service periods [60]. Also, the battery has several main drawbacks, such as a relatively short lifespan, which can be represented as a limited charge/discharge life cycle [16]. On the other hand, due to uncertainty in the availability and continuity of renewables, the battery might not be fully charged in some circumstances. Leaving a battery in a partial charge situation reduces its lifespan. Replacement of batteries results in environmental and disposal problems due to batteries' containing hazardous material [28]. Therefore, alternative EES technologies should be adopted, particularly for small-scale applications [16,63]. A small-scale CAES (SS-CAES) is a promising EES technology, presenting a great way to enhance energy extraction from RESs at an affordable cost, with the advantages of being environmental-friendly and having higher operational flexibility [16]. Moreover, since the RTE of CAES is relatively low, using the heat loss from the compression phase and the cold energy from the expansion phase for heating and cooling applications can play a crucial role in promoting overall CAES efficiency. The more detailed information about the critical characteristics of some popular EESs is listed in Table 2.1.

Generally speaking, the CAES system as a mechanical ESS stores energy in the form of high-pressure air, and as mentioned before it is one of the commercialized EESs, which exists from small to large scale capacities worldwide. The main components and working mechanism of a CAES are shown in Fig. 2.2. Generally, the operation of the CAES system is based on three

processes: compression, storage, and expansion process. Therefore, compressors use electricity to pressurize air during the off-peak demand in charging mode. The high-pressure and high-temperature air is cooled before being stored in an air reservoir.

The thermal energy can be dissipated into the atmosphere, stored in TES, or used for heating applications. In the discharging process, stored high-pressure air is released whenever the electricity is required. Then, it is preheated by an external heat source and expands via turbines generating electricity [64–66].

CAES has a high energy capacity and power rating, making it appropriate to use as a stationary and large-scale energy storage due to its ability to store a large amount of energy. However, CAES's energy and power density are low [57], which means that the amount of energy and power stored in a specific volume related to the air thermodynamic properties is low. Therefore, a larger storage container is needed to keep a significant amount of energy (like underground storage used for two commercialized CAES plants, Huntorf in Germany and McIntosh in the USA, at 532,000 m^3 [67] and 270,000 m^3 [68], respectively).

Table 2. 1. Characteristics of various types of EES systems using the data from Refs. [46,47,50,53,59,69–75].

EES	Mechanical					Electro-chemical		Electrical	Magnetic	Chemical
Characteristics	PHES	CAES		LAES	Flywheel	Lead-Acid	Li-ion	SCES	SMES	Hydrogen (FC)
		LS &UG	SS &AG							
Energy capacity (MWh)	100-20000	580-2860	<0.1	2.5	0.0052- 5	0-40	0-10	0-0.0005	0-0.015	0.312 developing 39
Power rating (MW)	1-5000	100-1000	0.003-10	1-300	0.1-20	0-40	0-100	0-0.3	0.1-10	0-50
Specific Energy (Wh/kg)	100-400	30-60	140 at 300 bar	214	5-100	30-50	80-200	0.05-15	0.5-75	800-10000
Specific power (W/kg)	---	---	---	---	400-1500	75-300	300-2000	500-10000	500-2000	5-800
Energy density (Wh/L)	0.5-2	2-6	> 6	50-200	20-80	50-90	100-500	10-30	0.2-6	500-3000
Power density (W/L)	0.5-1.5	0.5-2	>2	---	1000-2000	10-400	1000-10000	More than 100,000	500-4000	>500
Energy efficiency (%)	65-85	40-70	65-90	45-70	85-95	63-90	75-97	84-95	80-95	20-66
Discharge time	1-24h$^+$	1-24h$^+$	1-24h$^+$	1-12h$^+$	ms-15 mins	Mins-hrs	Secs-hrs	ms-1hrs	ms-8secs	Sec-24h+
Response time	Mins	Mins	Secs -mins	Mins	--	ms-sec	ms-sec	ms-sec	--	Sec
Daily self-discharge (per day)	Very small	Small	Small	Small	100	0.1-0.3	0.05-0.36	20-40	10-15	Very small
Storage duration	Hrs-months	Hrs-months	Hrs-days	Hrs-days	---	Mins-days	Mins-days	Secs-hrs	Mins-hrs	Hrs-months
DOD	80-100	40-50	40-50	---	75-85	50-60	80-90	100	---	---
Lifetime(year)	30-60	20-40	20-40	20-40	15-20	5-15	5-15	10-20	20-30	5-20
Cycle Capability	20000-50000	>13000	>13000		20000-100000	250-4500	1500-4500	>100000	>100000	20000
Power capital cost ($/kW)	2000-4000	400-1000	517-1550	300-1000	590-1446	615-750	463-966	286-331	303-761	2400-4700
Energy capital cost ($/kWh)	5-100	2-120	200-250	1300-2200	3000-6000	281-361.8	900-1300	926-1141	7209-9205	400-800
Maturity	Mature	Mature	Mature	premature	Mature	Mature	Mature	Premature	Premature	Premature/prototype

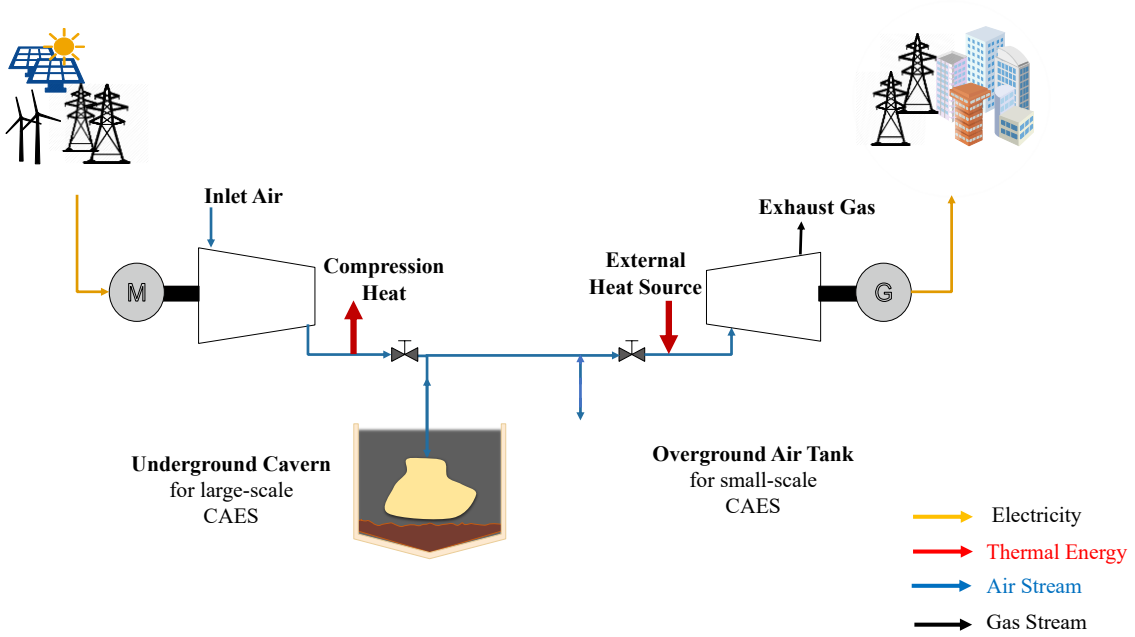

Fig. 2. 2. Schematics of the operating principle of the CAES plant.

In addition, CAES has relatively low energy efficiency. The range of energy efficiency is between 40-70%. Existing CAES plants have an energy efficiency of 42% (Huntorf) and 54% (McIntosh) [57]. In comparison, more advanced CAES units such as A-CAES have an energy efficiency of around 60% (e.g.. Goderich facility in Canada) and 67% (e.g.. Feicheng in China) [76]. Enhancing the RTE of CAES to approximately 80% could make it comparable with other EESs having a lower environmental impact. The relative daily self-discharge of CAES is small, which increases the storage duration and makes it suitable to store and discharge energy for a long time without wasting much energy. Depending on the CAES scale, it could take hours, days, and even months to reach an appropriate level of service in energy management applications (such as peak shaving, black start, renewable integration, and energy arbitrage). An attractive attribute of a CAES is its lifespan of more than 40 years and over 13000 cycles. CAES's energy (or power) cost is one of the lowest among all EESs, although its initial capital cost, like PHES, is relatively high [47]. In addition, in comparison with other EESs, CAES technology has a higher response time as it is multi-stage storage that includes a process involving several mechanical systems. Thus, it is not suitable for providing power quality and voltage/frequency regulation services, which require a fast response EES. The higher response time of CAES is less of a concern for energy management applications [57].

CAES has unique potential as an energy management tool [9]. Fig. 2.3 shows the position and application of CAES in the energy system environment. There are generally two potential applications for CAES: from the provider perspective (front-of-the-meter) and the consumer

perspective (behind-the-meter and stand-alone). On the energy supply side, transmission and distribution system operators are utilized CAES for bulk energy management services which requires the long-term ESS with a high power capacity, while response time is not a crucial concern [57,73]. The practical application of CAES on a global scale involves the category of grid services, including peak shaving, load shifting, black start, energy arbitrage, frequency restoration reserve, and renewable integration [46,53,57]. Most CAES facilities around the world operate as energy-shifting units because they can charge and discharge from hours to days economically and optimally due to the relatively low energy cost along with the high discharge time [46].

On the other hand, "Behind the meter" applications refer to end-users peak shaving and demand-side management (load-shifting). Consumers can utilize CAES to manage their energy consumption according to the energy price tariff (during the peak and off-peak hours) to minimize their energy costs [73]. CAES can also be applied as a backup power source that can be used as an alternative power source for hospitals, banks, and data processing centers.
CAES can be integrated into renewable energy systems, especially wind and solar energy. Such applications address the fluctuation of renewables [7,8] by capturing renewables surplus energy and storing it effectively, avoiding the renewable curtailment phenomenon [19,73]. Furthermore, CAES can serve as power engines in air-powered vehicles [77,78].

The utilization of CAES for poly-generation, either individually or combined with cogeneration systems in the energy hub framework, is another promising and feasible application of this system [7]. This means that CAES can either be used to generate cooling, heating, and power energy that improves its RTE efficiency or be coupled with cogeneration systems to improve the whole energy hub performance. A detailed review of a broad spectrum of research on poly-generation of CAES is found in Ref. [79]. Fig. 2.4 illustrates a framework of CAES applications in an energy hub based on data from Refs. [7,17,80,81].

Several literature reviews were published about CAES systems. A detailed comparison of previous review articles based on a different aspect of CAES is shown in Table 2.2. All articles are listed in order of the published year. They reviewed various aspects of this technology, such as technology development, characteristics, global status, different challenges, future trends of CAES, etc. For example, in Ref. [19], the authors briefly discussed CAES classification, application, and current global state. However, more attention was paid to reviewing China's most recent CAES developments considering their contribution to renewable energy penetration, their geological condition, and related government policies.

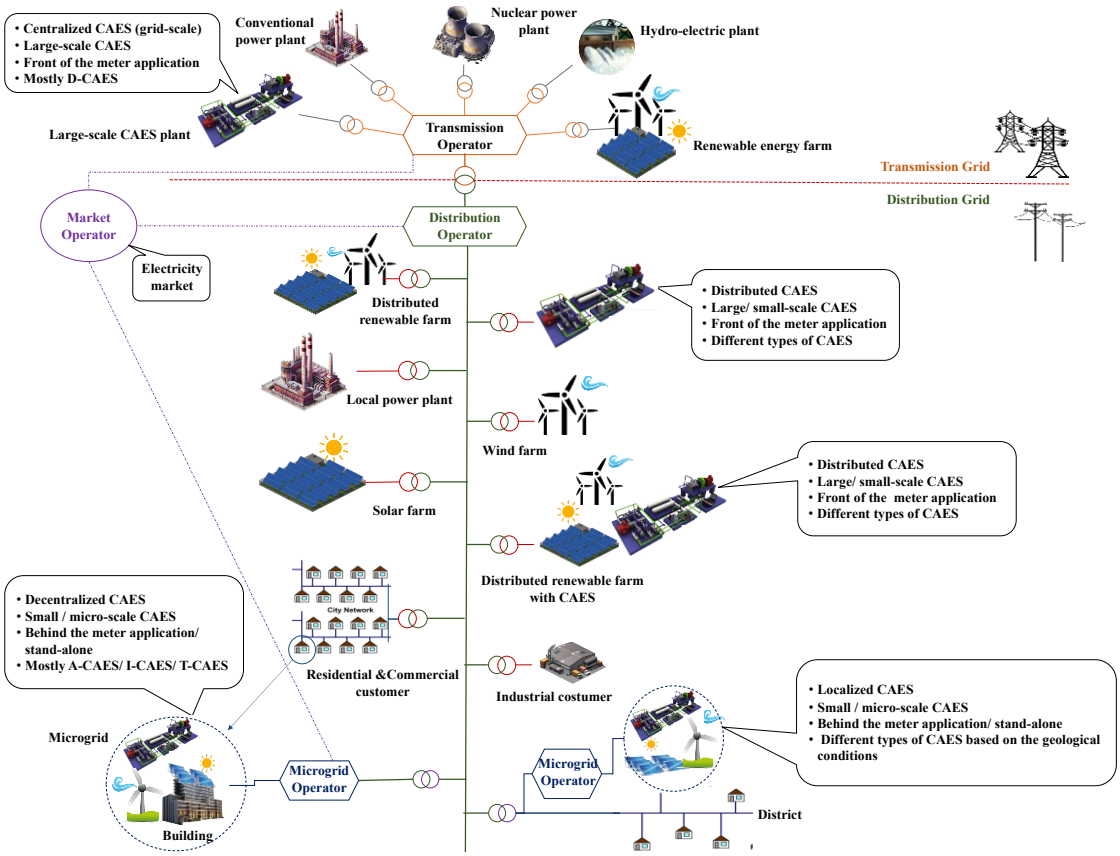

Fig. 2. 3. Application of CAES in the energy system environment.

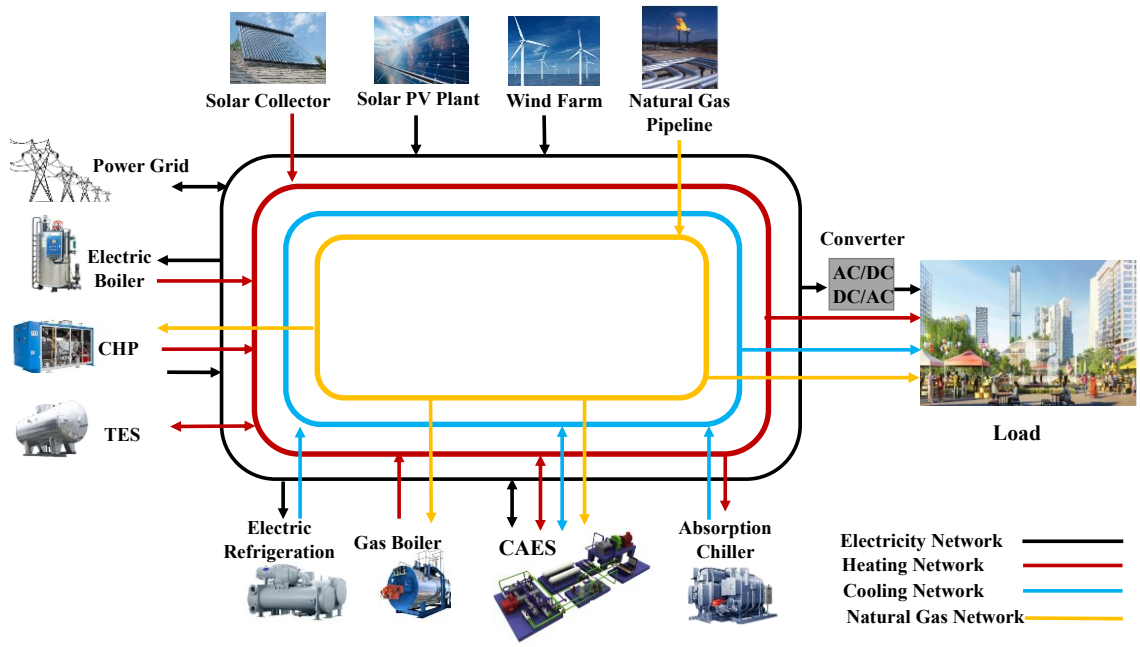

Fig. 2. 4. A framework of energy internet based on energy hub based on Refs. [7,17,80,81].

King et al. [76] not only briefly introduced several CAES technologies and current large-scale CAES projects but also presented several methods to store pressurized air using underground characteristics. In their study, there was a greater emphasis on examining and comparing the potential of integrating renewable electricity generation systems with an underground storage capacity of CAES plants in India and the UK for large-scale application. The geological considerations for developing air reservoirs and CAES plants in Canada and China were evaluated in Ref. [75].

CAES's operational stages and health & safety issues were explored in Ref. [59]. Additionally, various expander types suitable for different CAES technologies were analyzed. A similar approach was introduced earlier in Ref. [69] while the authors proposed guidelines for choosing appropriate expansion machines and expansion stage parameters to achieve high efficiency. Huang et al. [82] briefly discussed different classes of CAES in terms of scale, heat management, and integration to other technologies in parallel with introducing several application areas of CAES. The authors in Ref. [65] presented an overview of a CAES in terms of scale and fuel utilization with an analysis of the main subsystems of CAES. Furthermore, CAES application prospects in smart grid and energy internet were also illustrated to present CAES potential applications.

Wang et al. in Ref. [74] gave a brief overview of the different aspects of CAES technologies. A short discussion also was given on the challenges and future prospects of CAES. In Ref. [68], the other researchers also presented a detailed review of CAES's research trends in different areas of study, such as performance evaluation, economic analysis, and several control strategies of CAES systems. The need for correct fluid property data for the computation and design of CAES processes was emphasized by Budt [64].

Table 2. 2. Comparison of previous reviews on CAES.

Author	Year	Technology development	Characteristics	Heat regeneration (TES)	Application	States of CAES Commercialization	Challenges	Future trends	Other aspects and a short description
Tong et al. [19]	2021	√	×	×	√	√	×	×	Comprehensive feasibility analysis on CAES development in China
King et al. [76]	2021	√	×	×	×	√	×	×	The potential underground storage capacity in India and the UK
Olabi et al. [59]	2020	√	√	√	√	√	√	×	Health and safety and operational mode of system
Huang et al. [82]	2019	√	×	×	√	√	×	√	Application prospect of CAES
He et al. [69]	2018	√	√	×	×	×	√	×	Operating conditions of CAES, selection of air expansion machine
Li et al. [75]	2018	×	×	×	×	√	×	×	Geological considerations for CAES in Canada and China
Wang et al. [74]	2017	√	√	√	×	×	√	√	Research progress in CAES and the associated performance analysis
Wang et al. [73]	2017	√	√	√	√	√	√	√	Analyses the significant technological barriers/weaknesses
Venkataramani et al. [68]	2016	√	√	×	×	√	√	√	Research progress in CAES, CAES potential, economic analysis, and control strategies
Chen et al. [65]	2016	√	×	√	√	√	√	√	Elaborating critical subsystem of CAES
Budt et al. [64]	2016	√	×	√	×	√	√	√	Considering the exergy concept, discussing the importance of accurate fluid property data for the calculation, and design of CAES processes
Luo et al. [83]	2014	√	√	×	√	√	√	√	Overview of multi-scale CAES
Current Study	**2024**	√	√	√	√	√	√	√	CAES types and integration concept, designing, optimal planning, and scheduling in the different energy sectors

2.2. CAES technology development

To date, different CAES architectures have been proposed and developed based on various characteristics. Therefore, according to the literature, CAES can be divided into several categories, as shown in Fig. 2.5. For example, CAES can be characterized as large-scale (LS-CAES >50 MW), small-scale (SS-CAES in 10 MW class) and micro-scale (μS-CAES <100 kW) [65,82–84]. The most common classification of CAES is based on the structure aiming to enhance its technical and economic performance. Therefore, based on heat management techniques during the compression and expansion process, CAES can be classified into diabatic-CAES (D-CAES), adiabatic-CAES (A-CAES) with and without TES, Isentropic-CAES (I-CAES), Poly-generation CAES (PG-CAES). Advanced adiabatic_CAES (AA-CAES) is a kind of A-CAES with TES in which there is no energy loss in compression mode, and no fuel combustion is required before expansion [59,80]. Also, a review of different TES techniques for CAES can be found in Ref. [66].

In some studies [19,57,61,85], CAES was classified based on its different derivative concepts, such as liquid air energy storage (LAES), supercritical CAES (SC-CAES), under-water CAES (UW-CAES), and steam-injection CAES (SI-CAES). Callaghan et al. [86] carried out a comprehensive study on LAES technology as a subset of the CAES system. In addition, a state-of-the-art review on integration pathways and future perspectives of LAES was presented in Ref. [70]. More information about LAES can be found in Refs. [87,88]. In Ref. [65], CAES was categorized into supplementary fire CAES (SF-CAES) and non-supplementary fire CAES (NSF-CAES), which refers to the need for burning the fossil fuel for preheating the air before expansion [64]. In several studies, CAES was characterized according to the type of external heat source used toward the expansion phase. Thermal energy can be whether fossil fuel-based or from TES, which is classified according to the heat transfer methods (sensible heat, latent heat, and thermal-chemical) [66] or temperature degree of TES (high, medium, and low temperature) [64]. CAES may be categorized based on the form of air reservoir [85], which can be underground cavern (UG-CAES; natural salt caves, mines, aquifer storage, lined rock cavern, depleted gas field, well) [76,82], underwater reservoir (UW-CAES; ballasted rigid tanks or flexible fabric containers) [57] or aboveground tank or gas pipeline (AG-CAES) [89]. Another classification can be based on the state of the charge [64] in the storage reservoir, which could be iso-choric or iso-baric. In summary, detailed information about each type of CAES, such as description, advantages, and challenges, are listed in Table 2.3.

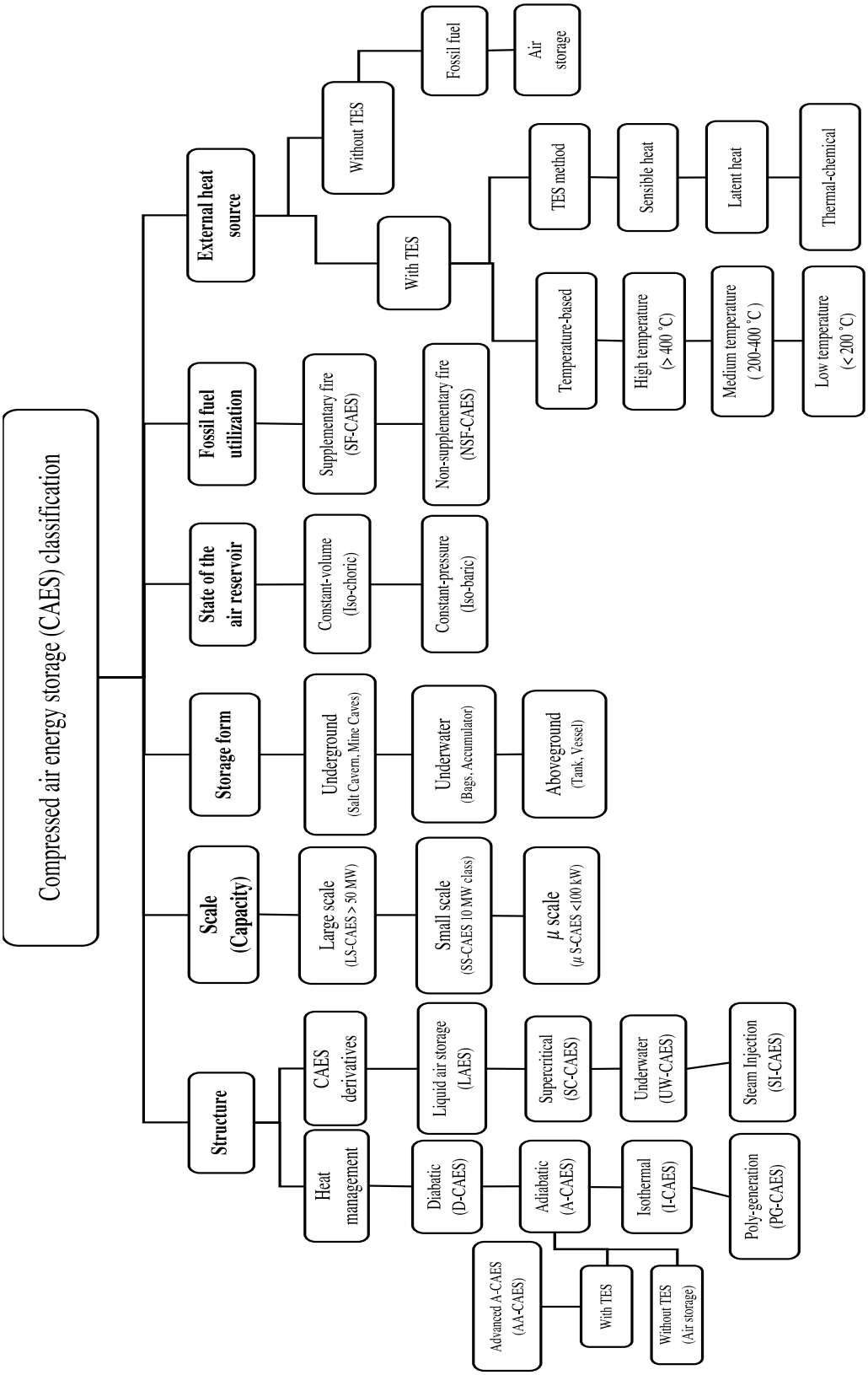

Fig. 2. 5. Comprehensive classification of CAES concept based on different characteristics.

Table 2. 3. Comprehensive classification of CAES concept with their advantages and disadvantages.

CAES type	Description	Expected efficiency	Advantages	Challenges	Latest research progress
D-CAES	The heat generated from the compression process dissipates into the atmosphere, and high-pressure air is preheated by burning fossil fuel in the combustion chamber before expansion.	46-54%	• Easy to install and control. • Capable of operating as a gas turbine in case the air reservoir is empty [90,91]	• Thermal loss; wasting a huge amount of energy in the form of thermal energy during the charging period • Fossil fuel dependency: environmental problems resulted by burning fossil fuel in discharging period to preheat the air before expansion • Geological restriction	[92]
A-CAES without TES	high pressure and temperature air generated from the compressor is stored in the same insulated storage tank/reservoir. [57].	Max 70%	• Environmental-friendly; the need for fuel has been eliminated. • The air does not need to be reheated for the expansion process. • The thermal energy loss is reduced [57].	• Decreasing the energy density of the air and then need for the larger tank to generate the same power • Material challenges for AST; storing high temperature compressed air needs more expensive storage vessels[57] • The air cannot be compressed to high pressures because it is not cooled, reducing its potential for storing energy [57]	[5,93,94]
A-CAES with TES	Storing air's thermal energy after each compression stage in separated TES and using that to preheat the discharged air before expansion[57].	40–50%[95] Max 70%-75%[57, 79]	• Environmental-friendly; the need for fuel has been eliminated • A smaller tank is needed for the same power generation, increasing roundtrip efficiency [57]	• High power consumption due to high-temperature rise during adiabatic compression [95] • Need for high-temperature TES in some cases [95] • Technical and safety issues associated with high-temperature TES • Cost of the TES element	[96–99]

I-CAES	The compression and expansion process occurs without the inherent challenges in temperature (in iso-thermal conditions)	Theoretically 100%[95] 80%[57]	• Environmental-friendly; the need for fuel and carbon emission has been eliminated[95] • Maximizing heat transfer during the compression or expansion phase and reducing heat loss due to heat exchange [100]. • Eliminating the need for TES[101] and the technical bottleneck of high-temperature TES [95] • Increase the efficiency of CAES, which makes it economical, and competent energy storage[59,101]	• Slow compression and expansion process to have enough time for heat exchange • It is challenging to attain near isothermal compression/expansion and maintain a constant temperature [57,95]. • The low heat transfer feature of conventional compressors is a significant challenge in achieving near-isothermal compression[101] • Attaining a high heat transfer rate[101] • Need for specialized machines to handle the heat transfer.	[62,95,100–103]
PG-CAES	Thermal energy from the compressor is used for heating, exhausted cold air from expansion is used for cooling demand, and power is generated in the expansion phase.	More than 100%[79]	• Environmental-friendly; the need for fuel and carbon emission has been eliminated[95] • Increasing the overall energy efficiency	• Lower electricity-electricity efficiency due to the lower inlet air temperature before expansion	[104–111]
LAES	In charging mode, Excess electricity is used to liquefy the air. The low-pressure liquid air is stored in a suitable insulated tank. In discharging mode, the low-pressure liquid air is pumped to the high pressure and vaporized and superheated to high-temperature vapor, which drives turbines to generate power [57,62].	53%[62]	• High energy and power densities (around 20 times higher than CAES) [62] • Needs for the smaller reservoir to store the same amount of energy (about 1/700th of the volume of gaseous air)[65] • Eliminating the geological restriction compared to D-CAES[57] • Having off-the-shelf components.[57]	• Relatively low cycle efficiency • The storage duration is shorter than CAES • Safety issues due to the leakages[57]	[86–88,112–114]

SC-CAES	Atmospheric air is compressed to its supercritical state and then stored in a reservoir after cooling. The air is pumped to supercritical pressure and reheated during discharge, generating gas to drive a turbine.	64.4%	Combines the advantages of LAES and A-CAES: • Environmental-friendly and relative high efficiency • High power and energy densities (18 times higher than D-CAES) • large power rating and storage duration	• The complexity of system flow	[112,115–117]
SI-CAES	The operation principle is similar to D-CAES, but steam injection into the high-pressure combustor before expansion is used to enhance the performance of gas turbines. Economizers, an evaporator, and a superheater (SPHT) are applied to generate the steam [118].	-	• Enhancing the output power of the turbine train by increasing the airflow rate and specific heat of combusted gas • Decreasing the local flame temperature in the combustor chamber due to introducing the steam with high specific heat • Reducing the thermal NOx generation [14]. • Eliminating the concern for surging the compressor due to steam injection. [118]	• Determining the ratio of the injected steam flow rate to the airflow rate at a certain level. • fixing a certain steam-to-air ratio needs to test each combustor. [118]	[118]
UW-CAES	The operation principle is the same as general CAES with the difference that high-pressure air is injected and stored in underwater containments to benefit from the hydrostatic pressure of water depth[89]. The water source can be a deep lake close to the coast, ocean sea, and onshore [100].	--	• Vessel technology is cheaper than underground [57,100,119] and vessel-related cost is independent of depth [119]. • Minimizing and simplifying the requirements for containment design structure due to the hydrostatic pressure (same pressure with the surrounding water) [89,119] • Because of constant pressure conditions in storage, turbine trains	• Need for suitable water source • Probability of leakage from storage unit (1.2 % /day)[61] • Pressure drop losses in the pipeline [61] •	[61,89,120–127]

			can work at their rated conditions without throttling down [57]. • Having a lower environmental and safety impact in case of failure [89]		
UG-CAES	The underground structure is employed for storing the high-pressure air[76]. The reservoirs are sited in underground salt, aquifers, porous rock, and hard rock [59]. Salt caverns, mine caves, expired wells, and abandoned natural gas reservoirs can be chosen as air storage for CAES[82].	--	• The potential of being at a very low cost: no more than $1/m3 and £0.09/kWh at 80 bar (less than half this for aquifers and depleted gas fields) [89,127] • Because of having a large volume, it is suitable for large-scale CAES applications [65,76].	• Need to excavation (if cavern doesn't exist). [119] • The challenges associated with the excavation of large caverns and detailed structural consideration to ensure the long-term integrity and avoid the collapse potential[119] • The cost of a reservoir is dependent on depth[119]. • Geological restriction; Finding and selecting the suitable geology and a site with specific geological formations, caverns, and mines[65]. • Several inherent issues are associated with these natural reservoirs, such as saltwater problems and animals like rats [59]. • The leftover air in the reservoir impacts CAES's overall efficiency [32].	[19,75,76,128] [64]

AG-CAES	Above-ground air storage such as high-pressure tanks or pipelines is employed instead of underground caverns for SS-CAES applications.	--	• Supplying higher energy density [59]. • Eliminating the dependency on geographical conditions • Presenting a flexible layout[65]. It can be installed onsite and anywhere [59]. • Reduce the need for leaving a large amount of air in storage during the discharge compared with underground reservoirs.	• Land requirement and availability. • Higher capital cost; storing a large amount of air by exploiting underground and underwater CAES is more cost-effective[59,65,89].	[19,64]
Constant pressure (Isobaric)	It reflects the state of the charge of air in the storage. The air pressure in the reservoir remains constant, and only storage volume is varied as it is filled and emptied during the charging and discharging period, respectively[59,89]. It can be underground, underwater, or aboveground [59,85].	--	• Allowing to have more efficient turbomachinery in both charging and discharging phases than with isochoric storage [89] • Improving the expansion efficiency by 10-15% is caused by eliminating the need to throttle down the air during discharge. • Higher energy density because there is no need for leftover air in the reservoir to support the external pressure posed by the weight of the surrounding earth, which causes the collapse of the underground reservoir[89].	• Isobaric storages are pretty complex [59]. • A deep air storage cavern or high-altitude water pond is needed to provide enough hydrostatic pressure by the water column. That compromises the economic attractiveness of such a structure [85].	[129–131]

Constant volume (isochoric)	The storage volume remains constant, and only the air pressure in the storage is varied as the storage is filled and emptied during the charging and discharging period, respectively [59,89,118].	--	• It can be underground or aboveground [32]. • Technically simple, and the installation cost is low [79]	• There will be the leftover air below the design pressure to observe the safety consideration of the reservoir and prevent the expander from operatingng at off-design conditions, which reduces the system efficiency[85]. • Need for throttling down the high-pressure air before expansion causes the massive amount of exergy to be destroyed [85]. • Changing the internal pressure and temperature of storage during the charging and discharging period can cause the compressor and the expander to work off the design point, affecting overall efficiency [85,118].	[27,84,132]

HT-CAES	The operation principle is similar to A-CAES but with single-stage high-temperature TES. High-pressure air is passed through the packed bed TES above 400 ºC to be cooled and heated up before storing in an air container and expanding in a turbine.	>70%	• The significant advantage is high cycle efficiency, up to 70%[64] • Using relatively inexpensive solid TES material[133]. • No additional heat exchange equipment is required because the TES material is in direct contact with the high-pressure air [133].	• Complex system engineering [64] • There is a need for a particular material to withstand thermal and mechanical stress simultaneously. • Higher start-up time (10-15 min) because of the need for high temperature [133]. • Controlling the high-pressure CAES (>70 bar) together with high-temperature TES (>400) is not straightforward [133]. • The jacket of the pressurized TES must be constantly cooled to ensure safe operation[133]. • A high construction and maintenance effort is needed because of the coexistence of high pressure and temperature air in TES [133]. • Interaction between air and TES medium might cause small particles to be released into the air, damaging the expanders (blades, wheels, etc.) [68]. • Designing the new compressors to be able to operate with high interstage and discharge temperatures [133].	[133,134]

MT-CAES	The operation principle is similar to HT-CAES but with two-stage TES below 400 ºC., TES media like molten salt or thermal oil PCM-filled packed bed TES is possible.	>70 %	• The lower efficiency than HT-CAES	• Start-up time is in the range of 10–15 min due to high thermal stress. • Interaction between air and TES medium might cause small particles to be released into the air [68].	[68]
LT-CAES	Heat transfer after every single stage occurs to reach low storage temperatures. TES includes a two-tank TES configuration with liquid media[133].	52-60%[133]	• Applicability of liquid TES medium, which is abundant, inexpensive, and environmental-friendly as well as being pumped easily [133]. • There is no interaction between compressed air and TES medium, making high-pressure air completely free of small particles and protecting expanders from damages [133]. • Eliminating the need for a particular material for the TES system • Applicability of and using standard heat exchangers and compression and expansion systems • Fast plant start-up of <5 min (faster start-up behavior) • Broad control range and suitable partial load behavior [133]	•	[133]

2.3. Integration of CAES

There is much interest in analyzing CAES integration potential with different cycles and renewable energy systems for different purposes considering techno-economic and environmental aspects. Literature in the context of CAES integration can be divided into two main subsections 1) integration with auxiliary or energy conversion systems (including renewable and non-renewable systems) in which mainly the steady-state model of CAES over one cycle is considered aiming at its performance improvement, 2) integration with conventional grid and RESs (e.g., wind and solar) where a transient and unsteady behavior of CAES is considered focusing on the potential application of CAES while smoothing renewable fluctuation and increasing their penetration.

2.3.1. CAES - auxiliary and energy conversion systems

Managing the heat generated and dissipated in the compression stage of CAES and reusing them to preheat the high-pressure air before expansion or for other applications is one of the main concerns of different researchers [135]. Another concern is burning fossil fuel to preheat the pressurized air before expansion and, consequently, greenhouse gas emissions during the discharge process. Therefore, integrating CAES with other technologies can be a promising way to improve the system's overall efficiency and recover the system's heat loss while eliminating the need for burning fossil fuel and consequently decreasing the size and cost of the storage [93]. The literature is mainly divided into two directions: 1) research on performance improvement of CAES systems after coupling to other cycles or technologies; 2) research on performance enhancement of integrated energy systems after combining with CAES technology. Such studies mainly focused on thermodynamic analysis of the system from the energy and exergy points of view. Besides, some economic [3,4] and environmental [5] aspects of integration concepts were evaluated in these studies. Table 2.4 summarizes previous studies in this area of CAES integration with other technologies and auxiliary service.

2.3.2. CAES- high TES (HTES)

Several studies have proposed adopting HTES as a replacement for conventional combustion chambers to eliminate the need to burn fossil fuel in D-CAES and efficiently use low-quality excess electricity from the grid or renewables to store and generate heat [134,136–138].

Table 2. 4. Summary of studies on coupling CAES with auxiliary and energy conversion systems.

Ref.	Integration concept	Fuel utilization	Analysis criteria	Performance results	RTE improvement
[134]	CAES-HTES	NSF	Energy analysis	Energy RTE of CAES-HTES: 53% Energy RTE of AA-CAES: 47%	6.5 %
[55]	CAES-HTES	NSF	Energy, exergy, and economic analysis	For CAES-HTES,energy RTE of 24.5-57.5% and total capital cost of 65-200 $/kWh For AA-CAES, energy RTE of 27.9-47.5% and total capital cost of 316.3$/kWh For D-CAES, energy RTE of 42-55% and total capital cost of 249-330 $/kWh	22.3 %
[136]	CAES-ORC-HTES CAES-KCS-HTES	NSF	Exergy and energy analysis	Exergy & energy RTE of CAES- HTES without WHR cycle: 43.46% and 49.84% Max Exergy & energy RTE of CAES-ORC; 44.63 % and 51.17 % Max Exergy & energy RTE of CAES-KCS; 44.20 % & 50.68%	2.67%
[137]	CAES-ORC- compression-absorption refrigeration-HTES	NSF	Exergy and energy analysis	Energy RTE of individual CAES-HTES; 57.57% Exergy & energy RTE of CCHP; 49.17 % and 65.17 %	13.15 %
[139]	CAES-MED-HTES	NSF	Energy analysis	Energy RTE of individual CAES-HTES; 56.24% Energy RTE of CAES-MED-HTES; 70%	24%
[138]	CAES-WT - compression-absorption refrigeration-HTES		Energy, exergy and economic analysis	Energy RTE of integrated system; 56.71%	11.9 %
[140]	CAES-ORC-CO_2 capture unit	SF	Energy and environmental analysis	Energy RTE of CAES-ORC-CO2; 43.95% CO2 recovery: 87.6%	---

[141]	CAES-MED-ORC-solar collector	SF	Energy, exergy and economic analysis	Exergy & energy RTE of the integrated system; 41.67 % and 65.2% Annual profit of 21,202 $	---
[142]	CAES-MED-TVC-solar heliostat	NSF	Energy, exergy, and economic analysis	Energy RTE of 48.7 % Total cost rate of 3056 $/h	---
[143]	CAES-BG	NSF	Exergy and energy analysis	Exergy & energy RTE of the integrated system; 64.28 % and 88.43%%	0.35%
[144]	CAES-GT-BG	NSF	Energy analysis	Energy RTE of 70% and electrical efficiency of 45%	---
[145]	CAES-SOFC-turbocharger	NSF	Exergy and energy & environmental analysis	Exergy & Energy RTE of CCHP; 58% % and 78% 0.06 kg/kWh CO2 reduction from SOFC	---
[146]	CAES-MultiPCM	NSF	Energy and exergy analysis	Energy RTE of CAES-MultiPCM; 70.83%	---
[135]	CAES-AD	NSF	Energy analysis	Energy RTE: 70%	---
[147]	CAES-ORC-RC-TEG	SF	Energy, exergy, and economic analysis	Exergy & Energy RTE of CAES without TEG: 28.72% and 34.23% Exergy & Energy RTE of CAES with TEG: 30.53% and 32.39%	1.84%
[148]	CAES-ORC-geothermal-solar collector	NSF	Energy, exergy and economic analysis	Exergy & Energy RTE: 31.17% and 35.41% At optimum point: exergy efficiency: 29% And total cost rate: 18%/hr	-4% (lower than CAES with fossil fuel)
[149]	CAES-ORC	NSF	Energy analysis	Energy RTE of: A-CAES with TES: 40.16% A-CAES with TES under variable pressure ratio:63% CAES/TES/ORC: 70.53%	56%-75%
[150]	CAES-PCM-solar collector-BG	SF	Energy and exergy analysis	Exergy & energy of gasifier and solar collector: Without CAES: 20.58% and 24.56% With CAES: 24.08% and 28.58%	16.3%

[151]	A-CAES-TES-BG, ICE	SF	Energy and exergy analysis	Exergy & energy of the integrated system (CHP):29% and 38%	----
[152]	CAES- BG, ground-source heat pump-absorption chiller	Biogas-SF	Energy and exergy and economic analysis	Exergy and Energy RTE: 31.52% and 90.06%	---
[153]	CAES-ORC-ejector system	SF	Energy and exergy analysis	Energy RTE of 68% and 71.9% before and after optimization.	5.7%

For instance, Houssainy et al. [134] introduced the concept of high-temperature hybrid CAES (HTH-CAES), in which two separated heating stages through LTES (hot/cold tank), and HTES were incorporated. Their thermodynamic analysis showed that the proposed configuration was more efficient by 6.5 % than AA-CAES with only LTES under the same condition.

In another study [55], this group presented a similar configuration named hybrid thermal-CAES (HT-CAES). They conducted a thermodynamic optimization to determine the optimal distribution scenario of importing energy between the CAES unit and HTES to maximize the energy efficiency and minimize the cost. Their results showed an RTE in the range of 24.5-57.5% and a capital cost of 65-200 $/kWh, which was about 33% -73% lower than that for D-CAES. An exergy efficiency and RTE of 49.84% and 43.46% were reported in Ref. [136] for CAES-HTES. Ramzi et al. in Refs. [137,138,154] also incorporated HTES to present a carbon-free cogeneration system based on CAES and refrigeration units. A RTE of 52.34 % in Ref. [137] was reported for individual CAES-HTES. This group also presented a RTE of 56.24 % for a similar configuration in Ref. [139].

2.3.3. CAES- organic ranking cycle (ORC)

There has been a vast interest in the literature to investigate integrating ORC into CAES for waste heat recovery. Such integration reduces heat loss and exergy destruction while enhancing total power generation and RTE [136]. For example, a combined cooling, heating, and power (CCHP) concept by combining CAES with HTES, ORC unit, and a hybrid compression-absorption refrigeration system was introduced by Razmi et al. [137]. In their proposed system, during the peak demand, when CAES switched to discharging mode, ORC extracted heat from exhaust gas released from the CAES turbine and then drove the chillers' compressor to provide cooling energy. Their results indicated the exergy efficiency of 49.17 % and the RTE of 65.15%, around 13.15 % more than the standalone CAES with HTES. In line with the previous study, Roushenas et al. [145] optimized the performance of a CCHP system based on CAES, ORC, and ejector systems. The results from optimization indicated RTE improvement of about 5.7% and exergy destruction reduction of approximately 16.7%. Soltani et al. [136] analyzed an integration of CAES with HTES and two waste heat recovery cycles of Kalina cycle and ORC to provide further power during the peak energy demand and consequently improve the efficiency of CAES. Their energy and exergy analysis indicated that applying a waste heat recovery cycle enhanced energy and exergy efficiency by 1.69–2.67% and 1.70–2.69%,

respectively. The maximum value belonged to the ORC recovery cycle. In another study, Fu et al. [149] have shown that AA-CAES and AA-CAES /ORC with variable pressure ratio improved the RTE of conventional A-CAES by 56% and 75%, respectively.

To improve a CAES system's GHG emission inventory and performance, CAES integration with ORC and a post-combusting CO_2 capture unit was proposed by Zeynalian et al. [140]. ORC was employed downstream of the CAES turbine to generate more power and recover its exhausted gas's heat to reduce its temperature for the CO_2 capture unit. Their results showed a CO_2 recovery of 87.6 % with a RTE of 17.4% and 43.95% for ORC units and the CAES system, respectively.

2.3.4. CAES- desalination

Several researchers combined CAES with desalination technologies to diminish heat dissipation and exergy destruction while supplying power and portable water [139,141]. For instance, Razmi et al. [139] achieved 70% RTE by integrating CAES with a multi-effect desalination (MED) system to recover the heat generated during the compression phase and turbine exhaust of the CAES system for electricity and unsalted water generation. In this study, a RTE improvement of around 24% was obtained. Javidmehr et al. [141] investigated the integration of CAES with MED, ORC, and solar dish collectors to simultaneously produce heat, power, and freshwater. MED was adopted instead of ORC's condenser to use high-quality vapor of ORC's turbine for water production. The optimization results were shown an exergy efficiency and RTE of 41.67% and 65.2%, respectively. Furthermore, the proposed configuration showed an annual profit of 21,202 $. Innovative integration of CAES with multi-effect thermal vapor compression desalination units (MED-TVC) and solar heliostat to produce power and portable water was introduced in Ref. [142]. In the proposed configuration, MED used the heat of the compression process to produce water. The RTE and total cost rate of 48.7% and 3056 $/h were achieved for the proposed system under optimal design conditions using artificial neural network and optimization algorithms.

2.3.5. CAES-biomass

In line with the heat management strategies in CAES, an integration concept named BIO-CAES technology was introduced by Llamas et al. [135]. Their proposed system used the heat generated during compression in anaerobic digestion (AD) to produce and store biogas as a means of chemical energy storage. Biogas was utilized in a combined heating and power (CHP)

system for expanding phase to preheat the compressed air and generate extra power. Their results showed that adequate thermal energy was generated from the compression process to operate an AD and produce biogas (instead of storing it in TES). Such heat management increased the BIO-CAES technology's overall nominal energy efficiency by more than 70%. Xue et al. [143], proposed coupling biomass integrated gasification combined cycle (BIGCC) into CAES system for heat recycling and performance improvement of CAES and integrated system. Their results demonstrated that the RTE of the integrated system improved by 0.35% compared with the standalone BIGCC. Besides, the RTE and exergy efficiency of around 88.43% and 64.28% were reported for CAES.

In studies focusing on the integration of CAES with various energy systems, the main objective is to know how much the energy systems' performance could be improved after integration with CAES. For example, Karapekmez et al.[150] presented a comprehensive thermodynamic assessment for an integrated system including a biomass-based power plant (with a biomass gasifier (BG)) and solar thermal storage units (with solar collectors and phase change materials (PCM)) coupled with CAES. They found energy and exergy efficiency improvements of 16.3 % and 17% for an integrated system. In this study, the average hourly solar radiation absorbed by the collector was considered instead of the dynamic behavior of solar radiation. A biomass-fueled CHP system based on a CAES, gasification unit, and gas turbine (GT) power plant was proposed by Razmi et al. [144] for waste heat recovery and peak shifting. The highest RTE of 70% and electrical efficiency of 45% were reported for the proposed hybrid system. A comprehensive techno-economic and environmental analysis for the similar hybrid system was carried out in Ref. [155]. A total and electrical RTE improvement of around 67% and 12% was achieved compared to the individual biomass plant. The results also highlighted a 25,764 tonnes/year carbon capture and 0.05 $/kWh cost of energy (COE). Diyoke et al. [151] introduced hybrid A-CAES and biomass gasification storage (A-CAES-BMGS) to generate electricity and domestic hot water. Their thermodynamic analysis was shown the RTE and exergy efficiency of 38 % and 29 %, respectively. In another study [156] this group conducted a techno-economic analysis of the wind-powered A-CAES-BMGS. They reported a total energy efficiency of 36.8 % and a COE of about 0.19 £/kWh. A unique CAES-based CCHP system fed by geothermal and biomass energy was proposed by Zhang et al.[152]. The pressurized air of CAES was combusted with biogas from a BG to generate power by a biogas turbine. Furthermore, the ground source heat pump and absorption chiller recovered the waste

heat of exhausted gas of the turbine to provide hot water and chilled water. The RTE of 90.06% and exergy efficiency of 31.52% were reported.

2.3.6. CAES-solar collector

In multiple studies, solar energy was used as a thermal energy source to preheat the high-pressure air before the expansion [141,148,150,157,158]. A combination of conventional CCHP system with CAES and solar collectors was presented in [158]. The multi-objective optimization results showed a minimum total investment cost of 1794 $ per total output power (kW) with an exergy efficiency of 52.71% at the maximum heating condition and a minimum cost of 1798 $/kW with an exergy efficiency of 44.84% for maximum cooling condition. Similarly, Mousavi et al. [148] carried out a thermo-economic evaluation of a CAES combined with ORC, which used solar and geothermal energy sources. A multi-objective optimization was carried out to maximize exergy efficiency and minimize the system's total cost. Although the proposed method was carbon-free, its RTE was about 4% lower than CAES with fossil fuel as a thermal energy source. In the studies mentioned above, the system's performance was evaluated at design conditions, and the dynamic performance of solar collectors and CAES was not considered.

2.3.7. CAES-fuel cell

Several studies have investigated performance improvements of power systems or CHP units based on CAES integrated with various fuel cell technologies such as solid oxide fuel cell (SOFC) [145,159–161], molten carbonate fuel cell (MCFC)[162,163], proton exchange membrane (PEM) fuel cell [164] . For instance, Roushenas et al. [145] evaluated an integrated CHP system consisting of SOFC, CAES, and turbogenerator to generate electricity and domestic hot water from the energy, exergy, and environmental perspective. It was found that their system could run with RTE and exergy efficiency of 78% and 58%, respectively. Moreover, an emission reduction of around 0.06 $kgCO_2/kWh$ was obtained compared to the individual SOFC. In another study, Roushenas et al. [161] reported an emission reduction of 6.6 % and RTE improvement of 38% by integrating CAES with SOFC-GT compared to the conventional SOFC-GT. An integration of compressed air and thermochemical energy storage with SOFC and GT was proposed by Zhong et al. [159]. An optimal RTE and COE of 89.76 % and 126.48 $/MWh was reported for the hybrid system, respectively. Zhang et al. [160] also achieved 17.07 % overall efficiency improvement by coupling CAES to SOFC, GT, and ORC

hybrid system. Khanmohammadi et al. [164] carried out triple objective optimization of a hybrid system comprised of CAES, PEM, ORC, and thermoelectric generator (TEG) for electricity and hot water production. The results demonstrated that the RTE and exergy efficiency of the proposed system were 1.6 % and 1.44 % higher than individual CAES, respectively.

2.3.8. CAES-other

Musharavati et al. [147] presented a combination of CAES with ORC, RC, and domestic hot water systems integrated with TEG, which mitigates wasting energy in the condensers of ORC and RC systems and boosts the thermal efficiency. Their results showed that the CAES with TEG had power and exergy efficiency of about 1.84% and 1.81% higher than the stand-alone CAES system. Ghorbani et al. [146] proposed a thermodynamic assessment for a hybrid wind turbine (WT) and A-CAES with multistage-PCM with RTE of 70.83 %. They concluded that applying TES in the form of PCM made the system more sustainable-friendly. It is worth mentioning that the average power production of WT farms was considered as the input energy of CAES, and wind power intermittency and dynamic behavior of CAES were not addressed. All the research mentioned in this section mainly investigated CAES performance under steady-state mode over only one cycle, even if the integration concept included the renewable energy source with intermittent behavior. There are still many gaps in this area of study that need to be addressed for further improvement, especially in the case of investigating dynamic behavior, optimization, and comprehensive economic and life cycle assessment of such hybrid systems.

2.3.9. CAES-solar-wind

Integrating CAES into intermittent RESs, especially wind and solar can enhance renewable penetration and add huge economic and environmental advantages to the energy system. There are several issues in terms of process design and operation of CAES that should be addressed to make this integration more energy-efficient and economical-friendly. The majority of the studies mainly investigated the performance of CAES, whether individually or coupled to other technologies, under design conditions or steady-state mode. In the latter cases, a monotonic variation for thermodynamic parameters is assumed over one charge/discharge cycle [27,147,156]. These assumptions have been adopted not only in thermodynamic analysis studies [146,148,150] but also in several studies that relied on techno-economic and environmental assessment [111,148,165–167]. However, integrating renewables such as wind

and solar requires CAES to absorb intermittent renewable power and respond to demand fluctuations. Accordingly, the operation of compressors and turbines must be adjusted respectively by renewable power output [22–24], and load demand [23,25,26] which makes the CAES system works unsteady and under off-design condition [22,26]. Operating under off-design conditions can significantly impact CAES efficiency and lifetime [168]. Until now, few numbers of related research have been carried out to address this mismatch caused by integration. Therefore, it is necessary to develop a time-dependent model to analyze CAES's operation and dynamic behavior over time and cycle to cycle.

Recently, research has been emerging in the development of design and operational strategies for techno-economic and environmental assessment as well as optimal scheduling of CAES integrated into conventional system and RES (mainly solar and wind, etc.). The literature explores three aspects: 1) designing of CAES; 2) feasibility studies for incorporating CAES, and 3) optimal scheduling of CAES at microgrid (MG), distribution power system (DPS), and energy market scales.

2.4. Conventional sizing vs. optimal sizing of CAES

The CAES system has no unique configuration due to its variety and complexity of having multi-interdependent sub-systems with different characteristics. Therefore, multiple studies proposed various design approaches for CAES integrated into renewables in different scales and applications. Rouindej et al. [29] proposed a design methodology named the user-centered approach for designing an A-CAES system integrated into the Ontario (Canada) grid. In their design strategy, energy capacity (kWh) and compressor/expansion size (kW) were achieved by calculating the frequency of occurrence or, in other words, probability of distribution (PD). This method was improved by Sarmast et al.[32], who proposed a coverage-percentage approach that used the outputs of the frequency occurrence method as upper limits to provide a more accurate way to size the A-CAES system.

A similar approach can be applied in the case of integrating CAES into the RES. Authors in [169] determined the size of the air storage tank (m^3) integrated into a solar home system based on the load demand and discharge time by modeling the downstream components of CAES, including generator, air motor, and storage tank. In another study [131], the air tank volume of CAES was calculated based on maximizing the amount of surplus power as the difference between the total renewables power and the load.

Therefore, according to the literature [29,32,51,131,169], two conventional design processes are presented in Fig. 2.6. Approach #1 (red boxes) is a sizing approach based on the worst-case scenario, which means maximum excess power is chosen as compressor train power capacity. On the other hand, the maximum deficit, which is the maximum difference between the load demand and power generation, is considered expander train power capacity [61]. Approach #2 (green boxes) is based on the design strategy proposed in Ref. [29] so that power generation can be from conventional sources or RESs. Some of the feasibility studies and optimal scheduling works adopted these approaches for sizing a CAES without using an optimization approach [51,131].

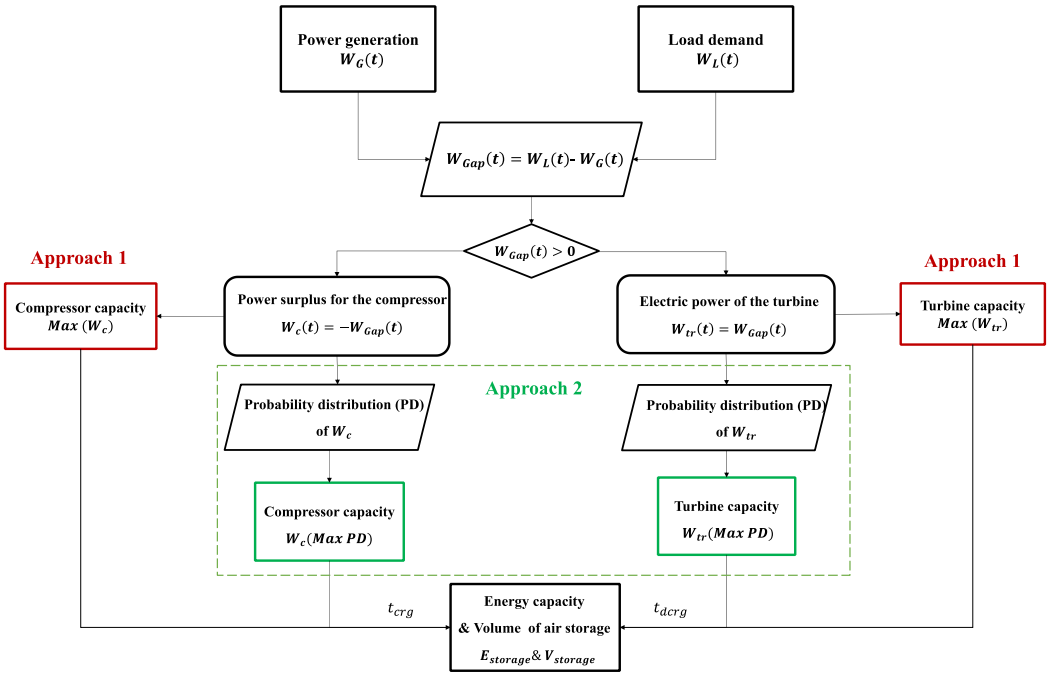

Fig. 2. 6. Descriptions of conventional sizing-design methodologies.

Some studies [20,51] proposed a sizing methodology considering the worst-case scenario in which the compressor train's power capacity and AST volume are estimated based on the maximum excess energy. An iterative numerical approach was proposed in Ref. [170] to size a small-scale standalone solar power plant with CAES to fulfill mobile base stations' electricity and cooling demand. The same strategy was performed in Ref. [171], mainly emphasizing on design and operating parameters of the standalone photovoltaic (PV) and CAES system. Their results showed that the proposed sizing-design strategy in which the size of the PV plant was based on the day with the worst solar radiation and maximum energy deficit led to the power plant oversizing and renewable curtailment. Conversely, the turbine train's capacity is

determined according to the maximum energy shortage (the maximum difference between the energy demand and renewable energy generation) [61]. The lack of consideration of economic aspects in sizing methodologies introduced in the previous studies can be seen as a significant limitation, as it may result in suboptimal designs that are not cost-effective in the long term.

Determining the appropriate CAES's rated power and energy storage capacity significantly impacts energy storage operation and profitability [172]. CAES can be sized according to its specific application and available energy sources in the whole energy system while considering techno-economic and environmental aspects. Optimization is necessary to avoid energy systems and CAES under-sizing and oversizing, decreasing the system's profitability [12]. Several studies have shown that having the oversized CAES causes it to be unusable most of the time, that increases the investment cost [173]. However, considering an undersized CAES system decreases the energy system's reliability, mainly if it is used for standalone applications where reliability is a more critical aspect than economic viability. On the other hand, from CAES itself perspective, there is a trade-off between energy capacity and power level. It means that, for any application with a specific power level, there is an optimum capacity for CAES components at a given pressure range of the air container [12].

In several research, for the sake of simplicity, it is assumed that the compressor and turbine have the same power rating. Some parametric studies have been conducted to investigate the effect of energy and power capacity on the cost and profitability of CAES systems [12,173]. The findings in [29] and [12] highlighted that a comprehensive assessment tool that can be customized based on the particular application and case study should be developed for optimally designing CAES in a hybrid system. Thus, assuming a specific structure can result in suboptimal performance and may not accurately reflect the potential of technology [174].

A few studies have been carried out to find the optimal size for CAES, either identifying the best value for compressor/turbine size and air reservoir volume based on an analytical model of CAES or identifying the optimal energy and power capacity of CAES integrated into other systems in the energy environment, considering techno-economic and environmental aspects. Table 2.5 provides a summary of optimal sizing studies for CAES.

An optimal sizing methodology was proposed by Wang et al. [172] to achieve optimal rated power and energy capacity of large-scale CAES technology under rated power constraints. The optimization process was developed according to CAES's several applications, such as energy arbitrage, wind power penetration augment, and load shifting, to relieve the load pressure on coal power plants. Therefore, a statistical method was adopted to assess power system operation

and wind power curtailment and, consequently, to find the best CAES power capacity. Their results showed that the maximum economic benefits of 10.5 M$/ year were obtained by introducing a CAES system with a total of 392 MW and 10 hr discharge time. In this study, optimal sizing of CAES (energy and power capacity) was conducted based on the operational characteristics of available power systems and wind power curtailment without considering the thermodynamic characteristics and limitations of CAES.

In Ref. [132], an optimum sizing of a grid-connected MG, integrating PV panel, iso-chronic CAES, and the grid, was carried out to satisfy the electricity demand of a building. A linear multi-objective model was developed to maximize the overall efficiency and minimize the energy-imported and energy-exported ratios from and to the grid. The simplex method was used to solve the optimization problem while obtaining the optimal value for the PV system's size, the AST volume, and the compressor's volumetric airflow rate. Their results indicated that the optimal design enhanced the building autonomy from 35% to 75%. No economic assessment was conducted. Aruta et al. [175] analyzed the feasibility of adopting hybrid PV and D-CAES for residential applications (1000-2000 buildings). They tried to achieve an optimal PV system size and the maximum level of air in AST to minimize carbon emission and a simple payback period according to simulated load demand and available solar radiation. A brute-force search method was employed to find the optimal design parameters. The results indicated that adopting an optimal PV/D-CAES system led to 51-55.5% carbon emission reduction. Moreover, in terms of economics, they reported a simple payback period in the range of 12.4-14.3 years for their proposed system. Yet, their proposed system used fossil fuels in the D-CAES unit. Therefore, they suggested further investigation for adopting an A-CAES system in which thermal energy storage (TES) can be employed to reduce or remove the need for fuel consumption by recovering the thermal energy generated during the compression process. In addition, they did not provide any information regarding their proposed system's long-term and transient operation or offer any insights on how their approach could contribute to achieving a self-sufficient building. A bi-level program was proposed by Ref. [176] for designing and planning islanded MG comprising distributed generations (PV, WT, diesel generator (DIG)) and iso-baric A-CAES. A sizing problem was solved at the upper level to achieve the optimal capacities of the components of MG while minimizing the total annual cost. In parallel, subject to these capacities, a unit commitment problem was formulated on the lower level to achieve the best schedule of MG while reducing the operation cost. The iso-baric A-CAES for spinning reserve requirement of MG was modeled in this study. Similar strategies were applied in Ref. [129].

Table 2. 5. Summary of studies on optimal sizing of CAES integrated into renewables.

Ref.	Hybrid system	End-user	Application of CAES	Energy supply	Scale	SOC	Objective function	Criteria	Decision variable	Opt. technique
[172]	WT/ Coal/Hydro /D-CAES	Grid-scale	• Bulk energy • Energy arbitrage • Wind penetration • load shifting	Electricity	LS	--	• Benefit of CAES	Economic	• Power capacity of compressors and expander • Energy capacity	Gradient method
[175]	PV/ D-CAES	Building	• PV penetration	Electricity	SS		• Carbon emission • Payback period	Economic Environmental	• Maximum level of air in AST • PV number	Brute Force
[132]	PV-A-CAES	Building	• PV penetration • Autonomy of building	Electricity	µS	Pressure	• Imported ratio, • Exported ratio • Storage efficiency	Reliability	• Tank volume (m3) • Air volumetric flow rate (m^3/hr) • PV install capacity	Simplex algorithm
[177]	PV/WT/CCHP/A-CAES	District	• Peak-shaving • Cogeneration • Renewable penetration	Electricity Cooling	SS	Pressure	Three-level programming: • Energy & exergy efficiency • TAC • TOC	Economic Environmental Reliability	• Expansion ratio • Power capacity of ICE, PV,WT, CAES	GA PSO

[130]	PV/WT/DIG/A-CAES	District	• Spinning reserve	Electricity	SS	Volume	Bi-level programming: • TAC • TOC	Economic	• Number of PV, WT ,DIG, air storage, • Power capacity of compressors and expanders.	UP:GA IL:CPLEX
[129,178]	WT/DIG/A-CAES	District	• Wind penetration • Power reliability	Electricity	SS	Volume	Bi-level programming: • TAC • TOC	Economic Reliability Environmental	• Number of WT, DIG • Tank Volume • Power capacity of compressors and expanders.	UP: QPSO IL:SQP

Optimal sizing and planning standalone MG, including WT, DIG, and iso-baric A-CAES considering the DRP was carried out by adopting a stochastic scenario-based bi-level programming method. Scenario generation and reduction techniques were adopted to evaluate the uncertainty of wind power and load demand. Their results showed that having the optimized design for EES combined with other generation systems in MG reduced the total daily cost by around 0.7% and 1.7% compared to oversize and undersized hybrid systems. The same approach was presented by Adib et al. [178], encompassing the A-CAES system's design and off-design conditions. They emphasized that adopting off-design situations is essential for achieving a more accurate system performance since using CAES during low charging and discharging chances becomes less probable.

Yan et al. [179] proposed hybrid CCHP (internal combustion engine) system integrated with PV, WT, and CAES to meet a residential community's heating, cooling, and electricity demand. They developed a tri-level collaborative optimization approach to find the optimal value of CAES parameters, optimal capacity of hybrid system configuration, and optimal dispatch strategy in the first, second, and third levels, respectively. Thus, a multi-objective optimization problem was formulated to minimize total daily cost and emission. It is worth noting that, in the sizing and planning stages, a black box approach was adopted, assuming CAES as a conventional ESS (such as a battery) with a specific capacity. Their results showed that the performance of the proposed hybrid system was improved considering the poly-generation feature of CAES as an advantage over conventional CCHP. In the second level, the economic and environmental benefits of CCHP integration into CAES were compared with CCHP coupling with a battery, indicating that introducing CAES is more cost-effective (5% less cost).

2.5. Techno-economic and environmental performance

Regarding the techno-economic and environmental assessment of incorporating CAES in energy systems, several studies focused on the potential of combining CAES with renewables, especially wind farms but in different ways [180–182]. The goal is to take advantage of the CAES system to smooth the high fluctuation of wind power by matching the power output of the integrated system with the grid power demand and improve renewable integration into the grid [22,183]. For example, An parametric study on large-scale CAES integrated into WT farm, and a national grid was conducted in Ref. [184]. The results showed annual savings of 5-11% and a 40% reduction in CO_2 emissions. Huang et al. [185] developed techno-economic

modeling to evaluate the CAES system's feasibility in enhancing the integration of WT into the power grid. A centralized D-CAES and distributed A-CAES were suggested with RTE of 53.6% and 57.6%, respectively. In another economic study [183], the higher profitability of D-CAES compared to A-CAES was shown as centralized and decentralized energy storage integrated into wind power and grid.

Large-scale integration: Fertig et al. [186] investigated the economic feasibility of a CAES-wind farm located in central Texas under various market electricity and gas prices scenarios. They reported that integrating CAES with WT was not economically viable and also a competitive method for their case study. Razmi et al. [186] evaluated the technical feasibility of incorporating large-scale A-CAES with HTES into two adjacent wind farms for smoothing the wind fluctuation and peak shaving. Their designed CAES had a maximum RTE of 52% in July, in which CAES delivered 93 kW to the national grid for 5 hours of peak demand. A design and performance analysis along with an economic evaluation of large-scale D-CAES for wind power at off-design and design conditions were presented by Meng [22]. The RTE of D-CAES at design conditions was 54.34%, and at off-design conditions under both constant and variable shaft speed mode of the compressors were reported 50.98% and 51.69%, respectively. Furthermore, the higher energy cost for CAES operation under off-design conditions was reported. In Ref. [187], Chen et al. investigated the feasibility of integrating large-scale A-CAES into the wind and solar energies in China. They analyzed the effects of operating variables on system performance. Similarly, He et al. [188] performed a techno-economic and environmental feasibility study. They reported the cost-effectiveness of bulk-scale CAES integrated to PV/WT in carbon reduction by 84% compared to conventional power plants fed by fossil fuel for countries with the appropriate geological situation.

Small-scale integration: In recent years, several researchers have investigated the feasibility study of using small-scale CAES as a BTM storage system integrated into the hybrid energy system (HES), either grid-connected or standalone [18,28,84,125,131,189]. Castellani et al. [28] proposed a small-scale PV/ CAES hybrid system to supply reliable power for a residential building with a peak demand of 2.2 kW. They used a simple energy balance based on solar power and energy demand, considering the pressure of air in a storage tank to evaluate the performance of CAES. They reported that although their proposed prototype CAES is technically feasible for dwelling applications capturing around 96% excess PV power and 26% demand coverage ratio in a typical day, it still has a lower efficiency (11-17%) than the battery bank for the same application. Therefore, the results showed that it is essential to consider

another aspect of such design to select the best energy storage solution. Similarly, Simpore et al. [189] studied the feasibility of a grid-connected HES, including PV, A-CAES, and grid to meet the demand of building (15 kW peak load) under different scenarios. They reported overall efficiency of 41% and a demand coverage ratio of 4% for A-CAES over a year. In another study, Zhang et al. [18] presented an integration concept including μs-CAES and WT, focusing on utilizing scroll compressors and expanders for flexible household power supply. The overall efficiency of the proposed CAES for one day operation was reported at 47.35%, while the integrated system efficiency, which reflects the energy utilization factor from wind power to household load demand, was 88.75%. However, their rough economic estimation indicated that the investment in installing CAES was marginally higher than the saved money from decreasing WT capacity. A dynamic model for evaluating the feasibility of A-CAES integrated into PV panels and electric grid to satisfy the building electrical demand under different scenarios was developed by Sidiki Simpore et al.[189]. The RTE of 41% and energy coverage ratio of 4% was reported for A-CAES. Furthermore, the higher coverage ratio was achieved under different parametric studies by increasing the compressor's PV panels area and volume flow rate. No economic evaluation was done in the studies mentioned above.

A grid-connected PV/CAES power system was proposed by Dib et al. [84], who presented a techno-economic approach aiming at reducing the percentage of load demand by the building sector in France and, consequently GHG emission reduction. Evaluating the system performance demonstrated that in the best configuration, the grid provided 35.7% of building energy demand while the self-consumption of the building was 64.3 %, in which PV had a share of 52.3% and A-CAES with RTE of 33.7% constituted 12.14%. According to the available market price, the economic analysis showed a cost reduction of 1.27 €/kWh resulted from increasing the A-CAES's storage pressure from 40 bar to 200 bar. In this study, the economics of integrating a whole hybrid system at the building scale were not considered. In another study, Sadeghi et al. [131] carried out a pre-feasibility techno-economic and environmental evaluation of integrating iso-baric CAES into a small-scale HES, including MCFC, GT, PV, and TES. The goal was to satisfy the district's electricity demand, including 500 households, and reduce the pollutant emissions from fossil fuel-burned GT plants. Parametric studies have been carried out to evaluate the proposed system's overall system efficiency, cost of energy, and CO_2 emission. Their results indicated that the overall energy efficiency of HES with CAES in storage mode was 72.7%, almost 25% higher than that when CAES was in the auxiliary mood (as a backup unit). Fiaschi et al. [125] proposed an off-shore platform to harness energy from renewables

(wave, wind, solar), integrating into supplementary fuel UW-CAES for off-shore applications such as villages, and tourist resorts, especially if they are located in a medium and small islands. The hybrid system was designed based on renewables availability, and the CAES tank volume was sized to supply electricity for 2 hr discharging at a specific mass flow rate during the peak demand. The yearly average efficiency of CAES was reported at 47.6%. Concerning the heat management of CAES, Cazzaniga et al. [190] proposed a novel configuration of small-scale I-CAES surrounded by water integrated into a floating solar PV plant for standalone application. Although a RTE of 80% was estimated, experimentations are required to approve this design idea. Additionally, a parametric study to evaluate the effect of components configuration and design parameters on HES performance and indicators has been carried out in the above-mentioned studies.

Multiple studies focused on the design and performance analysis of PG-CAES systems to satisfy the electrical, heating, and cooling demands. For example, Li et al. [111] took a first step toward developing a behind-the-meter PG-CAES system for supplying the energy demand of small-scale office buildings and domestic households. The results showed that with the appropriate design, the comprehensive RTE of PG-CAES in winter when the cooling energy was not required was higher (around 50%) than that in summer (30%). That is because of the high-power consumption of the compressor and inefficient expansion in summer, but the RTE was still more than the conventional system based on an absorption chiller. In this study, the turbine worked under the off-design condition to meet the demand while the compressor operated at the design condition. In this paper, no economic analysis was reported. Therefore, Lv [108] looked at the techno-economic feasibility of PG-CAES for small applications (hotels) for shifting the peak load based on electricity tariff. They concluded that the proposed system could reach an overall RTE of 76% and an annual money-saving of 53.9%. Several studies reported the coupling of PG-CAES with renewables [63,191]. Congedoe et al. [191] investigated the potential of μs-CAES with TES (high and low temperature) coupling with renewable energy generation to provide electricity, air conditioning, and domestic hot water. They tested their proposed plan to supply the energy demand of a single-family building. An A-CAES/PV/WT energy system for cooling and electrification of a rural mobile base station as an energy-intensive building in standalone mode was suggested by Zhao et al. [63]. Their results showed the proposed HES had high reliability with a loss of supply probability of 0.989% and an energy-saving ratio of 11.23%, even in extreme weather conditions with low available renewable energies. Besides, adopting a hybrid cooling strategy as a by-product of A-CAES

Table 2. 6. Characteristics of studies on the feasibility study of CAES for the small-scale application.

Ref.	Analysis aspects	Hybrid system	System mode		Application	Output energy	CAES structure	SOC	Analysis time	Performance criteria
			Grid-connected	SA						
[28]	Technical	PV-CAES	×	√	Historical Building (2-3 kW)	Electricity	CAES	Iso-choric	Daily (one day in summer)	Energy saving percentage (ESP) by storage Coverage ratio (C.R) System efficiency (S.E)
[189]	Technical	PV- CAES	√	×	Academic building (15 kW)	Electricity	A-CAES	Iso-choric	Yearly	System efficiency (S.E) Load coverage ratio (C.R)
[18]	Technical	WT-CAES	×	√	Household (40 kW)	Electricity	A-CAES	Iso-choric	Daily	System efficiency (S.E) Energy utilization factor
[125]	Technical	PV-Wave-WT-CAES	×	√	Off-shore application (> 100kW)	Electricity	UW-CAES	Iso-baric	Yearly	System efficiency (S.E)
[190]	Technical	PV-CAES	×	√	Off-shore application (SA) (6 kWh/day)	Electricity	I-CAES	Iso-choric	Daily	System efficiency (S.E)
[111]	Technical	-	√	×	Office building (>10 kW)	Electricity, heating, cooling	PG-CAES	Iso-choric	Seasonally	System efficiency (RTE)
[63]	Technical	PV-WT-CAES	×	√	Rural mobile bus station (3 kW)	Electricity, Cooling	PG-CAES	Iso-choric	Yearly	Loss of power supply probability (LPSP) Dump load ratio (DUMP) Relative fluctuation rate (DL) Energy saving ratio (ESR)
[191]	Technical	PV-chiller-CAES	√	×	Residential building	Electricity-Cooling Hot water	PG-CAES	Iso-choric	Daily and Seasonally	System efficiency (RTE)

[84]	Techno-economic	PV-CAES	√	×	Building (80 kWh/day)	Electricity	A-CAES	Iso-baric	Yearly	System efficiency (S.E) Load coverage ratio (C.R) Electrical load management (E.L.M) And LCOE
[108]	Techno-economic	-	√	×	Hotel building; peak shifting >100 kW)	Electricity, Heating, Cooling	PG-CAES	Iso-choric	Monthly	System efficiency (RTE) Money-saving
[131]	Techno-economic & environmental	PV-MCFC-GT- TES-CAES-Battery	×	√	Residential District (500 kW)	Electricity	A-CAES	Iso-baric	Daily (One day in Summer and winter)	System efficiency (S.E) , LCOE, and CO_2 emission

during discharging enhanced the RTE from 37.9% to 39.52%. In the end, a sensitivity analysis demonstrated that PV/WT configuration, storage volume, and pressure could most impact the systems' overall performance. Table 2.6 lists all studies on the feasibility study of CAES for small-scale applications.

2.6. Optimal operation and scheduling

There are several challenges in achieving an optimal combination of CAES and renewable technologies subsystems, considering uncertainties associated with renewable generation, load demand, and market energy prices. Furthermore, CAES as an EES has to be optimally controlled, taking into account its operation costs and physical constraints [192]. It is worth noting that CAES includes several components and is a mix of mechanical, electrical, and thermal engineering [27]. Therefore, the optimization and control of CAES's key elements individually do not mean the whole process optimal operation. So controlling the CAES at the system level and finding the optimal strategy for planning CAES is crucial, especially when integrated into the renewables [74]. The various efforts have been carried out in the direction with the above-mentioned issues from different levels of energy systems perspective, presented in the following subsections.

2.6.1. Scheduling and planning of CAES in local energy systems or microgrids

CAES as a subsystem of MG or decentralized HESs can be adopted for either behind-the-meter application or standalone applications. In the area of optimal operation-scheduling research, a limited number of scholars have explored the optimal operation of CAES systems as decentralized ESS within HES while considering it for different application potentials like renewable penetration and load shifting [61,173,193]. This scarcity is particularly evident when considering aspects related to the reliability and resiliency of such systems.

Studies that conducted optimal scheduling of CAES at the MG level are summarized in Table 2.7. For example, an operation model for SS-CAES for behind-the-meter applications was proposed by Anierobi et al. [173]. An optimization model was structured to manage the industrial customer's load demand while minimizing the annual electricity costs with and without CAES. The results indicated that incorporating SS-CAES was economically feasible with the specific electricity tariff rate structure. No thermodynamic model of CAES was used in this study. Heidari et al. [12] presented an operational strategy based on a thermodynamic model of I-CAES integrated into PV panels and grids. Their optimization results showed that

adopting CAES for residential buildings with a power demand less than 50kW was not economically feasible.

Sedighnejad et al. [51] introduced a control strategy to evaluate CAES's performance integrated into an isolated WT/DIG hybrid system using an energy harvest index (EHI). Their results showed that by targeting a maximum HEI tracking control, CAES could capture excess electricity and increase electricity generation using a hybrid power system, consequently decreasing pollutant emissions and bringing financial benefits. But no optimization was carried out in this study. Tiano et al. [61] optimized the hybrid system's operation, including PV, WT, and UW-CAES, to fully power the Sicily region. Dynamic programming was applied to optimize the plant operation while minimizing the annual electricity purchased from the national grid. The results indicated that their proposed system configuration could adequately manage and satisfy the load without dependency on the national grid and conventional power plant. Zhang [130] developed a bi-level optimization problem (BLP) for optimal sizing (upper level) and scheduling (lower level) of stand-alone MG, including PV, WT, DIG, and CAES used for joint energy and reserve application. They compared the bi-level dispatch strategy with other control dispatch strategies. Their results showed that MG's daily operation cost with other approaches was about 2.1 to 3.1% more than that with their proposed model. In other studies, Xu et al. [129] made optimal sizing and scheduling of off-grid MG, including WT, DIG, and CAES, aiming at minimizing daily capital costs and operating costs considering the DRP. They adopted a scenario-based bi-level programming method to address the uncertainty associated with renewables and load demand. Bagherzadeh et al. [193] surveyed the strategy of applying CAES in MG, including PV, WT, MT, CAES, battery, and grid. They proposed an energy management strategy for day-ahead optimal scheduling and unit commitment of an MG while considering the uncertainties of renewable resources and calling DRP. Their results showed a 7% reduction in total operation cost by incorporating CAES facilities and DRP. Jabari et al . [98] introduced a short-term optimal design and scheduling of a CCHP powered by a solar dish Stirling engine coupled with AA-CAES to supply residential’s cooling, heating, and electrical demands. The optimization model's results showed that AA-CAES could decrease the operational cost of the whole system by about 22.36% and 21.79% in the heating and cooling modes, respectively. In this study, the TES part and thermodynamic characteristics of AA-CAES were not investigated.

In another study, Jalili et al. [194] proposed a stochastic day-ahead optimal dispatch strategy for a grid-connected MG based on an energy hub to satisfy electricity, heating, and cooling

Table 2. 7. Characteristics of studies on optimal scheduling of CAES at the MG level.

Ref	Hybrid system		Energy storage		System mode		CAES characteristics		Application	Case study	Objective function
	Renewables	Other generators	CAES	Other ESS	Grid-connected	SA	SOC	Scale			
[130]	PV-WT	DIG	A-CAES	TES	×	√	Volume	SS	• Renewable penetration • Reserve capacity • Power reliability	Isolated MG (3 MW)	Bi-level problem, Min TAC Min TOC
[129]	WT	DIG	A-CAES	TES	×	√	Volume	SS	• Wind penetration • Power reliability	District (5 MW)	Bi-level problem, Min TAC Min TOC
[193]	PV-WT	Microturbine	I-CAES	Battery	×	√	Energy	SS	• Renewable penetration • Power reliability	Isolated-MG (2.5 MW)	Multi-objective: Min TOC Min CO_2 emission Max Reliability
[195]	PV-WT	DIG	D-CAES	×	√	×	Energy	SS	• Renewable penetration	University campus	Min TOC Two-Stage :
[196]	WT	DIG	D-CAES	×	√	×	LOA	SS	• Wind penetration	MG (3 MW)	Min power loss and voltage deviation Min TOC
[12]	PV	×	I-CAES	×	√	×	Pressure	μS	• Renewable penetration • Load shifting	Residential building (12 kW)	Min NPV
[173]	×	×	D-CAES	×	√	×	Energy	SS	• Load shifting	Industrial costumer	Min TAC

[61]	PV-WT	×	UW-CAES	×	√	×	Volume		• Renewable penetration • Power reliability	Island	Min Grid electricity
[98]	Solar dish Stirling heat engine	CCHP	AA-CAES	TES	√	×	LOA	μS	• Renewable penetration	Residential building (<100 kW)	Min Grid electricity
[179]	PV-WT	Energy hub	A-CAES	TES	√	×	Pressure	SS	• Renewable penetration • Peak shaving • Cogeneration	District (2-3 MW)	Tri-level: Max RTE Min TAC Min TOC
[194]	PV-WT	Energy hub	D-CAES	TES, ISC	√	×	Energy	SS	• Renewable penetration • Energy shifting • Power reliability	District (2 MW)	Min TOC

demand. The energy hub comprised CCHP, PV, WT, solar-powered D-CAES, ice storage conditioner (ISC), and TES. Their results showed that applying solar-powered D-CAES and ISC decreased the operation cost of MG by 2.6% compared with MG without any CAES and ISC.

Ref. [195] proposed the optimal management of grid-connected MG, including D-CAES, integrated with the PV and WT farm considering thermo-economic and environmental aspects. A dynamic programing algorithm was applied to minimize the power plant operational cost (maximizing profit) composed of the cost of purchasing the electricity and methane and revenue from the sale of excess energy. Their results displayed that incorporating the CAES led to a 74% CO_2 reduction and 80% cost reduction compared to the reference scenario (load satisfied by the main grid). In a related study, Daneshvar Garmroodi et al. [174] introduced a model-free strategy for optimizing the scheduling of an energy hub, which incorporates AA-CAES for various functions like heating, cooling, and electricity generation, even when operating under off-design conditions. The energy hub includes a MT, PV, WT, electric heat pump, gas boiler, absorption chiller, and A-CAES. Their study underscored the efficacy of adopting a safe-deep reinforcement learning approach in minimizing the energy hub's operational cost (gas consumption and trade-off with the grid) while satisfying the operational constraints. The adopted approach demonstrated superior performance compared to other alternative methods, such as state-of-the-art deep reinforcement learning and conventional mixed-integer linear programming methods.

2.6.2. Scheduling and planning of CAES in the distribution network

Recently, with a high penetration of distributed energy systems, including PV, WT, micro-turbines, dispatchable generators, and ESS, electric power networks have been transferred from passive distribution systems into active distribution systems [197]. Because of the inherent intermittency of renewable energies, the optimal operation of active distribution systems is one of the main challenges of power networks that distribution system operators (DSO) face. In this regard, developing a practical framework to cope with these issues is critical. Studies about optimal scheduling of distribution power systems in the presence of CAES have been carried out mainly in the area of peak shifting [45], renewable energy accommodation [1,196,198–201], reserve service [197,202], frequency regulation [201], voltage security [1], multi-generation of CAES [7,17,80,81]. In these studies, an optimization problem to achieve optimal

scheduling of DSO was formulated subject to constraints associated with the distribution network.

Haghifam et al. [197] attempted to present a day-ahead optimal energy and reserve scheduling of the active distribution system in the presence of CAES and an independent MG operator. A scenario-based stochastic bi-level programming method was implemented to minimize the total operation cost of DSO in the upper level while maximizing the benefits of MGO considering distribution network constraints in the inner layer. The results showed that incorporating CAES in DPS and intelligent parking lot in MG increased the generated power by conventional units and decreased the operation cost of DSO by about 1.25% while augmenting the benefits of MGO by approximately 1.37%. A two-stage optimization model for planning and scheduling the MG in the presence of CAES and preventive maintenance (PM) to avoid any failure in DPS was developed in Ref. [196]. In the first stage, a two-objective optimization model was solved to find the best size (MW) and location of MG while minimizing power loss and voltage deviation in the distribution network. In the second stage, an operation cost-minimization model was developed to achieve a stochastic scheduling model of MG. Furthermore, a risk assessment model, conditional value-at-credibility (CVaC), was adopted to hedge against wind power uncertainty. Their results indicated the usefulness of incorporating CAES and preventative maintenance in decreasing the MG operation cost and increasing the wind penetration and MG self-sufficiency while reducing the main grid dependency.

In another study, Panda et al. [1] developed an optimization model to evaluate a hydro-thermal-wind-solar-CAES hybrid power system's performance to achieve an optimal generation schedule while minimizing the operational costs and maximizing the voltage security. The operational constraints such as renewable intermittency and disruption were also considered. Their results displayed that an increase in renewable penetration from 20% to 40% resulted in 26 $/h saving in operating costs. Moreover, they showed that employing CAES in energy systems reduced the effect of fluctuation from renewable resources and improved the system's voltage security associated with the cost-effective operation even in high renewable penetration. Hence, the voltage of a hybrid power system with CAES was 6.5%-7.5% compared to that without CAES. Bai et al. [45], presented a tri-state dispatch model for AA-CAES taking into account its off-design characteristics for optimal scheduling of power distribution system with renewables and AA-CAES. They also showed the vital role of incorporating AA-CAES in operation cost reduction through renewable accommodation and peak shaving.

The variable power generation and CAES scheduling significantly impact static voltage stability as one of the crucial aspects of distribution network voltage security issues [199]. Therefore, several studies presented an optimal schedule for CAES as bulk energy storage in a security-constrained unit commitment (SCUC) framework for high wind penetration in DPS [198–200]. For example, Daneshi et al.[198] introduced deterministic SCUC with CAES and wind power generation considering fuel and environmental constraints. The overall results indicated that CAES could affect the peak-load reduction, system operation cost, and reliability as well as GHG emission and dispatch of the units. Stochastic SCUC models with CAES and wind power generation were introduced in Refs. [199,200] that not only considered wind uncertainty but also addressed static voltage stability constraint [199] and network contingency [200].

Furthermore, frequency dynamics management is essential to address the frequency deviation in power systems due to the abrupt loss of generation. Sedighizadeh et al. [201] proposed frequency dynamics-constrained unit commitment models in the presence of CAES and wind for optimal joint energy and reserve scheduling. The essential goal was to keep the dynamic frequency security by incorporating demand response and fast-response CAES following a generation loss. The results indicated that the proposed model in the presence of CAES guaranteed frequency security while decreasing the system operating cost. Although several studies suggested optimal energy and reserve scheduling of adopting D-CAES in DS, very few works have developed reserve capacity modeling for CAES. Hence, Li et al. [202] presented optimal joint energy and reserve scheduling for power systems by incorporating the reserve capacity model of AA-CAES. Some practical limitations and thermodynamic characteristics of AA-CAES were considered in the proposed model. The results showed that incorporating AA-CAES in the power system can decrease the energy and reserve costs of the system and mitigate wind curtailment. However, it is unsuitable for satisfying only the reserve demand of the system.

Several scholars have focused on optimal dispatching and scheduling of the multi-generation applications of CAES-based energy hubs integrated into the energy system. For instance, Li et al. [80] proposed a zero-carbon small Energy Internet (ZCE-MEI), including a DPS and district heating network (DHN) with an NSF-CAES hub to use heat and electric power in an integrated manner. A dispatching model was developed to maintain the voltage quality of DPS considering the dynamic behavior of TES and air pressure in ASTs. Results showed that

Table 2. 8. Optimal scheduling of DES in the presence of CAES

Ref.	Renewable generation	Storage	Other generators	Scale	Application	CAES Output energy	Case study	Objective function	Formulation	Uncertainty parameters
[197]	PV/WT	D-CAES, parking lot	TU	LS	Energy and reserve capacity	Electricity	IEEE 15-bus PDS	Bi-level programming: Upper level= Min TOC Lower level=Max profit	NLP	Wind/solar/load /electricity price
[196]	WT	D-CAES	DIG	LS	Wind penetration	Electricity	IEEE 33-bus radial PDS	Two-stage: First stage: Power loss and voltage deviation Second stage: Min operation cost	NLP	Wind power
[1]	Hydro/ WT/PV	D-CAES	TU	LS	Renewable penetration	Electricity	IEEE-30 bus PDS	Min operation cost	NLP	Wind/solar
[45]	WT	AA-CAES	-	SS	Wind penetration Peak shifting	Electricity	Modified IEEE 33-bus PDS	Min operation cost	MINLP	Wind power
[198]	WT	D-CAES	TU	LS	Wind penetration	Electricity	Eight-bus and IEEE 118- bus PDS	Min operation cost	MIP	---
[199]	WT	D-CAES	TU	LS	Wind penetration	Electricity	IEEE-30 bus PDS	Min operation cost	MINLP	Wind power
[200]	WT	D-CAES	TU	LS	Wind penetration	Electricity	Modified IEEE 30-bus PDS	Min operation cost	MILP	Wind power
[201]	WT	D-CAES	TU	LS	Wind penetration Frequency regulation	Electricity	6-bus PDS	Min operation cost	MINLP	Wind power
[202]	WT	AA-CAES	TU	LS	Wind penetration Energy and reserve capacity	Electricity	Revised IEEE 30 bus PDS	Min operation cost	MILP	Wind power Load demand

[80]	WT	NSF-CAES TES	-	SS	Wind penetration CHP	Electricity Heating	33-bus PDS, 8-node DHN	Min operation cost	MILP	-
[17]	Solar collector	AA-CAES, TES	Heat pump-GT	SS	CHP	Electricity Heating	IEEE 33-bus PDS and a DHN	Bi-level programming: Upper level= Min operation cost Lower level= Max profit	MILP	-
[7]	PV	AA-CAES, TES	-	SS	Wind penetration Reserve capacity CHP	Electricity Heating	Modified IEEE 33-Bus PDS	Max benefit of hub operator	MILP	Load demand Solar
[81]	WT	D-CAES, TES	CHP,boiler	SS	Wind penetration Reserve capacity	Electricity	Modified IEEE 33-bus PDS	Min operation cost	MILP	Wind

Although the proposed system could reduce operating costs and wind curtailment, the method could not deal with uncertainties. Similarly, an AA-CAES-based energy hub, along with its business model to exchange energy with a DPS and heating network under a time-of-use price mechanism, was introduced in Ref. [17]. The results indicated the interdependence of heat and electricity prices. In another study, Zhang et al. [7] proposed an optimal scheduling strategy for regional integrated energy systems based on an energy hub trading strategy and multiple applications of AA-CAES for cogeneration, reserve service, and PV consumption. The results showed that AA-CAES could increase the profit of energy hub operators by 21.89% and enhance the operational flexibility and energy autonomy of regional integrated energy systems. Li et al. [81] presented a robust and opportunistic day-ahead optimal scheduling for the district joint natural gas and power system based on an energy hub with high wind power penetration. D-CAES, along with demand response, was incorporated to reduce the operation cost of the system and wind uncertainty impacts. The results showed that CAES by itself led to around 5.16% and 46% reduction in operation cost and wind curtailment, respectively. Studies on optimal scheduling of DES in the presence of CAES are summarized in Table 2.8.

2.6.3. Scheduling and planning of CAES in the energy market environment

CAES systems can participate independently in the energy markets to purchase and sell electricity. However, the market price uncertainty is a challenging issue for CAES operators as one of the market players contributing to the day-ahead market [203,204]. Therefore, optimal bidding/offering strategies are essential to tackle these issues. Scholars have proposed different self-scheduling approaches (discharging/charging or purchasing/ selling the electricity) and presented optimal bidding and offering for CAES in the presence of energy market price uncertainties [90]. The goal of CAES as a participant in the energy market is to support the maximization of profit via energy arbitrage or providing other ancillary services. Table 2.9 indicates the characteristics of studies on optimal scheduling of CAES in the market environment. CAES's optimal operation for energy trading within a day-ahead electricity market was investigated by Nojavan et al. [90]. They presented a robust optimization approach to maximize the profit of the CAES system, taking into account market price uncertainty. Therefore, CAES's optimal offering and bidding curves that should be submitted to the market operator were achieved.

Meanwhile, risk management plays a vital role in the optimal scheduling of storage and generation units in any competitive electricity market. Therefore, the operational decisions of

every market player should incorporate the risk associated with price uncertainties [204]. Multiple studies addressed the risk in the objective function or some constraints in the scheduling problem [205]. CAES's offering and bidding curves schemes considering risks posed by market price uncertainty is studied by some researchers. For instance, Shafiee et al. [206] proposed different strategies to obtain hourly bidding and offering curves of a price-maker merchant CAES plant, which participates in a day-ahead electricity market. A mix integer linear programming (MILP) model was presented to manage the risks of uncertainties by robust optimization. In another study [6], this group proposed a risk-constrained self-scheduling operation strategy to provide the bid-offer curve for the merchant CAES facility participating in day-ahead energy markets. The information gap decision theory (IGDT) was adopted to model the market price uncertainty. A hybrid robust-stochastic strategy was introduced by Cai et al. [203] to achieve optimal bids and offers while maximizing the expected profit of CAES as one of the day-ahead energy market participants. A scenario-based stochastic method was used to consider the uncertainty of market price, while a robust optimization approach was implemented to assess the uncertainty of the cavern's maximum capacity. In another study, Nojavan et al. [207] developed a hybrid robust-stochastic method to present optimal biding and offering of CAES in both day-ahead of a real-time energy market. In this study, to cope with market price uncertainty, a stochastic framework was used for the day-ahead market, while a robust optimization approach was adopted for real-time energy arbitrage of CAES. A downside risk constraints (DRC)-based offering/bidding strategy was proposed by Ref. [204] in which a risk-based stochastic problem was developed to maximize the profit of CAES for a day-ahead energy market. Narayan Dash et al. [208] introduced the synthetic stochastic-robust approach to find optimal offers and bids for CAES while maximizing the profit of CAES considering the uncertainty of market price and cavern max capacity.

Besides providing energy arbitrage [90,91,203,204,206,207], the CAES systems can offer other ancillary services to the market, such as spinning and non-spinning reserve services [209,210] and regulation services [211]. For example, Shafiee et al. [210] developed the optimization-based self-scheduling approach for CAES in the day-ahead energy and reserve market , considering thermodynamic characteristics of CAES and price uncertainty. Similarly, Khatami et al. [211] presented a detailed model for investigating the optimal participation of CAES in energy and ancillary service (regulation and spinning) markets. However, in the aforementioned studies, the proposed reserve model cannot be used for A-CAES units due to the presence of TES limitations. Therefore, Drury et al. [209] presented an

energy and reserve self-scheduling optimization model for A-CAES and D-CAES to evaluate their potential value in U.S. markets. The developed reserve capacity model was not much accurate for day-ahead scheduling of CAES because only the maximum power limits were considered for compressor and expanders, respectively.

Several scheduling strategies for wind and CAES combined systems are studied [205,212,213]. CAES can be paired with wind turbines to increase the reliability of wind power to gain higher benefits [212]. Although the combination of wind and CAES units can be economically promising, an appropriate offering and bidding strategy are needed in which the uncertainty of wind power production and price forecast errors would be addressed effectively. Attarha [212] presented an adaptive, robust self-scheduling strategy for wind power paired with CAES participating in a day-ahead energy market. A market-driven model for assessing the profitability of join operation of the wind farm and UW-CAES in spot and the day-ahead market was developed in Ref. [214]. The results indicated a profit improvement of the wind farm by 19.2% in coordination with UW-CAES compared to without coordination. Li et al. [215] adopted a rolling day-ahead self-scheduling optimization model for wind farms integrated into D-CAES and A-CAES to evaluate the effect of the self-scheduling horizon on the profit of the whole system.

In addition to wind units paired with CAES, scheduling of other integrated power systems combined with CAES have been studied in Refs. [202,205,216–218]. Abbaspour et al. [216] presented and compared a short-term optimized operation scheduling of a GenCo owning the thermal power unit, wind farm, and CAES to maximize the company's profit in the energy market and minimize the cost. The results indicated that incorporating CAES increases the profit by 43% and decreases the operation cost by 6.7%. In Ref. [205], a stochastic programming-based optimal bidding for scheduling the same GenCo was found to be an efficient method for maximizing the profit in day-ahead energy and spinning reserve markets compared with a deterministic approach. In this study, conditional value at risk (CVaR) was implemented as a risk-controlling index. Ghalelou et al. [217] introduced a novel stochastic approach for self-scheduling the different systems, including thermal, wind, solar, and CAES unit in the day-ahead energy market to minimize the operation cost of CAES and thermal unit (TU) while considering the demand response program. This study evaluated the uncertainty associated with market price, load demand, temperature, solar radiation, and wind speed. The results showed that the stochastic self-scheduling of thermal and renewable units in the presence of CAES and demand response decreased the operation cost by about 5.15 % compared to that

Table 2. 9. Characteristics of studies on optimal scheduling of CAES in the wholesale market environment.

Ref.	Study field	Power system participant				CAES type	Market type	Market uncertainty	Uncertainty modeling	Formulation	Objective function
		CAES	WT	TU	PV						
[90]	Optimal bid/ Offer	√	×	×	×	D-CAES	Energy market (day-ahead)	Market price	Robust	MILP	Max profit
[206]	Optimal bid/ Offer	√	×	×	×	D-CAES	Energy market (day-ahead)	Market price	Robust	MILP	Max-Min profit
[91]	Optimal bid/ Offer	√	×	×	×	D-CAES	Energy market (day-ahead)	Market price	Robust-IGDT based	MINLP	Max profit
[203]	Optimal bid/ Offer	√	×	×	×	D-CAES	Energy market (day-ahead)	Market price	Robust-Stochastic	MILP	Max expected profit
[207]	Optimal bid/ Offer	√	×	×	×	D-CAES	Energy market (day-ahead & Real-time)	Market price	Robust-Stochastic	MILP	Max profit
[204]	Optimal bid/ Offer	√	×	×	×	D-CAES	Energy market (day-ahead)	Market price	DRC-based Stochastic	MILP	Max expected profit
[208]	Optimal bid/ Offer	√	×	×	×	D-CAES	Energy market (day-ahead)	Market price	Synthetic Stochastic &Robust	MILP	Max profit
[210]	Self-scheduling	√	×	×	×	D-CAES	Energy & Reserve market (day-ahead)	Energy and reserve market price	Deterministic	MILP	Max profit
[209]	Self-scheduling	√	×	×	×	D-CAES& AA-CAES	Energy & Reserve market (day-ahead)	Energy and reserve market price	Deterministic	MILP	Max revenue
[211]	Self-scheduling	√	×	×	×	D-CAES	Energy & reserve & regulation market	Market price Cavern air (day-ahead &real time)	Deterministic	MILP	Max profit
[212]	Self-scheduling	√	√	×	×	D-CAES	Energy market (day-ahead)	Market price Wind power	Adoptive Robust	MILP	Max-Min-Max profit
[214]	Self-scheduling	√	√	×	×	UWCAES	Energy market (day-ahead & spot)	Market price Wind speed	Deterministic	MINLP & MILP	Min cost
[215]	Self-scheduling	√	√	×	×	D-CAES	Energy market (day-ahead)	Wind power	Deterministic	MILP	Max profit

[205]	Optimal bid	√	√	√	×	D-CAES	Energy & Reserve market (day-ahead)	Energy and reserve market price Wind speed	Stochastic & CVaR & Deterministic	MILP	Max expected profit
[216]	Self-scheduling	√	√	√	×	D-CAES	Energy market (day-ahead)	Market price Load	Deterministic	MINLP	Max profit & Min operation cost
[218]	Self-scheduling	√	√	√	×	D-CAES	Energy market	Market price Wind speed Load	Look-ahead risk-constrained (CVaR)	MINLP	Min operation cost
[202]	Self-scheduling	√	√	√	×	D-CAES & AA-CAES	Energy & Reserve market	Market price Wind speed Load	Deterministic	MILP	Min operation cost
[217]	Self-scheduling	√	√	√	√	D-CAES	Energy market	Market price Wind speed Load demand Solar Radiation Temperature	Stochastic	MILP	Min operation cost

without CAES and demand response. A look-ahead risk-constrained method for scheduling different units, including wind, thermal, and CAES system, to minimize the total cost in the presence of demand response was proposed by Aliasghari et al. [218]. CVaR framework was considered to control the stochastic process. Li et al. [202] developed a reserve capacity model of AA-CAES to achieve optimal joint energy and reserve scheduling of power systems while minimizing the operation cost considering operation characteristics and limitations of AA-CAES.

2.7. Gaps and limitations

This chapter provides an updated review of the CAES, with a focus on evolving technology trends, CAES characteristics, and potential applications, particularly within the context of integration, design, and scheduling from various perspectives. It is evident from the literature that the CAES systems possess high energy capacity and power rating, making them suitable for stationary and large-scale applications with a lifespan of approximately 40 years. However it suffers from relatively low energy efficiency (between 40-70%). Consequently, there is significant interest in integrating CAES with different cycles to recover waste heat and reduce exergy destruction. Additionally, CAES can be combined with renewables to enhance renewable penetration and energy system reliability.

Moreover, the operation of CAES technologies as part of future electrical/thermal grids, particularly for small-scale applications, requires improvements to enhance competitiveness, affordability, and efficiency compared to other energy storage options. Therefore, optimization is crucial to determine the optimum capacity within the pressure range of the air reservoir, avoiding issues such as under-sizing, oversizing, decreased profitability, or reliability. It is important to note that achieving optimal operation of the entire integrated system is not necessarily attained solely through optimizing CAES's key components, especially when integrated with intermittent renewables and operating under off-design conditions.

In summary, the literature review highlights several gaps in previous studies focused on integrating A-CAES systems into decentralized energy applications:

1) A-CAES operation strategy:

- Underexplored role of TES; despite the potential advantages of incorporating TES, such as enhanced energy efficiency compared to D-CAES, prior studies have predominantly assumed its presence rather than conducting thorough evaluations. Existing literature on A-CAES with TES has not examined the function and optimal capacity of TES nor its

impact on system operation and performance. As such, the effect of TES operation and its integration and dynamic behavior on the performance of A-CAES and HES have not been studied. This gap emphasizes the need for in-depth investigations into the integration and optimal utilization of TES within A-CAES systems.

- Lack of comprehensive and accurate simulation model: From the above studies, it can be evident the lack of accurate simulation model for integration of A-CAES for decentralized application considering the physical limitations while ensuring the appropriate dynamic interaction of subsystems. So that, previous research [12,63,84,131] has only considered the effect of capacity and dynamic behavior of the air storage tank (of A-CAES) using a traditional energy management operation strategy (T-EMOS). Therefore, these T-EMOSs are not well suited for A-CAES, and HES performance evaluation as the effect of characteristics such as capacities of power conversion units and TES were neglected in simulation model.

2) Optimal sizing-planning:

- Absence of a customizable simulation-optimization model; while few prior studies have explored decentralized A-CAES systems' design and operation, they often employ multi-level programming approaches. These methods, while informative, may yield trade-off solutions and result in oversized or undersized systems due to analyzing the A-CAES based on short-term data to reduce dimensionality and avoid higher computational costs. Therefore, a critical gap in the literature is the absence of an independent, reliable planning simulation model enabling being coupled with a customizable optimization model. This integrated framework is essential not only for investigating long-term A-CAES system operation but also for optimally sizing the system to meet the specific requirements of diverse users and applications considering techno-economic and environmental aspects.
- Urban local A-CAES for joint renewable self-consumption and load-shifting; to the best of our knowledge, prior research has not explored urban-integrated local A-CAES systems designed to facilitate joint renewable self-consumption and load-shifting, particularly under applicable electricity tariff schemes. This application-specific research gap underscores the need for an investigation that thoroughly explores the complexities of optimizing A-CAES systems within urban area.
- Overlooking complex factors affecting system capacity; the previous body of works has primarily focused on determining the rated power capacity of PCSs (compressors and

turbine trains) and the energy capacity (e.g., AST volume) to establish optimal A-CAES configurations within HES. However, these studies often simplify the approach, overlooking influential factors such as the optimal number of compressor and turbine stages and the minimum and maximum allowable pressure levels within the AST. Similarly, assessing the optimal TES capacity to recover heat generated during compression can significantly enhance the system's techno-economic performance and reduce its environmental footprint. These factors represent crucial gaps in the literature that our study aims to address comprehensively.

3) Optimal operation-scheduling:

- Integration of planning and operation optimization: The existing evaluation methodologies, e.g., planning and scheduling, cannot fully capture the techno-economic role of A-CAES in local energy systems. An optimal configuration of HES and A-CAES capacity is required to ensure meaningful evaluation results, considering the techno-economic characteristics and limitations of A-CAES and other technologies. Therefore, the other gap pertains to the need for comprehensive performance assessment and detailed operational analysis of urban- integrated local HES with a limited energy sources and A-CAES system under various scenarios of grid connection using real-time data considering cost-effectiveness and resiliency aspects. Addressing these gaps requires the integration of planning and operation simulation and optimization for long-term and short-term horizon evaluations.
- Reliability assessment: Reviewing the previous studies acknowledged the gap in evaluating the resiliency scheme, recognizing that certain scenarios might compromise accessibility to specific resources due to failures. Under such circumstances, outages can diminish the resiliency of the system. To address this challenge, the proposed sizing and operation scheme should be designed with constraints prioritizing resilience, ensuring a robust system in the face of potential failures or disruptions.
- Response time of CAES system: Another significant research gap lies in the insufficient attention given to the detailed mechanical constraints of CAES systems, specifically regarding the transition time and response time of power conversion units such as compressors and turbines within HES. These mechanical intricacies play a pivotal role in influencing the reliability and resiliency of the storage unit and the entire energy system with limited energy sources, particularly in off-grid modes when sudden grid

outages occur. Addressing this gap is crucial for a more comprehensive understanding of A-CAES system dynamics and optimizing their performance in critical scenarios.

- Hybridizing energy storage systems: In addition, the literature rarely explored the hybridizing CAES system with other energy storage such as pumped hydro energy storage [122], flywheel [25,26,219], and supercapacitor. While CAES has the potential to be integrated with another energy storage like a battery, as suggested in [220] for increasing the self-sufficiency and resiliency of energy systems. This research gap is evident across various stages, from the initial design and planning phases to subsequent unit commitment and scheduling stages within HESS implementation.

Addressing the aforementioned research gaps is crucial for further promoting the utilization of CAES in decentralized applications. Therefore, the primary objective of this study is to bridge these gaps by conducting a comprehensive evaluation of a decentralized A-CAES system over its lifetime. This will be achieved through a multi-stage simulation and optimization procedure aimed at determining the optimal sizing and operation of such a system, considering thermodynamic, techno-economic, and environmental factors.

Chapter 3: Methodology

This thesis aims at making the decentralized A-CAES more feasible considering economic, environmental, and technical aspects by presenting a multi-stage simulation-optimization framework that includes three main modules: 1) Operation strategy module: Developing an accurate simulation model including EMOS logic for decentralized A-CAES operation and detail mathematical modeling of A-CAES sub-systems. 2) Optimal design module: presenting a user-based sizing- planning framework using the operation logic developed for A-CAES in the first module for not only customizing A-CAES system based on its application potential but also design an urban-integrated HES considering techno-economic, environmental and resiliency aspects during the project lifetime. 3) Optimal operation module: structuring unit-commitment model for optimal dispatch scheduling the HES components under different scenarios of considering response time of A-CAES system. It should be noted in this stage to achieve a most reliable and resilience energy system, the sizing-planning module is connected to operation-scheduling module to find the top-economic and most resilient configuration and operation for HES under different scenarios of grid- connection situation and A-CAES hybridization with other energy storage system such as battery.

3.1. Local hybrid energy systems

Fig. 3.1 illustrates the overall schematic diagram of HES examined in this thesis. The main components of the energy system include : 1) on-site solar PV serving as the primary energy source , 2) A-CAES system , 3) primary load demand, 4) a control unit including the energy management and dispatch strategy, responsible for measuring system parameters, evaluating operating conditions of each element, and planning the system operation at each time, 5) a converter system employed to convert DC to alternating current (AC) as the PV system's output power is direct current (DC).

Moreover, the A-CAES units consists of PCSs (e.g., compressor and expansion trains) and energy storage units (e.g., AST and TES with heat exchanger (HEX)).

Furthermore, during the model assessment, the HES is enhanced with the following components:1) The flexible load (electric boiler (e-boiler) in this thesis) is introduced to reduce the solar power curtailment and gas consumption by existing gas boiler (g-boiler) , 2) a Battey bank is hybridized with A-CAES to improve resiliency and avoid solar power curtailment. It

should be noted the presence of the electric boiler is investigated in Section 3.4, while the Battery bank is explored in Section 3.5.

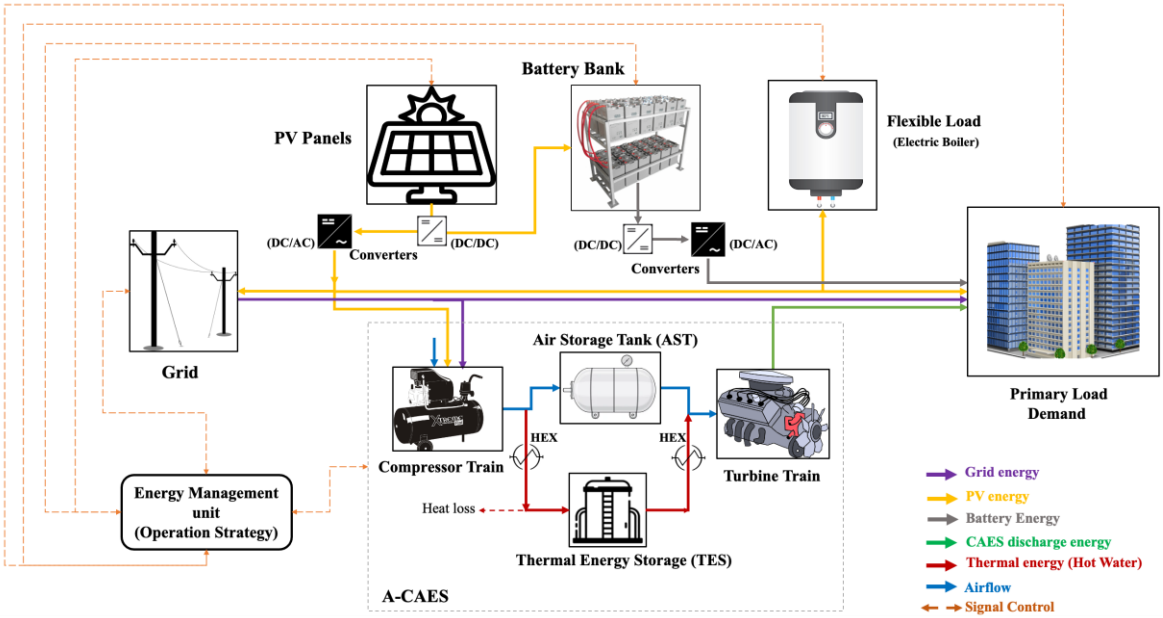

Fig. 3. 1. The overall schematic diagram of the local hybrid energy system.

3.2. An improved energy management operation strategy for integrating adiabatic compressed air energy storage with renewables in decentralized applications [20]

3.2.1. Research approach

In this section, an operation strategy, called I-EMOS for managing the energy flow in A-CAES system considering all components' models, limitations and interactions is established and compared with the traditional energy management operation strategy (T-EMOS). As mentioned earlier, in T-EMOSs, A-CAES is treated like a conventional battery where only the capacity of the energy storage unit, the air reservoir, is considered.

3.2.1.1. Model development

In this section, the mathematical formulation of PV panel and each component of the A-CAES based on their analytical model is presented.

3.2.1.1.1. Assumptions

For the convenience of modeling and analysis, the following assumptions are made in this work: 1) Air is treated as an ideal gas with a constant specific heat [179], 2) The AST is regarded as isothermal [63,179], 3) The operation mode based on the pressure of the compressor and expander is assumed constant-constant, 4) The inlet pressure of the turbine side corresponds to

the discharge pressure of the throttle valve, which equals the minimum pressure of the AST [63,179], 5) the outlet pressure of the compressor train equals the maximum pressure of the AST [63,179], 6) Heat loss and air leakage over the system are negligible, 7) Pressure loss in heat exchangers is reflected in the design input pressure of compression/expansion stages [149,221], 8) The hot and cold tanks in the heat recovery unit are set to be isothermal, 9) It is assumed that AST has a 50% charge at the initial time, 10) the compression and expansion processes are regarded as isentropic, 11) The same crankshaft is considered for compressors and turbines, 12) There is no limitation in purchasing and selling electricity from/to the electric grid, 13) The input air temperature to the first compressor is constant, 14) The analytical model for the output power of compressor and turbine train is considered a linear function of mass flow rate, which varies over time in response to changes in the renewable generation and load demand, 14) The efficiency of the power conversion systems including motor, compressors, turbines, generator is assumed to remain constant and at their design conditions.

3.2.1.1.2. PCS model (compressor/turbine train)

- Compressor train (charging mode)

The overall charging power of CAES (shaft-power of compressor) at time t can be written as [129,179]:

$$W_{CAES,crg}(t) = K_c \times \dot{m}_{c,a}(t) \quad (3.1)$$

where $\dot{m}_{c,a}$ represents the air mass flow rate of the compressor train and K_c is the power consumed by the compressor train per unit of mass flow rate in the charging process, and it is described below [222]:

$$K_c = \frac{1}{\eta_M} \sum_{i=1}^{N_c} \frac{C_{p,a}\, T_{c,i}^{in}}{\eta_{c,i}^{is}} \left(\pi_{c,i}^{\frac{\gamma-1}{\gamma}} - 1 \right) \quad (3.2)$$

where η_M presents the motor's energy conversion efficiency, N_c shows the number of compression stages, $C_{p,a}$ is the specific heat capacity of air at constant pressure, $T_{c,i}^{in}$ and $\eta_{c,i}^{is}$ represent the intake air temperature and the isentropic efficiency of the ith compressor, respectively, γ is the specific heat ratio and $\pi_{com,i}$ is the compression ratio for the ith compressor that is written as:

$$\pi_{c,i} = P_{c,i}^{out} / P_{c,i}^{in} \quad (3.3)$$

where $P_{c,i}^{in}$ and $P_{c,i}^{out}$ are the inlet and outlet air pressure of the ith compressor.

The electricity absorbed by the compressor train over a complete charging cycle can be calculated by [9]:

$$E_{CAES,crg} = \int_0^{t_{CAES,crg}} W_{CAES,crg}(t)dt \quad (3.4)$$

where $t_{CAES,crg}$ is the time required to fully charged the AST with a volume of V and reach the minimum pressure (P_{AST}^{min}) of the tank to maximum one (P_{AST}^{max}), given by:

$$t_{CAES,crg} = \frac{V_{AST}\,(P_{AST}^{max} - P_{AST}^{min})}{m_{c,a}^{r}\,R_a T_{AST}} \quad (3.5)$$

where $m_{c,a}^{r}$is rated air mass flow of compressor, R_a is ideal-gas constant and T_{AST} is the air temperature at the AST.

- Turbine train (discharging mode)

The overall discharging power of CAES ($W_{CAES,dis}$) at time t can be expressed as:

$$W_{CAES,dcrg}(t) = K_{tr} \times \dot{m}_{tr,a}(t) \quad (3.6)$$

where $\dot{m}_{tr,a}$ refers to the air mass flow rate of the turbine train and K_{tr} is the power delivered by turbine train per unit of mass flow rate in the discharging process, and it is described below:

$$K_{tr} = \eta_G \sum_{j=1}^{N_t} \eta_{tr,j}^{is}\, C_{p,a}\, T_{tr,j}^{in} \left(1 - \pi_{tr,j}^{\frac{\gamma-1}{\gamma}}\right) \quad (3.7)$$

where η_G presents the generator's energy conversion efficiency, N_{tr} is the number of the expansion stages, $\eta_{tr,j}^{is}$ represents isentropic efficiency of jth turbine, $T_{tr,j}^{in}$ and $\pi_{tr,j}$ are intake air temperature and expansion ratio of jth turbine, respectively with below relation:

$$\frac{T_{tr,j}^{out}}{T_{tr,j}^{in}} = \left(\pi_{tr,j}\right)^{\frac{\gamma-1}{\gamma}} \quad (3.8)$$

$$\pi_{tr,j} = P_{tr,j}^{out} / P_{tr,j}^{in} \quad (3.9)$$

where $P_{tr,j}^{\text{out}}$ and $P_{tr,j}^{\text{in}}$ present the inlet and outlet air pressure of the jth turbine.

Accordingly, the electricity delivered by turbine train over a complete discharge cycle can be calculated by [9]:

$$E_{CAES,dcrg} = \int_0^{t_{CAES,dcrg}} W_{CAES,dcrg}(t)dt \quad (3.10)$$

where $t_{CAES,dcrg}$is the time taken to fully discharge the AST and reach the maximum pressure (P_{AST}^{max}) of the tank to a minimum level (P_{AST}^{min}), given by:

$$t_{CAES,dcrg} = \frac{V_{AST}\,(P_{AST}^{max} - P_{AST}^{min})}{m_{tr,a}^{r}\,R_a T_{AST}} \quad (3.11)$$

where $m_{tr,a}^{r}$ is rated air mass flow of the turbine.

3.2.1.1.3. AST model

An AST has a dynamic behavior, and thus, its SOC depends on the level of energy stored in the reservoir in form of the air mass, which is measured by the compressor and expander train [129]. As mentioned above, the AST is set to be isothermal (T_{AST}) to facilitate the analyses [223]. Therefore, according to the ideal gases law (i.e. $PV = mRT$) and considering the isochoric AST (ΔV_{AST}=0), the air pressure (P_{AST}) in the AST at time t can be determined by:

$$P_{AST}(t) = \frac{M_{AST}(t).R_a.T_{AST}}{V_{AST}} \quad (3.\ 12)$$

where $M_{at}(t)$ is the accumulated air mass in the AST, and it is calculated as [129] :

$$M_{AST}(t) = M_{AST}(t-1) + \sum_{t=1}^{t_{CAES,crg}} \dot{m}_{c,a}(t)\,\Delta t \; - \sum_{t=1}^{t_{CAES,dcrg}} \dot{m}_{tr,a}(t)\,\Delta t \quad (3.\ 13)$$

where Δt is the time resolution.

The pressure state in the AST can be written as [45,202,223]:

$$P_{AST}(t) = P_{AST}(t-1) + \; \sum_{t=1}^{t_{CAES,crg}} \dot{P}_{c,a}(t)\,\Delta t \; - \sum_{t=1}^{t_{CAES,dcrg}} \dot{P}_{tr,a}(t)\,\Delta t \quad (3.\ 14)$$

$$\dot{P}_{c,a}(t) = \frac{R_a.T_{AST}}{V_{AST}} \dot{m}_{c,a}(t) \quad (3.\ 15)$$

$$\dot{P}_{tr,a}(t) = \frac{R_a.T_{AST}}{V_{AST}} \dot{m}_{tr,a}(t) \quad (3.\ 16)$$

where $\dot{P}_{c,a}$ and $\dot{P}_{\mathrm{tr},a}$ are the air pressure increasing and decreasing rates during charging and discharging the AST, respectively.

3.2.1.1.4. HEX model

Heat exchanger units are considered counter currents due to their excellent heat transfer capability compared to other designs [84,223]. In addition, water is selected as a thermal fluid due to its high specific heat capacity, which enables it to transfer and store more thermal energy at a low temperature [223]. Assuming counter flow heat exchanger and using the effectiveness–NTU method where $NTU = UA/C_{min}$ and s=C_{min}/C_{max}, the effectiveness (ε) of each heat exchanger can be evaluated as $\varepsilon = \frac{NTU}{1+NTU}$, considering s=*1* as assumed previously in [45]. NTU is the number of heat transfer units, U is the overall thermal conductance, A is the effective heat transfer area and $C = \dot{m}_c C_p$ is the heat capacity of the flow. Further details and comprehensive information can be found in [106]. Therefore, the total heat transfer power of heat exchangers during the charging and the discharging process can be calculated by equations (17) and (18), respectively [224].

$$\dot{Q}_c(t) = \dot{m}_{c,a}(t) C_{p,a}\, \varepsilon_{c,i}^{ex} \sum_{i=1}^{Nc} \left(T_{c,i}^{out} - T_{c,w,cold}^{in}\right) \quad (3.\ 17)$$

$$\dot{Q}_t(t) = \dot{m}_{tr,a}(t) C_{P,a}\, \varepsilon_{tr,i}^{ex} \left(\left(T_{tr,w,hot}^{in} - T_{AST} \right) + \sum_{j=1}^{Ntr-1} \left(T_{tr,w,hot}^{in} - T_{tr,j}^{out} \right) \right) \quad (3.18)$$

where $\varepsilon_{c,i}^{ex}$ shows the effectiveness of the cooling HEX after each compression stage, $\varepsilon_{\mathrm{tr,j}}^{ex}$ represents the effectiveness of the HEX in preheating the air before each expansion stage, $T_{c,i}^{\mathrm{out}}$ is the temperature of the outlet hot air from the ith compressor, $T_{tr,j}^{\mathrm{out}}$ is the temperature of outlet cold air from the j[th] turbine, $T_{\mathrm{c,w},cold}^{\mathrm{in}}$ and $T_{\mathrm{tr,w},hot}^{\mathrm{in}}$are the temperature of cold and hot water coming from TES, respectively.

3.2.1.1.5. TES model

In this study, a double hot/ cold tank is considered as TES, which has dynamic behavior determined by heat released during compression($\dot{Q}_c$) and heat supplied during an expansion ($\dot{Q}_t$). Therefore, The SOC of TES at time *t* can be expressed as [80,202]:

$$Q_{TES}(t) = Q_{TES}(t-1) + \sum_{t=1}^{t_{crg,TES}} \dot{Q}_c(t)\, \Delta t \; - \sum_{t=1}^{t_{dcrg,,TES}} \dot{Q}_{tr}(t)\, \Delta t \quad (3.19)$$

$where\ Q_{TES}(t)$ is the thermal energy state (kWh) in the hot tank with a volume of:

$$V_{TES} = E_{TES}/(C_w \rho_w (T_{hot} - T_{cold})) \quad (3.20)$$

$$E_{TES} = Q_{TES}^{max} - Q_{TES}^{min} \quad (3.21)$$

where E_{TES} is the energy capacity of TES while Q_{TES}^{max} and Q_{TES}^{min} are the TES's maximum and minimum energy capacity, respectively $C_w \rho_W$ equals 1.163 $\left(\frac{kwh}{m3,k}\right)$.

3.2.1.1.6. PV model

According to the hourly solar irradiance, the output power of a PV panel can be calculated as follows [63,179]:

$$W_{PV,DC}(t) = W_{PV}^{r} \left(\frac{I(t)}{I_{ref}}\right) \left[1 + N_T \left(T_{cell}(t) - T_{ref}\right)\right] \quad (3.22)$$

$$T_{cell}(t) = T_{am}(t) - \left(\frac{(NOCT-20)}{800} I(t)\right) \quad (3.23)$$

where $W_{PV,DC}$ presents the single PV system power output at time t in watts (W), W_{PV}^{r} reflects to the single PV-rated output power under standard conditions in watts, I is the solar irradiance at time t, I_{ref} shows solar irradiance at reference conditions (usually set as 1000 W/m^2), N_T refers to the PV temperature coefficient (-3.7×10 $^{(-3)}$ (1/°C) for monocrystalline and polycrystalline silicon [16]), T_{ref} is the cell temperature at the reference conditions (usually adjust at 25 °C), T_{cell} shows the cell temperature at time t calculated by Eq.3.23 in which T_{am}

is the ambient air temperature and $NOCT$ is the normal operating cell temperature (approximately 44-48 °C).

Considering the N_{PV} number of PV panels, the total AC power delivered by solar PV systems can be calculated by:

$$W_{PV,AC}(t) = N_{PV}\, W_{PV,DC}(t)\, \eta_{conv.} \quad (3.24)$$

3.2.1.2. Logic of improved energy management operation strategy (I-EMOS)

To establish and implement the simulation model, a logical energy management strategy is essential for handling each stream, including energy types (e.g. electric and thermal) and mass flow rates in A-CAES system. Fig.3.2 displays the logic of charging and discharging process of A-CAES system. In this EMOS for A-CAES charging and discharging, several steps are considered:

In this EMOS for A-CAES charging and discharging, several steps are considered:

1. Assessment of the current state of the AST and TES state
2. Assessment of nominal operating range of power conversion unit, including compressor and turbine trains
3. Energy management decision: Decide on storage, import/export, or the possibility of curtailment or deficit (loss of power supply)

A detailed explanation of the developed energy strategy and the interaction among different subsystems within the A-CAES system is provided in the subsequent subsection. This section details the integration of the A-CAES model with a fluctuating renewable energy model and load demand within the energy system environment to test and verify such a proposed strategy and simulation model of A-CAES. Consequently, a comprehensive account of the implementation of the simulation framework is provided, offering a thorough understanding of the dynamic interplay between the A-CAES system, renewable energy fluctuations, and energy demand considerations.

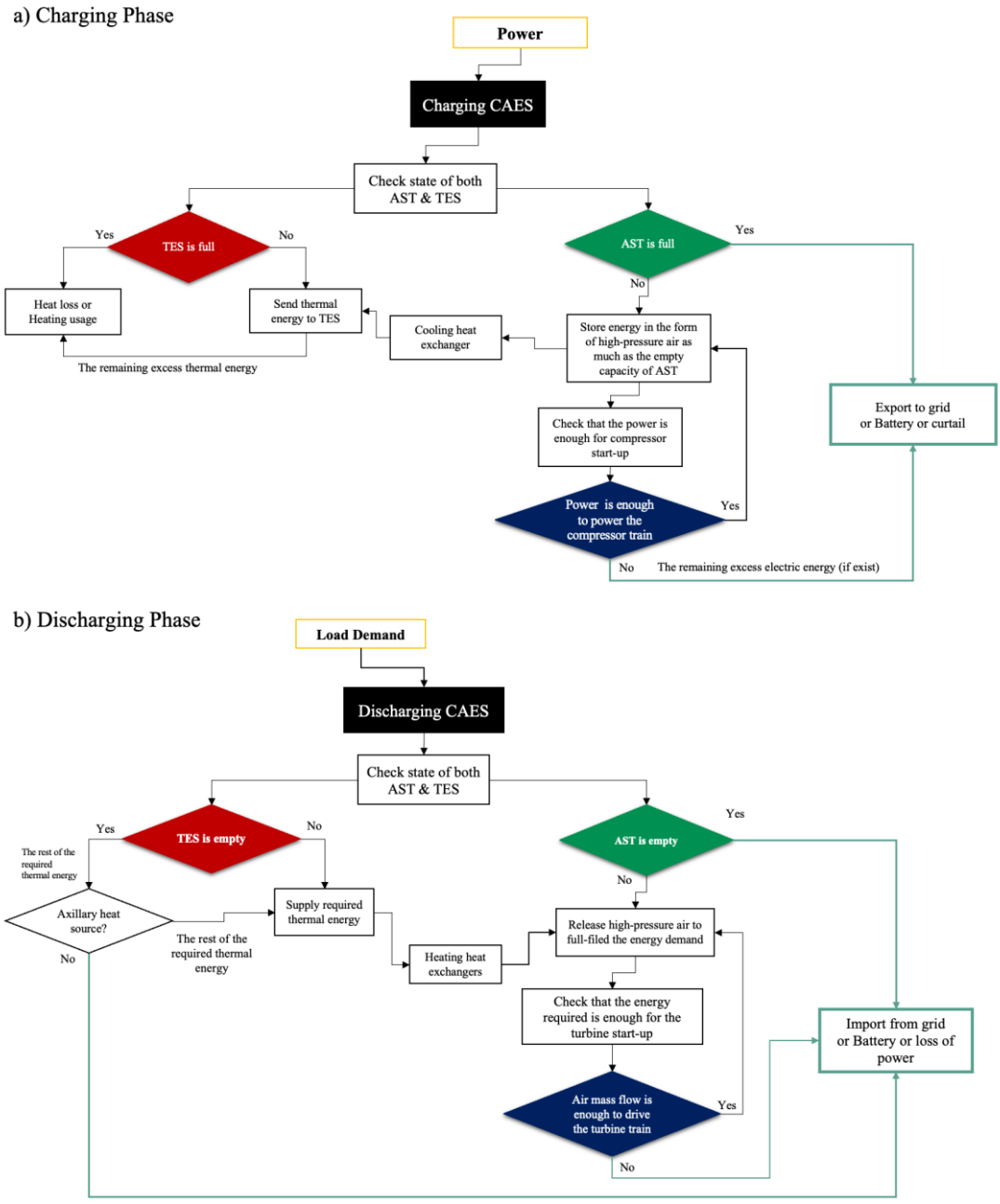

Fig. 3. 2. The logic of improved EMOS for A-CAES system operation

3.2.1.3. Simulation framework

Fig. 3.3a and b demonstrate a simplified flowchart of the T-EMOS and I-EMOS for HES to fulfill the electric load demand of an end-user with the role of renewable penetration. The grid is kept on the least priority and used when either generation units are unable to meet the load demand or there is excess electricity from PV generation, which can be sold back to the grid. As mentioned earlier, in T-EMOSs, A-CAES is treated like a conventional battery where only

the capacity of the energy storage unit, the air reservoir, is considered, as shown in Fig. 3.3a. However, A-CAES also includes power conversion systems. Thus, in T-EMOS, it is assumed that according to the state of the charge (SOC) of the A-CAES system, which is the level of air and its corresponding air pressure in the tank, in charging mode, all the surplus power from the renewables can be stored in the air storage tank until it is fully charged (the tank pressure reaches the maximum allowable pressure of tank). In the discharging mode, A-CAES can deliver energy to satisfy the energy demand until it is fully discharged (the tank pressure reaches the tank's minimum allowable pressure). Therefore, the surplus power that can be stored may violate the power capacity range of the mechanical system (their maximum and minimum power capacity), leading to many problems like choke, surge, etc. Therefore, it is crucial to consider the impacts of inherent fluctuation of renewables and energy demand along with the limitation associated with power conversion units like rated output power of motor/generator and compressors/turbines on the operation of A-CAES, something which is completely neglected in T-EMOS proposed in previous studies [63,84,170]. Furthermore, the function of A-CAES in the presence of TES considering its energy capacity and dynamic behavior, adds several limitations to the operation of A-CAES that should be addressed.

Fig. 3.3b displays I-EMOS considering all components' capacity limitations and the AST and TES dynamic behavior.

The steps of I-EMOS are as follows:

I) Reading the input data, such as characteristics of HES's components and year- around hourly solar irradiance and ambient temperature used to estimate the solar power generation,

II) Comparing the total power generated from renewable sources (W_G) with the electric load demand of end-user (W_L) on an hourly basis during a year,

III) Using the A-CAES/TES system as an energy buffer to store excess energy and compensate for energy shortage. This means that:

A) If the total power generated by solar PV panels is sufficient to satisfy the energy demand of the building, CAES units remain idle (off mode)

B) If the power generated by solar PV panels (W_G) is less than the load demand (W_L), which means the load demand cannot be served only by solar power, then:

- If the air pressure in the tank is more than the minimum allowable pressure ($P_{AST} > P_{AST}^{min}$), it could be released. Thus, the shortage power ($W_{Gap} > 0$) entirely or partially can be provided by A-CAES discharging power while remaining in a range of

working power of the generator and each turbine. Meanwhile, depending on the SOC of the TES tank (SOC_{TES}), the air mass flow rate can be fully or partially heated up using TES if $SOC_{TES} > SOC_{TES}^{min}$. Otherwise, the axillary heating source (e.g., fossil fuels) is needed.

- It should be noted that the discharging air mass flow rate can also be regulated according to TES's state of the charge (SOC_{TES}), eliminating the need for burning fossil fuels as an auxiliary heat source (the red arrow in Fig. 3.3b shows the regulating path).
- On the other hand, when either the air pressure in the tank is less than the minimum allowable pressure ($P_{AST} < P_{AST}^{min}$) or the desired load violates the operating range of turbines, generators, and TES capacity, in such cases, A-CAES is not able to provide the remaining demand entirely. Therefore, the power grid can compensate for the rest of the load demand.

C) If solar power generation (W_G) is greater than the load demand (W_L), there is excess power ($W_{Gap} < 0$), then:

- If the air pressure in the tank is lower than the maximum allowable pressure ($P_{AST} < P_{AST}^{max}$), the AST is not full. Then the excess power ($W_{Gap} < 0$) can be fed into A-CAES to charge it fully or partially, considering the motor's operating power range and the design air mass flow rate of each compressor. Meanwhile, depending on the SOC_{TES}, the heat energy generated during compression can be stored in a hot water tank when $SOC_{TES} < SOC_{TES}^{max}$. Otherwise, only a part of thermal energy can be stored, and the rest is dissipated or sent for other usages.
- On the other hand, when the AST is full ($P_{AST} > P_{AST}^{max}$) or the excess electricity violates the operating range of the motor, compressors, and TES, A-CAES cannot store the extra energy. Thus, the remaining excess energy is exported to the electric grid.

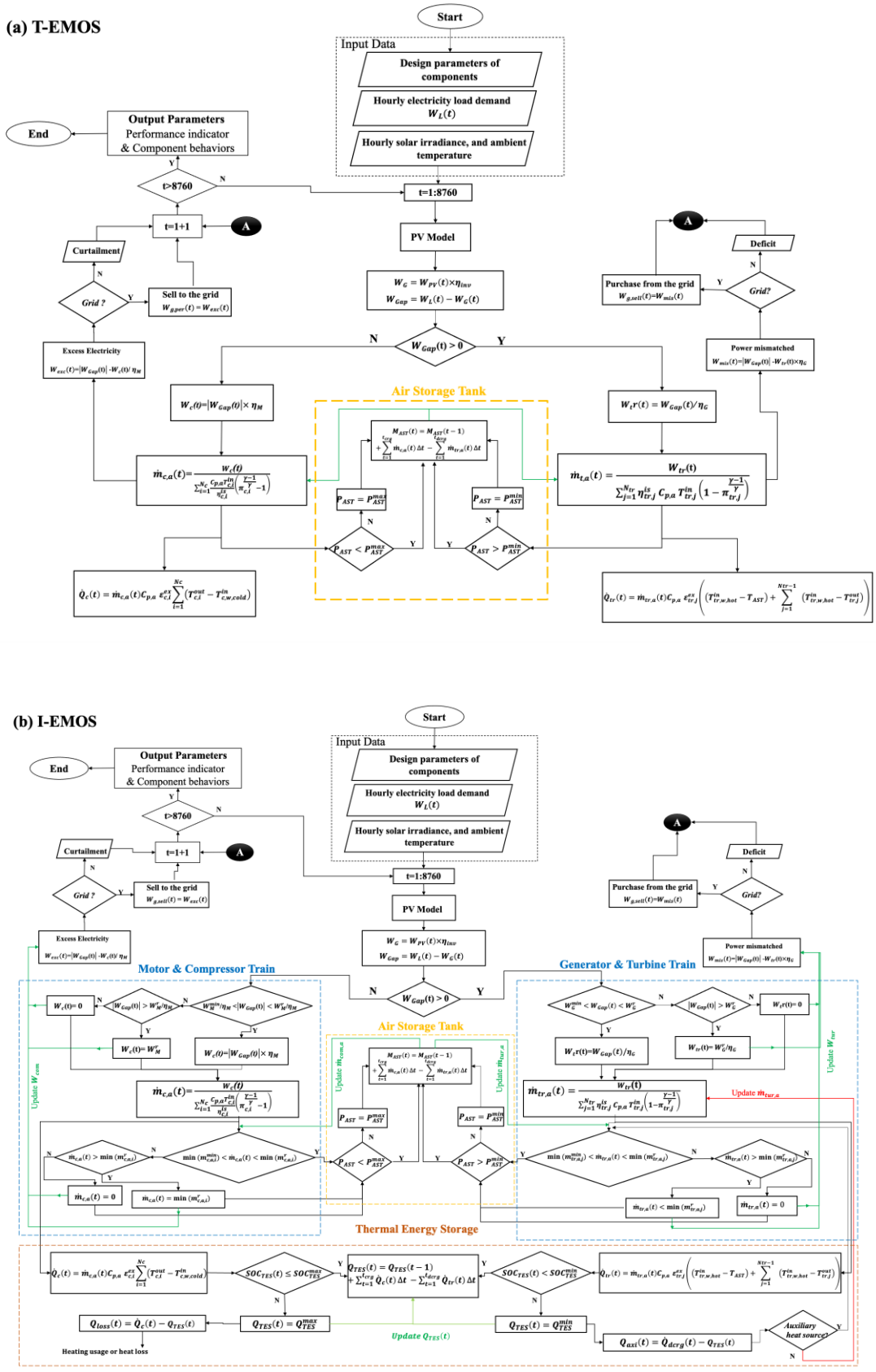

Fig. 3. 3. Flow diagram of two EMOSs of the A-CAES in grid-connected PV-based hybrid system for decentralized application a) T-EMOS, and b) I-EMOS.

3.2.1.4. Key performance indicators (KPIs)

Several indicators are defined to analyze the performance of the proposed HES. They are listed as follows:

1) Roundtrip efficiency of A-CAES (RTE), which refers to both cycle (RTE_{CAES_cycle}) and integrated efficiency (RTE_{CAES_int}) of A-CAES as a ratio of total expansion work to the total compressor work during a complete cycle and over a year (8760 hr), respectively [84].

$$RTE_{CAES\_cycle} = \frac{\sum_{t=1}^{t_{CAES,dcrg}} W_{CAES,dcrg}(t)}{\sum_{t=1}^{t_{CAES,crg}} W_{CAES,crg}(t)} \quad (3.25)$$

$$RTE_{CAES\_int} = \frac{\sum_{t=1}^{8760} W_{CAES,dcrg}(t)}{\sum_{t=1}^{8760} W_{CAES,crg}(t)} \quad (3.26)$$

2) Load coverage ratio of A-CAES (LCR_{CAES}), refers to the percentage of total building electricity load covered only by A-CAES. So, it is defined as the ratio of total turbine/generator work to the total building energy demand over a year [28]:

$$LCR_{CAES} = \frac{\sum_{t=1}^{8760} W_{CAES,dcrg}(t)}{\sum_{t=1}^{8760} W_L(t)} \quad (3.27)$$

3) Storage ratio of A-CAES (SR_{CAES}), reflects the percentage of total solar power generation stored in A-CAES. So, it is defined as the ratio of total compressors/motor work to the total renewable generation over a year and given by:

$$SR_{CAES} = \frac{\sum_{t=1}^{8760} W_{CAES,crg}(t)}{\sum_{t=1}^{8760} W_G(t)} \quad (3.28)$$

4) Electrical load management ratio (ELMR) implies the percentage of the total load demand (W_L) satisfied by energy coming from renewables (W_G) and A-CAES ($W_{CAES,d\mathrm{crg}}$). So, it is defined as follows [225]:

$$ELMR = \frac{\sum_{t=1}^{8760} min(W_G(t), W_L(t)) + W_{CAES,dcrg}(t)}{\sum_{t=1}^{8760} W_L(t)} \quad (3.29)$$

5) Import and export ratio, which reflects the percentage of building energy demand met by the electric grid (IMR) and the percentage of total renewable production exported to the electric grid (EXR), respectively[132]:

$$IMR = \frac{\sum_{t=1}^{8760} W_{g,per}(t)}{\sum_{t=1}^{8760} W_L(t)} = \begin{cases} \frac{\sum_{t=1}^{8760} W_L(t) - (W_G(t) + W_{CAES,dcrg}(t))}{\sum_{t=1}^{8760} W_L(t)} & W_L(t) > W_G\ (t) \\ 0 & W_G(t) > W_L(t) \end{cases} \quad (3.\ 30)$$

$$EXR = \frac{\sum_{t=1}^{8760} W_{g,sell}(t)}{\sum_{t=1}^{8760} W_G(t)} = \begin{cases} \frac{\sum_{t=1}^{8760} W_G(t) - (W_L(t) + W_{CAES,crg}(t))}{\sum_{t=1}^{8760} W_G(t)} & W_G(t) > W_L(t) \\ 0 & W_L(t) > W_G\ (t) \end{cases} \quad (3.\ 31)$$

3.2.2. Case study

In this section, the Concordia university, a high energy-intensive educational building located in Sir George Williams Campus in downtown Montreal (Quebec- Canada), is selected as a case study. To have a close look on A-CAES operation under proposed EMOSs, in this section, the Gina Cody School of Engineering and Computer Science (GCS_ENCS) 's electricity consumption is considered the only source of load demand. According to the measurement, the total annual electricity demand is 4,500 MWh, and the average hourly and daily electricity demand over a year are 513.5 kWh and 12.5 MWh, respectively.

Solar radiation information is obtained from the NASA surface meteorology and solar energy database for the city of Montreal [226] according to the location of the case study, 45°50′ N of latitude and 73°56′W of longitude. The total yearly solar radiation is 1308 kWh/m^{2,} and the annual average daily solar radiation is 3.58 kWh/m^2/day.

Hourly temperature data was obtained from the Montreal weather stats website [227]. The annual average temperature is 5.67°C.

The hourly energy demand, solar radiation, and air temperature over a year are presented in Fig. 3.4. Fig. 3.4 displays the hourly electricity demand profile of the GCS_ENCS (a), Montreal city's hourly solar radiation (b), and hourly air temperature (c) over one year.

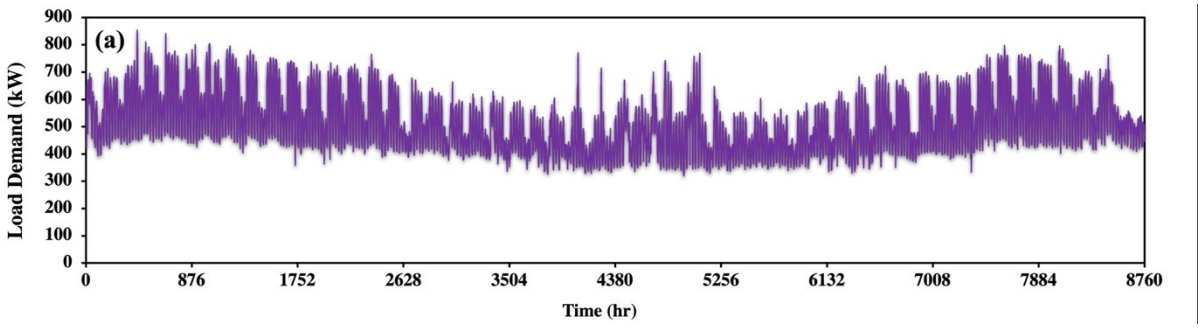

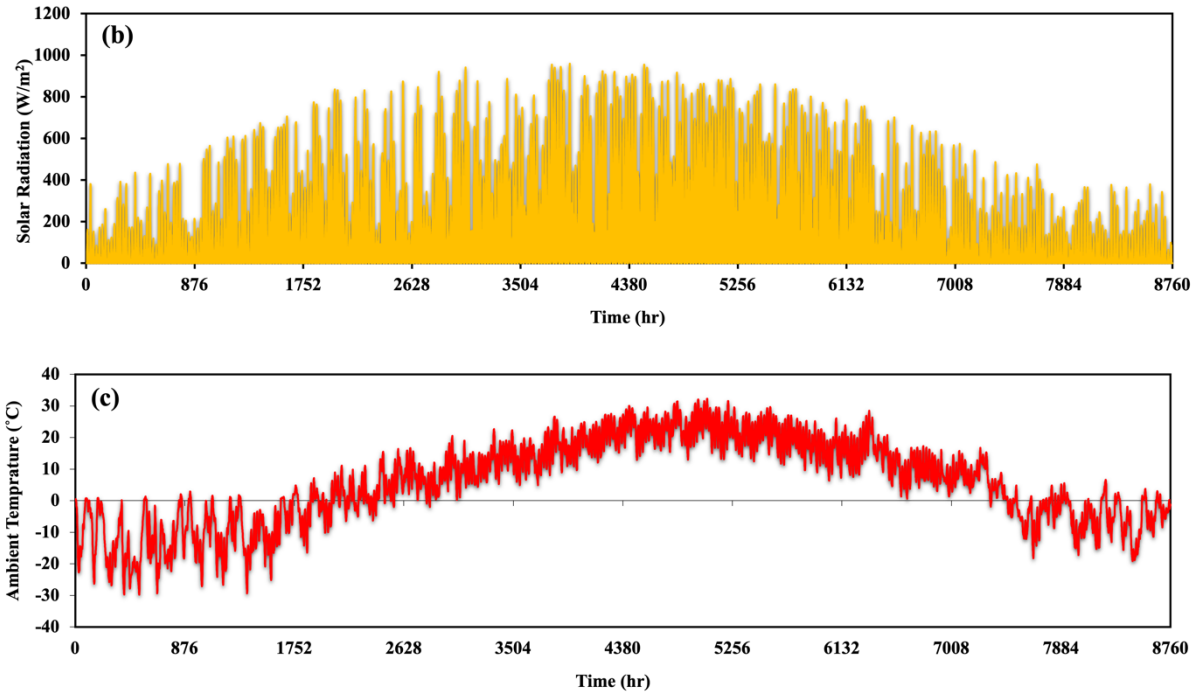

Fig. 3. 4. a) Hourly electricity demand profile, b) Montreal city's hourly solar radiation and hourly air temperature over one year in 2019.

3.2.2.1. Design conditions of components

In order to determine the HES configuration and evaluate its performance under the proposed EMOSs, input data and constraints are required. The information of the selected PV panel is listed in Table 3.1. According to the available roof area of 23,260 m^2 [228] and surface area of selected PV (around 1.64 m^2) [63], the maximum number of 14182 solar panels can be installed.

Since the A-CAES type used in this study has the closest similarity with the small-scale TICC-500 A-CAES pilot plant in terms of the type of compressor/turbine train, AST, and TES, the overall characteristics of this pilot plant [229] are considered as the reference for A-CAES configuration to validate the developed model. TICC-500 plant is the world's first multi-stage A-CAES demonstration plant with a 500 kW generation capacity and optimal electric efficiency of 37% [6], which was designed and built mainly for load shifting and RES utilization applications [229].

Fig. 3.5 shows the process flow diagram of the TICC-500 A-CAES pilot plant used in this study [27,221]. It includes a five-stage compressor train with the 315 kW driven motor, a three-stage turbine train with a single-shaft arrangement, a 500 kW generator, and two 50 m^3 steel tanks to store pressurized air with a working pressure ranging from 2.5 to 10 MPa [27]. It has

a regenerative heat unit, including cooling/heating heat exchangers, and a double- hot/cold water tank as a TES unit with pressurized water as a thermal medium. The volume of hot/cold water tanks is 12 m^3 with the corresponding designed temperatures of 120 °C and 45 °C, respectively [27,221]. Other required input data and constraints for compressors and turbines of CAES are listed in Table 3.2. In this section, one AST with a total volume of 100 m^3 is considered. Moreover, the minimum required power for compressor/turbine operations has been assumed to be 30% of their rated power capacity (listed in Table 3.2).

It is worth mentioning that the design parameters' values for all components of T-EMOS and I-EMOS are the same.

Table 3. 1. The specifications of the PV panel used in this study [63].

Term (Parameter)	Value
Panel type	Trina Solar Honey Plus TSM-DD05A (II)
Module material	Monocrystalline silicon
Panel dimensions/Cell number	1650 mm (L) * 992 mm (W) * 35 mm (H)/60
Maximum power	300 W
Open circuit voltage	39.8 V
Short circuit voltage	9.77 A
Maximum power point voltage	32.5 V
Maximum power point current	9.19 A
Module efficiency	18.3 %
NOCT	44 C
Temperature coefficient at maximum power	-0.0039/C

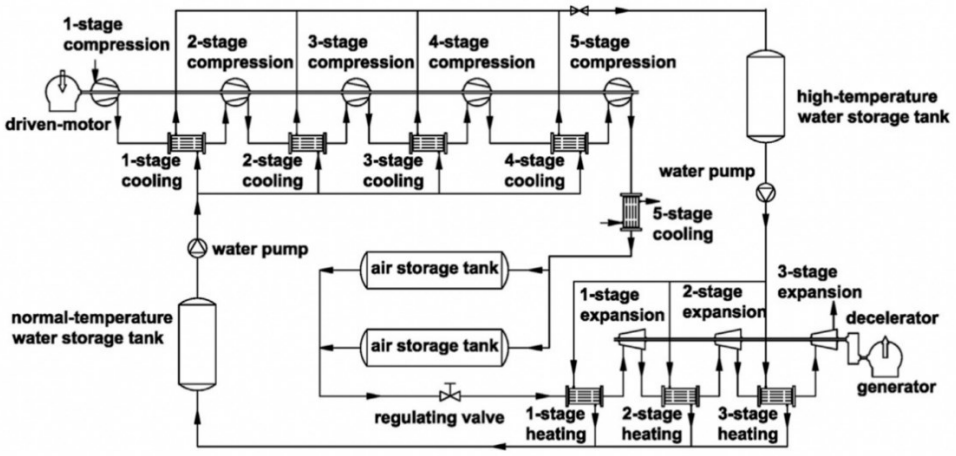

Fig. 3. 5. Process flow diagram of the TICC-500 A-CAES pilot plant used as a reference in this study [221].

Table 3. 2. The design parameters of each stage are compression and expansion [27,221].

Stage	Inlet pressure (MPa)	Outlet pressure (MPa)	Pressure ratio	Inlet temperature (°C)	Outlet temperature (°C)	Adiabatic Efficiency (%)	Shaft power (kW)
Compressors (i)							
1	0.1	0.35	3.5	25	153.0	74.4	76.7
2	0.34	0.91	2.67	45	146.7	77.5	59.4
3	0.89	2.40	2.69	45	147.6	80.5	57.8
4	2.35	5.80	2.46	45	142.2	82.4	49.4
5	5.72	11.23	1.96	45	109.1	83.0	36.3
Turbines (j)							
1	2.50	1.13	0.45	100	35	82.6	150.5
2	1.12	0.40	0.35	100	25	81.0	185.5
3	0.39	0.1	0.25	100	0.5	81.6	236.3

3.2.3. Results and discussions

The mathematical model mentioned in Section 3.3.1.1 and the EMOSs framework demonstrated in Section 3.3.1.3 as well as performance criteria defined in section 3.3.1.4 are implemented in MATLAB (version R2022a) [230] for system detailed analysis and discussion. To verify the model, the effects of the AST's volume and maximum pressure, and the TES's capacity on the HES performance are investigated. To assess the EMOSs and long-term operation of decentralized A-CAES system's integrated with HES in satisfying the electric energy demand, a yearly energy consumption profile and year-around solar availability are required (Fig.3.4)

3.2.3.1. Model validation

Regarding the validation of the developed models, the simulation result from running the model of A-CAES in the hybrid system under an I-EMOS is compared with the T-EMOS while validating by the tested results from the TICC-500 pilot plant. Table 3.3 presents the results from the proposed models and measured parameters of TICC-500 for A-CAES over a complete charging/discharging cycle at the design condition.

Since the considered design parameters and configuration of A-CAES under both EMOSs are the same (as presented in section 3.3.2.1), the cycle efficiency of A-CAES under T-EMOS and I-EMOS is almost the same and around 37%, which is close to the TICC-500 plant efficiency. However, the values of other parameters, particularly charging time, rated air mass flow rate, and generated thermal power of the compressor train, are far different under two

EMOSs, as listed in Table 3.3. It is worth noting that the cycle efficiency of A-CAES is mostly dependent on its design parameters and almost independent of the energy management strategy. As seen in Table 3.3, the result from I-EMOS and measured data of the TICC-500 facility are well-matching with an average of 94.6% similarity. Notably, the average errors of the parameters are about 5.4 % and 33.5% for I-EMOS and T-EMOS cases, respectively.

Table 3. 3. Comparing the results from the current EMOSs and measured parameters of the TICC-500 A-CAES pilot plant

	Current EMOS		TICC-500 [27,221]	Error %	
	T-EMOS	I-EMOS		T-EMOS	I-EMOS
A-CAES Cycle efficiency (RTE_{CAES_cycle})	37.4 %	37.3 %	37% (opt)	1	0.8
Charging time ($t_{CAES,crg}$)	1.35 hr	5.45 hr	5.59 hr	75.8	2.5
Discharging time ($t_{CAES,dcrg}$)	1 hr	1.07 hr	1.03 hr	2.9	3.7
Rated air mass flow rate of the compressor train ($m^r_{c,a}$)	6280 kg/hr	1547.6 kg/hr	1600 kg/hr	74.5	3.3
Rated air mass flow rate of the turbine train ($m^r_{tr,a}$)	8540 kg/hr	8540 kg/hr	8600 kg/hr	0.7	0.7
Rated generated thermal energy in charging	716 kW	178 kW	134 kW	75.1	24.8
Rated supplied thermal energy in discharging	635 kW	587 kW	600 kW	5.5	2.1

It is worth noting that the similarity between the results of T-EMOS (with 1 hour discharging time) and I-EMOS (with 1.07 hour discharging time) in the discharging process is due to the

generator/ turbine train characteristics of the TICC-500 pilot plant, designed to discharge 555 kWh energy to the power grid during 1.03 hour [27].

Fig. 3.6 also shows the dynamic behavior of air pressure inside the AST resulted from the simulation model and experimental case of TICC-500 plant for a charging/discharging cycle. As shown in Fig. 3.6a, the experimental results of the TICC-500 facility indicate that the air pressure of the air storage tank increased approximately linearly from 3.36 MPa to 9.34 after 4.3 hours during the charging process at design condition with an average air mass flowrate of 1554 kg/hr [221]. However, the simulation results of the TICC-500 plant showed that it takes 5.59 hours to fully-charge the air storage tank during which the AST pressure increases from 2.5 MPa to 10 MPa at design condition [27]. According to Fig. 3.6a, a similar charging behavior can be seen under I-EMOS when the motor/compressor train work at their full-load condition, occurring at the time when the excess PV power is higher than their nominal power capacity. In contrast, the different behavior for AST pressure can be seen under T-EMOS during the charging process. Therefore, at the time when there exists a high excess PV power, more than the rated power capacity of the compression unit, the motor/compressor train tends to send a massive amount of compressed air with a mass flow rate of 6280 kg/hr to fully charged the air storage tank in less than 2 hours.

As shown in Fig. 3.6b, during discharging process experiment, the AST pressure decreased from 8.65 MPa to 3.05 MPa in less than 1 hour with an average mass flowrate of 7760 kg/hr (10% less than the rated value) to generate stable power [221]. Comparing the experimental result with the results from the proposed simulation model indicates that, for T-EMOS case, at the highest load demand, the air storage is fully discharged after 1 hour, disregarding the generator power capacity limitation (500 kW). However, under I-EMOS, although the rated mass flowrate of 8540 kg/hr is achieved for a turbine train with a shaft power of 550 kW, the maximum mass flowrate of around 7896.1 kg/hr passes through the turbine-generator unit to reach 500 kW of power. Therefore, it takes 1.07 hr to fully-discharge the air storage tank (reaching from 10 MPa to 2.5 MPa) and generate more than 500 kWh of electricity. A similar behavior was reported in discharging process of the TICC-500 plant takes about 1.03 hours to generate 555 kWh to the power grid.

In summary, the results show that, in addition to AST, the operational capacity limitations of power conversion units and TES must be carefully considered to reach an improved operational profile for A-CAES. In case of I-EMOS, charging time, rated air mass flow rate of compressor train, maximum heat stored by TES per hour of charging, and dynamic behavior of

AST are very close to the measured data and experimental results of the existing plant. Conclusively, this proposed model and I-EMOS can serve as benchmarks for long-term operation and performance analysis (energy flow analysis) of A-CAES systems with different characteristics and for different applications.

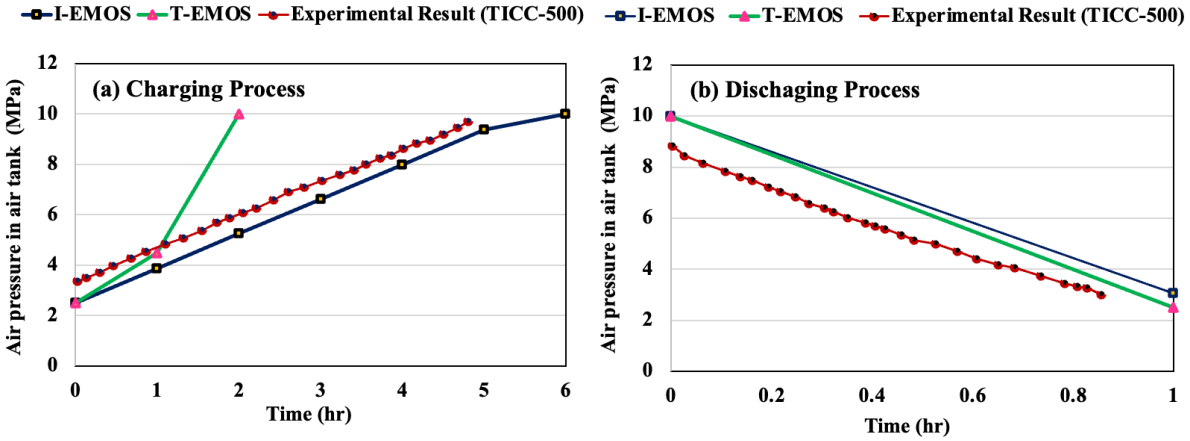

Fig. 3. 6. Air pressure in an air storage tank during (a) charging process and (b) discharging process under I-EMOS and T-EMOS versus the experimental result of TICC-500 A-CAES pilot plant at the design condition [221].

3.2.3.2. A-CAES operation under both T-EMOS and I-EMOS

PV is used as the primary electricity source to meet the case study's energy demand. At first, the PV's excess electricity is assumed to be utilized by compressors to pressurize the air and store it in the AST, considering the AST and operating power range of the motor/compressors. On the other hand, PV supply shortage is firstly compensated by the A-CAES system's turbine trains to satisfy the entire or a part of the unmet energy demand. In order to analyze the transient behavior of A-CAES under I-EMOS and T-EMOS, one week in January as a peak month of energy consumption is selected. Fig. 3.7 and Fig. 3.8 indicate the behavior of the main operating parameter of A-CAES under I-EMOS and T-EMOS for seven days in January, respectively. The red arrow in Fig. 3.7 implies the similarity between the PV generation profile and A-CAES behavior, while the black arrow shows the violation of parameters from their rated values. Depending on the fluctuating excess solar power and shortage load demand, the charging/ discharging air mass flow rate and works of compressors/turbines can get different values. At the time when the charging/ discharging air mass flow rate is more than the rated mass flow rate of compressors/ turbines or when the compressors/turbines operate over their nominal capacity, the violation happens. Violation can be calculated by taking the difference between the parameters' current values (in operation) and their nominal values presented in

Tables 3.3. Such a violation for main operating parameters can be observed under T-EMOS in Fig. 3.7 for compressors/turbines work, charging/ discharging mass flow rate, and later in Fig. 3.9a for charging/discharging thermal energy to/from TES. Fig. 3.7a and Fig. 3.8a illustrate the PV output electricity generation and the electric load demand profile of the building. As can be seen, the behavior of A-CAES under two EMOSs differs, particularly on their compression side. It is worth mentioning that the integration of A-CAES requires compressors and turbines to be adjusted by renewable and end-user energy demands. The operation of CAES under this condition often causes it to work unsteadily and over/under a range of operating conditions (its nominal power and energy capacity) as shown in Fig. 3.7 by the red arrow and black violation arrow at some points. In the real world, mentioned phenomena cause choke/surge problems in the mechanical sub-system and increase the risk of CAES failure, jeopardizing HES reliability. In Fig. 3.7b, energy used by the compressor and charging air mass flow rate has the same trend and behavior as PV excess output power. Since the operating range of motor/compressors is not considered in T-EMOS, compressors tend to consume the whole amount of available excess electricity, even less amount, to charge the AST with pressurized air considering only the air pressure state in the tank (as shown by the red arrows at some points in Fig. 3.7).

It can be noticed that the excess solar energy, compressors' operation, and air mass flow rate have the same behavior all the time. For instance, according to the plots in Fig. 3.7, the five compressors (with positive work in Fig. 3.7b) utilize all PV excess electricity from hours 150 to 160 to compress the air for charging the empty AST. However, at around hours 252, 276, and 300, compressors consume a massive amount of PV excess energy for 1 hour until the AST is fully charged and reaches the maximum allowable pressure of 10 MPa (Fig. 3.7d).

Nevertheless, as shown by black arrow in Fig. 3.7b, operational work of each compressor violates from its nominal capacity presented in Table 2. The rest of the excess electricity is exported to the grid. Meanwhile, the hourly charging air mass flow rate of 6280 kg/hr violates the rated air mass flow rate of the compressor train, which is 1600 kg/hr, as reported in Table 3.3. Under T-EMOS, compressors, and turbines even start operating to consume and generate energy less than the minimum power (it is supposed to be 30% of rated power) that they need to start running, as seen around hour 230 in Fig. 3.7. During night, when there is no PV power generation, the electrical demand is satisfied by the energy released by the turbines (with negative work in Fig. 3.7b). Turbines/generators also have the same behavior. They tend to discharge air mass as much as is available in the AST to generate the electricity required by the end-user.

Such an A-CAES operation often causes compressors and turbines to work out of their design condition and operating range, leading to failure and surge/choke problems [168]. It seems that, under T-EMOS, one big compressor and one giant turbine are considered, which can charge and discharge a specific amount of energy depending on excess electricity and load demand during a short charging/discharging time, considering the AST's SOC.

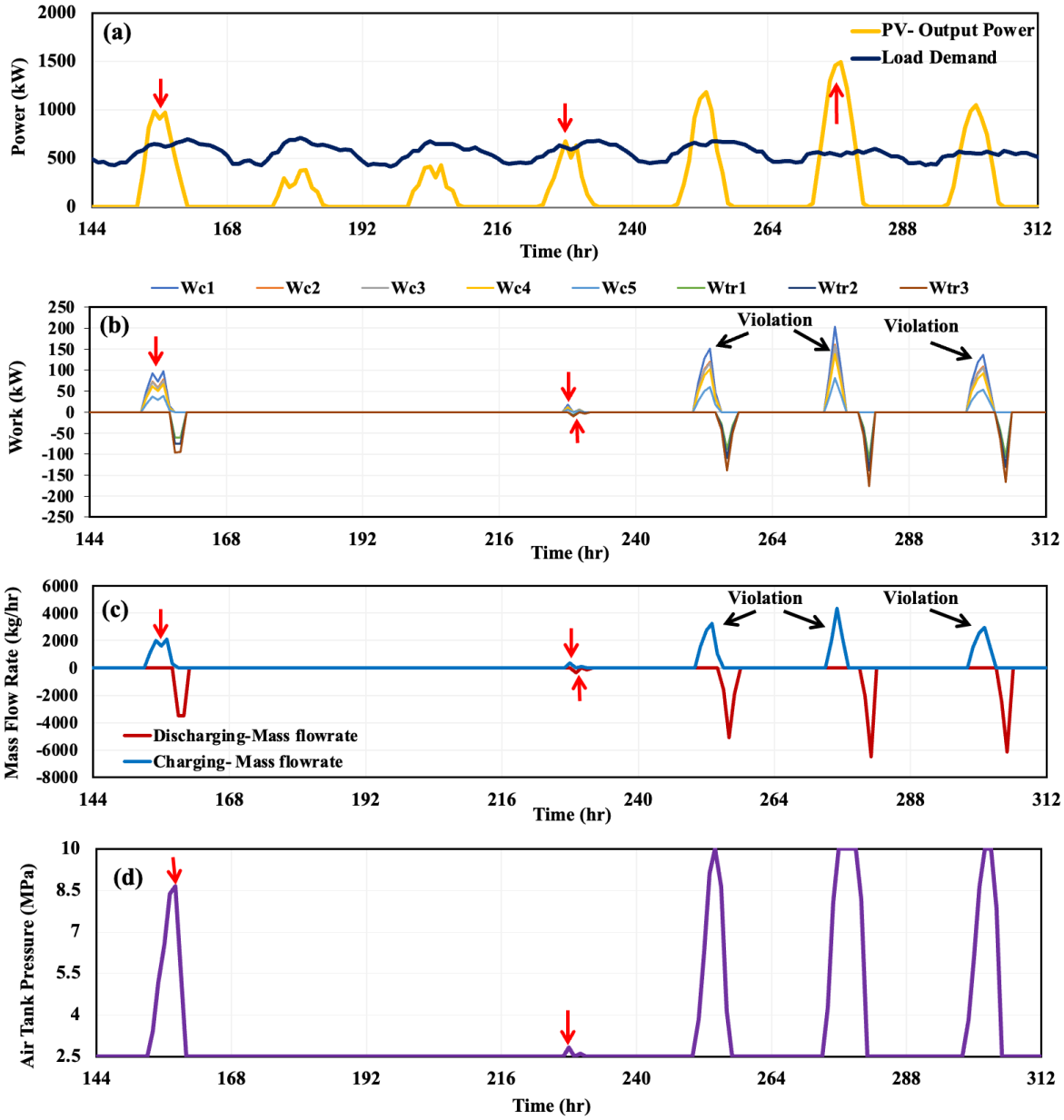

Fig. 3. 7. Hourly behavior of the main operating parameters of A-CAES under T-EMOS during one week in January.; a) PV output power and load demand, b) work of turbines and compressors, c) charging/discharging mass flow rate, and d) dynamic behavior of AST.

While in practice, compressors can use excess electricity as much as their nominal power in each hour. Therefore, despite T-EMOS, the maximum charging time of A-CAES under I-

EMOS is around four times more than that of T-EMOS. Thus, it takes nearly 5.45 hours to fully charge the AST from a minimum pressure of 2.5 to a maximum allowable of 10 MPa under I-EMOS. Hence, adopting the whole characteristics and limitations of power conversion units in EMOS causes A-CAES to work differently and close to the existing A-CAES pilot plant and protect it from any type of failure.

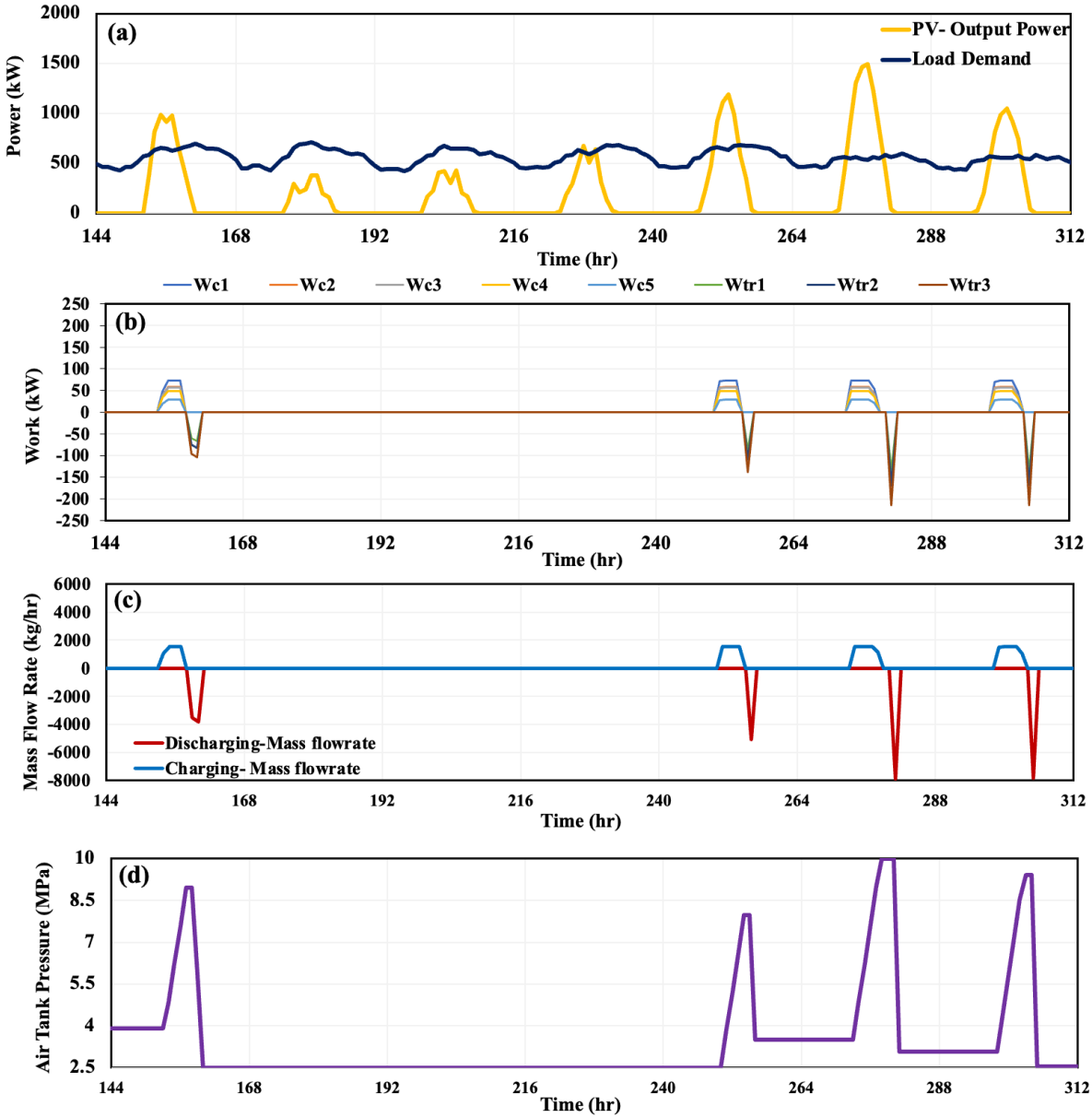

Fig. 3. 8. Hourly behavior of the main operating parameters of A-CAES under I-EMOS during one week in January.; a) PV output power and load demand, b) work of turbines and compressors, c) charging/discharging mass flow rate, and d) dynamic behavior of AST.

From Fig. 3.8b is evident that five compressors and three turbines are working at their operating range (equal to or less than their nominal power capacity and more than the least

power they need to start operating). In fact, the AST can be charged for a maximum of 5.45 hours depending on available excess electricity and SOC of the AST. Furthermore, A-CAES remains in idle mode when the extra energy from PV and deficit energy demand are less than the minimum power required by the compressor and turbine train's start-up power. For example, in Fig.3.8 b, c, and d, around hour 230, A-CAES does not work under I-EMOS compared to its operation under T-EMOS shown in Fig. 3.7.

Besides, as shown in Fig.3.8b, c, and d, at around hours 252 and 300, since excess PV power is not sufficient for being used by compressors, the AST is not fully charged. While at around hour 276, when the excess electricity is enough and even more, the AST can be completely charged. On the other hand, at night and whenever there is no solar energy, turbines can generate electricity depending on the air availability in the AST and the minimum air mass flow rate they need to operate. This fact is the reason behind the behavior of the AST (not getting fully discharged) at the time around hours 255, and 280 (Fig. 3.8d).

3.2.3.3. A-CAES cycling metrics

The A-CAES system's key cycling metrics, such as the number and duration of charging /discharging time (ramp-up and ramp-down period) under both EMOSs, are estimated and compared in Table 3.4. It is observed that, generally, the A-CAES undergoes several full and partial charge/discharge cycles to follow the electric energy supply/demand profile. However, the metrics' values differ under both EMOSs. Since the charging time of A-CAES under I-EMOS is around four times more than that under T-EMOS, the operating time of the compressor train under I-EMOS is higher (approximately 500 hours more). In comparison, the working time of the turbine train under T-EMOS is 1.6 times higher than that under I-EMOS over a year. The reason is that, under T-EMOS, A-CAES follows the supply/demand profile, and sometimes it tends to charge/discharge energy even if the amount of required energy is lower or higher than the minimum and maximum operating rated power of compressors and turbines, respectively. That's because, in T-EMOS, the capacity limitation of power conversion units (compressors and turbines) are not considered, which is one of the main difference between T-EMOS and I-EMOS. Therefore, the number of times that ramp-up/ ramp-down is needed under T-EMOS is more than that under I-EMOS. This fact is the same for the required full charge/discharge. Accordingly, around 266/330 and 186/174 required yearly full charge/discharge are estimated for A-CAES under T-EMOS and I-EMOS, respectively. This must be considered a significant factor in the A-CAES design, mainly when it is used for

decentralized applications where it must be adjusted with the energy supply/demand profile. Calculating accurate values for each metric is also essential in the case of maintenance planning and degradation of A-CAES systems for a long time.

Table 3. 4. A-CAES cycling metrics for one year.

Metrics	EMOSs	
	T-EMOS	I-EMOS
Operating time compressor train	1080	1577
Operating time turbine train	748	470
Number of times Ramp-up is needed	338	325
Number of times Ramp-down is needed	338	300
Number of full charges	266	186
Number of full discharges	330	174
Longest duration of charging	1.35	5.45
Longest duration of discharging	1.00	1.07

3.2.3.4. TES operation

It is assumed that in A-CAES, heat generated by compressors is stored in TES during the charging phase and reused by turbines during discharging phase. Based on the TICC-500 specifications [221] and Eq. (3.21), the maximum capacity of TES is calculated at around 1047 kWh, and the maximum hourly stored/delivered heat by TES during charging/discharging is 134 kWh / 600 kWh (because the rated thermal energy transferred in cooling/heating heat exchangers are 134 kW/600 kW, respectively). Therefore, according to the Table 3.3, the hourly stored/delivered thermal energy under both EMOSs is different because their charging/discharging times are not the same. This fact can be observed in Fig. 3.9, which shows rated generated/supplied heat in charge/discharge phases of A-CAES under T-EMOS and I-EMOS over a year. It can be seen under both EMOSs, generated/required heat profiles are similar to their compressor/ turbine train behavior. Therefore, under T-EMOS (Fig. 3.9a), a considerable amount of heat (maximum 716 kWh) generated by the compressor train should be stored in the TES during only one hour, which is far from the TICC-500 plant (maximum 134 kWh). The reason is the lack of consideration of power conversion units' capacity limitations under T-EMOS. However, under I-EMOS, the maximum hourly thermal energy of 178 kWh can be sent to the TES, which is close to 134 kWh of TICC-500 units (around four times less

than T-EMOS). Similarly, in discharging phase, the maximum thermal energy of 587 kWh is required over one hour under I-EMOS but 635 kWh under T-EMOS.

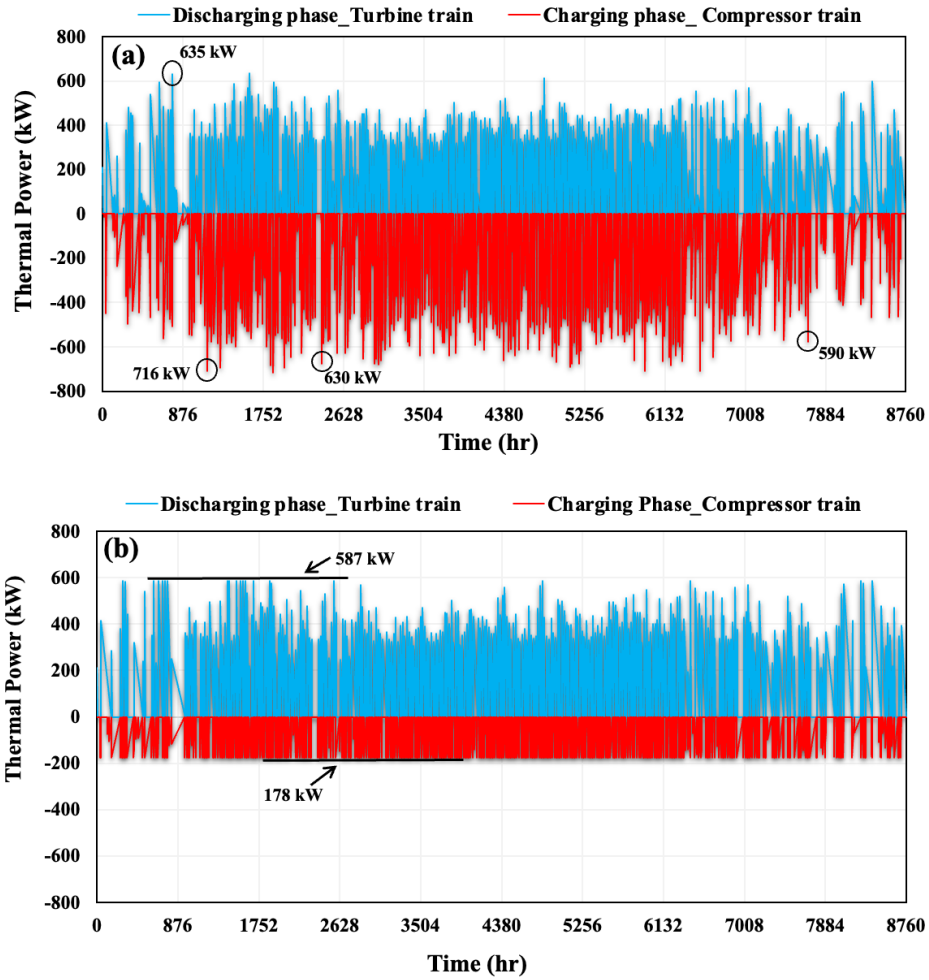

Fig. 3. 9. Thermal power generated in charging phase (red) and supplied in discharging phase (blue) over a year under two developed EMOSs: a) T-EMOS and b) I-EMOS.

Fig. 3.10 also illustrates the hourly thermal energy flow in the system under I-EMOS, including generated/supplied thermal power, SOC of TES (in kWh), and amount of heat loss/ required auxiliary heat during the compression/ expansion phase for one week in January. However, depending on the SOC of TES, a part of the thermal energy generated in the compression phase might be stored (Fig. 3.10b), and the rest is lost or used for other thermal applications (Fig. 3.10c). Moreover, it is shown that the thermal energy stored in TES is enough for the expansion phase, and there is no need for additional auxiliary heat sources. Observing TES behavior plays an essential role in designing and analyzing the A-CAES function, especially when it is linked to the heating and cooling demand of end-users.

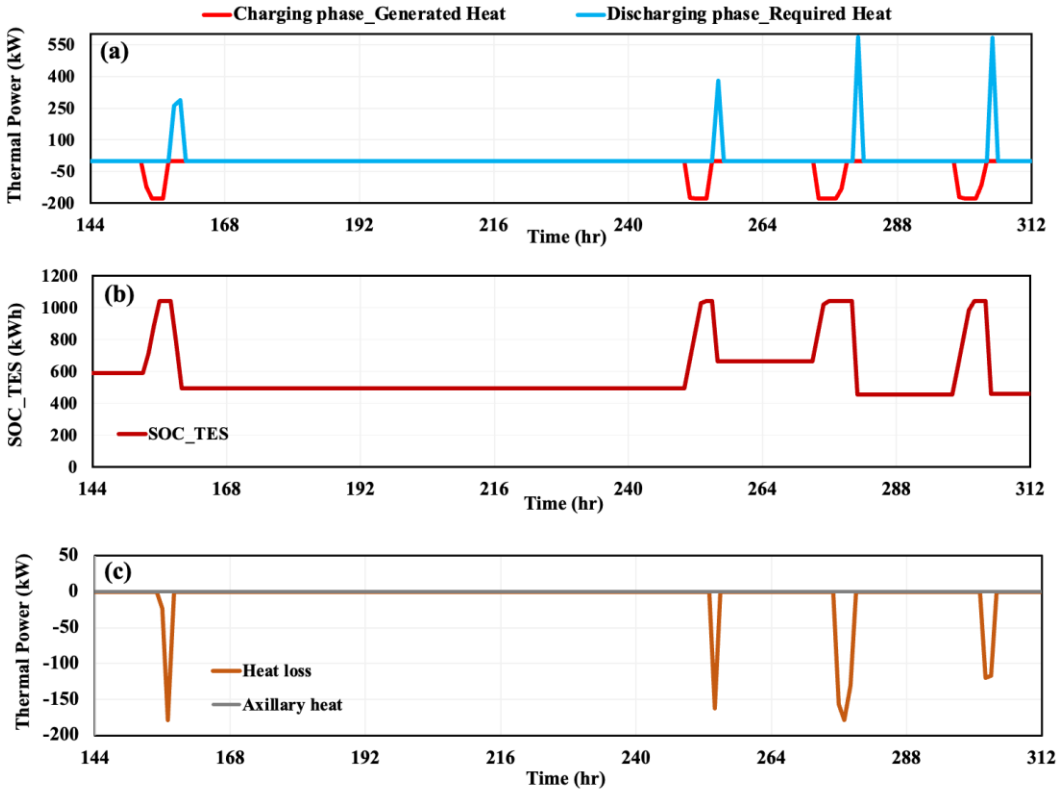

Fig. 3. 10. Hourly a) generated/required thermal power, b) SOC of TES (in kWh), and c) amount of heat loss/ required auxiliary heat during the compression/ expansion phase under I-EMOS for one week in January.

3.2.3.5. Energy and power balance analysis

Fig. 3.11 displays the hourly power balance of the proposed HES with several sources of energy (solar PV, CAES, TES, power from the grid, and power to the grid) and the building load demand during four days in January under both EMOSs. As can be seen, in many situations, power derived from solar PV panels does not meet the electric load demand of the building. Therefore, the other available energy sources must be used to meet the load demand. It can be noticed that A-CAES operation affects the performance of the whole system. For example, according to Fig. 3.11a, during the 10^{th},11^{th}, and 12^{th} days, the compressor of A-CAES and excess PV production have the same behavior. However, they have different trends under I-EMOS in Fig. 3.11b. Besides, different behaviors of A-CAES and other components in the proposed HES on each day can be observed in Fig. 3.11. For instance, on day 9^{th}, since there is no excess PV production and stored energy in the AST, A-CAES does not work in Fig. 3.11a and Fig. 3.11b. On the 10^{th} day, under T-EMOS (Fig. 3.11a), A-CAES starts charging and discharging with a low amount of energy, while under I-EMOS (Fig. 3.11b), it cannot begin

operating since the amount of power is less than the minimum required power for compressor/turbine start-up. Therefore, the electrical energy is exchanged with the grid.

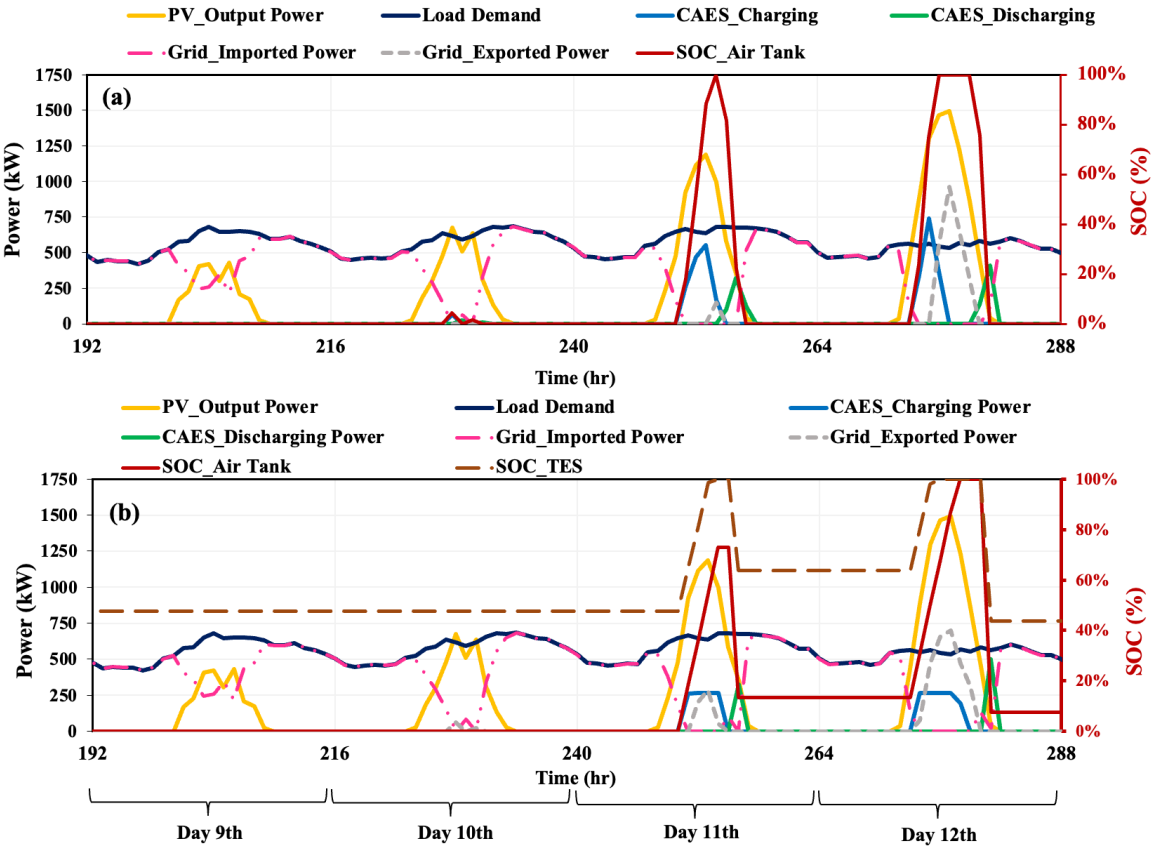

Fig. 3. 11. Hourly power balance of the proposed HES for four days in January under both EMOSs a) T-EMOS and b) I-EMOS.

The main difference between the two studied EMOSs can be observed on days 11th and 12th. The behavior of different energy sources on days 11th and 12th can explain the importance of considering the capacity limitation of the power conversion unit of A-CAES. For example, in Fig. 3.11a, as can be seen, the compressor train uses excess PV production as much as the remaining capacity of the AST, and the rest of the solar PV output is sold to the grid after the AST is fully charged.

However, under I-EMOS in Fig. 3.11b, charging the AST and exporting power to the electrical grid occur simultaneously. Therefore, this operation impacts the AST's behavior. So, during discharge time, when PV production is not enough AST is fully discharged under T-EMOS, opposite to the I-EMOS under which the AST is not fully discharged because the remaining air in the AST does not create the minimum required mass flow rate for turbine operation. The SOC of TES is also displayed in Fig. 3.11b under I-EMOS, in which the

limitations of TES are applied. The result shows that TES is big enough to store a significant amount of energy and meet the heat demand of the turbine train.

Table 3.5 compares the simulation results, including the defined assessment indicators, for the proposed HES under both EMOSs. The yearly charge and discharge energy of A-CAES under I-EMOS are 377 MWh/yr and 141 MWh/yr., respectively, 9.3% and 9.6% less than those under T-EMOS. This reduction is due to the limitations of TES and power conversion units, including motor/compressors and generator/turbines. However, the ratio of discharging and charging energy which refers to the integrated electricity-electricity efficiencies for both EMOSs, are the same (around 37.42%). Accordingly, the LCR and SR of A-CAES under I-EMOS decrease by 9.5 % and 7.2%, respectively, compared to the T-EMOS, as reported in Table 3.5.

Table 3. 5**.** Comparison of the simulation results of the proposed HES under both EMOSs over a year.

Assessment criteria	Unit	EMOSs	
		T-EMOS	I-EMOS
Total A-CAES charging energy	MWh/yr.	416	377
Total A-CAES discharging energy	MWh/yr.	156	141
The integrated efficiency of A-CAES ($\boldsymbol{RTE_{CAES\_int}}$)	%	37.42	37.43
Storage ratio of A-CAES ($\boldsymbol{SR_{CAES}}$)	%	9.21	8.33
Coverage Ratio of A-CAES (L$\boldsymbol{CR_{CAES}}$)	%	3.46	3.14
Coverage Ratio of PV panels	%	42.19	42.19
Electrical load management ratio ($\boldsymbol{ELMR}$)	%	45.66	45.33
Import from the grid (IMR)	%	54.34	54.66
Export to the grid (EXR)	%	48.83	49.71

Meanwhile, exporting energy to the grid and importing energy from the grid increase by around 1.8 % and 0.6 %, avoiding renewable curtailment and compensating for the deficit. Generally, under I-EMOS, solar PV panels account for 42.19%, A-CAES contributes around 3.14 %, and the grid affords the rest 54.66% of the total energy generation.

On the contrary, under T-EMOS, PV panels, A-CAES, and grid fulfilled the building demand by contributing around 42.19%, 3.46 %, and 54.33%, respectively. Hence, the ELMR is over 45% under both EMOSs due to the slight difference in the A-CAES's SR. Of course,

these differences would be varied according to the case study (load demand profile) and weather conditions.

3.2.3.6. Sensitivity analysis

In the technical analysis of A-CAES and HES, the indicators defined above can be affected by changing the critical and independent parameters of the system. Besides, finding the best value for each parameter determines the optimal design of inter-connected components in a HES. Therefore, in this study, the influence of AST volume, maximum AST pressure, and TES capacity on the behavior of HES are investigated. The following sections compare and assess criteria variation under both developed OSs, including T-EMOS and I-EMOS.

3.2.3.6.1. Effect of AST volume

Fig. 3.12 presents the influence of AST volume on system performance, including A-CAES charging/ discharging energy, charging/discharging time, and HES's evaluation indicators under both EMOSs, considering fixed design parameters and PV panel numbers of 11000. Increasing the volume of the AST means that with a specific air pressure range in the storage tank, more air can be accumulated in the tank. Obviously, the AST volume variation has a much lower impact on HES's performance under I-EMOS compared to T-EMOS. For example, Fig. 3.12a and Fig. 3.12b illustrate the total A-CAES charging/discharging energy implying yearly compression/expansion works under T-EMOS and I-EMOS, respectively. Thus, along with the increased AST volume, A-CAES stores more PV power output and delivers more energy to answer the load demand. However, due to the fixed rated output power of the compressor and turbine train, the power stored and generated under I-EMOS remains constant for an AST volume of more than 200 m^3, as represented in Fig. 3.12b. That means, A-CAES cannot manage and generate energy more than their nominal power with the increased AST volume.

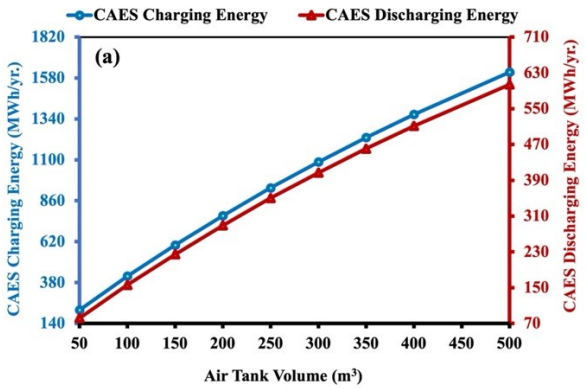
CAES Charging Energy
CAES Discharging Energy
(a)
CAES Charging Energy (MWh/yr.)
CAES Discharging Energy (MWh/yr.)
Air Tank Volume (m³)

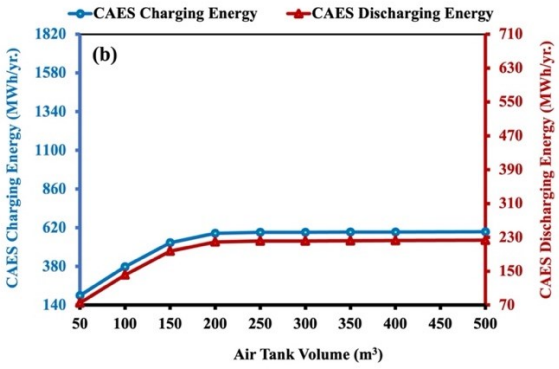
CAES Charging Energy
CAES Discharging Energy
(b)
CAES Charging Energy (MWh/yr.)
CAES Discharging Energy (MWh/yr.)
Air Tank Volume (m³)

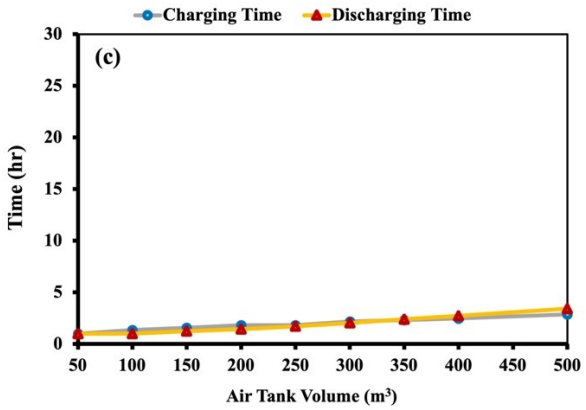
Charging Time
Discharging Time
(c)
Time (hr)
Air Tank Volume (m³)

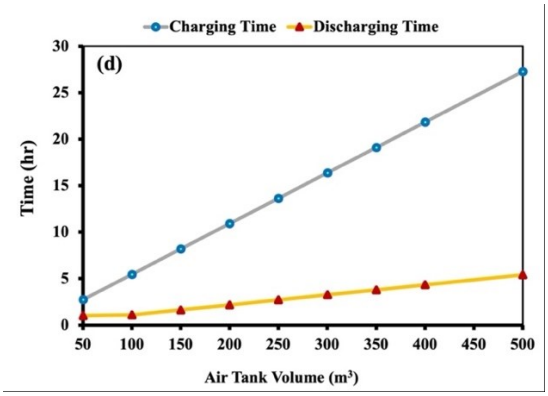
Charging Time
Discharging Time
(d)
Time (hr)
Air Tank Volume (m³)

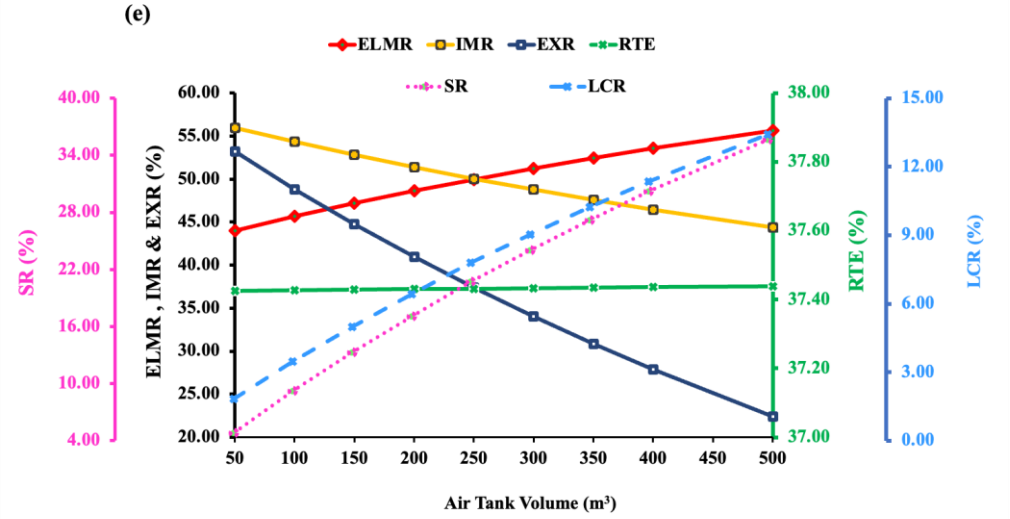
(e)
ELMR
IMR
EXR
RTE
SR
LCR
SR (%)
ELMR , IMR & EXR (%)
RTE (%)
LCR (%)
Air Tank Volume (m³)

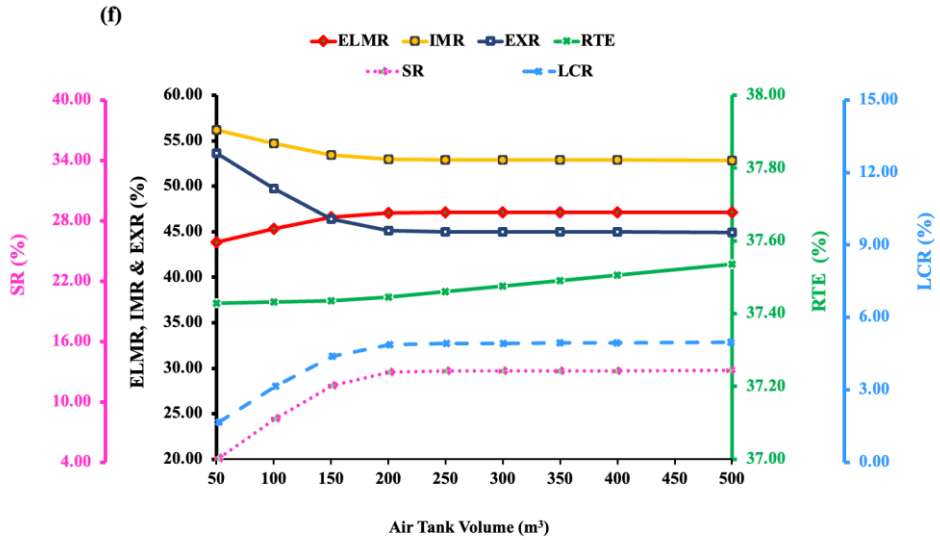

Fig. 3. 12. The effect of AST volume on a) A-CAES charging/ discharging energy under T-EMOS, b) A-CAES charging/ discharging energy under I-EMOS, c) charging/discharging time under T-EMOS, d) charging/discharging time under I-EMOS, e) HES's evaluation indicators under T-EMOS, and f) HES's evaluation indicators under I-EMOS.

On the contrary, A-CAES compression/expansion works increase monotonically under T-EMOS, as shown in Fig. 3.12a. These results can be proved by the ones presented by Zhao [63]. Meanwhile, the larger AST volume leads to a longer A-CAES charge/discharge time. But under I-EMOS, as depicted in Fig. 3.12d, charge and discharge times are highly affected by the AST volume variation compared to T-EMOS, in which A-CAES can absorb/deliver a huge amount of energy in a shorter duration (Fig. 3.12c). Therefore, both charging and discharging times have a positive trend with increased AST volume but a small variation scope. As a result, in such a case, both the A-CAES's SR and LCR would rise monotonically, indicating a lower EXR and IMR to/from the grid, respectively (Fig. 3.12e). Thus, the ELMR rate also has an improved trend with the raised AST volume.

However, under I-EMOS, the storage volume variation has a low impact on HES's indicators, as shown in Fig. 3.12f. As an example, a 10-fold increase in the AST volume increases the A-CAES storage and LCR by 7.4 times under T-EMOS while only three times under I-EMOS. Therefore, the most A-CAES's SR and LCR values in I-EMOS and the least EXR and IMR can be achieved with a minimum of 200 m^3 of AST volume. In other words, by increasing the tank volume by more than 200 m^3, all evaluation criteria remain constant.

It should be noted that A-CAES efficiency has a negligible variation with raised AST volume under both EMOSs. Such assessments help us select the proper EMOS to find the

optimal size for AST storage to avoid oversizing A-CAES, which not only influences its performance but also its economy can be affected.

3.2.3.6.2. Effect of AST pressure

Fig. 3.13 represents the influence of the upper pressure of the AST on system performance, including A-CAES charging/ discharging energy, charging/discharging time, and HES's evaluation indicators under both EMOSs considering fixed design parameters and PV panel numbers of 11000. Raising the maximum pressure of the AST implies storing more air at a higher pressure, which is expected to increase the total compression/expansion work. Thus, as depicted in Fig. 3.13a, this elevated trend is monotonic under T-EMOS, leading to an increase in the A-CAES's SR, LCR, and ELMR (Fig. 3.13e) while the IMR and EXR decrease monotonically. However, different behavior can be seen for A-CAES compression/expansion works under I-EMOS (Fig. 3.13b). In such case, there is an optimal value for a maximum pressure of air (14 MPa) which leads to the highest SR, CR and correspondingly lowest IMR and EXR, as shown in Fig. 3.13f.

Moreover, the maximum ELMR can be achieved at an optimal value of 14 MPa for upper AST pressure (Fig. 3.13f). This is because the last compressor must reach the maximum pressure of the AST, and its mass flow rate decreases. Thus, the storage pressure variation negatively affects the A-CAES system performance. Furthermore, according to Fig. 3.13a and Fig. 3.13b, due to the higher variation of compressor work compared to the turbine work with raised storage pressure, the A-CAES efficiency is decreased monotonically by nearly 23% under both EMOSs. The results also show that the higher maximum pressure of the AST can result in a longer charging duration under I-EMOS due to the limited rated output power of the compressor train. It is worth noting that the storage pressure variation has a very small and negligible impact on the charging/discharging time of A-CAES under T-EMOS because there is no limitation on the operational power capacity of the compressor/turbine.

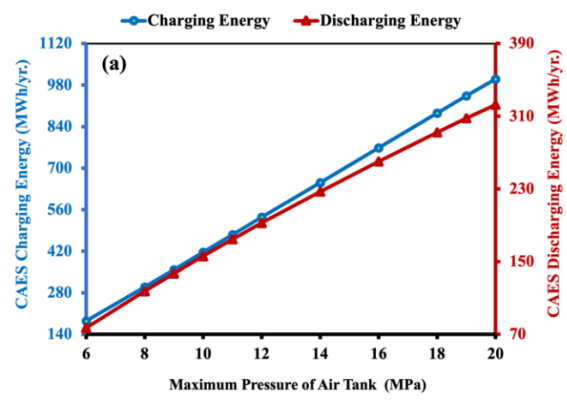
Charging Energy
Discharging Energy
(a)
CAES Charging Energy (MWh/yr.)
CAES Discharging Energy (MWh/yr.)
Maximum Pressure of Air Tank (MPa)

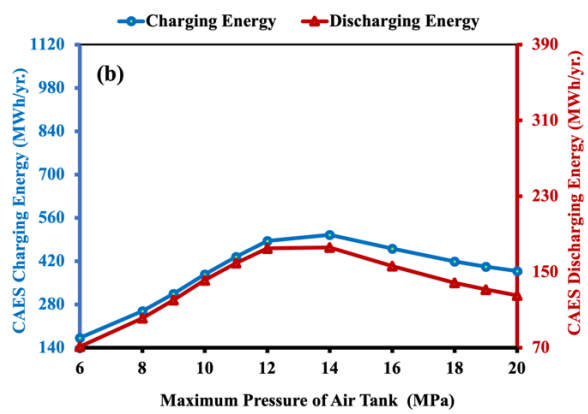
Charging Energy
Discharging Energy
(b)
CAES Charging Energy (MWh/yr.)
CAES Discharging Energy (MWh/yr.)
Maximum Pressure of Air Tank (MPa)

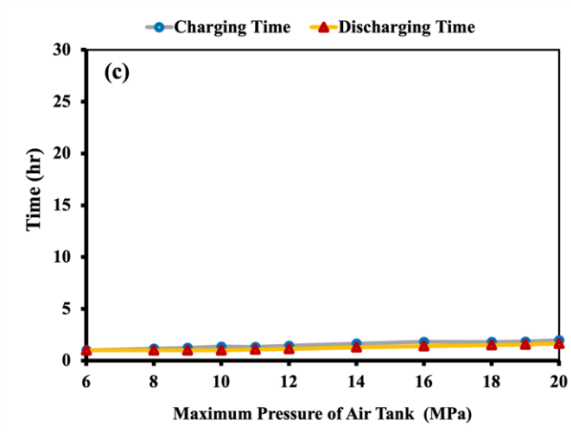
Charging Time
Discharging Time
(c)
Time (hr)
Maximum Pressure of Air Tank (MPa)

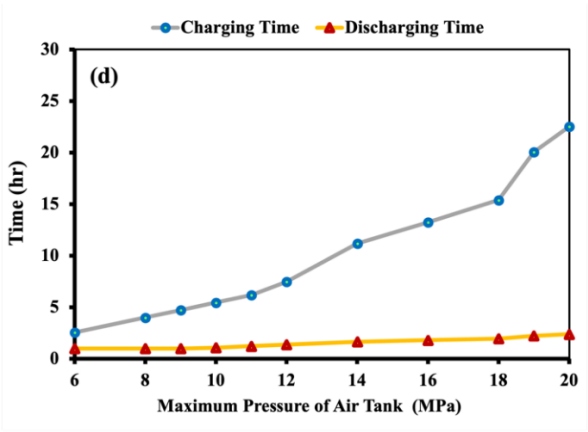
Charging Time
Discharging Time
(d)
Time (hr)
Maximum Pressure of Air Tank (MPa)

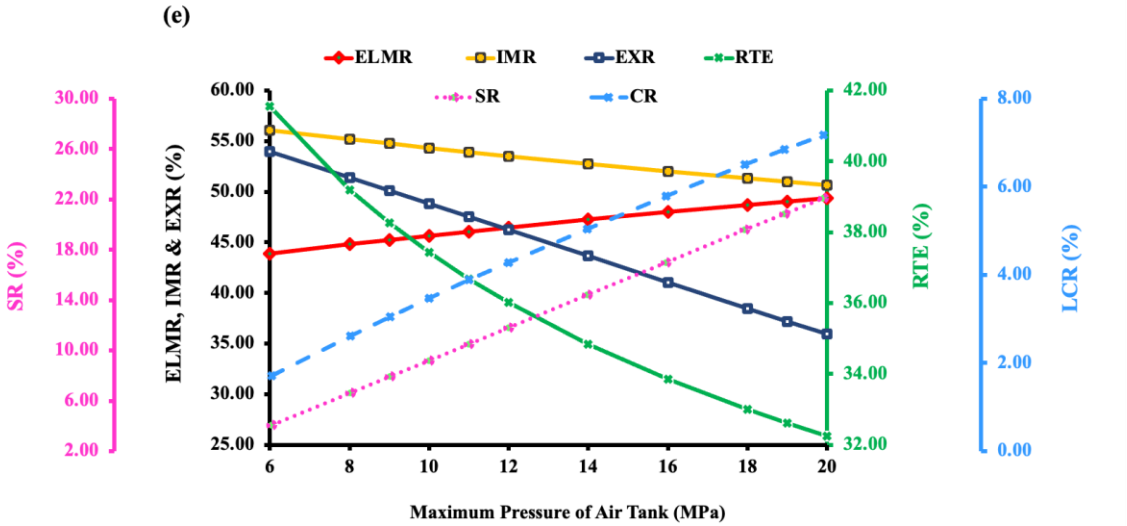
(e)
ELMR
IMR
EXR
RTE
SR
CR
SR (%)
ELMR, IMR & EXR (%)
RTE (%)
LCR (%)
Maximum Pressure of Air Tank (MPa)

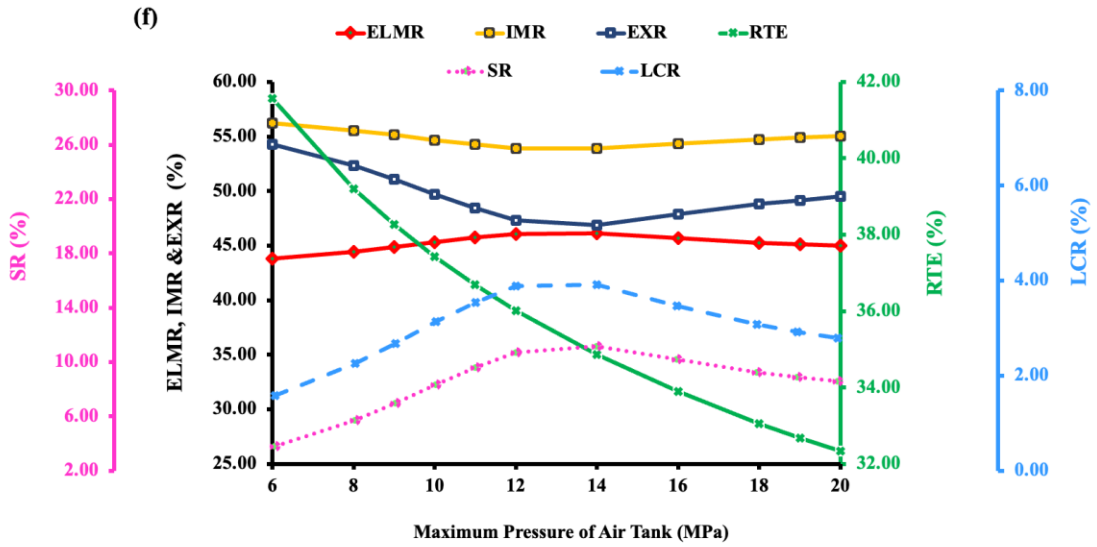

Fig. 3. 13. The effect of maximum pressure of AST on a) A-CAES charging/ discharging energy under T-EMOS, b) A-CAES charging/ discharging energy under I-EMOS, c) charging/discharging time under T-EMOS, d) charging/discharging time under I-EMOS, e) HES's evaluation indicators under T-EMOS, f) HES's evaluation indicators under I-EMOS.

3.2.3.6.3. Effect of TES capacity

This study assumes that TES is the only heat source required for the expansion phase, and no axillary heat source exists. Therefore, based on the thermal energy available in TES, discharging air mass flow rate from the AST would be regulated during discharging time. The amount of stored thermal energy in TES highly depends on the volume and capacity of TES. Fig. 3.14 shows the impact of TES volume on essential parameters of A-CAES and HES. As can be seen, with raised TES volume, yearly A-CAES discharge energy increases because TES can capture more thermal energy.

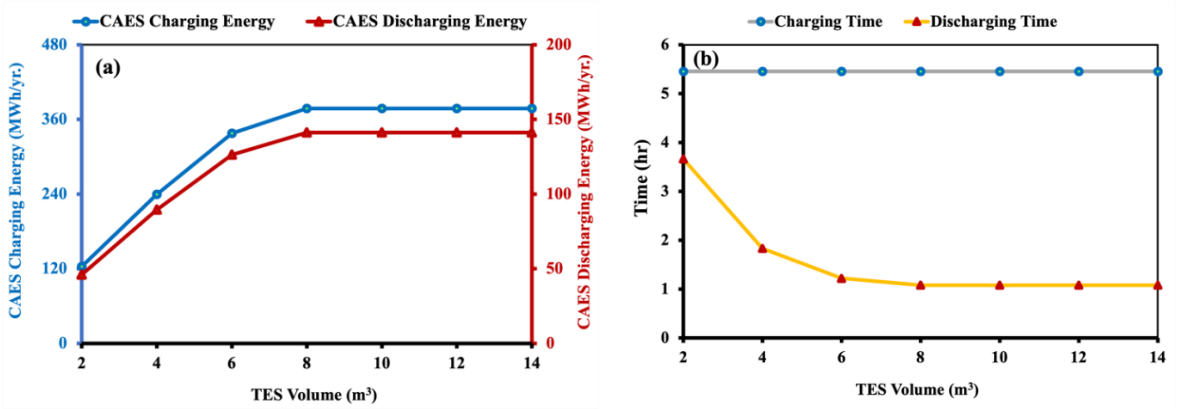

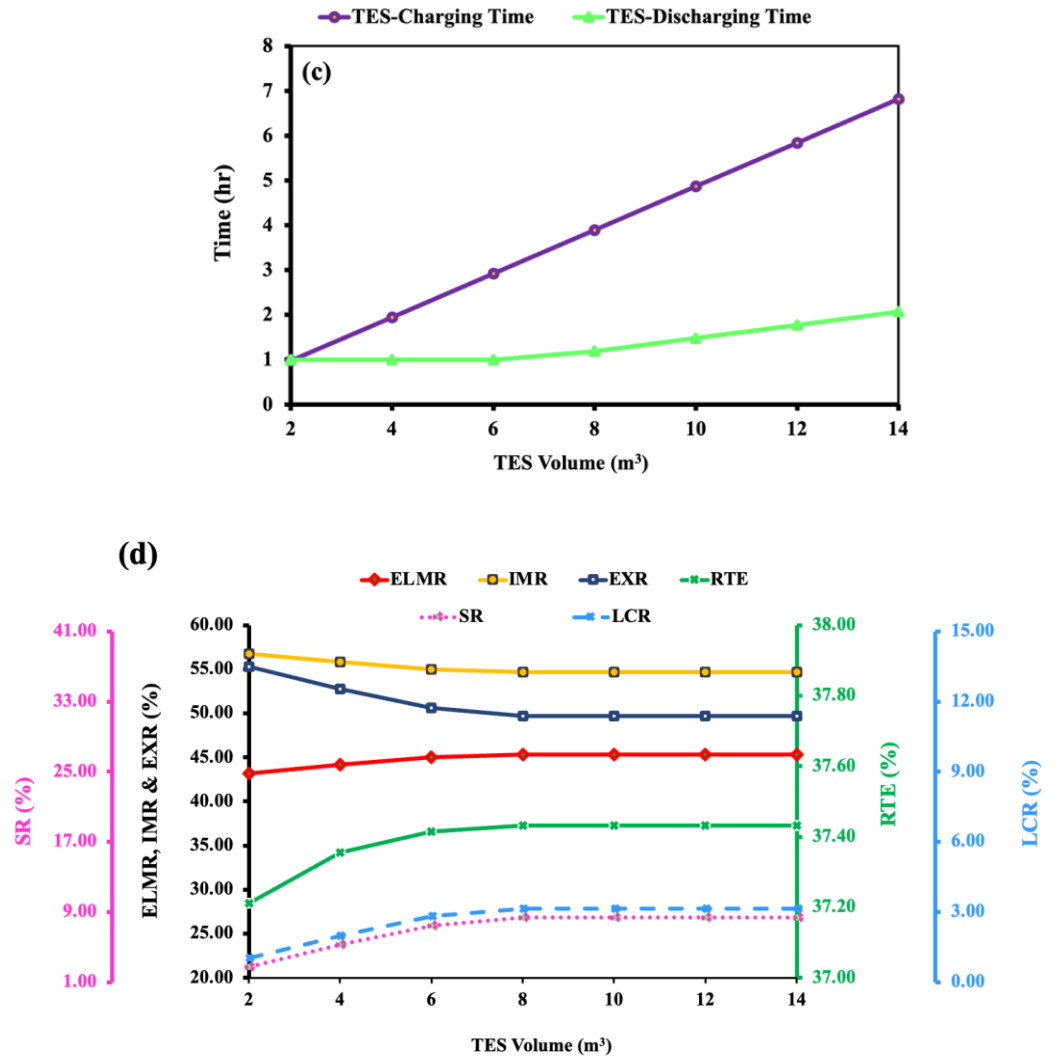

Fig. 3. 14. The effect of TES volume on a) A-CAES charging/ discharging energy, b) charging/discharging time, c) charging/discharging time of TES, and d) HES's evaluation indicators under I-EMOS.

Meanwhile, the discharging time of A-CAES decreases. But this improvement in discharging energy and reduction in discharging time is not monotonic; after reaching a specific value for TES volume, they remain constant. On the other hand, although the A-CAES charging time is constant (Fig. 3.14b), the yearly charging energy also has the same trend as discharging energy (Fig. 3.14a). The reason is that the operation of the turbine train affects the SOC in the AST, and consequently, it impacts the compressor train's function in the following times. Similarly, according to Fig. 3.14d, the CAES's LCR, SR, ELMR, and integrated efficiency first improve and then remain unchanged with the increased TES volume of larger than 8 m^3, whereas both the import and export ratio decrease.

Moreover, TES's charging/discharging times increase monotonously by raising the TES volume because it can capture and release more thermal energy. More information regarding

the effects of TES capacity on CAES performance and operation, along with a brief environmental investigation, can be found in section 3.3 [21].

3.3. Effect of low-temperature thermal energy storage on hybrid PV- compressed air energy storage operation [21]

3.3.1. Research approach

Similar to section 3.3 (paper1), the considered HES in this section is composed of five key components: PV, CAES, grid, control system, and building load demand. The distinguishing factor is that, in certain scenarios, the CAES system includes a combustion chamber in addition to the motor/compressor train, generator/turbine train, heating/cooling heat exchangers, and a double cold/hot tank as TES.

In a broad sense, this section delves into the details of the TES parts of the EMOS introduced in previous section (3.3). The overarching operation strategy managing the energy flow in the (HES) remains consistent as illustrated in Fig. 3.3. However, the key distinction lies in the consideration of various heating sources in this section, particularly during the discharging phase, affecting CAES's operation and performance. This implies that the thermal energy required for expansion can be sourced from either TES or auxiliary heat, such as burning fossil fuels. This consideration has implications for the operation and performance of the CAES system.

In such a case, two scenarios are defined based on two different operational conditions of CAES concerning thermal energy sources as follows:
for the operation condition of the CAES with respect to thermal energy sources as follows:

Scenario 1 (Scen.1): The required heat is exclusively provided by TES. Therefore, when TES does not have enough energy (less than the amount needed for expansion), the mass flowrate of high-pressure air released from the AST is regulated accordingly. If compressed air is less than the minimum mass flowrate required by turbines, CAES stops discharging, and further power deficit is compensated by purchasing electricity from the grid (TES scenario).

Scenario 2 (Scen.2): the initial heat requirement is met by the TES. If the thermal energy available from TES is insufficient to meet the turbines' needs, an auxiliary heat unit is employed to compensate for the additional thermal energy required. In this study, the auxiliary heat unit is represented by a combustion chamber (TES and auxiliary heat scenario).

3.3.1.1. Model development

The model for all HES's components employed in this section remains consistent with the previous section 3.3 (chapter 1), except for the incorporation of the combustion chamber model (as an auxiliary heat source).

3.3.1.1.1. Combustion chamber model

When using axillary heat, the compressed air should be burned with natural gas (NG) in the combustion chamber. Therefore the required heat can be calculated by [202]:

$$\acute{Q}_t(t) = \dot{m}_{t,a,ax}(t) C_{p,a} \times \left(\sum_{i=1}^{Nt} T_{t,j}^{in} - T_{AST} - \sum_{j=1}^{Nt-1} T_{t,j}^{in} \left(\pi_{tur,j}\right)^{\frac{\gamma-1}{\gamma}} \right) \quad (3.321)$$

where $\dot{m}_{tur,air,ax}$ is part of the compressed air mass flowrate burned in the combustion chamber. The equivalent fuel consumption can be estimated as follow:

$$FC = \frac{\acute{Q}_t(t)}{H_f \times \eta_f} \quad (3.33)$$

where H_f shows the heat value of gas (38.8 MJ/m^3) and η_f is gas combustion efficiency (85% in this study).

3.3.1.2. KPIs

The indicators utilized in this part are the same as those in section 3.3, including ELMR, LCR, SR, and RTE. However, due to the inclusion of auxiliary heat in current investigation, the formulation of the RTE is modified as follows:

$$RTE_{CAES\_cycle} = \frac{\sum_{t=1}^{t_{dcrg}} W_{CAES,dcrg}(t)}{\sum_{t=1}^{t_{crg}} W_{CAES,crg}(t) + \frac{\acute{Q}_t(t)}{\eta_f}} \quad (3.34)$$

3.3.2. Case study

The same case study as considered in section 3.3 (paper 1) is considered for the current investigation.

3.3.3. Results and discussions

The case study and design parameter considered in current evaluation is the same as in the previous section (3.3). As mentioned before, the design and behavior of TES as a sub-system of CAES influence the whole system's performance. In this section, the aforementioned issue is investigated considering two defined scenarios (section 3.4.1) to evaluate and verify the

developed operation strategy for every possible condition that might be happened in the CAES system, especially when it is adopted for decentralized application.

3.3.3.1. Thermal energy flow in the system

The behavior of the compressor and turbine in generating/ consuming heat during charging/discharging is already displayed in Fig. 3.9b in previous section 3.3.

3.3.3.2. Effect of TES capacity

CAES is a complex system with interdependent components. Therefore, each element's design and operation influence one another's performance and, consequently, the whole hybrid system's function. This section analyzes the effect of TES capacity on the proposed system's operation under two defined scenarios (section 3.4.1).

3.3.3.2.1. Performance analysis

Fig. 3.15 displays the impact of TES capacity on the charging and discharging times of the AST and TES. From Fig.3.15a, it is observed that TES's charging/discharging times increase monotonously by raising the TES volume because it can capture and release more thermal energy. However, the increase in charging time is sharper than discharging time because the heat generated during the compression phase is more than the required heat for expansion according to the characteristics of considered CAES in the current study. It should be noted that this behavior is the same for both scenarios because the charging and discharging time of TES depends on its capacity and the rated heat of the compressor/turbine. Therefore, it is not affected by adopting other axillary heat sources.

In contrast, with raised TES capacity, the discharging time of the AST decreases in scen.1 while remaining constant in scen.2 as shown in Fig.3.15b. This phenomenon is due to the strong dependence between TES capacity and mass flowrate of the turbine, which is regulated according to the available thermal energy when TES is the only source of heat (scen.1). In such a case, the turbine operation depends on the available heat capacity in the system. However, discharging time does not change when there is another axillary heat source because it can be compensated for the capacity shortage of TES. On the other hand, the full charging time of the AST under both scenarios is constant because there is no regulation on the rated mass flowrate of the compressors at steady-state conditions based on the TES capacity.

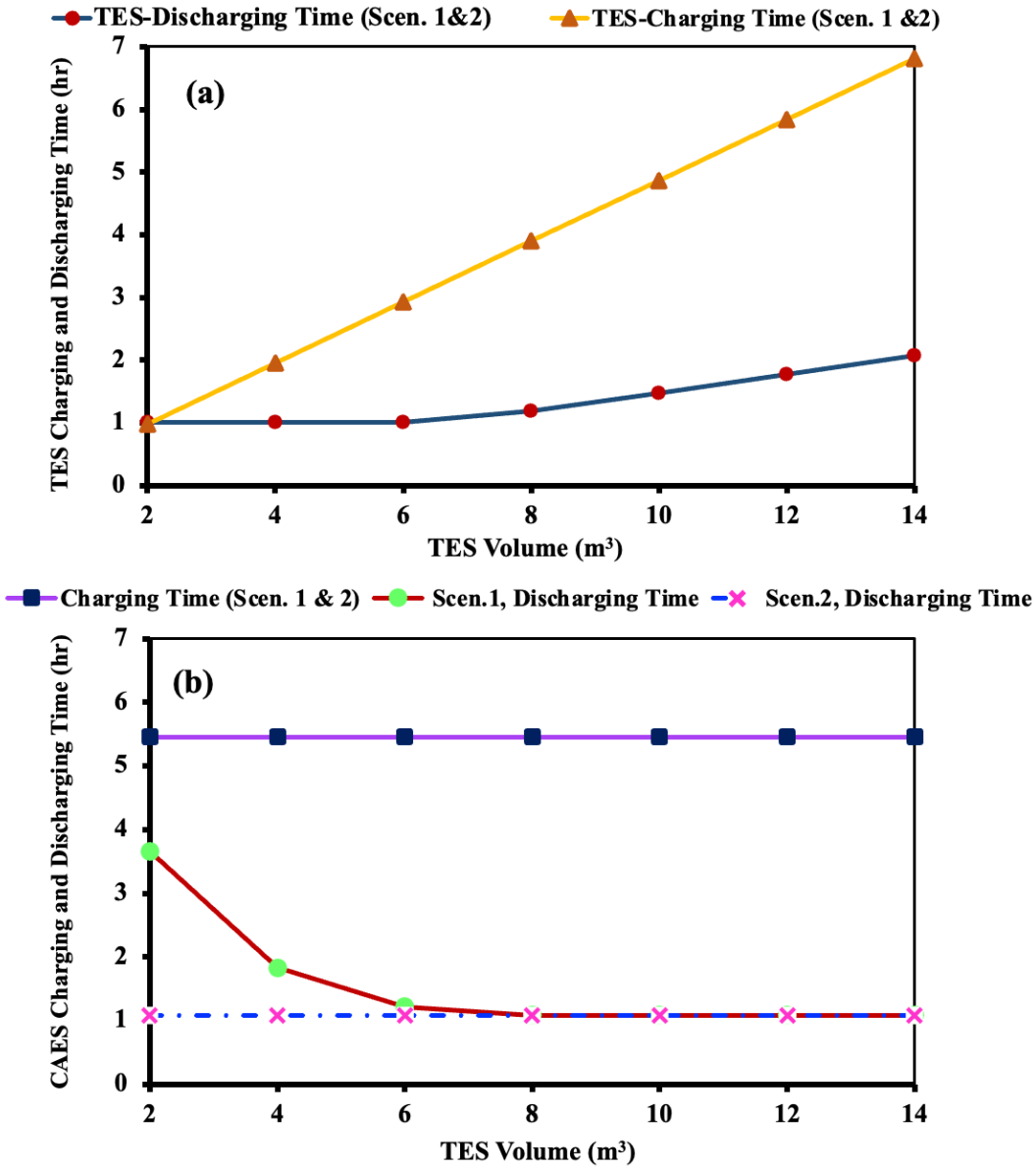

Fig. 3. 15. The effect of TES capacity on the charging and discharging time of a) TES and b) CAES.

Fig.3.16 shows the impact of TES capacity on the performance of the proposed system. From Fig.3.16a illustrates that with increased TES capacity, CAES's integrated, and cycle RTE remain constant in scen.1 while they increase in scen.2. That is because in scen.1, raised TES capacity affects the turbine's rated mass flowrate positively and discharging time negatively. Therefore, the turbine and compressor work ratio remain constant considering one complete cycle. However, ELMR has the exact opposite trend under both scenarios, as demonstrated in Fig.3.16b.

Since the TES affects the turbine operation and subsequently the AST state and the compressor train operation in the following steps, the integrated efficiency of CAES is also constant. However, both LCR and SR are improved first by raising TES volume in Scen.1, as shown in Fig.3.16c. However, for TES volume higher than 8 m^3, the variation of LCR and SR is not considerable. In contrast, in scen.2, increased TES volume positively impacts both integrated and cycle efficiencies (Fig.3.16a). At the same time, SR and LCR remain constant, as can be seen in Fig.3.16c. The reason is the reduction of the NG usage share in preheating the compressed air.

3.3.3.2.2. Heat management in the system

As mentioned before, using TES to recover the heat generated during the compression phase mitigates the system energy loss and emission while improving efficiency. However, finding the optimal size for TES to reach the above-mentioned goal is essential. Fig.3.17 shows the system's heat loss during a year. Obviously, with increased TES capacity, the system's heat loss reduces in scen.2 because, along with the raised TES volume, more thermal energy generated during the charging process can be captured by TES. These phenomena can be proved by Fig.3.18, which displays the share of heat loss and thermal energy managed by TES in the total thermal energy generated during the compression phase.

On the other hand, in scen.1, changing the TES volume alters the operation hour of turbine and compressor trains. Hence, with raised TES capacity, the heat released from the compression phase becomes larger, resulting in a higher heat loss, as demonstrated in Fig.3.18. Thus, an increase of TES volume from 2 m^3 to 8 m^3 increases and decreases the yearly heat loss by about 3 and 2.3 times in scen.1 and scen.2, respectively. However, the further increase in the TES volume (more than 8 m^3) does not impact heat loss for both scenarios.

Fig. 3.19 also illustrates the TES impact on the share of TES and NG in providing the heat required by the turbine train during the discharging process. As can be seen, TES volume positively impacts TES share in supplying heat for both scenarios. However, in scen.2 the rest of desired thermal energy is compensated by burning NG, resulting in carbon emission.

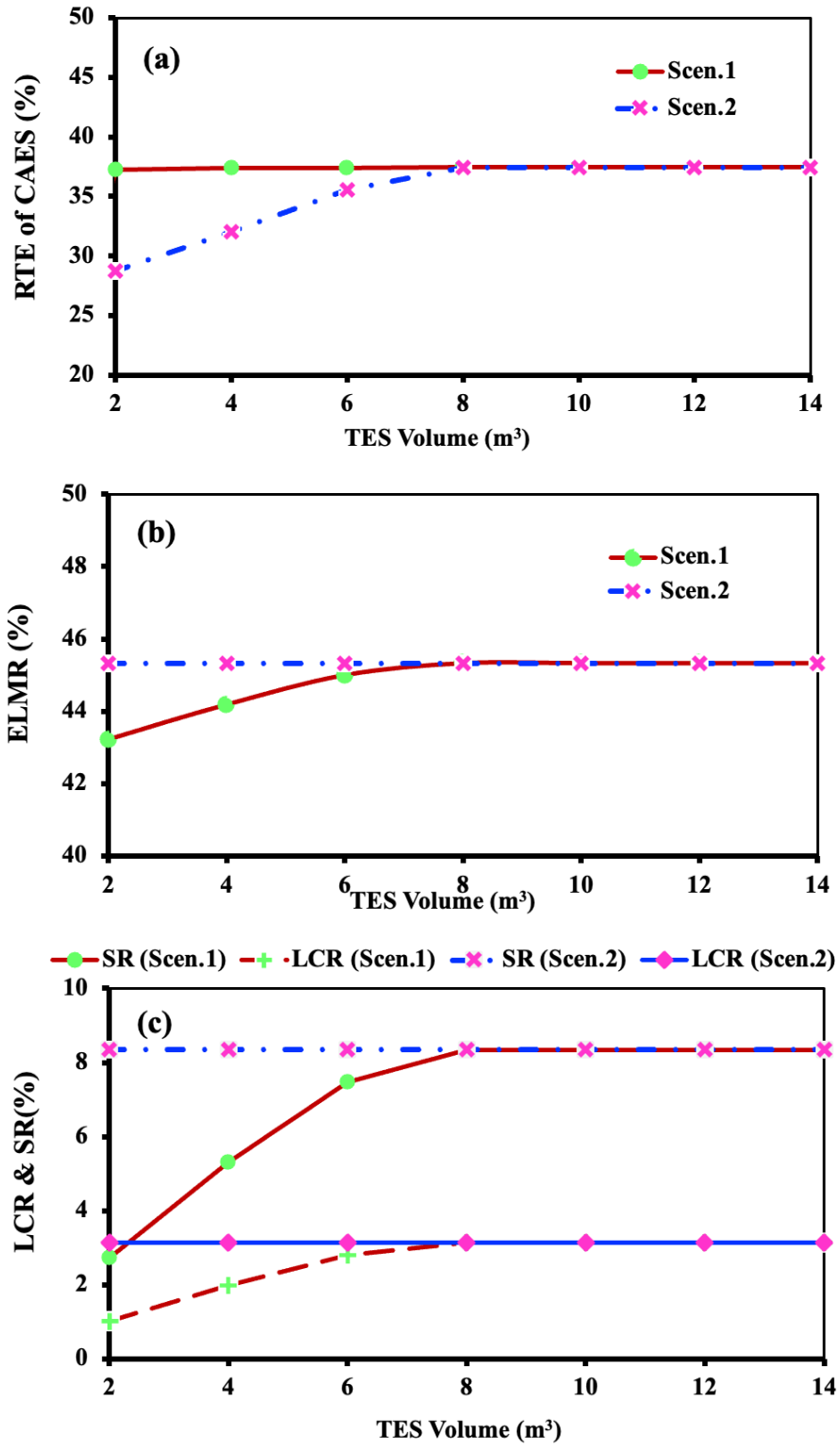

Fig. 3. 16. The effect of TES on the a) RTE of CAES, b) ELMR, and c) LCR and C.R.

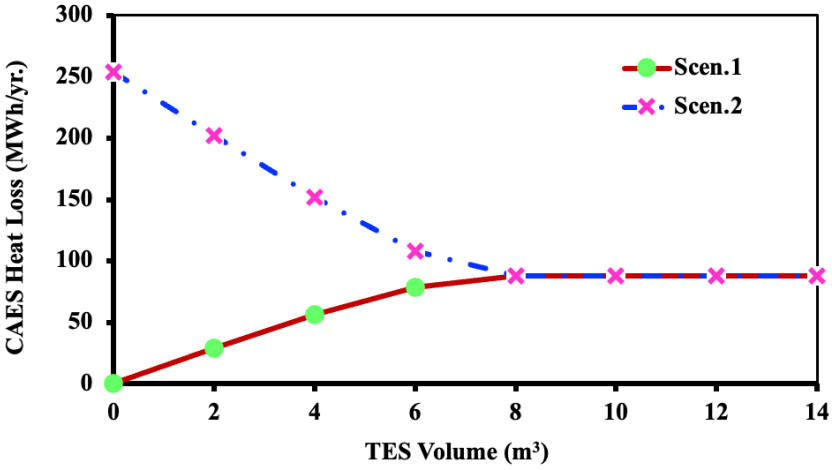

Fig. 3. 17. The effect of TES capacity on yearly heat loss from CAES.

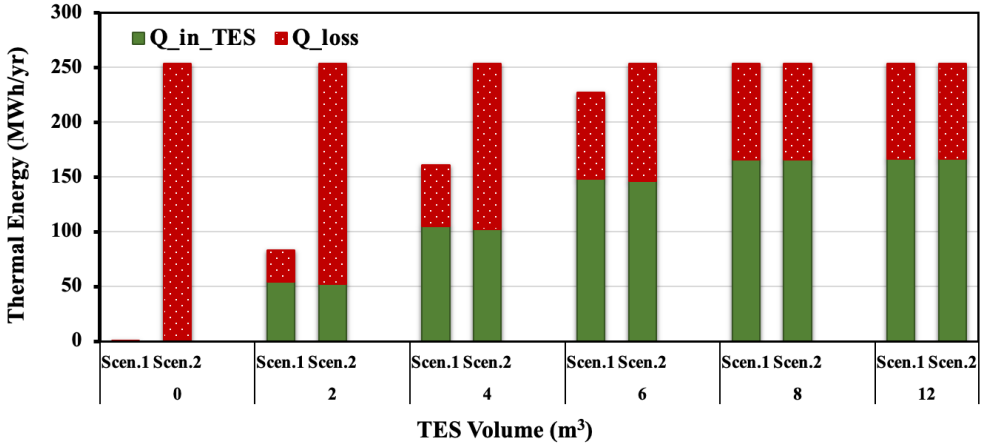

Fig. 3. 18. The effect of TES capacity on the portion of captured heat by TES and heat loss during the charging phase.

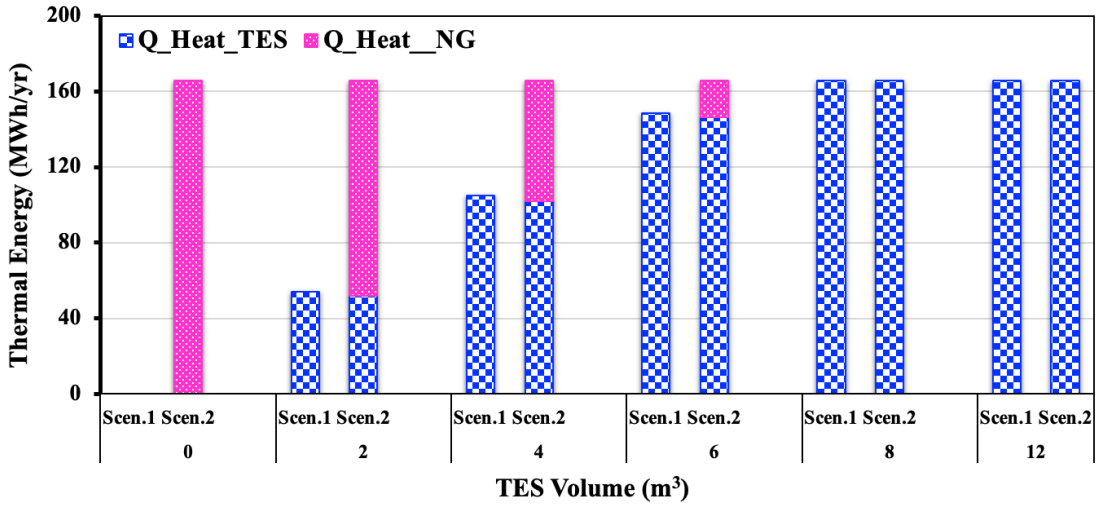

Fig. 3. 19. The effect of TES capacity on the portion of TES and NG in supplying thermal energy during discharging phase.

3.3.3.2.3. Operational condition in the system

To better understand the system's dynamic operation, three days of January (from 10th to 12th) are selected as a representative to evaluate the different possible operational conditions of HES components. Fig. 3.20 displays the PV panel's output power and electric demand of the case study (building in this work) for these representative days.

As can be seen, a part of building demand is fulfilled by solar energy in these three days. However, there is an excess PV power output on days 11^{th} and 12^{th} that can be stored in CAES. While on the day 10^{th}, since the excess electricity is less than the compressor start-up power, extra energy is sold back to the grid. This also can be seen in Fig.3.21a and Fig.3.22a, which show the hourly work of the compressor (Wc) and turbine (Wtr).

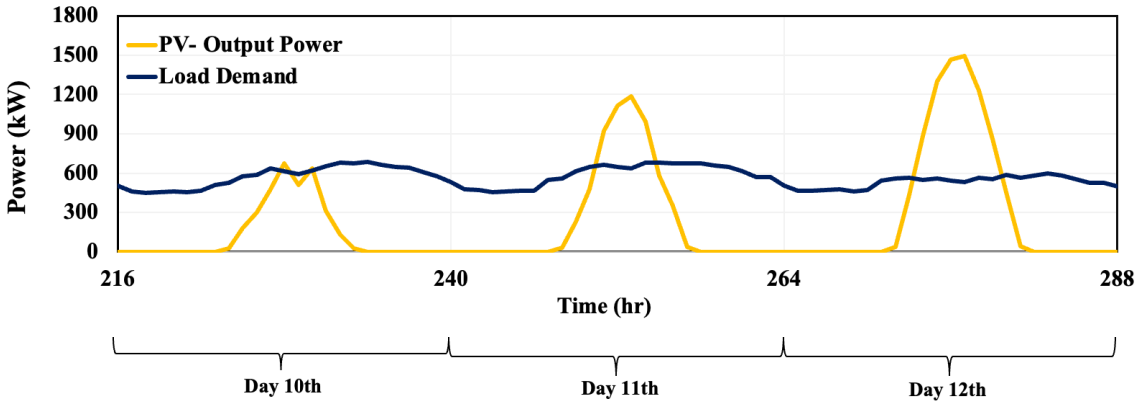

Fig. 3. 20. Profile of the PV output power and building electric load demand during the three days of January.

Furthermore, the effect of TES capacity on the operational condition of compressor/turbine, AST, TES, and hourly heat loss /required by turbine train are shown in Fig.3.21 and Fig.3.22 for scen.1 and scen.2 respectively.

Obviously, the TES has the same operational behavior in two scenarios (Fig. 3.21c and 3.22c), and the change of TES volume will alter the amount of stored thermal energy and thus TES behavior. However, unlike scen.2, in scen.1, since the operation hour of the turbine train and, subsequently, the compressor train are affected by TES volume variation (Fig. 3.21a), the SOC of the AST is changed (Fig. 3.21b). Therefore, the increased TES capacity implies a larger thermal energy discharge. Thus, more air mass flow is discharged from the AST resulting in higher electric power generation by turbine train. The results also indicate that for the TES volume higher than 8 m^3, the system's operational condition variation is the same (except SOC of TES).

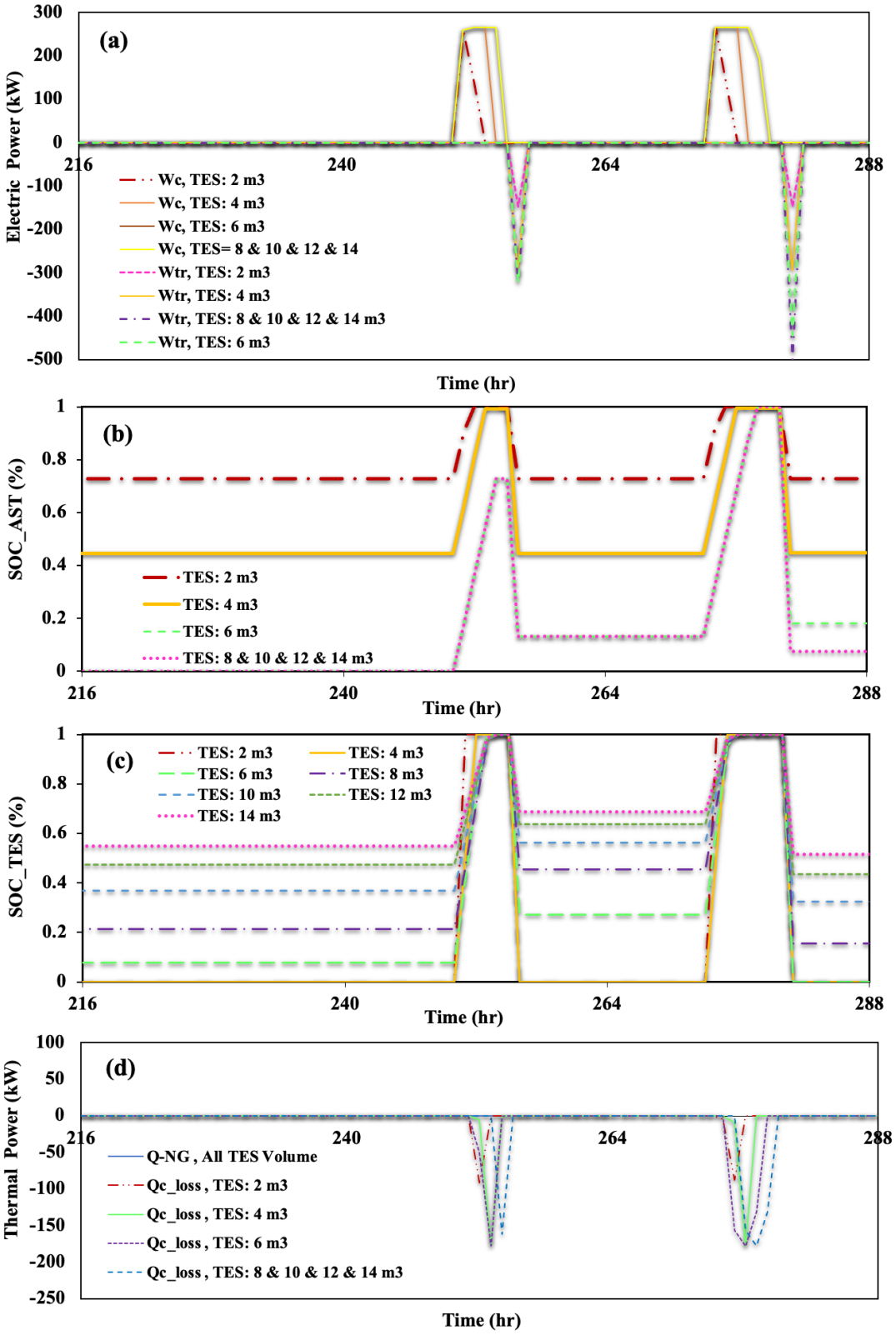

Fig. 3. 21. The effect of TES capacity on the dynamic operation of a) compressors and turbines, b) SOC of AST, c) SOC of TES, and d) compressor heat loss and NG usage under Scen.1.

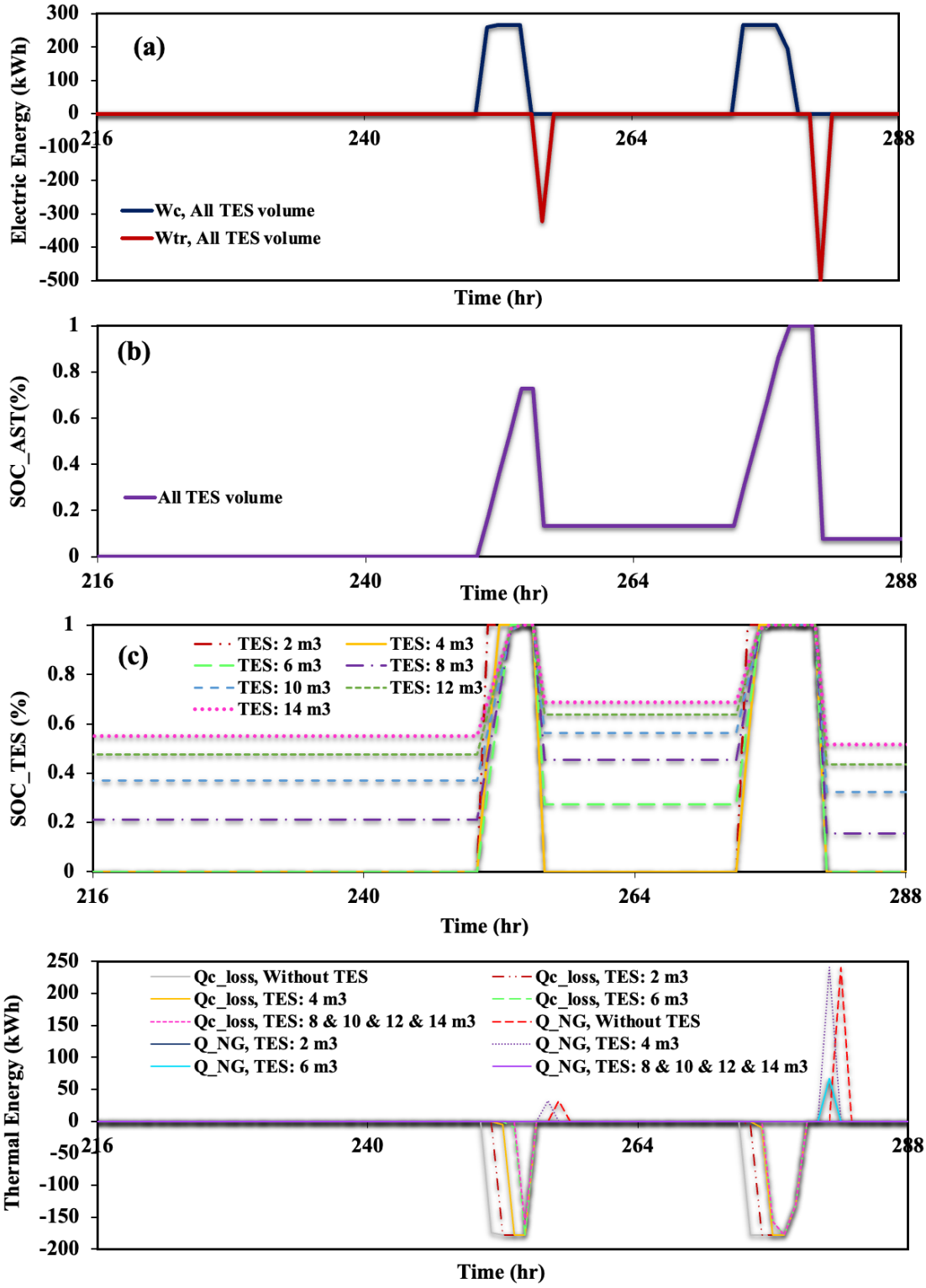

Fig. 3. 22. The effect of TES capacity on the dynamic operation of a) compressors and turbines, b) SOC of AST, c) SOC of TES, and d) compressor heat loss and NG usage under Scen.2.

As highlighted before, in scen.2 (Fig. 3.22) the variation of TES capacity does not affect the operation of the turbine/compressor train (Fig. 3.22a) and thus SOC of AST (Fig. 3.22b).

Such behavior is due to the presence of axillary heat in the system that can compensate for the TES shortage to provide the desired heat of the turbine train.

3.3.3.3. Emission analysis

It is assumed that the combustion chamber of CAES considered in scen.2 is the only source of carbon emission. The result shows that increasing TES volume from 0 to 8 m^3 mitigates the amount of CO_2 emission of the system by around 100% (from 32.5 to 0 m^3) while converting it to zero-emission energy storage.

3.4. Optimal planning and configuration of adiabatic-compressed air energy storage for urban buildings application: Techno-economic and environmental assessment [231]

3.4.1. Research approach

The components of the generic system consist of solar PV as the primary energy source, a load, a converter, a power dispatch controller, and A-CAES system and e-boiler as a source of flexible-load demand.

3.4.1.1. Alternative PDSs

Alternative PDSs, as listed in Table 3.6, are proposed and compared according to various application potentials of A-CAES for urban buildings.

Table 3. 6. Description of proposed operation strategies.

PDS	Purpose	CAES-Grid interaction at the off-peak hour (charging)	Renewable generation (primary energy source)
A	Renewable integration	No	Yes
B	Load shifting	Yes	No
C	Joint A and B	Yes	Yes
D	Joint A and B, seasonally	Yes (High LD*) /No (Low LD)	Yes
O	Primary power system (Grid)	No	No

*LD: load demand

The EMOS of A-CAES is demonstrated in Fig. 3.2, where the limitation associated with the rated power capacities of PCSs and energy capacities of AST and TES, as well as their interconnections, are adopted during the charging and discharging process. The explanation of A-CAES sub-systems' operation (as shown in Fig. 3.3b) is merged into the description of the

following proposed PDSs. More details was explained in the section 3.3 (paper1).

Fig. 3.23 illustrates different proposed PDSs in line with services offered by A-CAES for decentralized applications (e.g., building load demand shifting and renewables integration).

Strategy (A) corresponds to renewable integration aiming to increase solar energy penetration in energy-intensive buildings, as shown in Fig. 3.23a. When PV generation exceeds the load demand at time t, A-CAES can be charged depending on the rated capacity and operation range of the compressor train as well as the AST state of the charge (SOC), which should be less than the maximum allowable pressure in AST (see Fig. 3.2). Then the excess electricity (if exists) is either sold back to the grid or used for another application. Meanwhile, the heat generated during the compression process can be stored in TES depending on its SOC. Otherwise, the surplus heat is dissipated into the atmosphere. When PV generation cannot meet the load demand at time t, the load can be satisfied by A-CAES discharging depending on the turbine train's operation range and AST and TES's SOC. If TES and AST are not empty, meaning that the air pressure is more than the minimum required pressure in AST, A-CAES could discharge as long as the thermal energy could provide heat for the air mass that must be enough for turbine start-up and less than the rated mass flow rate. Otherwise, the energy shortage is compensated by importation and purchasing power from the grid. The whole system bidirectionally interacts with the grid, as observed in this strategy, while there is no interaction between the grid and the A-CAES system.

Strategy (B) refers to the building’s load demand shifting by charging CAES in an off-peak hour and discharging it during peak hour, as presented in Fig. 3.23b. At off-peak hours of the time of use (TOU) tariff, electricity is imported from the grid not only to satisfy the energy demand but also to charge the CAES depending on the SOC of AST and operating range of the compressor train. Meanwhile, the heat generated during the compression phase can be stored in TES depending on its SOC. Otherwise, the heat is lost. At peak hours, the load is satisfied by discharging the CAES first, depending on the SOC of both TES and AST and the operational range of the turbine to substitute the expensive grid power followed by the purchasing from the grid (grid importation).

Strategies (C) and (D) aim to plan the A-CAES system for joint renewable integration and load shifting, which is a combination of strategies (A) and (B). These strategies utilize PV generation as the first priority to meet the load demand, as demonstrated in Fig. 3.23 c and d.

Strategy (C) operates the same as the A-CAES charging process in PDS-A when there is excess PV power generation during peak hours. However, during the off-peak hour, grid

importation is also conducted (after excess PV penetration) to fully charge the A-CAES system. In contrast, in PDS-C, when load demands exceed the PV generation at the off-peak hours of the TOU tariff, the strategy operates the same as in PDS-B; the electricity is first imported from the grid to fulfill the demand, followed by the fully charging of the A-CAES before the next peak hour. While at peak hours of the TOU tariff, the strategy acts the same as the CAES discharging process in PDS-A.

Strategy (D) has a similar process as PDS-C during the peak months of the year when the building has higher load demand (more than the average monthly load, mainly in the fall and winter). While during the rest of the months (with lower load demand mainly in spring- summer with good solar irradiance), the PDS-D manages the energy flow the same way as the PDS-A only for solar integration (disregarding the peak/off-peak hours).

Strategy (O) refers to the primary power system corresponding to the current building electrification situation in which the load demand is only satisfied by the energy purchased and imported from the grid.

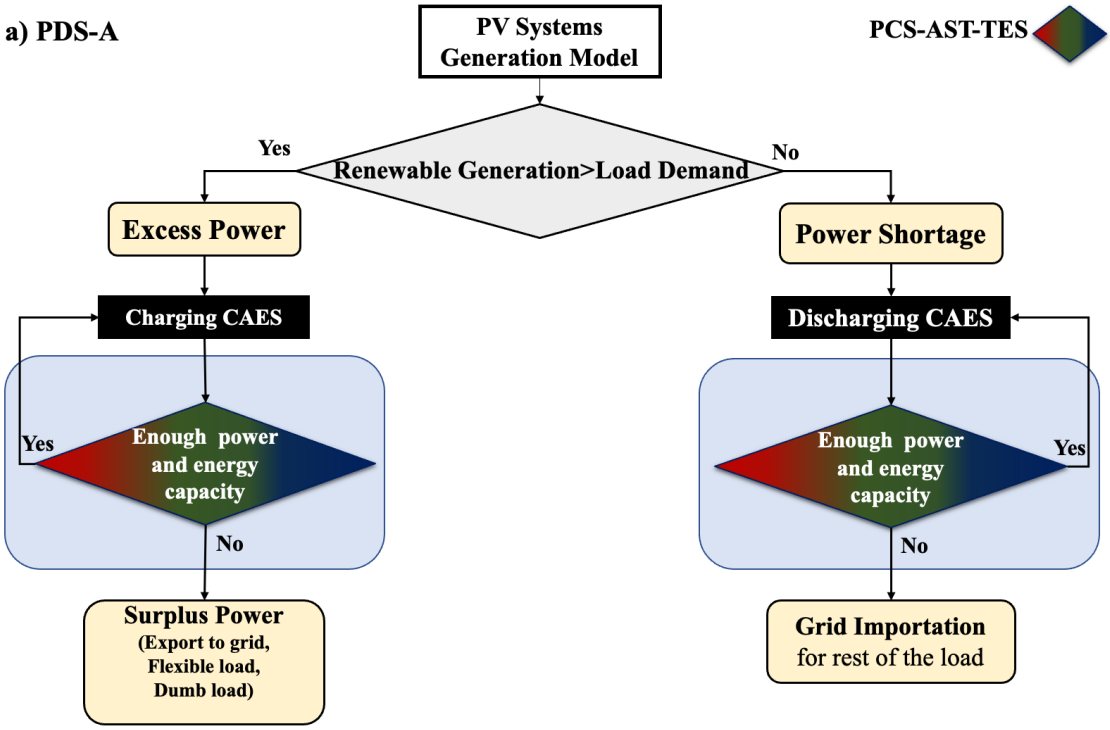

b) PDS-B

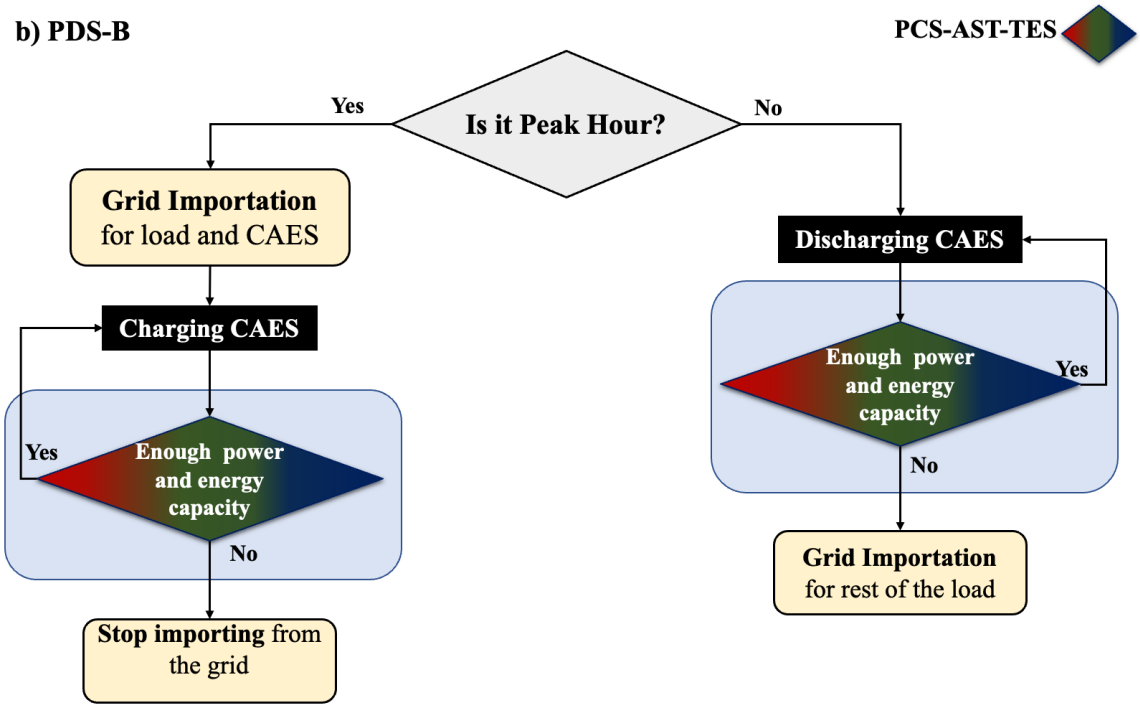
PCS-AST-TES
Is it Peak Hour?
Yes
No
Grid Importation
for load and CAES
Charging CAES
Enough power
and energy
capacity
Yes
No
Stop importing from
the grid
Discharging CAES
Enough power
and energy
capacity
Yes
No
Grid Importation
for rest of the load

c) PDS-C

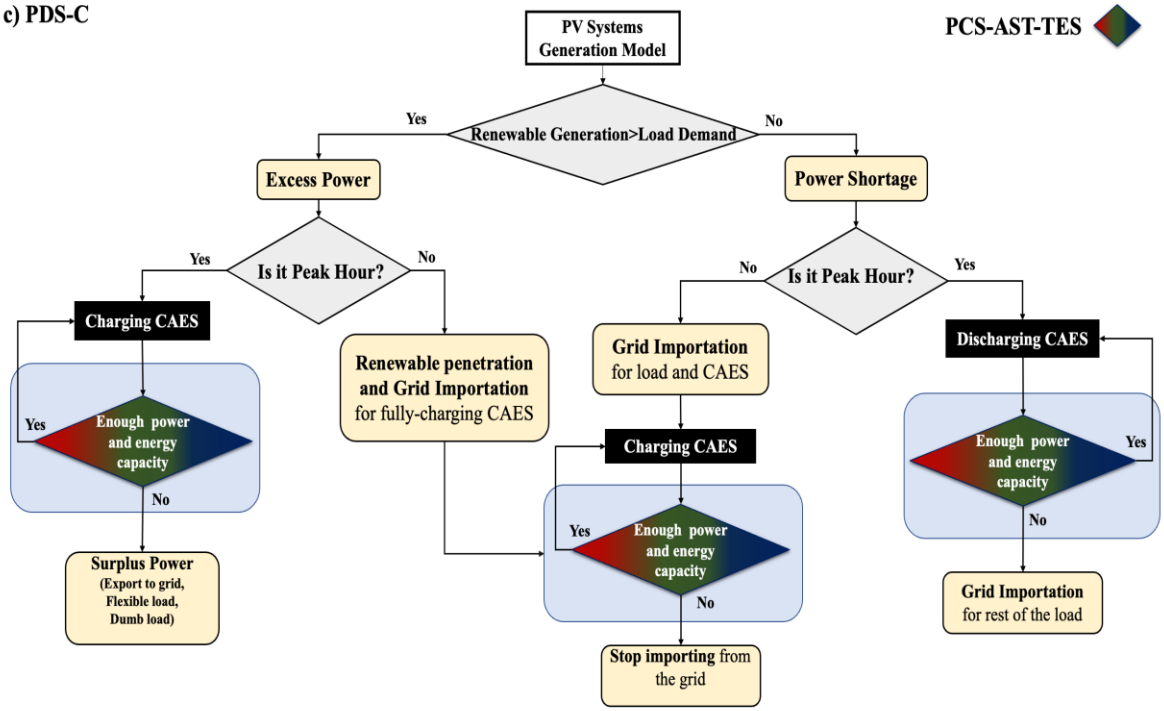
PCS-AST-TES
PV Systems
Generation Model
Renewable Generation>Load Demand
Yes
No
Excess Power
Power Shortage
Is it Peak Hour?
Yes
No
Charging CAES
Enough power
and energy
capacity
Yes
No
Surplus Power
(Export to grid,
Flexible load,
Dumb load)
Renewable penetration
and Grid Importation
for fully-charging CAES
Is it Peak Hour?
No
Yes
Grid Importation
for load and CAES
Charging CAES
Enough power
and energy
capacity
Yes
No
Stop importing from
the grid
Discharging CAES
Enough power
and energy
capacity
Yes
No
Grid Importation
for rest of the load

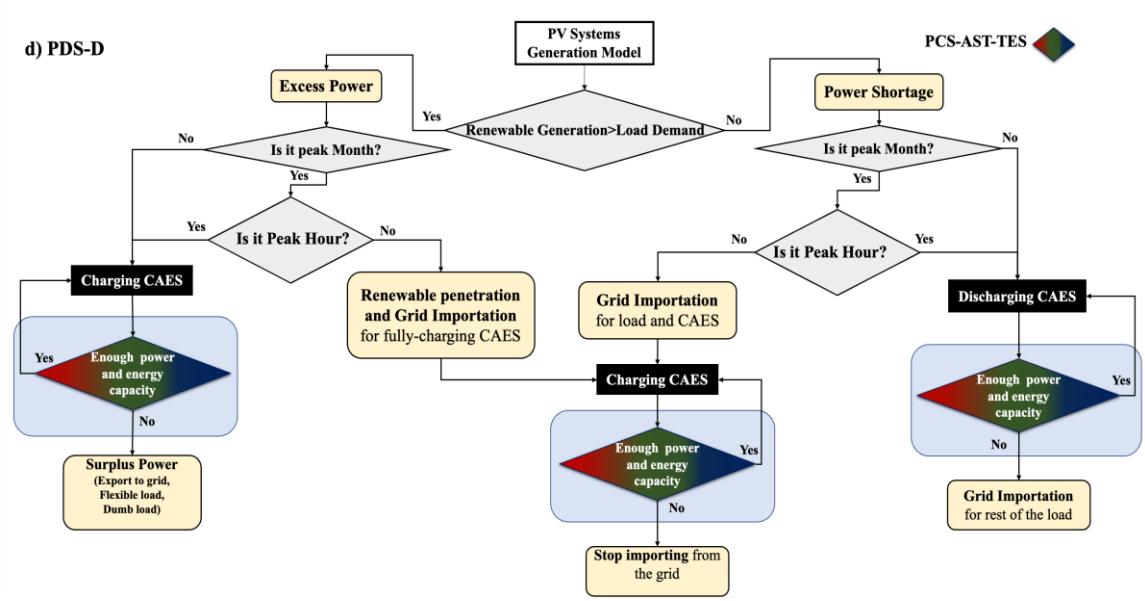

Fig. 3. 23. The flowchart of the different proposed PDSs.

3.4.1.2. Scenarios

This study investigates several scenarios subject to managing the extra PV output power (the energy that is not stored due to the A-CAES capacity limitation and restriction associated with selling power to the grid, as follows:

Scenario I: There is a limitation on selling back the grid (Worst case scenario).

Scenario II: There is no limitation on selling back to the grid (Best-case scenario).

Scenario III: There is a flexible load to use PV-surplus power (for another application, such as an e-boiler for hot water required for the heating, ventilation, and air conditioning system.)

By analyzing the results of these scenarios under the proposed PDSs, it is possible to observe the effect of managing PV-surplus power and energy exchange between HES and grid on the feasibility of the proposed HES, enabling us to find the best scenarios under which A-CAES system has the highest techno-economic viability. Fig.3.24 also displays the logic behind the managing the PV-surplus power by adopting electric boiler as a flexible load.

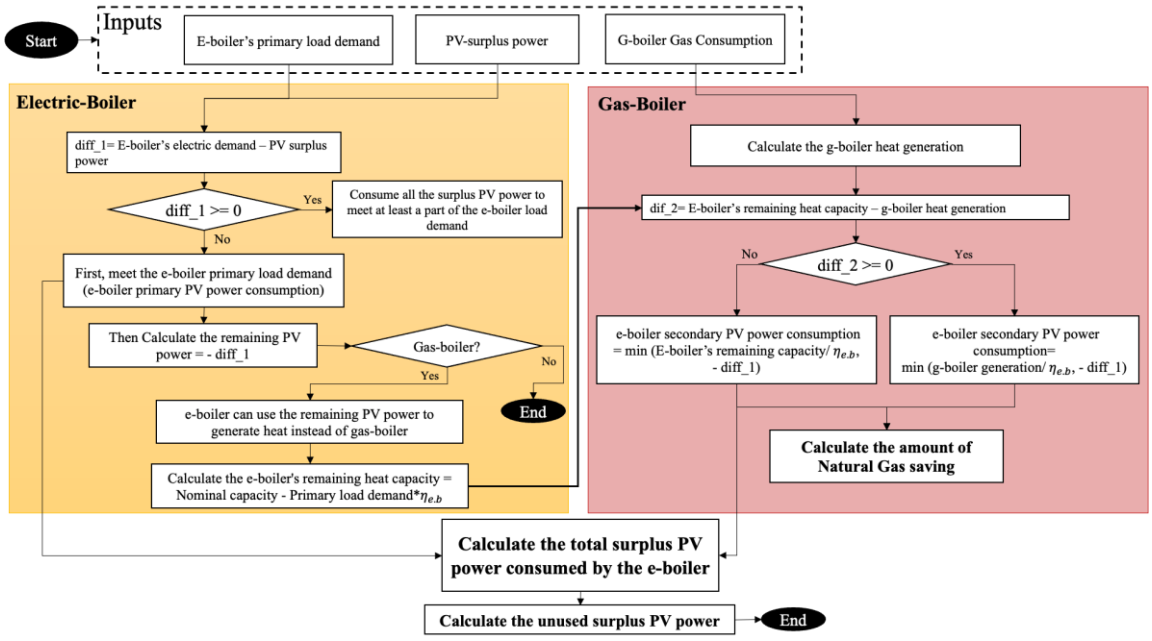

Fig. 3. 24. The flowchart of introducing electric-boiler as flexible load to manage the PV-surplus power.

3.4.1.3. Generic model development

In this section, a generic mathematical model for the A-CAES system, suitable for optimal sizing-designing, is proposed. The model is formulated as a function of design variables to facilitate the simulation and optimization processes. The studied design variables related to each component of the A-CAES system are shown in Fig. 3.24. The independent design variables (green) represent the decision variables in the optimization problem. Meanwhile, the dependent variable is defined as intermediate variables, which are formulated as a factor of independent variables.

Fig. 3.25 demonstrates a typical structure of a small-scale A-CAES system, including several inter-connected sub-systems such as; 1) motor and multi-stage compressors; 2) generator and multi-stage expanders (turbines); 3) AST for storing high-pressure air; 4) heating and cooling HEX units 5) double hot and cold water tanks for storing the thermal energy (TES unit), and 6) throttle valve to adjust inlet air pressure to AST and turbine train. Moreover, the model of the PV panel was presented in section 3.3.1.1.

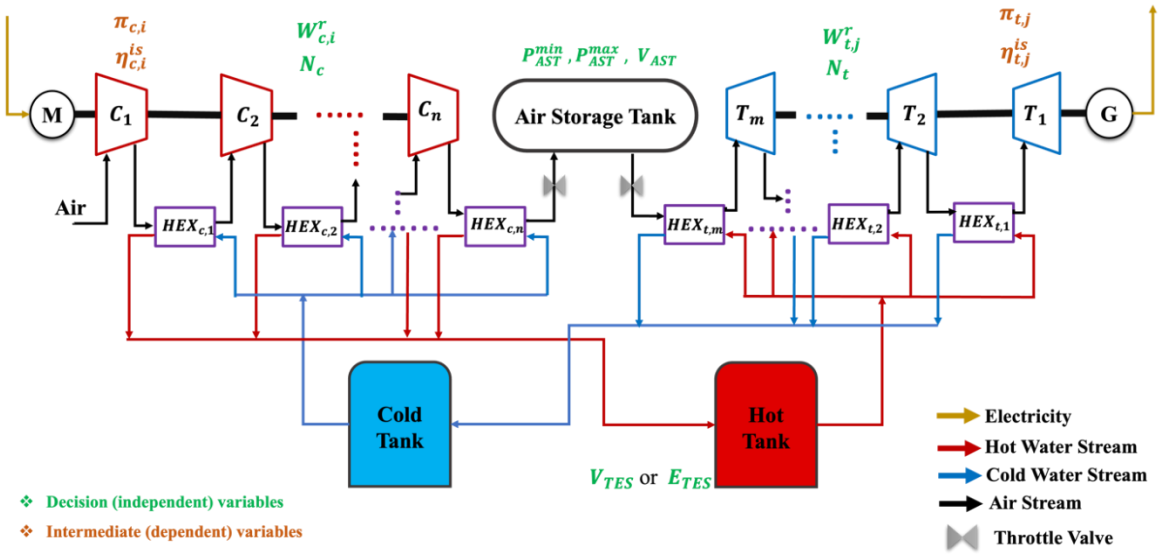

Fig. 3. 25. A schematic of the A-CAES structure.

3.4.1.3.1. Assumptions

In order to formulate the global mathematical model, several assumptions are made. They are: 1) Air is considered an ideal gas with constant specific heat; 2) Input and output power to and from the A-CAES is AC; 3) All compressors (turbines) have the same characteristics in terms of nominal power, isentropic efficiency, pressure ratio, etc.; 4) The constant-constant operation corresponding to the pressure of compressors and expanders of A-CAES is considered. This means that the pressurized air is throttled before entering the AST during the charging phase and after being released from the AST before expansion during the discharging phase. Further information can be found in the related references [45,232]; 5) The minimum working pressure of the AST corresponds to the discharge pressure of the throttle (regulator) valve, which is the inlet pressure of the turbine [84] 6) The pressure of the output air of the last compressor is the same as the maximum pressure of the AST; 7) The temperature of ambient input air to the compressor of A-CAES as well as the temperature in AST and TES, is constant [27]; 8) The input air temperature at each stage of compression and expansion remains constant; it means that the air after each compression/ expansion stage could be cooled down/heated up to the same level [129]; 9) The analytical model for the output power of compressor and turbine train is considered a linear function of mass flow rate, which varies over time in response to changes in the renewable generation and load demand; 10) The efficiency of the power conversion systems including motor, compressors, turbines, generator is assumed to remain constant and at their design conditions.

3.4.1.3.2. PCS model (compressor/turbine train)

The overall A-CAES system's charging power consumed by the compressor train ($W_{CAES,crg}$) and overall discharging power generated by the turbines ($W_{CASE,dcrg}$) can be expressed as Eq. (3.32) and (3.33):

$$W_{CAES,crg}(t) = N_c \dot{m}_{c,a}(t) C_{p,a} T_{c,i}^{in} \left(\pi_{c,i}^{\frac{\gamma-1}{\gamma}} - 1 \right) / \eta_M \eta_{c,i}^{is} \quad (3.35)$$

$$W_{CAES,dcrg}(t) = N_t \dot{m}_{tr,a}(t) C_{p,a} T_{tr,j}^{in} \left(1 - \pi_{tr,j}^{\frac{1-\gamma}{\gamma}} \right) \eta_G \eta_{tr,j}^{is} \quad (3.36)$$

where N_c and N_t are the number of compression and expansion stages, respectively. $\dot{m}_{c,a}$ and $\dot{m}_{tr,a}$ represent the charging and discharging air mass flow rate, respectively. $T_{c,i}^{in}$ and $T_{tr,j}^{in}$ show the temperature of inlet air to compressors and turbines, respectively. $C_{p,a}$ refers to the specific heat capacity. η_M and η_G are the efficiencies of the driven motor and generator, respectively. γ is the isentropic factor, which equals 1.4. $\pi_{c,i}$ and $\pi_{tr,j}$ which are compression and expansion ratios, can be defined as Eq. (3.34) and (3.35)[129]:

$$\pi_{c,i} = P_{c,i}^{out} / P_{c,i}^{in} = (P_{AST}^{max} / P_{am})^{\frac{1}{N_c}} \quad (3.37)$$

$$\pi_{tr,j} = P_{tr,j}^{in} / P_{tr,j}^{out} = \left(P_{AST}^{min} / P_{am} \right)^{\frac{1}{N_{tr}}} \quad (3.38)$$

where P_{AST}^{max} and P_{AST}^{min} represent the maximum and minimum air pressure in AST, respectively. While P_{am} is the ambient air temperature. On the other hand, $\eta_{c,i}^{is}$ and $\eta_{tr,j}^{is}$ are the efficiency of compressors and turbines and can be calculated by the empirical Eq. (3.36) and (3.37), respectively. These relations were proposed in [233] as a result of the performance evaluation of Bryton-Cycle engines:

$$\eta_{c,i}^{is} = 0.91 - \frac{(\pi_{c,i})^{\frac{1}{N_c}} - 1}{300} \quad (3.39)$$

$$\eta_{tr,j}^{is} = 0.9 - \frac{(\pi_{tr,j})^{\frac{1}{N_{tr}}} - 1}{250} \quad (3.40)$$

3.4.1.3.3. AST model

Since AST has a constant volume (iso-choric), the pressure of the AST increases or decreases depending on the high-pressure air charging and discharging duration, respectively. Therefore, the air pressure in AST at time t is determined as follows [110,234]:

$$P_{AST}(t) = P_{AST}(t-1) + \dot{P}_{c,a}(t) \Delta t_{crg} - \dot{P}_{tr,a}(t) \Delta t_{dcrg} \quad (3.41)$$

$$\dot{P}_{c,a}(t) = \frac{R_a.T_{AST}}{V_{AST}} \dot{m}_{c,a}(t) \quad (3.42)$$

$$\dot{P}_{tr,a}(t) = \frac{R_a.T_{AST}}{V_{AST}} \dot{m}_{tr,a}(t) \quad (3.43)$$

where P_{AST} is the air pressure in AST, V_{AST} shows the volume of AST, T_{AST} is the air temperature in the AST, R_a is the gas constant, and Δt is the time resolution. $\dot{P}_{c,a}$ and $\dot{P}_{tr,a}$ show the pressure of airflow during the charging and discharging process, respectively.

Accordingly, the SOC of CAES can be determined as follows:

$$SOC_{AST}(t) = \frac{P_{AST}(t) - P_{AST}^{min}}{P_{AST}^{max} - P_{AST}^{min}} \quad (3.44)$$

3.4.1.3.4. HEX model

Assuming counter flow heat exchanger and using the effectiveness–NTU method where $NTU = UA/C_{min}$ and $s = C_{min}/C_{max}$, the effectiveness (ε) of each heat exchanger can be evaluated as follows [106]:

$$\varepsilon = \begin{cases} \frac{1-exp\,[-NTU\,(1-s)]}{1-s\,exp\,[-NTU\,(1-s)]} & for \;\; s < 1 \\ \frac{NTU}{1+NTU} & for \;\; s = 1 \end{cases} \quad (3.45)$$

where NTU is the number of heat transfer units, U is the overall thermal conductance, A is the effective heat transfer area and $C = \dot{m}_c C_p$ is the heat capacity of the flow. Further details and comprehensive information can be found in [106]. Notably, in this study, the *s=1* is considered as previously assumed in [45].

Thus, considering all the equations mentioned above, the heat exchangers' total heat transfer during charge ($\dot{Q}_c$) and discharge ($\dot{Q}_t$) process can be determined using Eq. (3.43) and (3.44), respectively.

$$\dot{Q}_c(t) = \dot{m}_{c,a}(t) C_{p,a} \varepsilon_{c,i}^{ex} \left(N_c T_c^{in} \pi_{c,i}^{\frac{\gamma-1}{\gamma}} - N_c T_{in,cold}^{w} \right) \quad (3.46)$$

$$\dot{Q}_{tr}(t) = \dot{m}_{tr,a}(t) C_{p,a} \varepsilon_{tr,j}^{ex} \left(N_{tr} T_{in,hot}^{w} - T_{AST} - (N_{tr} - 1) T_{tr}^{in} \pi_{tr,j}^{\frac{1-\gamma}{\gamma}} \right) \quad (3.47)$$

3.4.1.3.5. TES model

Usually, a low-temperature TES is selected for a small-scale A-CAES system [11]. This study considers a sensible heat TES in the form of double hot/cold water. The TES dynamism in terms of energy at time t can be expressed as below:

$$Q_{TES}(t) = Q_{TES}(t-1) + \dot{Q}_c(t) \Delta t_{crg} - \dot{Q}_{tr}(t) \Delta t_{dcrg} \quad (3.48)$$

where Q_{TES} is the cumulative thermal energy stored in TES. Thus, the volume of the single hot/cold water tank (V_{TES}) can be determined as follows:

$$V_{TES} = E_{TES}/(C_w \rho_w (T_{hot} - T_{cold})) \quad (3.49)$$

$$E_{TES} = Q_{TES}^{max} - Q_{TES}^{min}$$

where E_{TES} is the energy capacity of TES while Q_{TES}^{max} and Q_{TES}^{min} are the TES's maximum and minimum energy capacity, respectively. Accordingly, the SOC of the TES unit can be determined as follows:

$$SOC_{TES}(t) = \frac{Q_{TES}(t) - Q_{TES}^{min}}{Q_{TES}^{max} - Q_{TES}^{min}} \quad (3.50)$$

3.4.1.4. Optimization problem formulation

In this section, a mix-integer nonlinear problem (MINLP) is defined to design the proposed HES optimally. The main goal is to formulate a cost-effective, reliable, and environmental-friendly HES consisting of several decision variables as below:

$$X = \left[W_c^r, W_{tr}^r, N_c, N_t, V_{AST}, E_{TES}, P_{AST}^{min}, P_{AST}^{max}\right]$$

where X is the vector of decision variables (x_v) in which N_c and N_{tr} are discrete and the rests are continuous variables.

The optimization problem is formulated as follows:

$$Minimize \ \ LCOE = f(X) \quad (3.51)$$

Subjected to the following constraints:

$$x_v^{min} \leq x_v \leq x_v^{max} \ \ \forall \, x_v \ \in \ X \quad (3.52)$$

$$LCR_{A-CAES} \geq LCR_{min} \quad (3.53)$$

$$0 \leq LPSP \leq LPSP_{max} \quad (3.54)$$

where LCOE refers to the levelized cost of energy of the HES, implying the life cycle cost (LCC) per unit of electricity generated over the project's lifetime [155]. In the local generation scenario, an upper and lower allowable amount for the design variable (X_v^{min} and X_v^{max}) of each component is defined according to the available surface area of the buildings (such as the roof or façade area for installing PV panels, or indoor space for A-CAES). The constraint associated with load coverage ratio (LCR) reflects the contribution of the A-CAES system as the primary system to absorb the excess PV power output before being exported for other usage. Besides, loss of power supply probability (LPSP) refers to the system's reliability, especially for scenarios when there is a limitation on purchasing electricity from the grid. The definition and

formulation of LCOE, LCR, and LPSP are expressed in following section 3.4.1.5. Fig. 3.26 illustrates the coupled simulation and optimization framework. It should be noted that the particle swarm algorithm (PSO) algorithm is used for solving the optimization problem, as explained in section 3.4.1.6.

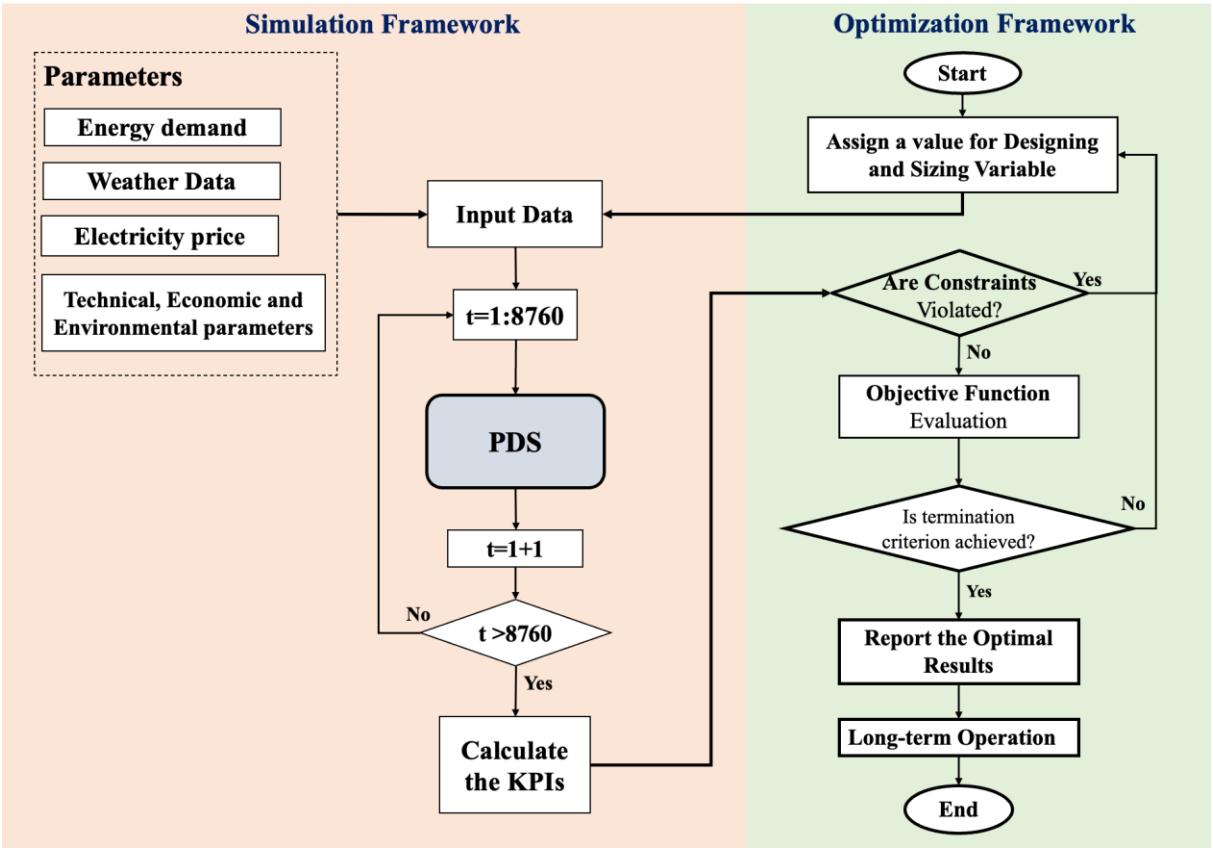

Fig. 3. 26. The block diagram of the designing simulation-optimization framework.

3.4.1.5. KPIs

The HES performance is usually evaluated from a techno-economic and environmental perspective [235]. The technical aspects focus on the energy flow among HES's elements and their contribution. In this study, the economic factors pay attention to the cost of energy and profitability of the proposed hybrid system. While the environmental part mainly centers on the systems 'carbon footprint. The economic, technical, and environmental indicators addressed in this study are listed in Table 3.7and 3.8, 3.9, respectively. Several technical criteria are defined to investigate the performance of the decentralized A-CAES and the entire HES. A HES would be economically viable when it can satisfy the load demand at an acceptable cost. The economic indicators used in this study to evaluate the system feasibility and conduct the economic analysis include the LCC and, LCOE, and PBP.

Table 3. 7. A list of technical performance indicator

Technical performance Indicator	Description	Formula	Ref.
A-CAES system			
Round trip efficiency	The ratio of the A-CAES system discharging and charging energy over a complete cycle ($t=t_{discrg}/t_{crg}$) and the entire year (t=8760 hr)	$RTE = \frac{\sum_{t=1}^{t} W_{CAES,dcrg}(t)}{\sum_{t=1}^{t} W_{CAES,crg}(t)}$	[20]
Load coverage ratio	The contribution of the A-CAES system to fulfill the load demand	$LCR = \frac{\sum_{t=1}^{8760} W_{CAES,dcrg}(t)}{\sum_{t=1}^{8760} W_{L}(t)}$	[20]
Storage ratio	The ability of the A-CAES system to absorb excess PV system's output power and inexpensive grid power	$SR = \frac{\sum_{t=1}^{8760} W_{CAES,crg}(t)}{\sum_{t=1}^{8760} W_{ren}(t) + \sum_{t=1}^{8760} W_{imp,offpeak}(t)}$	[20]
Heat recovery ratio	The ability of the A-CAES system to recover the heat generated during the compression process	$HRR = \frac{\sum_{t=1}^{8760} \dot{Q}_{tr}(t)}{\sum_{t=1}^{8760} \dot{Q}_{c}(t)}$	[20]
HES			

Electrical load management rate	The fraction of the total energy delivered to the load demand coming from renewables and A-CAES	$ELMR = \frac{\sum_{t=1}^{8760} min(W_{ren}(t), W_L(t)) + W_{CAES,dcrg}(t)}{\sum_{t=1}^{8760} W_L(t)}$	[20,84]
Loss of power supply probability	Referring to the capability of power system in meeting the load demand	$LPSP = \frac{\sum_{t=1}^{8760} W_L(t) - (min(W_{ren}(t), W_L(t)) + W_{CAES,dcrg}(t) + W_{g,per}(t))}{\sum_{t=1}^{8760} W_L(t)}$	
Self-consumption rate	the ability of system to consume the generated renewable energy	$SCR = \frac{\sum_{t=1}^{8760} min(W_{ren}(t), W_L(t)) + W_{CAES,crg}(t)}{\sum_{t=1}^{8760} W_{ren}(t)}$	

Table 3. 8. A list of economic performance indicator

Economic performance Indicator	Description	Formula	Ref.
Life cycle cost	The net present value of all expenditures during the project's lifetime	$LCC = CAPEX + (OPEX_{yr}/CRF)$	[236]
Total capital cost of HES	Including the capital cost of all energy conversion systems in HES	$CAPEX = CAPEX_{PV} + CAPEX_{Conv.} + CAPEX_{CAES}$	[20]
Total capital cost of A-CAES	Investment cost of the A-CAES system is the summation of the initial cost of all	$CAPEX_{CAES} = CAPEX_c + CAPEX_{tr} + CAPEX_{AST} + CAPEX_{TES} + CAPEX_{HEX}$	[20]

	components (Table D.1)		
Total operation cost of HES	Summation of operation cost associated with PV, converter unit, CAES, and grid	$OPEX = (OPEX_{PV} + OPEX_{conv.} + OPEX_{CAES} + G_{net})$	[20]
Total operation cost of CAES	Summation of operation cost of turbine and compressor trains, AST, HEXs, TES and fuel (if needed)	$OPEX_{CAES} = OPEX_c + OPEX_{tr} + OPEX_{AST} + OPEX_{TES} + OPEX_{HEX} + OPEX_{fuel}$	[20]
Net energy purchasing from the grid	The difference of energy imported from the grid (including main and flexible load) and energy exported to the grid	$G_{net} = \sum_{t=1}^{8760} C_{per}(t)\, W_{g,per}(t) - \sum_{t=1}^{8760} C_{sell}(t)\, W_{g,sell}(t)$ $W_{g,per}(t) = W_{L,per}(t) - W_{flex,per}(t)$	[12]
Capital recovery factor	In order to consider the interest rate (I_r) in the lifetime (n) of the project, the net present value of operation cost is calculated using the capital recovery factor	$CRF(I_r, n) = \frac{I_r(1+I_r)^n}{(1+I_r)^n - 1}$	[237]
Real interest rate	Indicating the real interest rate (I_r) adjusted to consider the effects of the inflation rate (I_f) in the nominal interest rate (I_n).	$I_r = 1 - \frac{1+I_n}{1+I_f}$	[237]
Levelized cost of energy	Implying the LCC per unit of electricity generated, which is the summation of total annual served energy (primary load demand, selling back to grid, other	$LCOE = \frac{LCC \times CRF}{E_{served}}$	[155]

	application)		
Payback period	Time required to recover the CAPEX of the project while reaching the break-even point	$SPBP = \frac{CAPEX}{CF}$	[12]
Cash flow	Electricity saving cost (cash flow) due to the adopting PV/A-CAES system. Net electricity purchased from the grid in the basic power system (only grid) and current scenario (after adopting HES)	$CF = Basic\ Scenario - Current\ Scenario = G_{net}^{bps} - OPEX$	[12]
Cumulative Cash flow (profit)	The profitability of adopting PV/A-CAES system. The DPBP is the year when profit gets the value of zero.	$Profit = \sum_{ii=1}^{n} \frac{CF}{(1+I_r)^{ii}} - CAPEX$	

Table 3. 9. A list of environmental performance indicator

Environmental performance Indicator	Description	Formula	Ref.
Total carbon emission reduction by HES	Total carbon emission reduction by adopting HES emits	$TCER\left(\frac{kg}{year}\right) = CER_{CAES} + CER_{grid} + CER_{boiler}$ $CER_{CAES} = EM_{D-CAES} - EM_{A-CAES}$ $CER_{grid} = EM_{grid}^{bs} - EM_{grid}^{cs}$ $CER_{boiler} = EM_{gboiler}$	--

Total emissions from HES	Total emission that HES emits	TEM= $EM_{CAES} + EM_{grid} + EM_{gboiler}$	
CAES emission	The multiplications of emission factor and the amount of fuel consumption. For A-CAES system $\dot{Q}_{tr}^{'}(t) = 0$, while for D-CAES $\dot{Q}_{tr}^{'}(t) = \dot{Q}_{tr}(t)$ (Eq.(13))	$EM_{CAES}(kg) = \sum_{t=1}^{8760} Ef \frac{\dot{Q}_{tr}^{'}(t)}{H_{fuel} \times \eta_{fuel}} \times \Delta t$	[81]
Grid emission	The carbon emission equivalent to the imported energy from the grid	$EM_{grid}(kg) = \sum_{t=1}^{8760} \lambda_e \times W_{g,per}(t) \times \Delta t$	[81]
Gas boiler emission	The multiplications of emission factor and the amount of fuel consumption	$EM_{gboiler} = \sum_{t=1}^{8760} Ef * m_{NG}$ $m_{NG} = \frac{(PV\ power - eboiler\ demand) > 0}{H_{fuel} \times \eta_{fuel}}$	-

3.4.1.6. Optimization algorithm

The design of a HES can be a complex task due to the uncertainty of renewable resources and the constraint related to the components and specific case studies. Among all optimization techniques, meta-heuristic methods can handle nonlinearity and effectively approximate global solutions with better convergence and accuracy at high speed [235].

As reported in [238], the particle swarm algorithm (PSO) and genetic algorithm (GA) are the most-used optimization techniques for solving design optimization problems in terms of both performance and flexibility. PSO and GA were inspired by animal social behavior and laws of natural evolution, respectively [239]. This study uses the PSO technique to solve the design optimization problem while its performance is compared with GA. In PSO, the candidate solutions are called particles which have their own positions and velocities. The movements of these particles are updated in the search space to reach a better position according to their own personal best, and the direction toward the global best of the swarm achieved so far. The velocity (V_z^k) and position (X_z^k) of zth particle at iteration k is updated as follows:

$$V_z^{k+1} = \omega\, V_z^k + c_1 r_1 (P_{best,z}^k - x_z^k) + c_2 r_2 (G_{best}^k - x_z^k) \quad (3.55)$$

$$X_z^{k+1} = X_z^k + V_z^{k+1} \quad (3.56)$$

where $P_{best,z}^k$ and G_{best}^k show the personal and global best positions, ω represents the inertia weight which is initially set to 0.9, reducing linearly to 0.4 in proportion with iteration number, r_1 and r_2 are the random parameters between 0 and 1, c_1 and c_2 are constant parameters representing the self-confidence range (1.5 to 2) and swarm-confidence range (2 to 2.5), respectively.

Fig. 3.27 shows the flowchart of the PSO algorithm for solving the proposed design optimization problem. At first, the algorithm considers a random value for the velocity and position of each particle and their corresponding local and global best positions. Then the algorithm's iteration begins, and the fitness of particles (objective function) is calculated using the HES'hourly-based PDSs running throughout the year. Accordingly, P_{best} and G_{best} are evaluated and stored according to the particles' personal and global best experiences. Afterward, the iterative loop repeats, and the new position and velocity are estimated, and correspondingly the objective function is calculated, and P_{best} and G_{best} become updated (by comparing with the previous values). The algorithm's loop is ended when the termination criterion, which is the number of iterations (N_k) is satisfied. The PSO method's control parameters considered in this study are shown in Table 3.10.

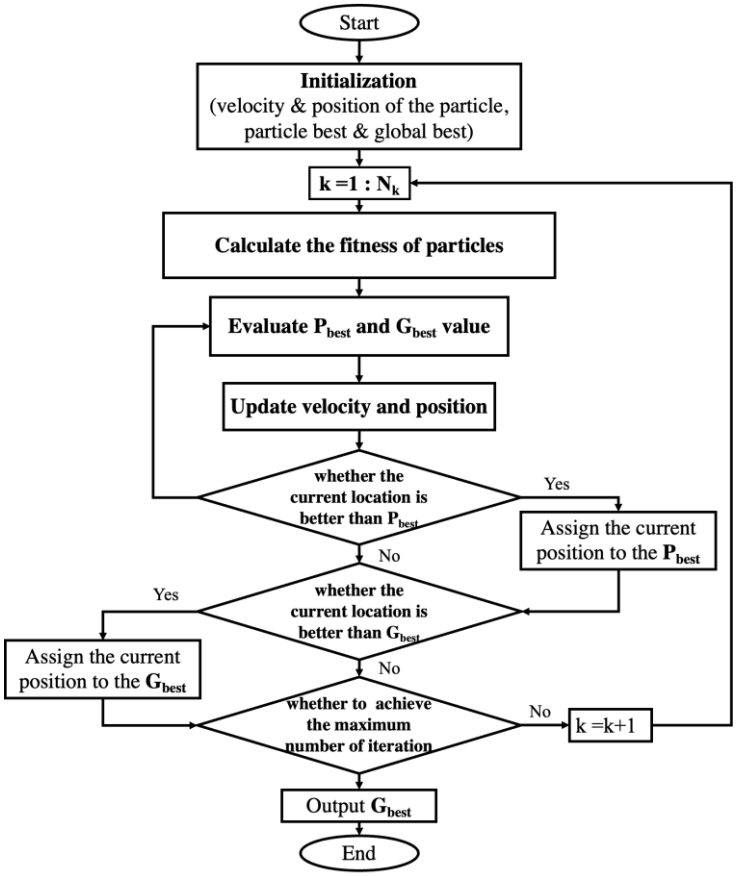

Fig. 3. 27. The block diagram of the PSO optimization algorithm.

Table 3. 10. Parameters of the PSO algorithm [240].

Parameter	Value
Dimension of the problem	10
Population size	20
Inertia weigh	decreases linearly from 0.9 to 0.4
Maximum iterations (N_k):	100
Weighting factors (c1 and c2)	2

3.4.2. Case study

The case study is the John Molson School of Business, known as the MB building, one of the main buildings of the Concordia University, located in downtown Montreal, Canada with 45°50′ N of latitude and 73°56′W of longitude. MB is a high energy-intensive building with annual 5645 MWh energy demand, which equals at least to 506 household energy needs in Canada. Within this building, there are two emergency and regular transformers measuring the total load demand of the MB building. The regular and emergency circuits in the building are split to make the generator's wiring and distribution much simpler. Approximately one-third of the lighting in the MB building is connected to the emergency circuits, along with a few critical

mechanical systems such as the boiler, pumps and controllers, smoke extraction and pressurization systems, and elevators. The regular circuits are used to power the remaining two-thirds of the lighting, plug loads, audio/video equipment, and the chillers and cooling towers. Based on the taken measurement, the MB building has the average, maximum, and minimum hourly electricity consumption of 645 kWh, 1604 kWh, and 271 kWh over a year, respectively. The yearly total electric load demand of the corresponding building is presented in Fig. 3.28(a).

Figs. 3.28 (b) and (c) show the solar irradiance and ambient temperature in Montreal provided by NASA in 2021. According to the measurement, the average daily solar radiation is 3.58 kWh/m^2/day, while the maximum and minimum average daily solar radiation of 6.47 and 1.20 kWh/m^2/day are observed in July and December, respectively.

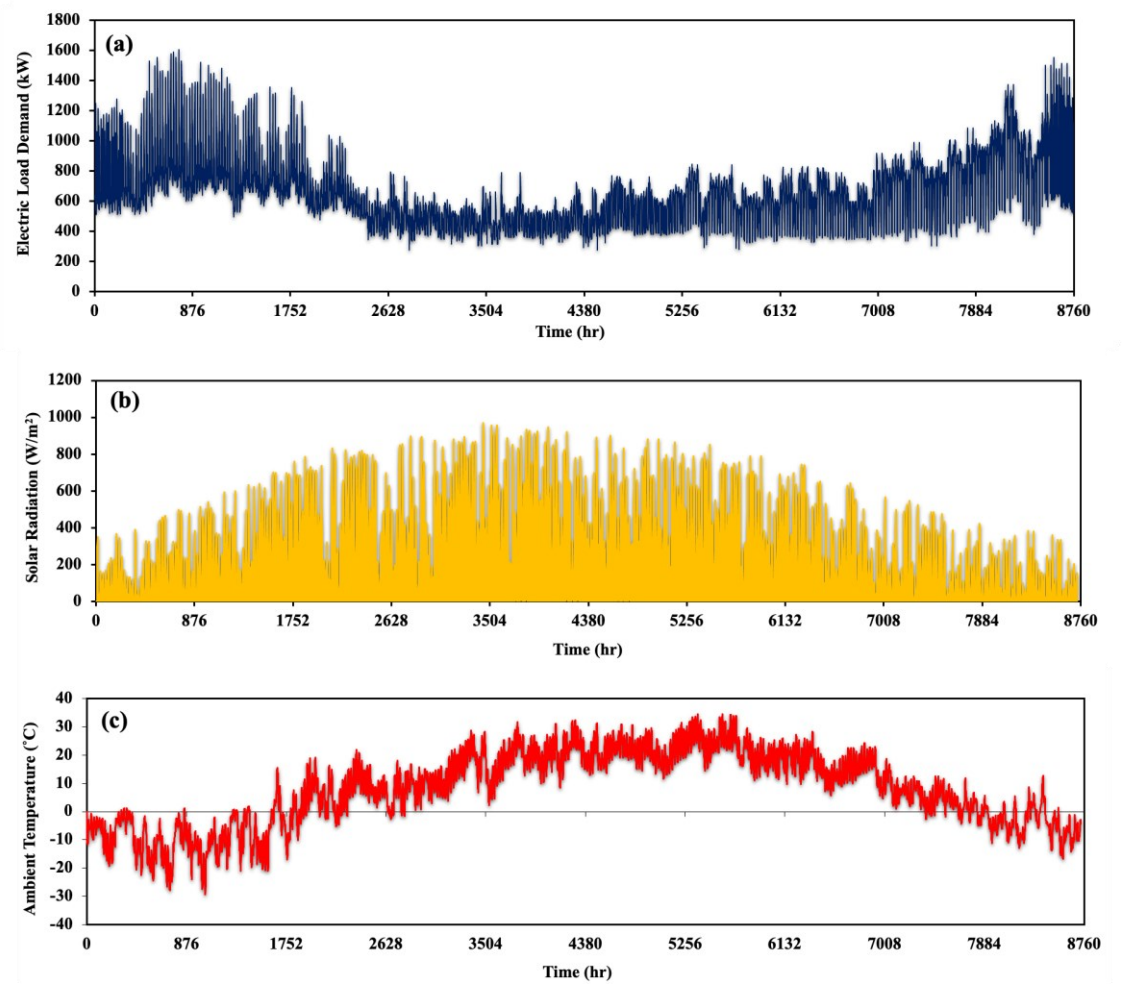

Fig. 3. 28. Hourly-around yearly profile of (a) building load demand, (b) solar radiation, (c) ambient temperature of Montreal city in 2021.

Furthermore, in another building of the Concordia campus (EV building), there are electric boiler (e-boiler) and natural gas boiler (g-boiler), which are used to provide hot water for the HVAC system. In this study, the load demand of an electric boiler (with power capacity of 1000

kW) is considered the flexible load, which is answered by PV-surplus power when A-CAES capacity is full. By adjusting flexible loads to match the surplus renewable energy, the need to dump or curtail the renewable generation is reduced while making better use of clean energy resources and increasing the system's cost-effectiveness. The load demand of the electric boiler and natural gas (NG) used by the g-boiler are shown in Fig. 3.29.

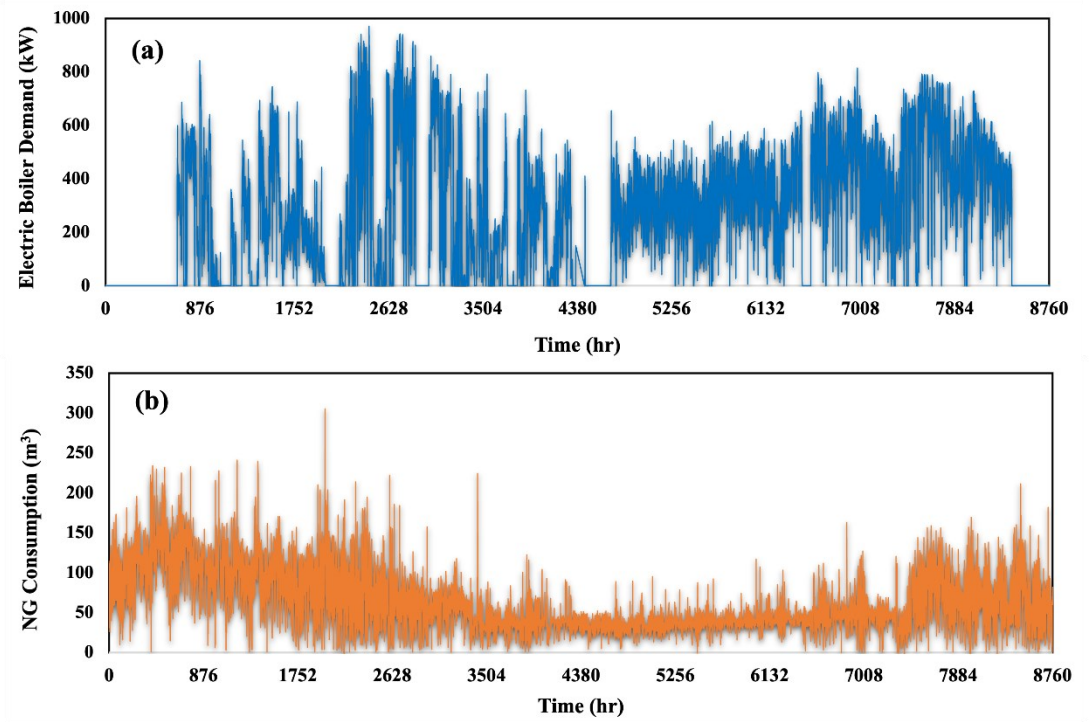

Fig. 3. 29. a) electricity demand of electric boiler, b) NG consumption of gas boiler.

3.4.2.1. Electricity market in Montreal and proposed TOU tariff

Due to Quebec's reliance on hydroelectric power for electricity generation, the cost of electricity in the province is relatively lower compared to other provinces in Canada. Therefore, only two different electricity prices corresponding to the two-period time-of-use (TOU) tariff are implemented by a utility company named Hydro-Quebec.

In this study, a TOU tariff scheme is proposed and utilized according to the flex Rate M [241] of double-daily electricity tariffs specified by hydro-Quebec for large consumers as well as Concordia University's monthly contract-based electricity price. The TOU tariff is divided into high electricity prices at peak hours from 6 am to 9 am and 4 pm to 8 pm and low electricity prices at off-peak hours throughout the year. Thus, the peak-hour electricity price is considered according to the flex M rate, which is 0.51967 cents/kWh only for winter (from December to March). Similarly, we assume half of the winter peak-hour price for summer days to have double-tariff pricing (2-period TOU tariffs) in summer as well (from April to November). Table

3.11 shows the electricity tariff scheme in peak hours for winter and summer. Concordia University's monthly contract-based electricity price, shown in Fig.3.30, is considered the electricity price at off-peak hours, holidays, and weekends for each month of the year.

Table 3. 11. Peak-hour electricity price based on the flex M rate of Hydro-Quebec.

Season	Peak Hours	Electric Price (CAD/kWh)
Winter	6:00 – 9:00 16:00 - 20:00	0.51967
Summer		0.2598 (assumption)

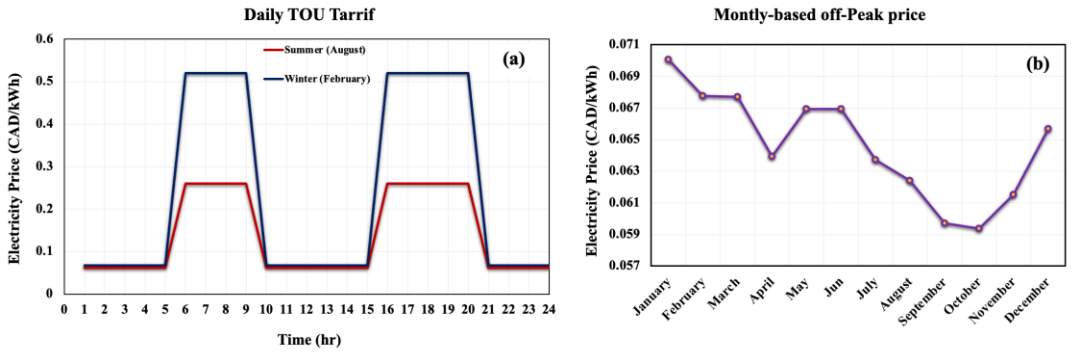

Fig. 3. 30. a) Daily TOU tariff, and b) monthly-based off-peak electricity price

As mentioned in the literature, the electricity export price is around two to four times less than the import price, depending on the time of the day [12]. Therefore, since Hydro-Quebec implements no tariff for export electricity price, half of the double-tariff purchase price is assumed for the selling price for the entire year.

3.4.2.2. Techno-economic and environmental parameters

To conduct the simulation and optimization, a proper value for the parameters of each component in the proposed PV / A-CAES hybrid system should be collected first. The economic parameters of PV, battery, converter, and A-CAES sub-systems and their corresponding economic models are presented in 3.5.2.2. The technical parameter of the studied A-CAES systems are listed in Table 3.13. Notably, most of the technical parameters of A-CAES components were selected based on the actual A-CAES pilot plant named TICC-500 [27]. The economic, environmental parameter and project specifications are listed in Tables 3.12, 3.14 and 3.15, respectively. The characteristics of the PV panel considered in this study are detailed

in our previous research [20]. It should be noted, in this study, the lifetime of all components is the same as the project lifetime. Table 3.16 presents the lower and upper bounds of design-decision variables optimized by PSO. It is worth mentioning the search range of design variables is chosen according to the actual situation of the case study, as presented earlier. According to TICC-500 pilot plant average value for design variable is considered to validate the new simulation model as listed in Table 3.17.

Table 3. 12**.** Economic parameters of HES's components.

Components*	CAPEX ($)	$OPEX_{fix}$ ($/yr)	Ref
PV panels	930 ($) N_{PV}	2% (CAPEX)	[242]
Converter (95%)	296.61($/kW) W^{r}_{conv}(kW)	2% (CAPEX)	[242–244]
Battery	525 ($)$N_B$	0.5% (CAPEX)	[245]
Compressor	253 ($/kW) $N_c W^{r}_{c}$(kW)	2% (CAPEX)	[34,246,247]
Turbine	225($/kW) $N_{tr} W^{r}_{tr}$(kW)	2% (CAPEX)	[34,246,247]
AST	$(42\ P_{max}(\text{kPa}) + 1.4) \times (710\ V_{AST}(\text{m}^3)^{0.54})$	1% (CAPEX)	[12]
Heat exchanger	$130\left(\frac{A_{HEX}(\text{m}^2)}{0.093}\right)^{0.78}$	1% (CAPEX)	[131,152]
TES (Hot/Cold tank)	20 ($/kWh) E_{TES}(kWh)	1% (CAPEX)	[34,248]

Table 3. 13**.** A-CAES input technical data.

Process parameter	Values	Refs
Ideal gas constant (R_{air})	287 J/kg/K	[129]
Specific heat of the air (C_{air})	1004.5 J/kg.K	[129]
Isentropic factor (γ)	1.4	[129]
Ambient air pressure (p_{am})	101.3 kPa	[129]
Ambient air temperature (T_{am})	298 K	[129]
Air Storage Tank		
Air temperature (T_{AST})	298 K	[129]
Compressor		
Efficiency of motor(η_M)	90%	[129]
Inlet temperature (T_c^{in})	298 K	[129]
Minimum output power (δ_c)	30% of rated power	[34]
Turbine		

Efficiency of a generator (η_G)	95%	[34]
Inlet temperature (A-CAES) (T_{tr}^{in})	373 K	[129,221]
Minimum output power (δ_{tr})	30% of rated power	[34]
TES		
Hot Tank (TES) temperature ($T_{in,hot}^{w}$)	393 K	[34]
Cold tank temperature ($T_{in,cold}^{w}$)	298 K	[34]
Heat exchanger effectiveness	95%	[249]
Overall heat transfer coefficient	300 W/m^{2}K	[249]
Combustion Chamber		
Heating value of NG (H_{fuel})	1 kJ/kg	[21]
Efficiency of combustion chamber (η_{fuel})	95 %	[21]

Table 3. 14. Environmental input data.

Parameter	Value	Ref.
CO_2 emission factor of fuel (Ef)	1.877 kg/m^3	[81]
Electricity emission coefficient (λ_e)	0.972 gr/kWh	[81]

Table 3. 15. Project specification.

Parameter	Value	Ref.
Lifetime (n)	25 years	[248]
Nominal interest rate (I_n)	4.25%	[250]
Inflation rate (I_f)	6.8%	[251]

Table 3. 16. Decision variables and their simulation ranges.

Decision variable	Unit	Lower boundary	Upper boundary	Variable type
N_c	Number	1	5	Discrete
N_{tr}	Number	1	5	Discrete
W_c^r	kW	50	350	Continuous
W_{tr}^r	kW	50	350	Continuous
V_{AST}	m^3	50	300	Continuous
E_{TES}	kWh	0	8000	Continuous
P_{AST}^{max}	MPa	6	20	Continuous
P_{AST}^{min}	MPa	1	2.5	Continuous

Table 3. 17. The quantity of design variables in TICC-500 A-CAES pilot plant.

Design Variable	N_c	N_{tr}	W_c^r	W_{tr}^r	V_{AST}	P_{AST}^{max}	P_{AST}^{min}	V_{TES}	E_{TES}
TICC-500 [27,221]	5	3	63 kW	166.67 kW	100 m^3	10 MPa	2.5 MPa	12 m^3	1.05 MWh

3.4.3. Results and discussions

This part of study aims to design and plan a decentralized A-CAES system under four PDSs based on its different application potentials for building infrastructures. The simulation and optimization have been conducted to investigate the optimal techno-economic and environmental performance of a proposed HES designated to satisfy the load demand of the high energy-intensive urban building. Moreover, four PDSs were presented and compared in order to accomplish the LCC assessment of the studied HES. A-CAES system's dynamic behavior and energy flow, technical and environmental indicators based on hourly-based yearly operation are analyzed while the economic criterion during the project lifetime is evaluated. The effect of the size of energy sources (number of solar PV panels and allowable power purchased from the grid) and AST volume on different indicators of various strategies are investigated. It is important to emphasize that the size of the PV system and AST volume specifically refer to the available space within the building. A simulation model, including a mathematical model and proposed PDSs, along with the optimization model consisting of the optimization problem and PSO algorithm, were implemented in MATLAB software (version 2022a) running on an Intel Core i7-7500U CPU @ 2.7 GHz. Moreover, the simulation has been performed with a time step of one hour and operates on data for one year (8760 samples/year). The information related to the input parameters is presented in previous section 3.5.2.

3.4.3.1. Validation and verification of simulation and optimization models

In this part of study, the A-CAES system is designed optimally using a coupled simulation-optimization model. To validate the reliability of the simulation model, including the mathematical model and PDSs, the design parameters of a well-known A-CAES pilot plant named TICC-500 were set as an input of the simulation framework. Then, the quantity of crucial operational parameters resulting from the adopted model is compared with their quantity in the considered pilot plant at the design condition. TICC-500 facility includes a five-stage motor/compressor train and a three-stage generator/turbine train with different characteristics from one another and a nominal power capacity of 315 kW and 500 kW, respectively. Since it

is assumed that the compressors and turbines have the same characteristics (see section 3.5.1.3), the average power capacity and isentropic efficiency of compressors/turbines are considered as input design variable values, as presented in Table 3.17 (section 3.5.2.2).

Table 3.18 shows the value of operational parameters obtained from the simulation model and actual A-CAES pilot plant under design conditions. Comparing the simulation result and real available data indicates a similarity of over 75% for all operational parameters, while the average similarity is around 88%. The main reasons for the differences are the values of input design parameters: in reality, the compressors and turbines of the TICC-500 pilot plant have different characteristics each, while the average values for them are assumed in this study. For example, it is assumed that each compressor stage has a nominal power capacity of 63 kW with an average isentropic efficiency of 80%, while each turbine stage has a rated capacity of 166.67 kW with an average isentropic efficiency of 81%. However, the results still show a fair agreement between the simulation results and actual data, considering the assumption adopted in the current model.

On the other hand, to verify the performance of PSO methods in optimal designing the A-CAES system, the results of the PSO under different PDSs are compared against those obtained through Genetic algorithm (GA) techniques, utilizing the same number of iterations (#100) and agents (#20). It should be noted that both methods aim to find the optimal design of the proposed HES to minimize the LCOE while maximizing the electrical load management. Fig. 3.31 displays the iteration curves of two methods applied for four different PDSs. Comparing the results of both optimization techniques shows the better performance of PSO in terms of convergence speed, optimization times, and in some cases, the better fitness function value. In other words, the fastest convergency, shortest optimization time, and minimum LCOE is achieved for all PDSs while employing the PSO method. Hence, the PSO technique is selected as an optimization algorithm for optimal designing the HES.

It's important to note that heuristics methods, like PSO, don't guarantee the global optimum but provide estimates of achieving it. A trial process was conducted to assess the robustness of the PSO algorithm (ensuring global optimal), following a methodology suggested in the literature [129,178]. This process involves multiple optimization runs, and the fitness values obtained in each run are analyzed. The minimum LCOE (fitness function) was achieved under

Table 3. 18. The A-CAES system's operational parameters resulted from the current simulation model and TICC-500 pilot plant with the same characteristics (Validation of simulation model).

	RTE (%)	$\mathbf{t_{crg}}$ (hr)	$\mathbf{t_{dcrg}}$ (hr)	Charge AMFR (kg/hr)	Discharge AMFR (kg/hr)	Output Energy (kWh)	Input Energy (kWh)	Q_c (kWh)	Q_{tr} (kWh)
Current model	39	4.35	1.17	2016	7483	585	1369	980	618
TICC-500 operational parameters [27,221]	37	5.59	1.03	1600	8600	555	1360	747	600
Similarity	95%	78%	88%	79%	87%	95%	99%	76%	85%

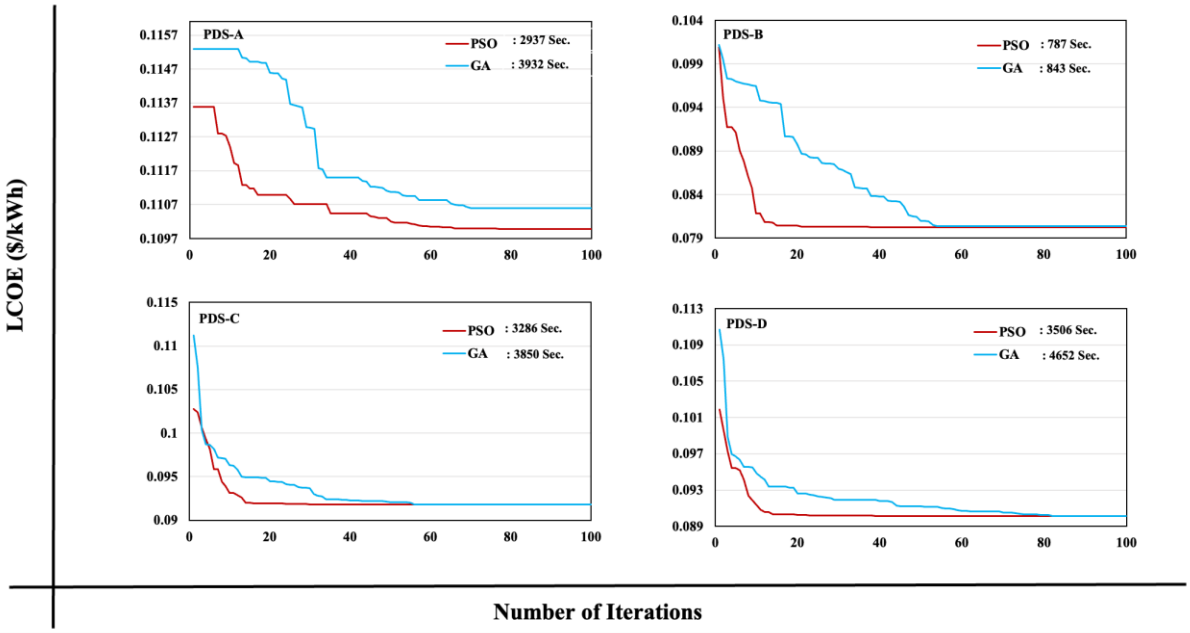

Fig. 3. 31. Variation and convergence of the fitness function (LCOE) for four PDSs using PSO and GA algorithm.

different PDSs labeled as A, B, C, and D, which are 0.110, 0.080, 0.092, and 0.090 $/kWh, respectively. These values were obtained over multiple optimization runs (8 for PDS A, 8 for PDS B, 8 for PDS C, and 7 for PDS D), as shown in Fig.3.32. The observed consistency in achieving these values across multiple runs indicates a convergence to a global optimum solution.

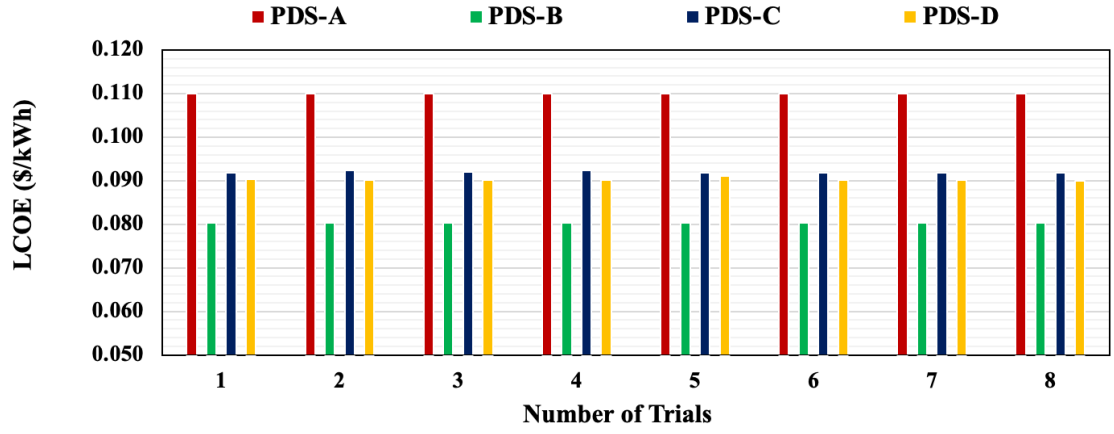

Fig. 3. 32. The fitness function (LCOE) value in 8-time trials for different PDSs using the PSO algorithm.

3.4.3.2. Optimization results

Following section analyzes the optimization results of four proposed PDSs.

3.4.3.2.1. Optimal configuration

Table 3.19 presents the optimal configuration of the top-economic A-CAES system under each PDS. According to Table 3.19, although the same AST volume of 300 m^3 is selected for all HESs, the A-CAES system operating under PDS-B has the largest size in terms of energy (i.e., highest AST pressure of 17.51 MPa and TES capacity of 5.59MWh/50.84 m^3) and power capacities (1400/929.8 kW compressor/turbine). On the other hand, the smallest A-CAES system is achieved under PDS-A, featuring a total compressor/ turbine capacity of 556.06/457.4 kW, an AST with a pressure of 12.12 MPa and a TES capacity of 3.05 MWh (equivalent to 27.74 m^3). Comparing the optimal configuration of A-CAES under strategies C and D reveals that seasonally planning the A-CAES (PDS-D) concerning the load-shifting results in the larger energy/power capacity to take advantage of both grid price and solar availability optimally.

Table 3. 19. The optimal configuration of the A-CAES system for different PDSs.

Design variable	PDS-A*	PDS-B	PDS-C*	PDS-D*
N_c (#)	5	4	5	5
N_{tr} (#)	4	5	5	5
W_c^r(kW)	111.21	350	157.56	167.80
W_{tr}^r(kW)	114.35	185.96	142.48	148.82
V_{AST} (m^3)	300	300	300	300
P_{AST}^{max}(MPa)	12.12	17.51	15.71	16.43
P_{AST}^{min}(MPa)	2.50	2.50	2.50	2.50
E_{TES} (MWh)	3.05	5.59	4.64	4.96
V_{TES} (m^3)	27.74	50.84	42.21	45.13

* Strategies including 7394 PV panels and 2100 kW Converter system

It is worth mentioning that since the maximum volume of AST (300 m^3) is selected by the optimization algorithm for all systems, a much more increase in the energy capacity of A-CAES led to an increase in the maximum pressure of AST. Hence, for the optimal system under PDS-B, eliminating the PV systems results in a rise in AST maximum pressure of almost 44.5%, 11.45%, and 6.6% higher than those of A, C, and D (see Table 3.19). Hence, it can be concluded

that the size of A-CAES highly depends on its long-term storage services and operation (PDS) in addition to the pattern of load demand, solar availability, and electricity tariff.

3.4.3.2.2. Technical performance analysis

The technical performance of optimal HESs for each PDS is introduced in Table 3.20. It should be noted that the performance indicators are described and formulated in Table 3.6. As shown, although the optimal A-CAES system designed for load-shifting (PDS-B) has the highest LCR of around 24.9 %, the largest electrical load management ratio (ELMR) of 52.1 % belongs to the system planning for joint solar penetration and seasonally load-shifting (PDS-D). So, the ELMR of the HES under PDS-D is around 4.22%, 28.6%, and 109% more than PDSs of C, A, and B, respectively. As can be seen, the higher storage ratio (SR) of 43.7% and LCR values of 24.9% belong to A-CAES of the HES operating under PDS-B, focusing on building electricity bill management while shaving the peak load demand for the 4.40 hr discharge process during peak hours. The higher percentage of the storing and delivering energy under PDS-B is mainly due to its single function of load-shifting and unlimited energy sources from the grid, leading to the A-CAES configuration with higher energy and power capacity. However, since the hybrid system does not plan for solar energy penetration, the ELMR is less than other systems.

Table 3. 20. The technical performance of the A-CAES system for different PDSs.

KPI	PDS-A*	PDS-B	PDS-C*	PDS-D*
ELMR (%)	40.5	24.9	49.9	52.1
LCR (%)	6.1	24.9	15.4	17.7
SR (%)	23.3	43.7	25.1	35.3
RTE (%)	48.1	43.4	46.4	45.9
HRR (%)	82.2	80.0	85.1	84.3
t_{crg} (hr)	8.73	6.15	9.00	9.00
t_{dcrg} (hr)	5.60	4.40	5.06	5.11

* Strategies including 7394 PV panels and 2100 kW Converter system

Moreover, comparing the round-trip efficiency (RTE) of A-CAES under different PDSs shows that the systems with the higher maximum pressure in AST have lower RTE. Thus, the A-CAES system under PDS-A has the highest RTE (e.g., 48.1%), and the less efficient A-CAES is achieved under PDS-B (e.g., 43.4%). The relation between the volume and pressure of AST can

explain such RTE values. As shown in Table 3.18, at the same AST volume (300 m^3), the higher the upper pressure in the tank, the larger the compressor power capacity and, correspondingly, the less RTE (see Table 3.20). Therefore, the most efficient A-CAES is obtained under PDS-A (renewable integration), while the less efficient A-CAES belongs to PDS-B (load shifting). Meanwhile, a heat recovery ratio (HRR) of over 80% is achieved for all configurations, among which the highest value belongs to the system operating under PDS-C with 85.1% HRR. The reason is the compressor/ turbine power capacity ratio of the A-CAES under strategy C is around 1.1, which is 1.7 %, 9%, and 26.6% less than that for the system under strategies D, A, and B.

Fig. 3.33 compares PV-surplus power under all PV excess energy management scenarios for the optimal configuration involving renewable energy (e.g., strategies A, C, and D). As can be seen, the highest PV-surplus power under scenarios of zero selling and flexible load (e-boiler) belongs to the HES, designed with PDS-C when load-shifting is conducted over an entire year. In contrast, the system planned under PDS-D (seasonally load-shifting) has the lowest unused PV power in all scenarios concerning PV-surplus energy management.

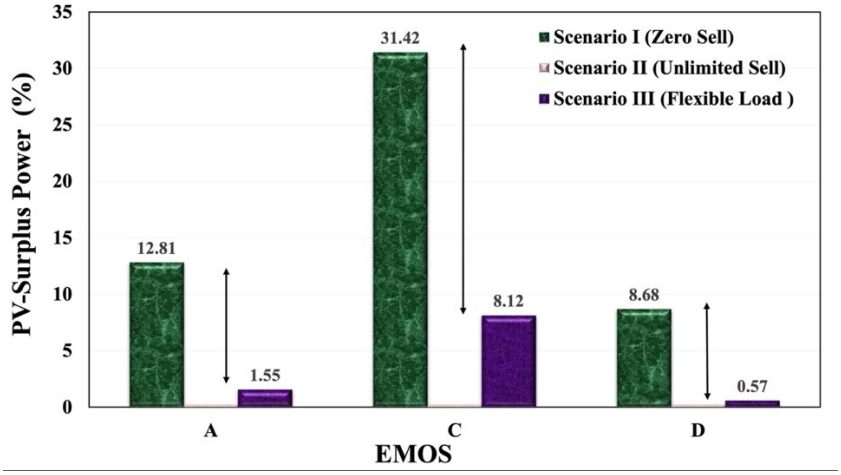

Fig. 3. 33. Comparing PV-surplus power under all scenarios for strategies involving renewable energy.

Thus, a PV self-consumption rate of up to 92% is attained for a system designed according to strategy D. While in PDS-C at worst case scenario (scenario I; zero sell), around 31.41% of PV output power remains unused, which is the highest compared to other strategies. Except in the presence of a flexible load (e-boiler in this study), the unused solar power drops by 3.8 times (under PDS-C). However, it is still more than other strategies of A and D, with 1.55% and 0.57% extra PV power under flexible load scenarios.

It is worth mentioning that the scenarios involving the use of excess electricity for other applications, apart from the primary load of the studied building, are explored as the alternatives for managing PV-surplus energy. Therefore, it does not make any changes in the optimal configuration and, subsequently, the technical performance of HES and A-CAES operations in the building. However, the economic and environmental indicators are changed.

3.4.3.2.3. Economic analysis

According to Table 3.21 and Fig. 3.34a, under the worst-case scenario (Scenario I; zero sell, see section 3.5.1.2), the LCOE values of 0.080, 0.090, 0.092, 0.110 $/kWh obtained for HES designed under PDSs of B, D, C, and A, with a maximum ELMR of 24.9 %, 52.1%, 49.9%, 40.5%, respectively. Nonetheless, the PDSs of B, D, C, and A have corresponding LCC values of 8.40, 9.41, 9.59, 11.39, and 11.04 M$. Under scenario I, except HES with PDS-A, the other optimal configurations are economically viable options compared to a primary power system (PDS-O) with an LCOE of 0.105 $/kWh. That shows that in the worst-case scenario (which is the basic scenario for the studied building), adopting an A-CAES system only for solar energy penetration is not financially viable as its LCOE of 0.110 $/kWh is around 4.76 % more than the primary power system. Thus, the optimal structure's discounted payback period (DPBP) under PDS-A is more than the project lifetime (25 years) in the worst-case scenario I, as shown in Fig. 3.34.

On the other hand, under the best-case scenario (Scenario II; unlimited sell), the minimum LCOE belongs to the optimal structure under PDS-C with a value of 0.073 $/kWh as around 31.42% of PV output power (PV-surplus power as shown in Fig. 3.33) is sold back to the grid.

Subsequently, the configurations with PDSs of B, D, and A exhibit LCOE values of 0.08, 0.084, and 0.101 $/kWh, respectively. It should be noted that the economics of the optimal system under PDS-B remains unchanged for all scenarios, as A-CAES is planned only for load-shifting under the respective strategy (there is no solar PV system).

Moreover, comparing the economics of optimal systems under all scenarios concerning managing the unused PV power shows that for all HESs, the lowest LCOE is achieved under scenario III, where the solar PV-surplus power is used for the available flexible load (e-boiler in this study). Consequently, analyzing the results of scenarios II and III indicates that although the lowest LCC value of 8.40 M$ belongs to the PDS-B (no PV/converter systems), the system of PDS-C demonstrates the minimum LCOE of 0.073 $/kWh and 0.072 $/kWh under scenario II and III, respectively. The reason is the presence of a term related to the served total load

demand in the denominator of LCOE formulas.

Table 3. 21. Economic results correspond to the optimal configurations for all PDSs under three scenarios concerning PV-surplus power management.

	PDS-A*	PDS-B	PDS-C*	PDS-D*	PDS-O (Grid)
Indicator	Scenario I (zero sell)				
LCOE($/kWh)	0.110	0.080	0.092	0.090	0.105
LCC (M$)	11.04	8.40	9.59	9.41	11.04
CAPEX(M$)	3.39	1.07	3.64	3.68	0
OPEX (M$/yr)	0.44	0.40	0.32	0.31	0.60
Net saving ($/kWh)	<0	0.025	0.013	0.015	0
DPBP (yr)	> 25	5.5	16.5	15.5	0
SPBP (yr)	21.53	5.36	13.26	12.87	0
Profit (M$)	-0.47	2.64	1.45	1.62	0
	Scenario II (unlimited sell)				
LCOE($/kWh)	0.101	0.080	0.073	0.084	0.105
LCC (M$)	11.26	8.40	8.98	9.24	11.04
CAPEX(M$)	3.39	1.07	3.64	3.68	0
OPEX (M$/yr)	0.42	0.40	0.29	0.30	0.60
Net saving ($/kWh)	0.004	0.025	0.032	0.021	0
DPBP (yr)	24.5	5.5	13.5	14.5	0
SPBP (yr)	19.8	5.36	11.5	12.45	0
Profit (M$)	-0.22	2.64	2.05	1.79	0
	Scenario III (flexible load)				
LCOE($/kWh)	0.099	0.080	0.072	0.083	0.105
LCC (M$)	11.01	8.40	8.50	9.05	11.04
CAPEX(M$)	3.39	1.07	3.64	3.68	0
OPEX (M$/yr)	0.41	0.40	0.26	0.29	0.60
Net saving ($/kWh)	0.006	0.025	0.033	0.022	0
DPBP (yr)	24.4	5.5	12.5	14.4	0
SPBP (yr)	18.41	5.36	10.92	12.02	0
Profit (M$)	0.023	2.64	2.54	1.99	0

* Strategies including 7394 PV panels and 2100 kW Converter system

That means achieving the minimum LCOE does not necessarily imply the lowest LCC and

vice versa, given how managing the PV-surplus power. Consequently, the economic assessment shows that the systems designed for load-shifting purposes (PDSs of B, C, and D) are financially viable (long-term cost-effectiveness) even in the worst-case scenario (scenario I) as their LCOE is less than the primary power system (PDS-O) under all scenarios, as shown in Fig. 3.34a. While, for the PV/A-CAES system to be a viable economic system, at least a part of PV-surplus power should be exported to the grid or used for other applications.

Meanwhile, among all strategies, the least capital expenditure (CAPEX) and operation expenditure (OPEX) belong to the optimal configuration under PDS-B (no PV/converter systems), planning A-CAES for building load-shifting, taking advantage of grid off-peak prices.

However, the capital cost of the A-CAES system in PDS-B is around 1.07 M$, which is 48.9%, 26.2%, and 23.5% higher than that of configurations under strategies A, C, and D, respectively.

To better compare the economic impacts of each component in optimal HESs, Fig. 3.34b shows the capital cost broken down by sub-systems for the four optimal configurations (as listed in Table 3.19). It should be noted that since all optimal structures under different scenarios are fixed, the CAPEX remains unchanged. In other words, the only OPEX of HESs varies across different scenarios concerning PV-surplus power management. According to Fig. 3.34b, for all HESs involving renewable energy (PV systems), the investment cost of the PV system is the most significant portion (around 60-65%) of the capital cost. In fact, the PV system and converter are the key cost components of the three HESs under PDSs A, C, and D. Notably, the initial cost of the A-CAES system is the least portion of the system's capital cost in these strategies. Regarding the A-CAES, for the HESs under strategies A, C, and D, the highest percentage of initial cost belongs to heat exchangers and compressor train. While in PDS-B, the compressor train has the highest share of 33% in A-CAES capital cost, followed by the heat exchanger, turbine train, AST, and TES with portions of 25%, 19%, 13%, and 10%, respectively. Such a cost-sharing can be proved by the A-CAES power and energy capacity, as presented in Table 3.19.

Fig. 3.35 illustrates the cumulative cash flow of optimal systems for different PDSs under various scenarios during the project lifetime. As can be seen, the least and most payback period (PBP) belongs to the system operating under PDS-B (only load shifting) and PDS-A (only renewable integration) for all scenarios, respectively. Hence, adopting the proposed HES for only solar system integration is not significantly profitable. Therefore, the A-CAES planned under PDS-A for only solar integration might be less attractive to investors than other HESs

with less LCOE and shorter PBP. The reason is the longer PBP increases the risk of the power projects becoming unprofitable or failing altogether. That shows adopting the A-CAES system for the building's electricity bill management and grid peak-shaving (PDS-B) is the most attractive option concerning the payback time. However, in some cases, depending on the amount of positive cash flow generated after the even-break point, the system with a longer PBP can be more attractive to investors than the project with a shorter payback period.

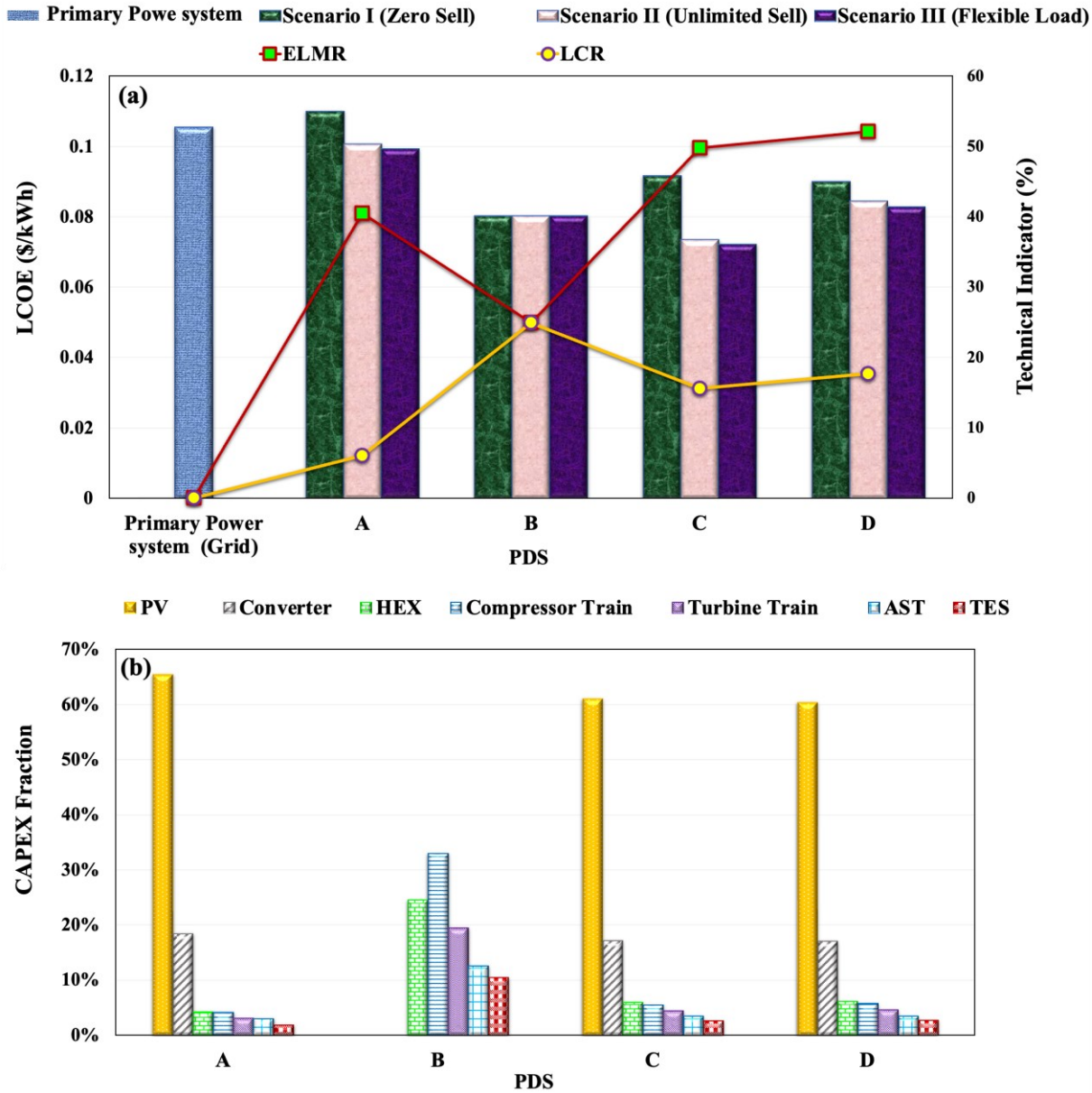

Fig. 3. 34. a) LCOE, ELMR, and LCR of HES, b) capital cost breakdown of HES's components under all scenarios for different PDSs.

As shown in Fig. 3.35, for example, under scenario III (flexible load) at the end of the project, the cash flow of systems under PDS-C and PDS-D is only 4% and 24% less than PDS-

B despite having PBP around 7 and 9 years longer. Furthermore, it is worth mentioning that although in scenario I, the PBP of strategy D is shorter than strategy C, the situation gets reversed in scenarios II and III, where the system with PDS-C has a more extended payback period than PDS-D. As mentioned earlier, higher PV-surplus power under PDS-C can lead to such outcomes.

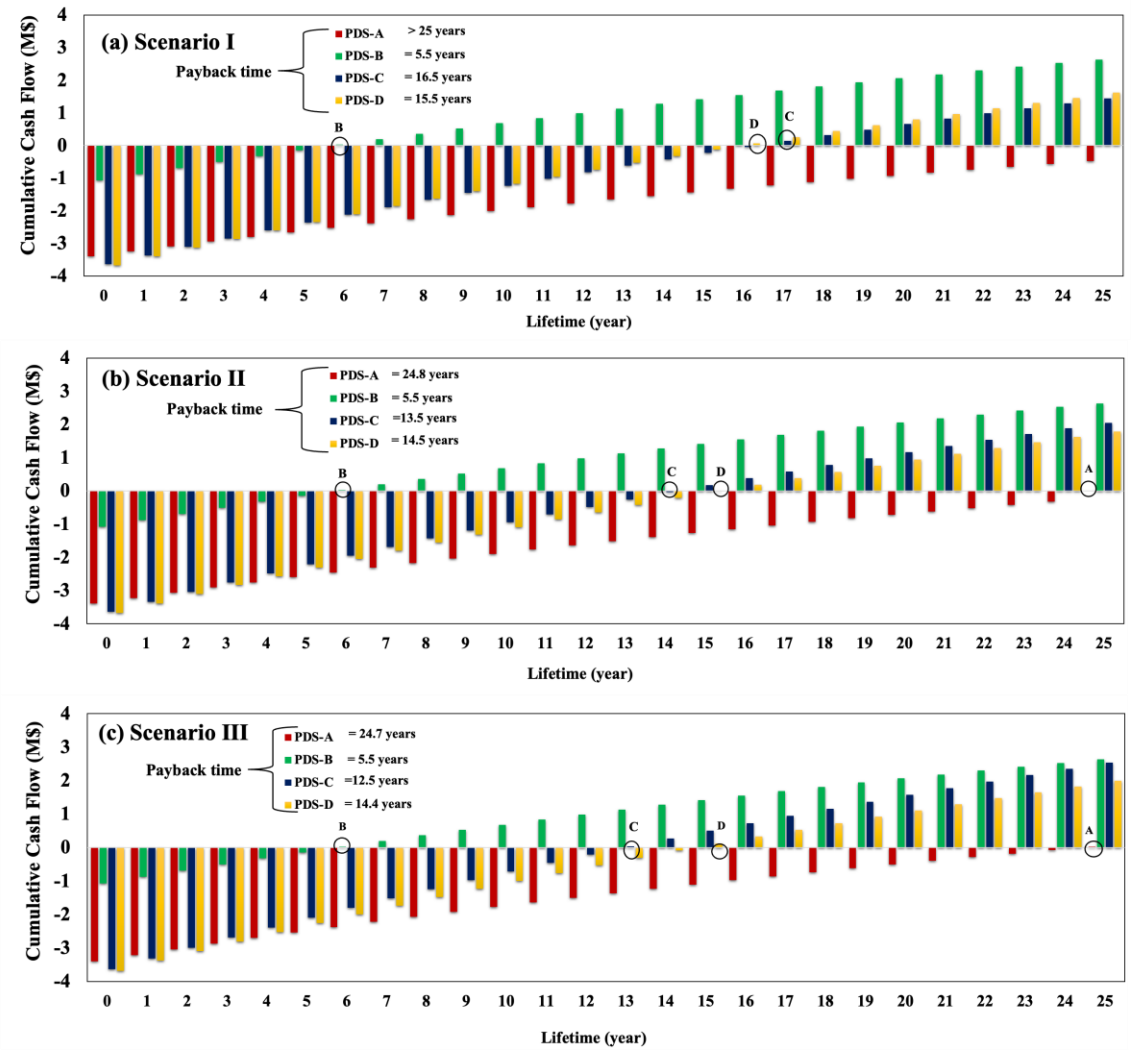

Fig. 3. 35. The optimal systems' cumulative cash flow (profit) for different PDSs under various scenarios over the project's lifetime.

Therefore, among all scenarios, maximum energy cost savings of 0.033, 0.025, 0.022, and 0.006 $/kWh were achieved for optimal configuration under strategies C, B, D, and A for scenario III. However, the least DPBP values of 5.49 years belong to the system operating under PDS-B (only load shifting) with less CAPEX compared to other strategies for all scenarios. It is worth noting that a project with a lower LCOE than the other system (especially the primary power system) can produce energy at a lower cost over its lifetime. It could be due to factors

such as lower capital cost, higher energy production, or more efficient technology. So, a project can have a lower LCOE than others but a longer PBP. This situation arises when the project incurs high CAPEX that is eventually offset by revenue generated over the project's lifetime.

3.4.3.2.4. Environmental analysis

Transparently quantifying environmental emissions is critical in selecting the best planning strategy among various operation strategies alongside the techno-economic assessment. This thorough evaluation enables well-informed decision-making, considering economic and environmental aspects to identify the optimal configuration and most suitable PDS [252]. Table 3.22 and Fig. 3.36 illustrate and compare environmental performance, including Carbon emission (CE) and total Carbon emission reduction (TCER) associated with the optimal configurations for all PDSs under all scenarios. It is worth mentioning that the grid is the only source of emissions for the current optimal HESs. Moreover, since around 95% of grid energy comes from renewables (e.g., hydro) in Quebec, only 5% of imported energy from the grid is assumed as the source of carbon emission. Thus, the quantity of CE of HES is independent of the scenarios concerning PV-surplus power management. However, the amount of TCER varies across the different scenarios as the emission associated with the sub-systems of current power systems is compared with the conventional components that use fossil fuel to generate energy. For example, A-CAES considered in current optimal systems is compared with the traditional CAES systems (D-CAES), which have a combustion chamber instead of a TES unit. Another example is e-boiler employment in current systems (as flexible load in scenario III) to manage the PV-surplus power instead of using a g-boiler to provide the same energy.

As shown in Fig. 3.36 and Table 3.22, given that the only grid is the emission source, the amount of CE is proportional to the grid importation for all strategies. In other words, the less solar availability, the more significant grid power penetration, and the higher the carbon footprint. So, the most significant CE belongs to HESs designed for load-shifting (PDS-B). More specifically, strategy B results in a configuration that emits Carbon by around 363.90 tonnes/year, 25% more than the PDS-O (grid). That is due to the unlimited grid power imported to meet the load demand while charging the A-CAES during the off-peak hour. Nonetheless, the CE from current optimal HESs with PDS of A, D, and C correspondingly are about 40.5 %, 28.3 %, and 19.03%, less than the PDS-O (grid).

On the other hand, although the system planned for renewable integration with PDS-A exhibits the lowest CE of 163.21 tonnes/ year, it also has less TCER than other systems under

all scenarios due to its lower grid power importation and smaller A-CAES size. Conclusively, the highest TCER is achieved for the optimal configurations with PDS-D under all scenarios.

Table 3. 22. Environmental results correspond to the optimal configuration for all PDSs under three scenarios regarding PV-surplus power management.

Indicator	PDS-A*	PDS-B	PDS-C*	PDS-D*	PDS-O (Grid)
	Scenario I (zero sell)				
CE** (tonne/yr)	163.21	363.90	222.11	196.72	274.33
TCER (tonne/yr)	204.10	322.98	307.68	370.43	-
CER_CAES	92.98	412.54	255.46	292.82	-
CER_Grid	111.13	-89.56	52.22	77.62	-
CER-eBoiler	0	0	0	0	-
	Scenario II (unlimited sell)				
CE** (tonne/yr)	163.21	363.90	222.11	196.72	274.33
TCER (tonne/yr)	223.06	322.98	354.17	383.27	-
CER_CAES	92.98	412.54	255.46	292.82	-
CER_Grid	130.08	-89.56	98.70	90.46	-
CER-eBoiler	0	0	0	0	-
	Scenario III (flexible load)				
CE** (tonne/yr)	163.21	363.90	222.11	196.72	274.33
TCER (tonne/yr)	230.76	322.98	374.58	389.67	-
CER_CAES	92.98	412.54	255.46	292.82	-
CER_Grid	111.13	-89.56	52.22	77.62	-
CER-eBoiler	26.66	0.00	66.90	19.23	-

* Strategies including 7394 PV panels and 2100 kW Converter system

** Grid is the only source of carbon emission at the current power systems (since in the considered case study, around 95% of energy comes from hydro, 5% of total energy from the grid is considered for estimating CE in both primary and current power systems)

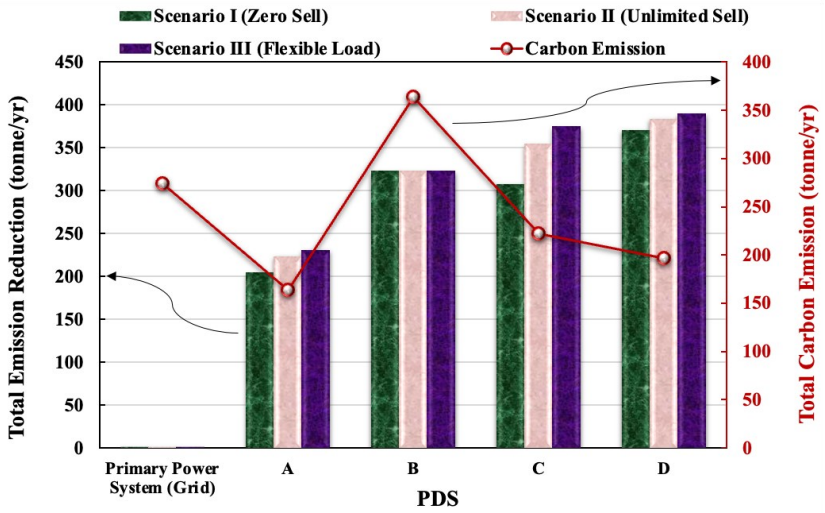

Fig. 3. 36. Comparison of CE and TCER for HESs for different PDSs under all scenarios.

Furthermore, in Fig. 3.37, the left figures depict the primary and secondary power consumption of the electric boiler (e-boiler), while showcasing the diminished NG consumption by the existing gas boiler (right figures) under Scenario III, which involves a flexible load in PDSs with integrated renewables. The observations align with the findings reported in Table 3.22 for Scenario III. Specifically, under PDS-C, it is evident that the surplus- PV power surpasses that of strategies A and D. Moreover, the reductions in gas consumption and the CER-eBoiler are notably more under this scenario compared to the other strategies.

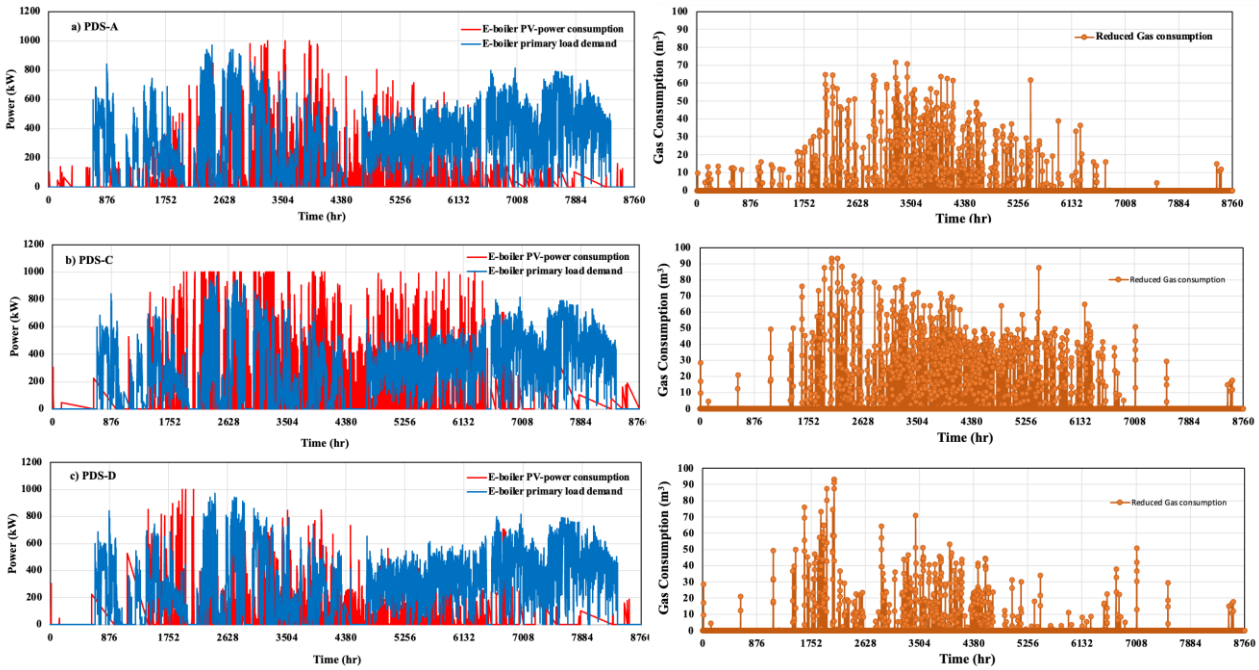

Fig. 3. 37. The primary and secondary power consumption of e-boiler (left figures), the reduced NG consumption by existing gas-boiler under the scenario III (flexible load) for PDSs involving renewable integration.

3.4.3.2.5. A-CAES operation analysis

This section elaborates on the operation and characteristics of the A-CAES system under each PDS, evaluating cycle by cycle and annually. Table 3.23 displays the other important design parameters of the A-CAES system under each PDS. According to Table 3.23, comparing design parameters for four systems shows that the same isentropic efficiency of 89.6% and the pressure ratio of 1.9 are achieved for turbine train of systems planning under strategies B, C, and D. The reason is the dependency of expansion ratio to the number of turbine stage and a minimum pressure of AST which are the same for respective systems. Nonetheless, the A-CAES designed under PDS-A, with one expansion stage less than other systems, has an expansion ratio of 2.2, 13.63 % higher.

In contrast, since the maximum pressure of AST for all systems is different, the compression ratio and, subsequently, the isentropic efficiency of compressors are not identical across the various configurations. As shown in Table 3.23, the maximum pressure ratio belongs to the system operating under PDS-B, which has a four-stage compressor and the highest AST's maximum pressure (17.5 MPa), 27%, 25%, and 22% higher than strategy A, C, D.

Fig. 3.38 also illustrates and compares the charging/ discharging time and air mass flow rate (AMFR) during a complete cycle. The results show the different charging/discharging times and AMFRs depending on the employed PDS. As shown in Table 3.23 and Fig.3.38, A-CAES can store energy for up to 9 hr when planning for joint renewable integration and load-shifting applications (strategies C and D and almost A). Nonetheless, the highest charging/ discharging AMFR and the least charging / discharging time belong to PDS-B planning for load-shifting. It can be said that the more charging/discharging AMFR, the less charging/discharging time. It can be concluded that charging time and AMFR of A-CAES are significantly influenced by uncertainty and availability of power resources. Hence, due to the uncertainty associated with solar availability, the A-CAES systems planned with PDS-A, C, and D have a higher charging time and less AMFR than strategy B (with a certain and unlimited power source).

Fig. 3.39 demonstrates the dynamic behavior of AST in the form of the SOC (%) and the air pressure for systems for different PDSs over a year on an hourly basis. It is evident that under PDS-A (see Fig. 3.39a), an AST capacity remains largely unused during winter due to the lower solar radiation and higher load demand than in the summer. However, under PDS-B (see Fig. 3.39b), the most capacity of AST is used in winter due to the higher energy demand and electricity price at off-peak hours. Such behavior of AST becomes more intense for the system

operating under PDS-C (see Fig. 3.39c) due to the desire of A-CAES to absorb excess PV energy and off-peak grid electricity to supply on demand at peak hours. Therefore, a considerable part of AST capacity is useless in summer under PDS-C as A-CAES is mostly at its full-charged state or close to it. As illustrated in Fig. 3.39d, the system under PDS-D has the behavior of a combination of PDS-A (in summer) and PDS-C (in winter). Therefore, unlike other strategies, a small portion of AST remains unused during the year. The behavior of TES is approximately similar to the AST for each PDS with the same reasons as presented in Fig. 3.40.

Table 3. 23. A-CAES systems' design parameters for each PDS under all scenarios.

	$\pi_{c,i}$	$\eta^{is}_{c,i}$ (%)	$\pi_{t,j}$	$\eta^{is}_{t,j}$ (%)	Charging AMFR (kg/hr)	Discharging AMFR (kg/hr)	t_{crg} (hr)	t_{dcrg} (hr)
PDS-A	2.6	90.5	2.2	89.5	3865.5	6025.0	8.73	5.60
PDS-B	3.6	90.1	1.9	89.6	8565.7	11961.8	6.15	4.40
PDS-C	2.7	90.4	1.9	89.6	5151.7	9165.4	9.00	5.06
PDS-D	2.8	90.4	1.9	89.6	5430.8	9572.9	9.00	5.11

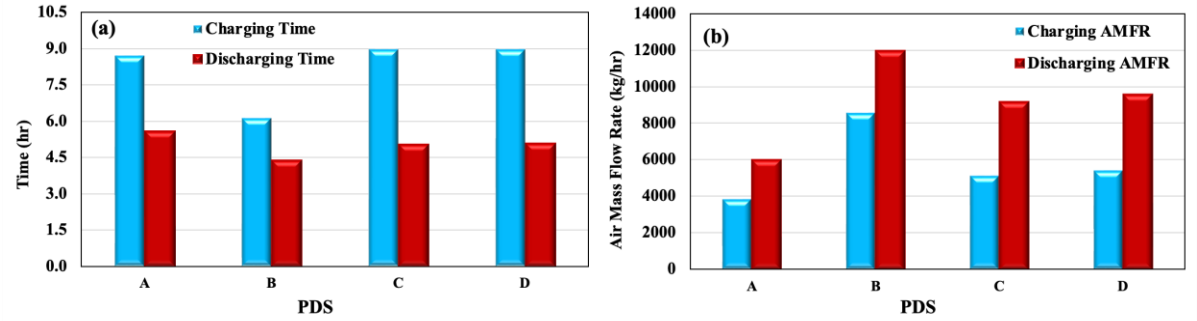

Fig. 3. 38. Comparing the charging and discharging a) time and b) air mass flow rate (AMFR) for optimal configurations under all strategies.

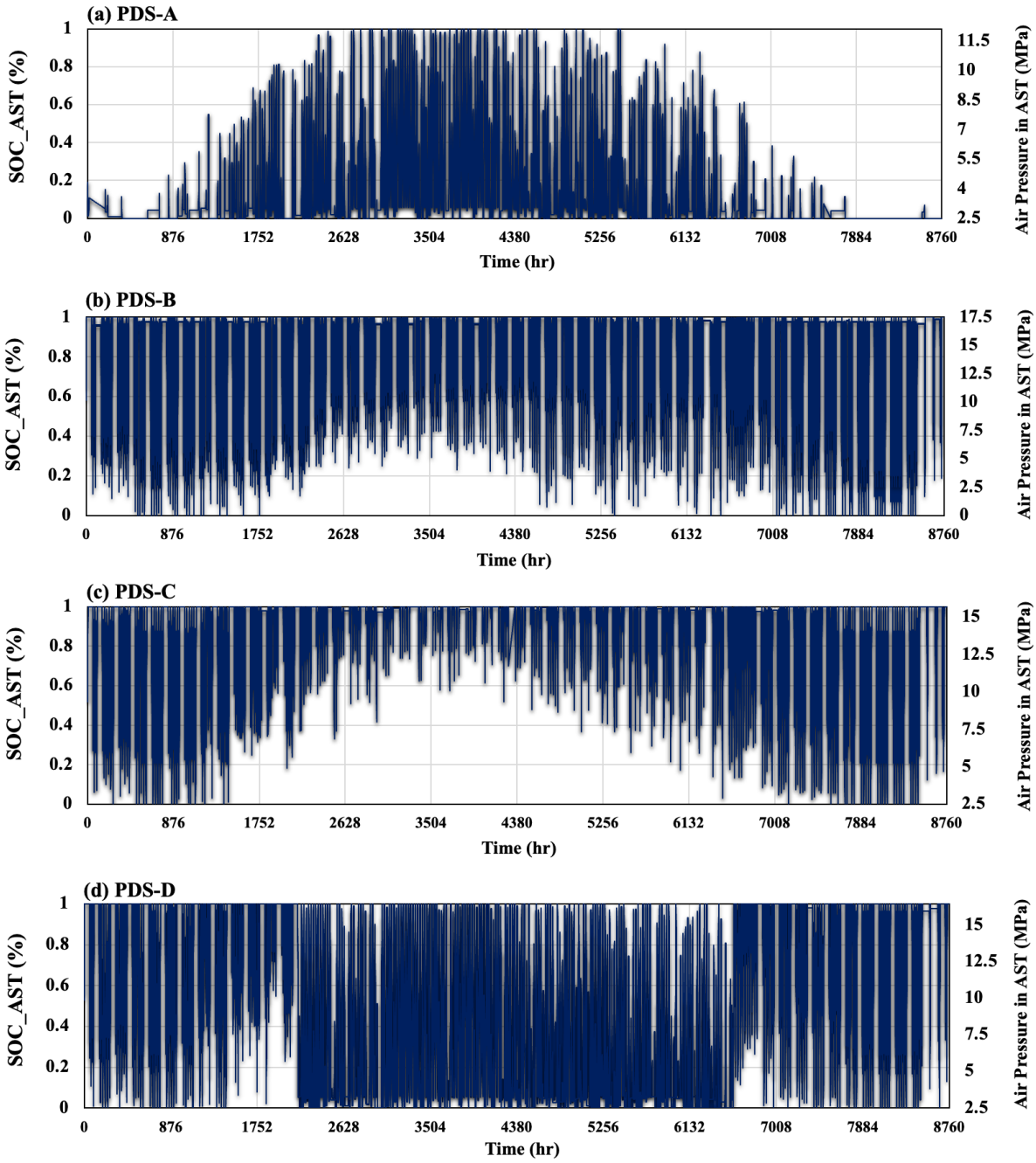

Fig. 3. 39. The SOC and air pressure in AST over a year for different PDSs under all scenarios.

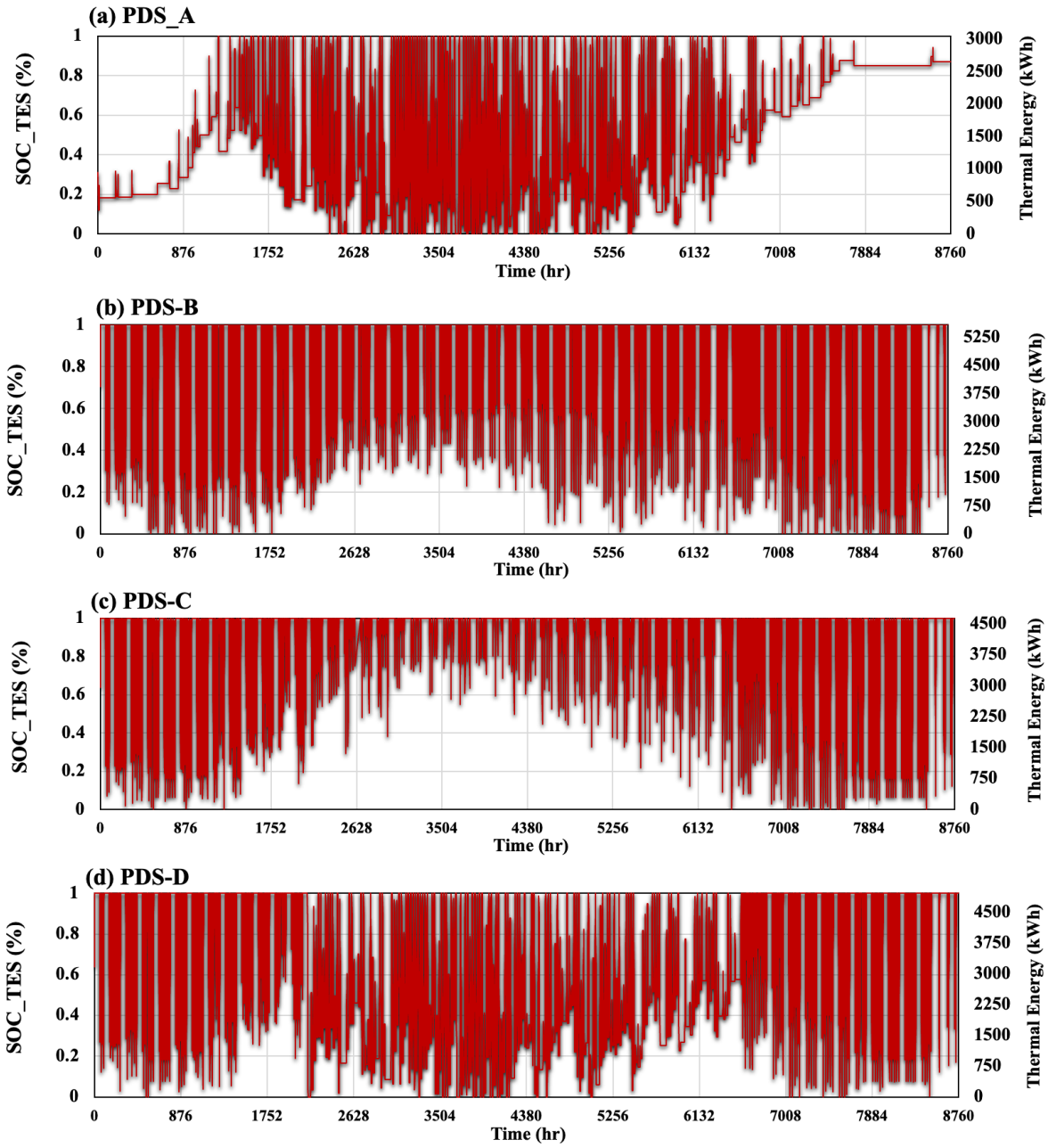

Fig. 3. 40. The SOC and stored energy in TES under different PDSs for all scenarios.

3.4.3.2.6. Electrical analysis

Fig. 3.41 presents the contribution of all energy sources (solar, A-CAES, grid) to meet the energy demand of building for different PDSs over months of the year. Almost all available power sources are employed to satisfy the building electricity demand across all systems. However, the distinctive contribution of the A-CAES system specifically highlights its contrasting role in meeting the load requirements in various PDSs. Given that the same solar PV capacity is utilized for the configuration involving renewables, the contribution of solar energy to answer the load demand remains consistent across strategies A, C, and D (see Figs.

3.40 a, c, and d).

As can be seen, the PV self-consumption in March and August is around 211.5 MWh, higher than the rest of the months, even though May and June are peak months in terms of solar intensity. That is due to the higher load demand in March and August compared to May and June. However, solar energy has the highest share of around 54% and 55.7% in the total supplied power to meet the demand in May and June, respectively, consistent with the higher solar irradiance and lower energy demand (see section 3.5.2). Conversely, since the weak solar irradiance coincides with the peak demand period (e.g., the first and last two months of the year), the solar power contribution to the building demand reaches less than 20% during this period. Accordingly, for the system with PDS-A, under which the A-CAES is planned only for renewable integration, the charging/ discharging and, subsequently, the contribution of A-CAES depend on the solar-PV generation potential (see Fig. 3.41a). Therefore, the A-CAES contribution in fulfilling the electricity requirement during periods characterized by high demand and low solar intensity (e.g., the two first and last three months of the year) ranges from 0.02% to 2.35 %. This contribution is considerably less compared to the months when A-CAES accounts for 6.5% to 18% of the power supply, coinciding with lower load demand and higher solar intensity, predominantly in the remaining months of spring and summer.

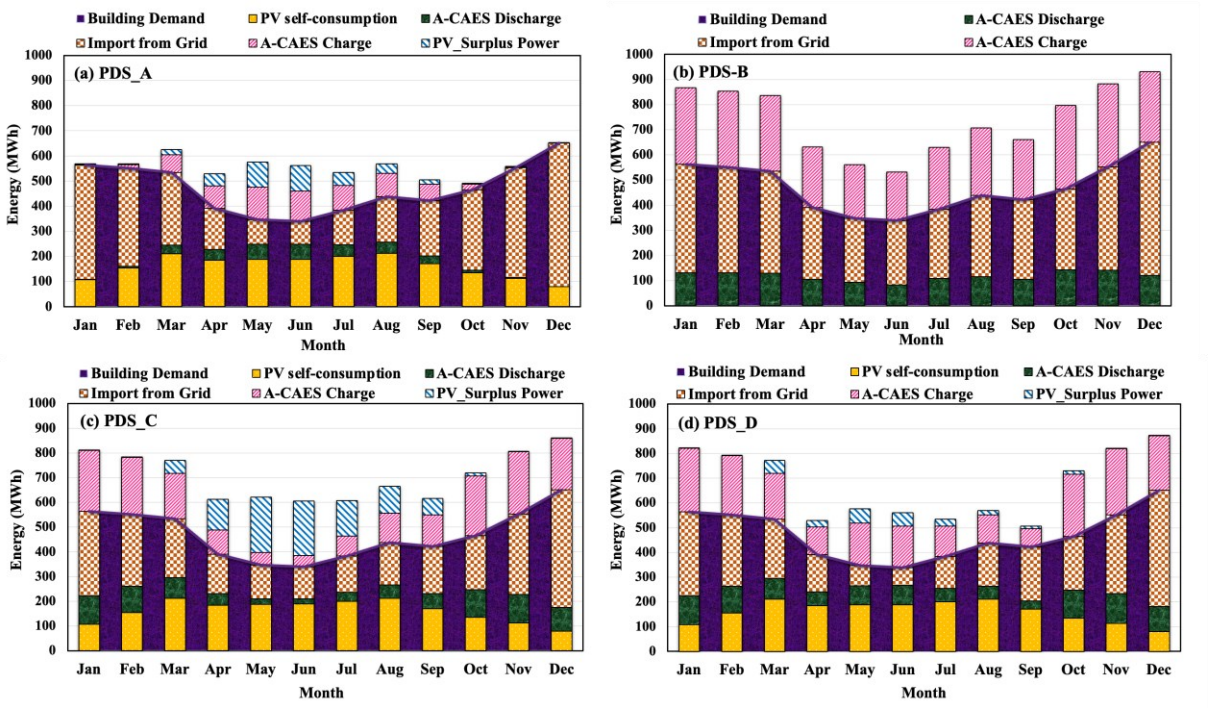

Fig. 3. 41. Monthly different energy sources responding to building model electrical energy demand for different PDSs under scenario I (zero sell).

Conversely, the A-CAES system planned with PDS-C (see Fig. 3.41c) exhibits a contrasting

pattern as it is strategically allocated throughout the year for both renewable integration and load-shifting purposes. Consequently, during the time with the lower solar intensity but higher building energy demand and peak-hour electricity prices, the A-CAES system holds a larger share in the electricity supply, ranging from 14% to 24%. However, the A-CAES system demonstrates the smallest contribution in supplying energy during the summer months despite the occurrence of both solar integration and load-shifting. This behavior can be proved by the SOC of the AST, as depicted in Fig. 3.41c for PDS-C.

Moreover, due to interacting with the grid during the peak hours and the alignment of abundant solar availability with lower load demand during the summer, the A-CAES remains at its fully-charge state most of the time, resulting in significant solar PV-surplus power. However, to take advantage of solar radiation potential, especially in spring and summer, the load-shifting task within the framework of PDS-D is confined to the high-demand months of the year, predominantly in winter and fall. As shown in Fig. 3.41d, the A-CAES system supplies more energy when operating under PDS-D compared to strategies A (during winter) and C (during Summer).

Notably, among all strategies, the proportion of A-CAES to the load demand is the highest (falling within the range of 18-31%) when employing PDS-B, aiming at managing the building bill management through load shifting. This is attributed to the unlimited grid being the only energy source to meet the building load demand.

Fig. 3.42 and Fig. 3.43 illustrate the hourly power balance of the designed system based on different PDSs for three days in Winter (February) and Summer (June). Given that the same PV power generation and load demand are considered for all HESs, the A-CAES dispatch strategy plays a crucial role in dictating energy flow dynamics within the system. Hence, the A-CAES system's performance and grid transmission distinguish the different HESs from one another.

According to Fig. 3.42, in the HESs incorporating solar energy (strategy A, C, and D), the PV output energy is generated during the daytime, with a peak value occurring at noon throughout the year. As expected during daylight hours, the PV output power is prioritized and directly supplied to meet the load demand. Meanwhile, any excess solar energy beyond the load demand can be stored in A-CAES depending on the amount of extra PV power, SOC of AST, and nominal capacity of the motor/compressor train.

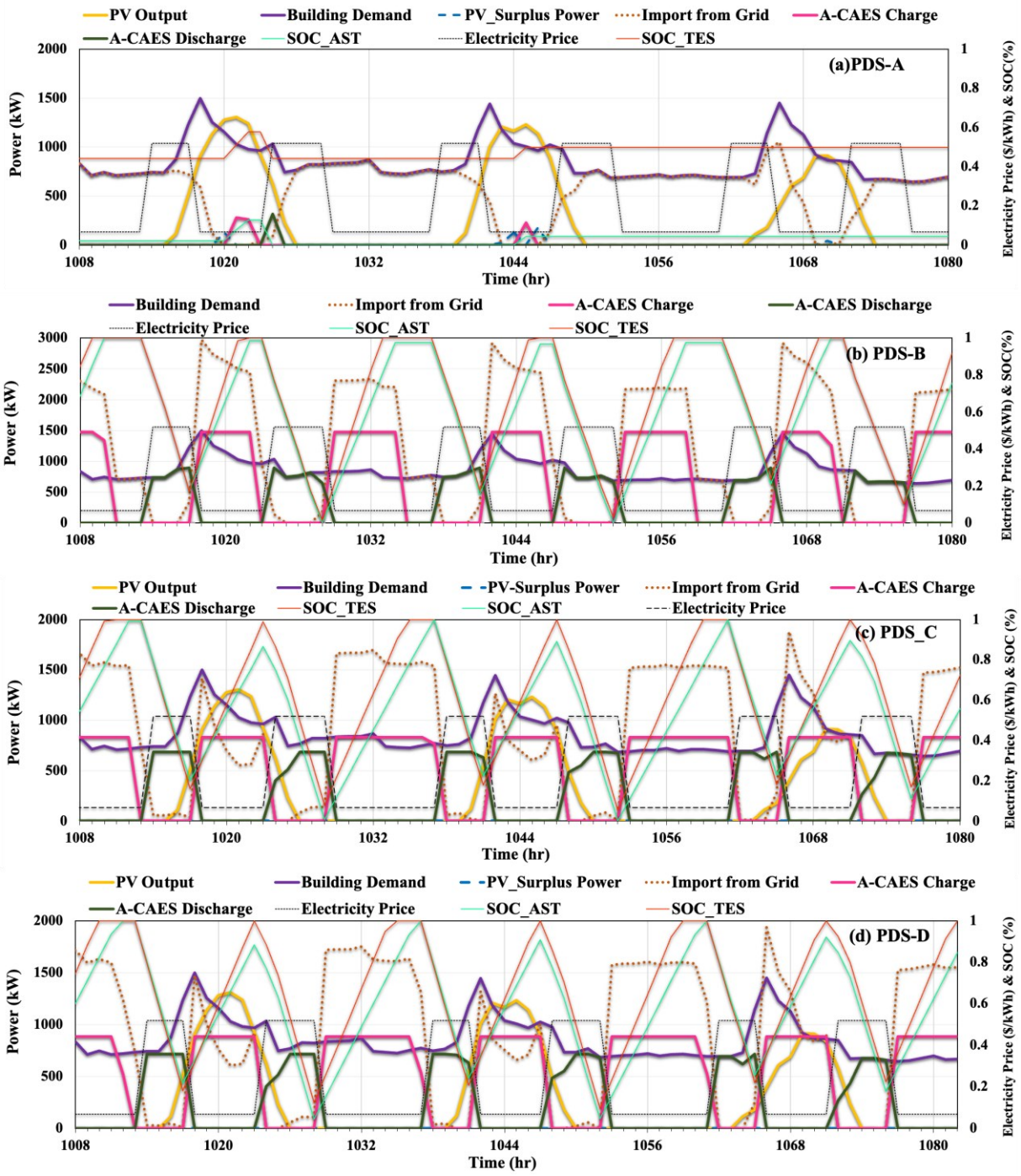

Fig. 3. 42. The hourly power balance in the optimal configuration for each PDS over three days in Winter (February) under scenario I (zero sell).

Based on Fig. 3.42a, for the HES operating under PDS-A, the limited extra PV power system results in the A-CAES system storing and supplying a low quantity of energy for a short time. Consequently, the SOC of AST and TES mostly remains unchanged. Furthermore, sometimes, when solar energy is insufficient, the PV power output is solely allocated to meet the load demand while the A-CAES system remains inactive. Therefore, importing power from

the grid compensates for the energy shortage. Moreover, since the A-CAES can supply energy on load demand according to the available energy in AST, TES, and turbine train nominal power capacity, the grid importation and A-CAES discharging might be conducted simultaneously to keep the HES reliable.

Fig. 3.42b shows the load electrification during peak and off-peak hours of the grid under PDS-B. It can be seen during grid valley hours; the system utilizes the grid electricity to satisfy the load while simultaneously charging the A-CAES for up to 4.15 hours to minimize the grid importation for load demand later during peak hours. Under such a strategy, the A-CAES is designed according to the load demand and dynamic electricity price profiles. As shown in Fig. 3.42b for all three days, at midnight (first hours of the day), when the electricity is cheap, the energy is purchased from the grid to charge the A-CAES for up to 6.15 hours until the AST is fully charged. While in the early morning, during peak hours (6:00 to 9:00 AM), the A-CAES system (turbine side) starts discharging the energy to answer the entire electricity load demand. As it is evident, most of the time, the releasing power from A-CAES converses total load demand during peak hours. When the electricity price decreases during off-peak hours (9:00 AM to 4:00 PM), the A-CAES (compressor side) starts consuming energy from the grid for 6 hours to fully charge the AST by pressurized air. Then, from 4:00 to 8:00 PM, A-CAES starts discharging again during the peak hours.

As depicted in Fig.3.42c and d, during the winter season, when the A-CAES system is configured to incorporate joint solar integration and load shifting, strategies C and D exhibit similar and comparable operational characteristics, combining elements from strategies A and B. Every day, during midnight (12:00 to 6:00 AM), A-CAES stores inexpensive electricity from the grid until it reaches full charge. This stored energy is then utilized in the early morning during peak hours (6:00 to 9:00 AM) in conjunction with solar energy to meet the electricity demand. From 9:00 AM to 4:00 PM, as solar energy availability almost coincides with the off-peak hours, the load demand is met by energy from PV systems (as a priority) and the grid. Meanwhile, the A-CAES undergoes charging using both grid importation and any excess PV power that might exist during the corresponding period. As a result, the compressor train of A-CAES primarily operates under their design condition. Subsequently, when the grid experiences peak hours in the evening, the turbine of A-CAES switches on to compensate for the insufficient PV power in meeting the load demand. Consequently, as illustrated in Fig. 3.42 c and d, during the peak hours of the day, the A-CAES system effectively could reduce the reliance on costly grid energy while covering nearly the entire load demand. When comparing the operation of A-

CAES during the winter, it becomes apparent that in the systems implementing load-shifting (e.g., strategies of B, C, and D), A-CAES operates predominantly at design or full load conditions. As a result, both AST and TES are fully charged and discharged during the corresponding time.

During the summer (see Fig. 3.43), the HES operation differs from winter across various PDSs. The primary factors contributing to this difference are the increased potential and availability of solar energy as well as the decreased load demand. For example, according to Fig. 3.43a for the system operating under PDS-A, although the compressor train of A-CAES operates at full-load conditions during the charging phase, there are instances where a portion of solar energy remains unutilized. The operation of A-CAES under PDS-B in summer (Fig. 3.43b) closely resembles its operation in winter (Fig. 3.42b). The only difference is that AST and TES are not fully discharged due to the lower load demand. Consequently, the generator/turbine train work at their partial load condition based on the load demand pattern.

On the other hand, in contrast to the winter season, the operation of A-CAES during summer under PDS-C is significantly different from PDS-D. While in terms of AST and TES, it resembles that of PDS-B to some extent, with most of the storage remaining unused and maintained in a high SOC. Therefore, this leads to an A-CAES being unable to absorb the excess solar energy during the daytime in summer.

As shown in Fig. 3.43c, the PV power generated during the daytime (6:00 AM to 6:00 PM) is sufficient to meet the load due to the favorable alignment of high solar energy availability and low load demand. Therefore, there is no need for any energy from A-CAES as it is already fully charged by utilizing inexpensive grid energy during the early hours of the day (midnight). Consequently, the AST and TES usually remain at their high SOC (full capacity), and A-CAES cannot store any excess energy from the PV system. In other words, since the A-CAES is specifically engineered to enable load-shifting and renewable integration during summer months with lower load demand, during the early morning (6:00 to 9:00 AM), the available solar energy is abundant enough to fulfill the load demand without necessitating the discharge of the A-CAES system.

On the contrary, as shown in Fig. 3.43d, PDS-D bridges the gap left by strategy C, explicitly dealing with the PV-surplus power and untapped A-CAES capacity during the summer when solar energy alone is almost sufficient to fulfill the load demand. Since the A-CAES system is only planned for renewable integration in summer (off-peak month) under PDS-D, the AST and TES possess enough capacity to accommodate the PV power generated during periods of high

solar availability. Therefore, a minor portion of solar energy remains unutilized.

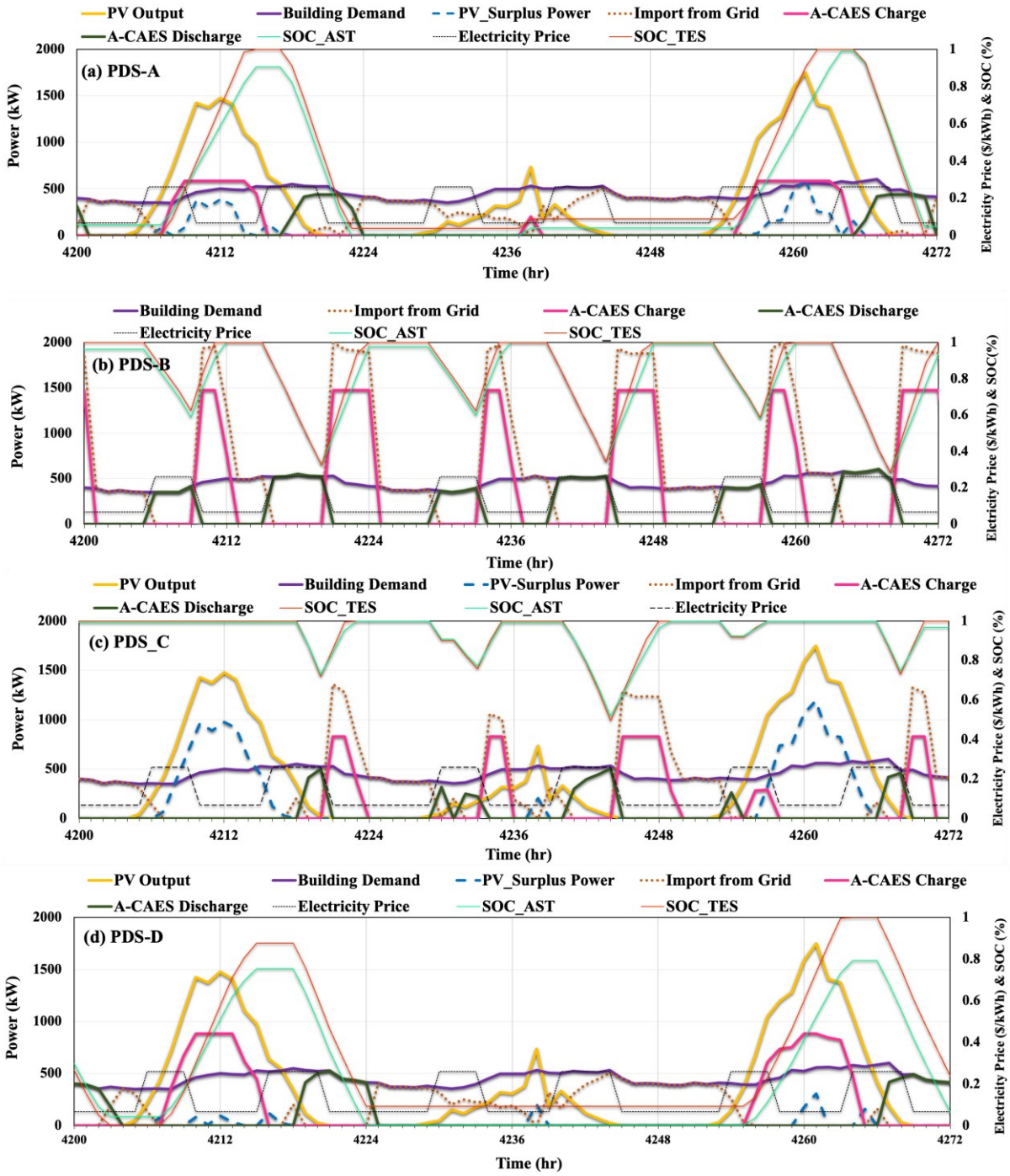

Fig. 3. 43. The hourly power balance of the optimal configuration for each PDS over three days in summer (June) under scenario I (zero sell).

It should be noted that the behavior of HESs under scenario II (unlimited sell) and scenario III (flexible load) differs in terms of PV-Surplus power. However, the operation of A-CAES, grid importation, and solar PV power are the same across all scenarios. For example, in scenarios I and II, the PV-surplus power is entirely dumped and sold back to the grid,

respectively. On the other hand, in scenario III, a portion of PV-surplus power is utilized for flexible load while the remaining PV-surplus power is discarded.

Furthermore, Fig. 3.44 shows the primary and shifted load demand of the studied building from the grid for strategies implementing load-shifting during a weekday in March. It is worth highlighting that most of the renewable integration and load-shifting, which lead to the grid peak–shaving, occurs at this time of the day (from 9:00 AM to 4:00 PM). Moreover, it is evident that optimal HESs under strategy D followed by C have a greater contribution to grid peak shaving compared to strategy B.

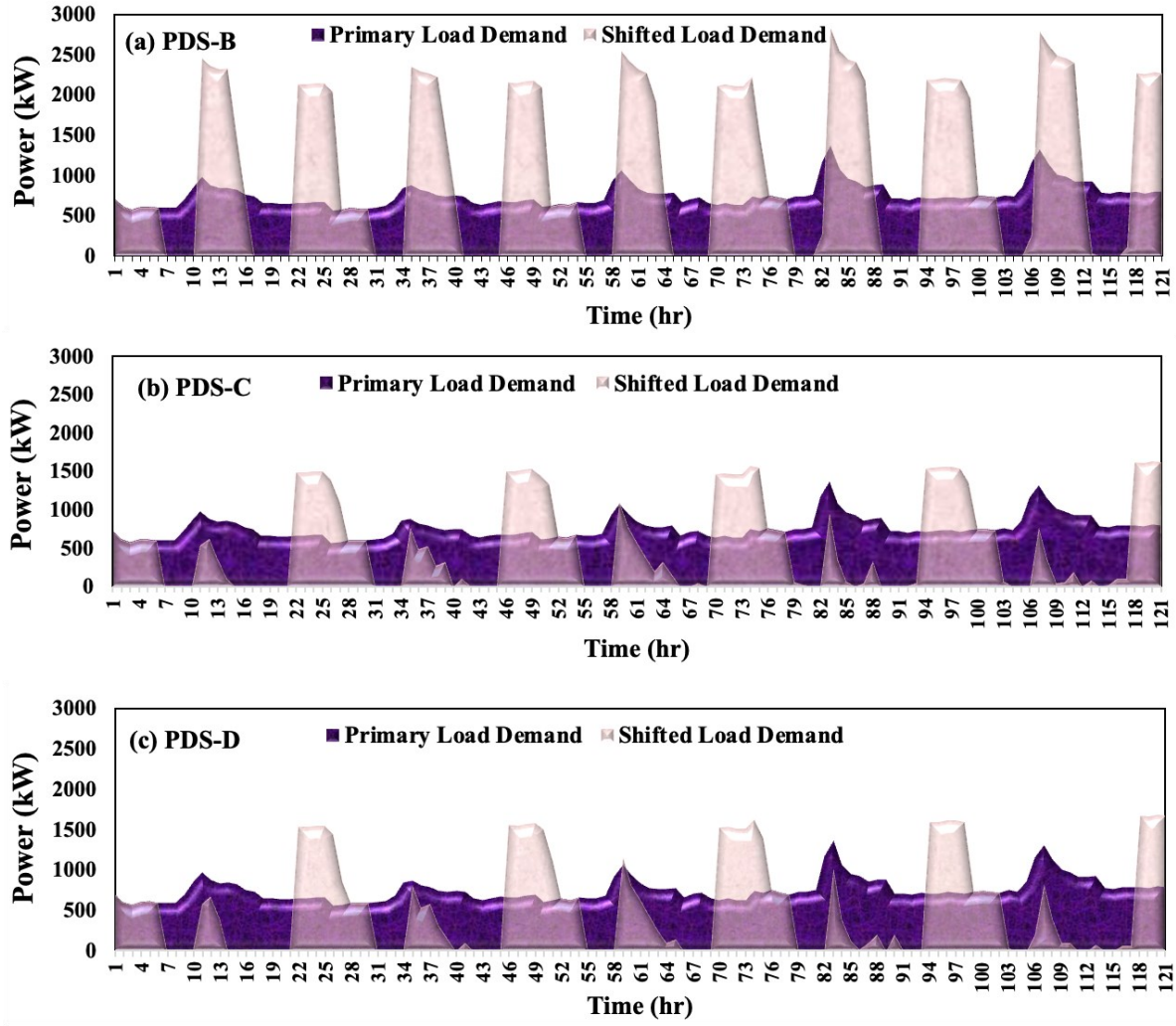

Fig. 3. 44. The primary and shifted load demand from the grid for strategies implementing load-shifting during a weekday in March under all scenarios.

3.4.3.3. Sensitivity analysis (post optimization)

To ensure the model's applicability to the different case studies and verify its accuracy concerning the variations associated with influential input parameters, the widely-employed

approach is to analyze the sensitivity of the developed model toward those parameters [236,252].

In this section, the focus is on examining the effect of energy source quantity (e.g., number of PV panels and maximum allowable grid importation) and the upper bound of AST volume (referring to the available surface area for installing A-CAES) on optimal design, A-CAES contribution and overall performance of HES. The results of sensitivity analysis are elaborated upon in subsequent sub-sections.

3.4.3.3.1. Number of PV panels

Generally speaking, the total PV power output will increase with the raised PV panel numbers. The effect of the number of installed PV panels (depending on available rooftop area) on ELMR of HES and LCR of optimal A-CAES system under all PDSs involving PV panels is depicted in Fig. 3.45.

According to Fig. 3.45a, as expected, with increasing the number of PV panels, the ELMR of the HESs under strategies A, C, and D monotonically improves. But this improvement is sharper under strategies A and D compared to strategy C. So, for smaller PV system capacities (less than 6000 PV panels), the ELMR of the optimal HES under PDS-C is higher than the ELMR values obtained under other strategies of D, A, and B. When the number of PV panels exceeds 6000, the ELMR of the optimized system under PDS-D surpasses the ELMR of the system under PDS-C. The reason is that although the solar energy penetration increases with raised PV panel numbers, the variation patterns in the LCR of A-CAES systems differ for the corresponding strategies, as depicted in Fig. 3.45b. So, as the number of PV panels increases, the LCR of the A-CAES system consistently improves under strategies A and D but declines under PDS-C. Such a behavior highlights that planning the A-CAES system for simultaneous solar integration and load-shifting throughout a year for such a case study with the higher capacities of PV systems is not an efficient option. Because when load demand is low during the summer, the PV power output can meet a considerable portion of load demand, rendering the need for A-CAES to discharge energy. Consequently, a significant part of the SOC of AST remains unchanged during the summer.

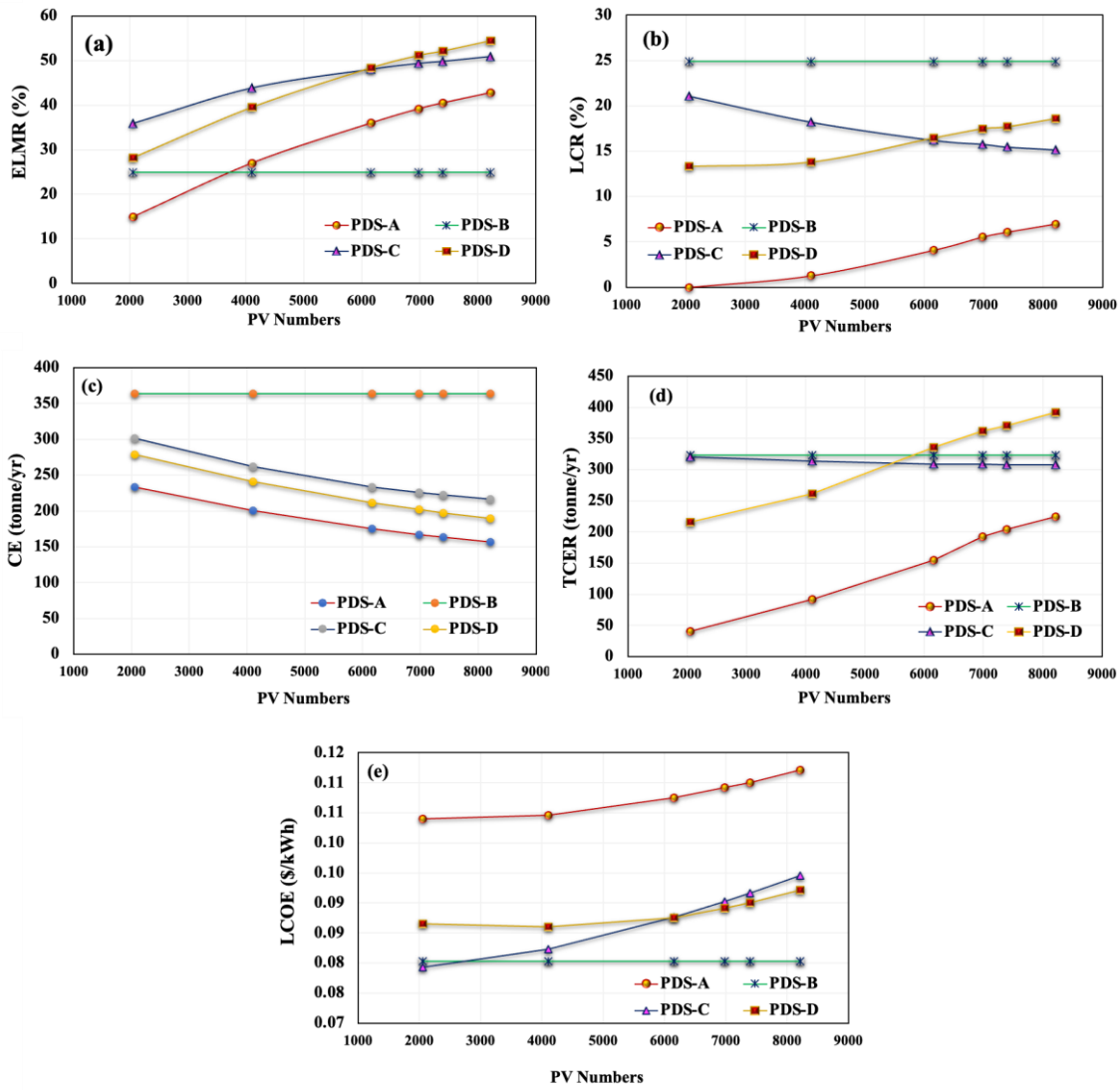

Fig. 3. 45. Effect of PV panel numbers on (a) ELMR, (b) LCR, (c) CE, (d) TCER, and (e) LCOE of the optimal HES for all strategies under the scenario I (zero sell).

On the contrary, seasonally planning the A-CAES for load-shifting (PDS-D) demonstrates effectiveness in higher-capacity solar systems. Notably, the optimum configuration exclusively intended for load-shifting (PDS-B) purposes exhibits a higher LCR across various PV system capacities than other strategies. However, except for strategy A for PV numbers less than 4000, the system under PDS-B demonstrates lower ELMR for the varying number of PV panels compared to all other strategies.

Fig. 3.45e indicates the variation in LCOE as the PV panel numbers are changed. As shown, the LCOE tends to rise with higher solar PV capacities, mainly for the systems operating under strategies A, C, and D. However, this increase in LCOE for the system planned under PDS-C is sharper than other systems. Therefore, for the PV numbers exceeding 6000, the LCOE of the

system under PDS-C surpasses that of PDS-D. That can be attributed to the contribution of the A-CAES system in covering the load demand across various PV capacities, as mentioned earlier. It is worth noting that, for a smaller number of PV systems around 2000, the LCOE of HES under PDS-C amounts to 0.78 $/kWh, 2.5% less than the system under PDS-B, which has the lowest LCOE of 0.08 $/kWh across different numbers of PV panels.

Fig. 3.45c and d present the effect of PV numbers on the environmental impact of the optimal HES across different strategies. As shown in Fig. 3.45c, The CE demonstrates an approximately linear negative correlation with the PV numbers for strategies A, C, and D. Besides, the HES implemented under strategies A, C, and D exhibits lower CE values compared to the system under PDS-B, even in the small number of PV panels.

In contrast, the TCER follows a similar pattern of variation as the LCR of A-CAES for strategies A, C, and D, as depicted in Fig. 3.45d. Thus, for PV panel numbers below 6000, the higher TCER belongs to strategies B and C, whereas for higher capacities of solar systems, the system operating under strategy D demonstrates the higher TCER.

3.4.3.3.2. Allowable grid importation

Fig. 3.46 presents the influence of restricting the imported power from the grid on the techno-economic and environmental performance of the optimized HES for all strategies under the worst-case scenario (zero sell). As it is evident, there is a correlation between the level of A-CAES interaction with the grid and sensitivity to variation in the maximum allowable power imported from the grid. That means the less A-CAES interaction with the grid, the less sensitivity to the variation of power imported from the grid. Therefore, there are considerable changes in optimal design and, subsequently, the techno-economic and environmental performance of HES, especially planned for load-shifting (PDS-B) purposes where A-CAES has direct and significant interaction with the grid (see Fig. 3.46). Furthermore, increasing the grid importation power leads to a larger capacity requirement for A-CAES in PDSs involving load-shifting (B, C, D). This explains the observed reduction in the LCOE with increased imported power from the grid for the corresponding strategies, as depicted in Fig. 3.46e. Put simply, a larger-size A-CAES has the advantage of being able to absorb a greater inexpensive power to meet the load demand at peak hours.

On the contrary, the design and overall performance of HES planned under PDS-A, focusing on solar penetration, exhibits less sensitivity to the quantity of power purchased from the grid as far as the reliability constraint is met (LPSP less than 1%). As a result, almost for all HESs

under different strategies, when the grid-imported power is below 1000 kW, the LPSP exceeds the 1% threshold, indicating a lower level of reliability for the achieved HES.

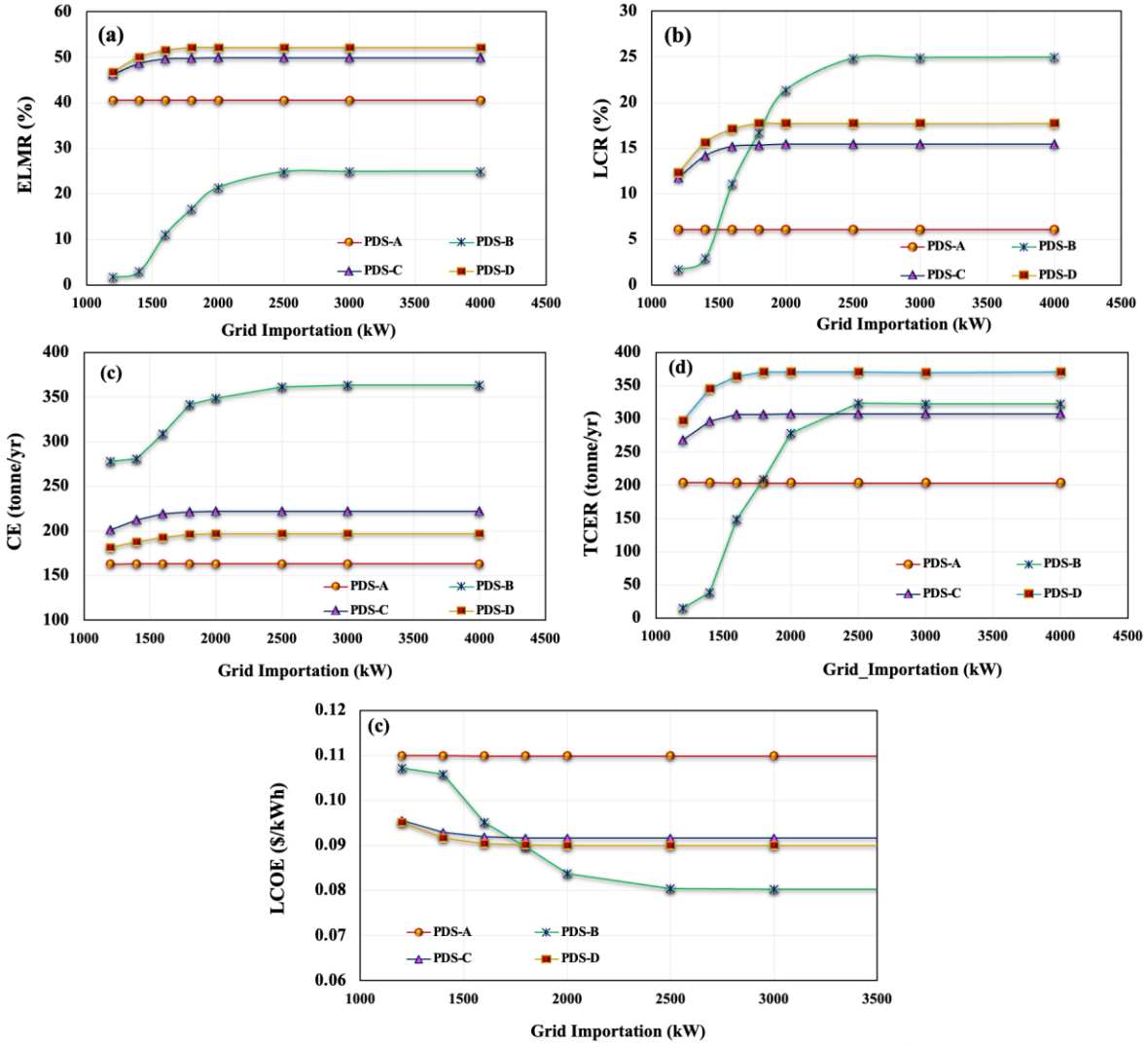

Fig. 3. 46. Effect of the allowable grid importation on (a) ELMR, (b) LCR, (c) CE, (d) TCER, and (e) LCOE of the optimal HES for all strategies under the scenario I (zero sell).

Indeed, the LCR of A-CAES initially improves with an increase in the imported power from the grid, resulting in an increase in the ELMR for HESs designed under load shifting-involved PDS such as B, C, D. However, there exists a threshold of imported power from the grid for each strategy beyond which the design and performance of HES remain constant. This threshold is approximately 1800 kW for strategies C and D, while for PDS-B is around 2500 kW.

As presented in Fig. 3.46c, considering that the grid is the only source of emissions in the current systems, there is an initial rise in CE when the imported power from the grid increases up to the threshold for each strategy. Beyond this threshold, the CE levels off and remains

constant, mirroring the patterns observed in ELMR and LCR (Fig. 3.46a and b). Similarly, the TCER also follows a similar trend, as illustrated in Fig. 3.46d. Even with an increase in imported power from the grid, the reduction in emissions achieved by implementing a higher-capacity A-CAES system outweighs the decrease in emission reduction attributed to greater grid importation.

When comparing different strategies, it is essential to note that, for the grid importation levels below approximately 1800 kW, the LCR of the A-CAES system under PDS-B is lower than that of strategies C and D. Similarly, for the grid importation level below 1500 kW, the LCR of the HES under PDS-B is also lower than that of PDS-A. However, for grid importation levels exceeding 1800kW, the HES under PDS-B demonstrates the lowest LCOE compared to other strategies. That means that for smaller values of power imported from the grid (less than 1800 kW), the LCOE of HES under PDS-D, followed by PDS-C, is the minimum among all systems.

Furthermore, across all levels of power imported from the grid, the HES under PDS-B exhibits the least ELMR (Fig. 3.46a) and most CE (Fig. 3.46c) compared to other strategies. Conversely, the maximum ELMR and TCER (Fig. 3.46d) belong to HES-implemented PDS-D, focusing on renewable integration and seasonal load-shifting, surpassing other strategies across different quantities of power imported from the grid.

3.4.3.3.3. Maximum volume of AST

The space required for AST of the A-CAES system is one factor that limits the A-CAES incorporation in buildings with limited space. In this work, the upper limit of AST volumes considered in the optimization problem's constraints refers to the available space in the specific case study. As explained earlier and reported in Table 3.19, the maximum AST volume is consistently obtained for all HESs across different strategies. This observation emphasizes that the AST volume is a variable significantly influencing the system's design and performance for such a case study. This section shows how changing the upper limit of AST volume (reflecting the available space area) affects the optimal configuration and overall performance of HESs for all PDSs. Table 3.24 shows the optimal structure of the A-CAES system with various values across different upper limits of AST volume under each PDS. Analyzing the optimum results indicates that to have the minimum LCOE, the optimization tends to select the maximum volume of AST while selecting the smaller maximum pressure in the tank.

Fig. 3.47 illustrates how the optimal maximum pressure in the tank is reduced by increasing

the upper limits of AST volume. That is why, in the largest AST volume of 1500 m^3, the lower

Table 3. 24. The effect of volume of AST on optimal configuration of A-CAES for all strategies.

Design variable	AST Volume					
	200	300	500	750	1000	1500
	PDS-A					
N_C (#)	5	5	5	5	5	5
N_{tr} (#)	3	4	4	4	3	3
W_C^r(kW)	95.94	111.21	130.37	120.60	133.57	128.39
W_{tr}^r(kW)	146.68	114.35	109.01	111.42	161.24	154.22
V_{AST} (m^3)	200	300	500	750	1000	1266
P_{AST}^{max}(MPa)	13.33	12.12	9.53	7.18	6.51	6.00
P_{AST}^{min}(MPa)	2.5	2.5	2.5	2.5	2.5	2.5
E_{TES} (MWh)	1.99	3.05	3.83	3.78	3.63	3.88
V_{TES} (m^3)	18.16	27.75	34.90	34.42	32.99	35.34
	PDS-B					
N_C (#)	4	4	4	3	3	3
N_tr (#)	5	5	5	5	5	5
W_C^r(kW)	350	350	350	350	350	350
W_{tr}^r(kW)	165.07	185.96	184.38	177.21	183.47	194.68
V_{AST} (m^3)	200	300	500	750	1000	1500
P_{AST}^{max}(MPa)	20	17.51	11.57	8.55	7.06	6.00
P_{AST}^{min}(MPa)	2.5	2.5	2.5	2.5	2.5	2.5
E_{TES} (MWh)	4.34	5.59	5.63	5.64	5.66	6.76
V_{TES} (m^3)	39.51	50.84	51.22	51.27	51.46	61.47
	PDS-C					
N_C (#)	5	5	5	5	5	5
N_{tr} (#)	5	5	5	5	4	4
W_C^r(kW)	175.62	157.56	150.76	147.37	145.32	146.86
W_{tr}^r(kW)	136.26	142.48	143.26	151.44	189.29	202.12
V_{AST} (m^3)	200	300	500	750	1000	1345
P_{AST}^{max}(MPa)	20	15.71	10.79	8.26	6.94	6.00
P_{AST}^{min}(MPa)	2.5	2.5	2.5	2.5	2.5	2.5
E_{TES} (MWh)	4.34	4.62	4.89	5.36	4.80	5.21
V_{TES} (m^3)	39.51	42.21	44.55	48.74	43.72	47.46
	PDS-D					
N_C (#)	5	5	5	5	5	5
N_{tr} (#)	5	5	5	5	4	4
W_C^r(kW)	178.88	167.80	160.90	157.08	153.45	152.79
W_{tr}^r(kW)	136.70	148.82	153.41	161.70	202.02	207.58
V_{AST} (m^3)	200	300	500	750	1000	1399
P_{AST}^{max}(MPa)	20	16.43	11.26	8.59	7.18	6.00
P_{AST}^{min}(MPa)	2.5	2.5	2.5	2.5	2.5	2.5
E_{TES} (MWh)	4.34	4.96	5.17	5.62	5.02	5.43
V_{TES} (m^3)	39.51	45.13	47.03	51.14	45.68	49.37

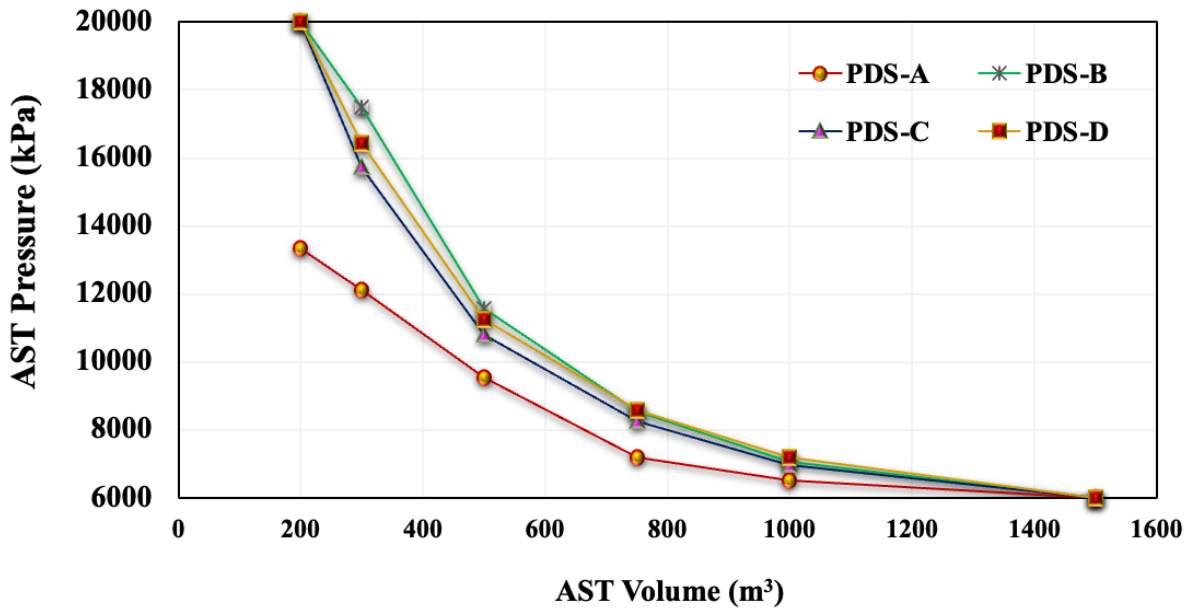

Fig. 3. 47. The variation of AST pressure versus AST volume.

limits of maximum air pressure in the tank are selected. While for the smallest AST volume of 200 m^3, the upper bound of maximum allowable pressure in AST is obtained for PDS-C, D, and B. Due to such a reverse change in pressure and AST volume, the energy capacity of AST remains approximately constant across different AST volumes. This explains the minimal positive variation observed in ELMR and LCR for all strategies when increasing the AST volume, as depicted in Fig. 3.48a and b. This can be attributed to the efficiency improvement resulting from a reduction in optimal operating pressure within the AST with raised volume and, subsequently, reducing the compressor train's size and increasing the turbine train's capacity, as reported in Table 3.24. Consequently, the CE of HESs exhibits a gradual and modest decrease, as illustrated in Fig. 3.48c.

Furthermore, LCOE exhibits a gradual decrease, although this decrease is more pronounced in strategies where A-CAES has a larger size within HES. According to Fig. 3.48e, the LCOE reduction with raised AST volume is particularly significant for the optimal configurations under PDS-B compared to other strategies. It is observed that the capacity of A-CAES plays a crucial role in influencing the magnitude of change in LCOE. As mentioned earlier, such a reduction in LCOE results from the decrease in the maximum pressure of AST, which subsequently leads to a reduction in the size of the compressor train. It can be said that the size of the compressor train, as a main contributor to A-CAES's initial cost, affects the LCOE of the HES. Hence, given that a HES under PDS-B is associated with the largest compressor train, the LCOE is more sensitive to changes in AST volume under this corresponding strategy compared

to other PDSs.

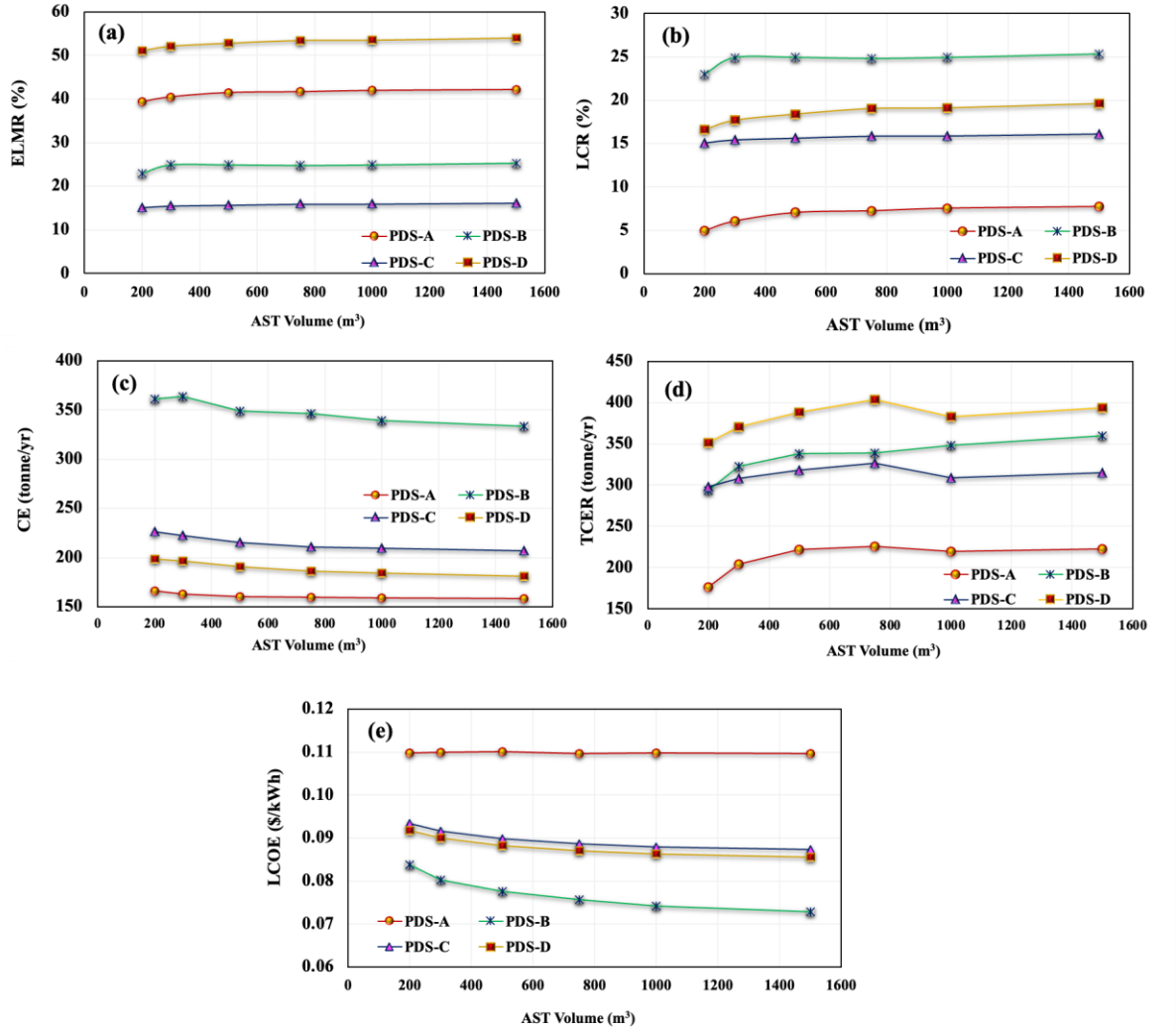

Fig. 3. 48. Effect of the AST volume on (a) ELMR, (b) LCR, (c) CE, (d) TEMR, and (e) LCOE of the optimal HES for all strategies under the scenario I (zero sell).

3.5. Resilience-centered optimal Sizing and Scheduling of a building-integrated PV-based energy system with Hybrid Compressed Air Energy Storage and Battery System [253]

3.5.1. Research approach

In this section, the components of the generic system consist of solar PV as the primary energy source, a load, a converter, a power dispatch controller, and both A-CAES and Battery units.

3.5.1.1. Proposed sizing-scheduling approach

Fig. 3.49 illustrates the overall flowchart of the implementation of the two-stage sizing-

scheduling approach. In this diagram, the process begins by receiving year-round system operation boundary conditions such as hourly electric load demand, meteorological information, electricity tariff, as well as other techno-economic characteristics of the case study. In this approach, the sizing-planning stage achieves the energy system's optimal capacity and quantity of components. The operation-scheduling stage simulates and optimizes the operation of each element within the HES while considering the more detailed mechanical limitations of the A-CAES system, specifically charging-discharging transition time and responsiveness. The overall cost of HES consists of the total capital cost, fixed O&M cost of devices, replacement cost, and cost of energy import /export cost (grid). The sizing-planning stage's objective is to minimize the HES's overall cost of energy during the project lifetime, considering the time horizon of 8760 hr/year. Differently, the objective of the scheduling stage is to minimize the daily variable operational cost, including the cost of energy import /export cost (grid) and penalty cost associated with the loss of power supply (LPS), renewable energy curtailment, and excess heat considering the time horizon of 24 hr/day. Therefore, the unit-commitment model can be run separately 365 days a year. More elaboration on the proposed framework and assessment indicators are presented as follows.

In the first layer, the optimal sizing starts with reading the case study characteristics and the initial quantity of sizing variables assigned by the optimization algorithm as input data. Therefore, as shown in Fig.3.50, the rule-based PDS is used to dispatch the power among components and manage the energy stream at each timestep over a year. Then, the constraint violation is checked, and the LCOE (objective function) corresponding to the optimal configuration is reported after achieving the termination criterion.

In the second layer, the result from the first layer, including the top-economic and resilient configuration and long-term renewable power generation along with the hourly electric load demand and electricity tariff, feeds the optimization problem for short-term optimal scheduling. In this stage, the objective function of the problem is the minimization of the operational costs while achieving the minimum loss of power supply probability (LPSP) for day-to-day resilient and cost-effective operations. Ultimately, the optimal schedule and unit commitment are achieved for an already optimal designed system.

To ensure the resilience of the energy system in terms of both configuration and operation (through both sizing and scheduling), an appropriate value for the minimum possible LPSP is determined, with yearly LPSP considered during the sizing stage and daily LPSP during the operation stage. The optimization process is carried out iteratively until the minimum LPSP

(indicating maximum resilience) is achieved through both long-term and short-term evaluations.

It is important to note that the methodology and results in the first layer are independent of the second layer, meaning that the method here is not bi-directional or bi-level programming, working based on short-term horizon data, as proposed in [178]. Therefore, it is not conducted concurrently. The reason is that the dispatch strategy in the first layer is based on rule-based PDS (to decrease the computational burden and consider a more detailed model of components). In contrast, it is a unit-commitment model in the second layer [11].

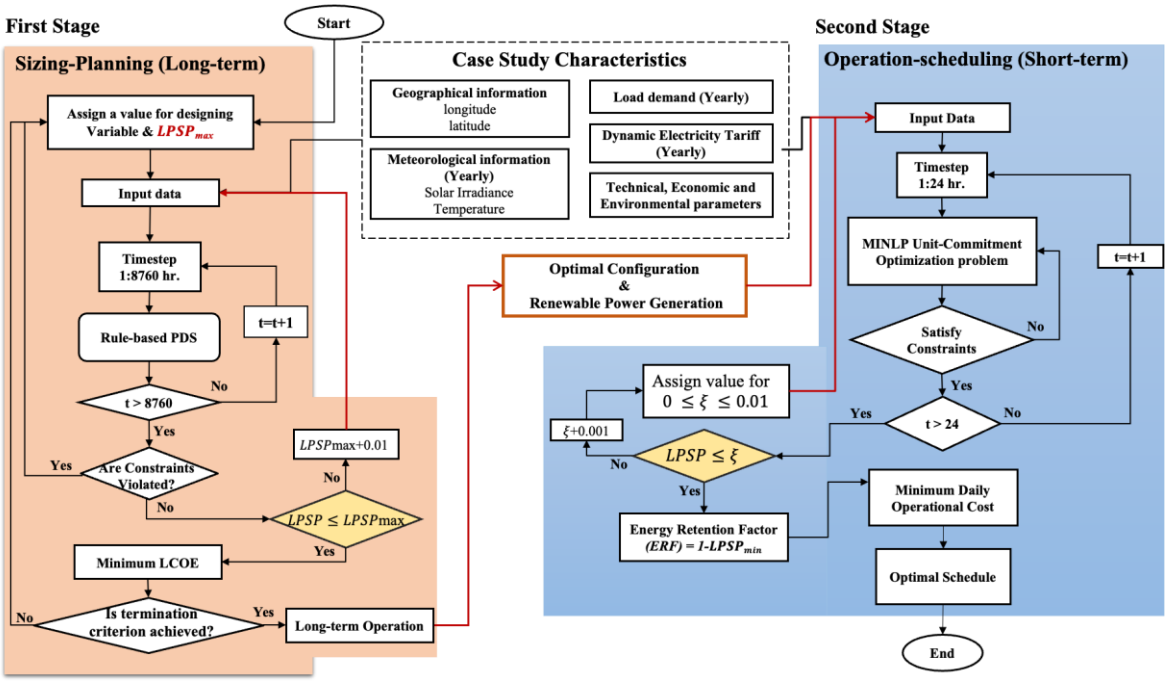

Fig. 3. 49.The proposed two-stage sizing-scheduling approach.

Fig. 3.50 illustrates the primary energy flow routes from the proposed HES to meet the load demand. It showcases the rule-based PDS, which is crucial for simulating the long-term operation of all components, particularly energy storage in the first layer.

a) During periods of solar PV generation, route one is chosen to supply power to the end-user's load demand. If the generation surpasses the building load requirements, excess power charges the A-CAES through route 2, where the compressor train generates and sends high-pressure air to AST according to its rated power capacity and state of the charge (SOC) of AST. Meanwhile, the heat generated during the compression process is stored in the TES according to its SOC; otherwise, it dissipates to the atmosphere (or can be used for other usages). When the AST of A-CAES reaches full capacity, the

battery initiates charging via route 3. Upon the battery reaches full charge (i.e., battery SOC=SOC_{max}), any surplus energy is directed to route 4. So that, in the event of additional excess electricity from the PV, the extra energy can either be exported to the grid or discarded.

b) When the PV generation falls short of meeting the load, the A-CAES discharges through route 2 in conjunction with route 1. However, if the load demand exceeds the nominal power capacity of the turbine train, or if it is less than the minimum nominal capacity and one of the AST and TES, or both, are empty, the battery discharges through route 3. When the battery's SOC reaches a minimum, load requirements are fulfilled through route 4, utilizing electricity purchased from the grid. In a scenario with limited access to the grid, a portion of the load might remain unmet, leading to a loss of power supply.

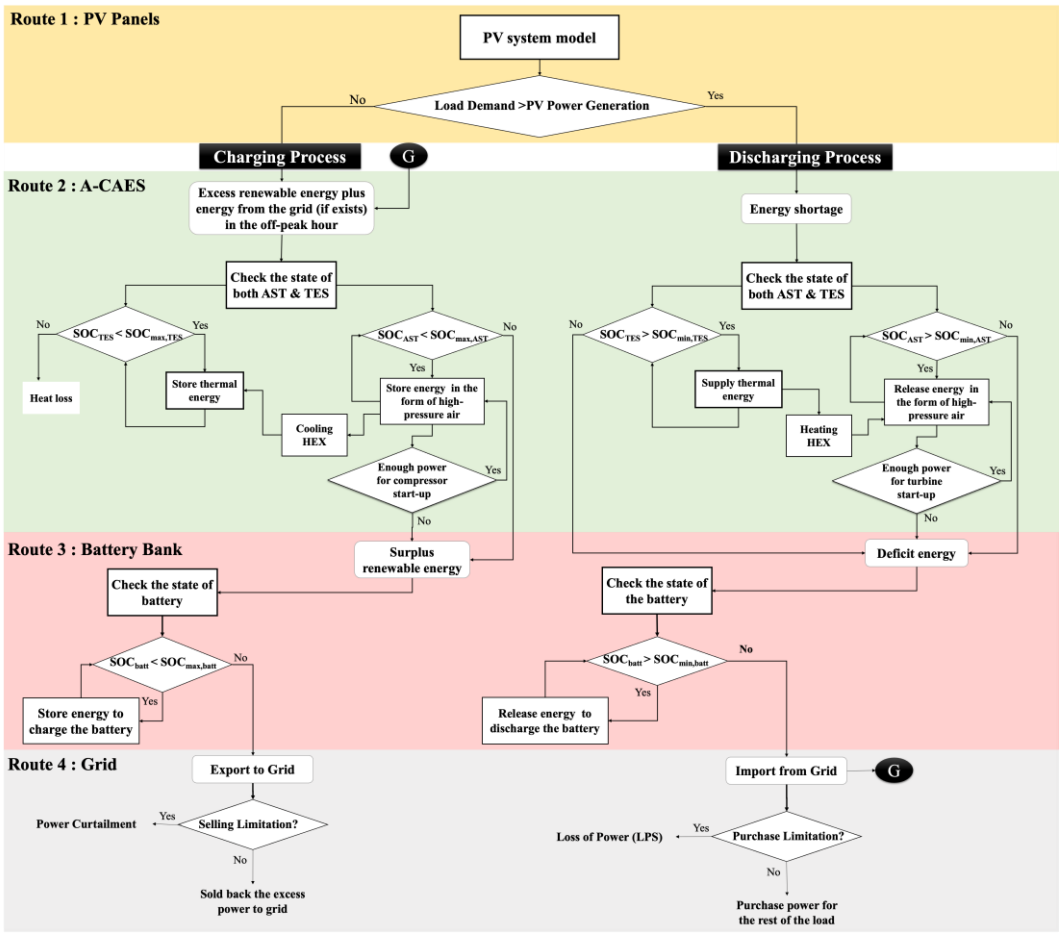

Fig. 3. 50. Flow diagram of PDS for the PV/A-CAES/Battery/grid hybrid system

It should be noted that Fig. 3.50 illustrates the overall PDS. However, depending on the case study and the defined scenario, each route can be replaced, removed, or relocated. For example, in a scenario of a HES without a battery, route #3 (battery) is excluded, and route #2 (A-CAES)

is followed by route #4 (grid). A deep understanding of the A-CAES operation strategy can be found in [20].

3.5.1.2. Mathematical model of components

3.5.1.2.1. PV model

The PV model described in section 3.3.1.1.6 is utilized.

3.5.1.2.2. A-CAES model

The generic thermodynamic model of the A-CAES system proposed in section 3.5.1.3 is employed to determine the operation condition of its sub-systems in both stages. The compression and generation powers are computed using Eq. (3.32) and (3.33). The air pressure (P_{AST}) in the AST and the thermal energy (E_{TES}) in the TES at each hourly-basis time step, t, can be calculated using Eq. (3.38) and Eq. (3.45), respectively. Eq. (3.43) and (3.44) express the thermal power, transferring during the compression and expansion stages [15, 31].

3.5.1.2.3. Battery model

The stored energy in the battery is formulated using Eq. (3.57):

$$E_B(t) = E_B(t-1)(1-\sigma) + W_{B,crg}(t) * \eta_{crg} - \frac{W_{B,dcrg}(t)}{\eta_{dcrg}} \quad t > 1 \qquad (3.57)$$

3.5.1.2.4. Converter model

The required power capacity for the converter can be calculated as follows [1]:

$$W_{conv.} = (N_{PV} W_{PV}^r + N_B W_B^r)\, \eta_{conv.} \qquad (3.58)$$

A converter with an efficiency ($\eta_{conv.}$) of 90% is considered [30].

3.5.1.3. Optimization problem formulation

Expanding on the details discussed in Section 3.6.1.1, this section introduces a two-stage optimization model for sizing and scheduling the proposed HES. This model accounts for both long-term and short-term horizons, providing a holistic evaluation of the energy system's performance. In the first stage, sizing-planning problems are formulated under scenarios of a limited grid power source. In the second stage, the unit-commitment model is executed under scenarios of grid-connected (same as the first stage) and off-grid (grid outage) systems. The model, as explained in Fig. 3.49, ensures that the system runs optimally in the short-term (second stage) after optimizing its size and planning it for the long-term (first stage) operation,

considering the resiliency of the hybrid system in the form of LPSP (or energy retention factor (ERF=1-LPSP)) in both stages. This approach ensures that each part of the system reaches its best size and state after integration.

3.5.1.3.1. First stage: sizing-planning scope

The proposed sizing-planning approach involves a simulation model including rule-based PDS, a mathematical model of each component, and the optimization model with a specific emphasis on long-term measures (8760 hr/year). Further details on optimal sizing problem formulation will be provided in this section. The objective function of the first stage is to minimize the LCOE, implying the life cycle cost (LCC) per unit of energy demand served (E_{served}) over the project's lifetime as follows:

$$Min\ LCOE = (LCC \times CRF)/E_{served} \quad (3.\ 59)$$

where LCC is determined by aggregating the net present values of all system costs, including capital expenditures (CAPEX), operation and maintenance expenditures (OPEX) and replacement expenditures ($REPEX$) [235].

$$LCC = CAPEX + OPEX_{yr}/CRF + REPEX \times SPPWF_B \quad (3.\ 60)$$

$$OPEX_{yr}=OPEX_{fix} + \sum_{t=1}^{8760}(C_{per}(t)\ W_{g,per}(t) - C_{sell}(t)W_{g,sell}(t)) \quad (3.\ 61)$$

where CAPEX, OPEX, and REPEX could be calculated by summation of the sub-systems expenditures as shown in Table 3.12. C_{per} and C_{sell} are the dynamic electricity price per unit of purchased power from the grid ($W_{g,per}$) and sold back power to the grid ($W_{g,sell}$), respectively. CRF stands for capital recovery factor to convert the present value to annual value and vice versa, as defined by Eq. (3.62). $SPPWF_B$ reflects the single payment present worth factor for the components that need to be replaced several times over the project lifetime, used to convert the replacement cost to present value, as defined by Eq. (3.63) [254].

$$CRF_{proj.}(I_r, n) = \frac{I_r(1+I_r)^n}{(1+I_r)^n-1} \quad (3.\ 62)$$

$$SPPWF_B = 1 + \frac{1}{(1+I_r)^{mb}} \quad (3.\ 63)$$

where I_r indicates the real interest rate adjusted to consider the effects of the inflation rate (I_f) in the nominal interest rate (I_n) [237] as expressed in Table 3.8. It should be noted that, in this study, the battery, which has a lifespan of 15 years (mb), is the only system requiring replacement once within the 25-year project lifetime (n). The lifetimes of the other components are assumed to be equal to the overall project lifespan.

To optimize the objective function (Eq. 3.59), the problem must comply with specific constraints. These constraints primarily relate to the restrictions on the number and size of the components (X_z) as well as a renewable curtailment (DL) and resiliency-oriented constraint (LPSP) as follows:

$$X_z^{min} \leq X_z \leq X_z^{max} \quad (3.641)$$

$$0 \leq LPSP \leq LPSP_{max} \quad (3.65)$$

$$0 \leq Curtailment \leq DL_{max} \quad (3.66)$$

where LPSP represents the loss of power supply probability, and $LPSP_{max}$ is the maximum allowable LPSP specified by the end-user. It can be defined as follows:

$$LPSP = \frac{\sum_{t=1}^{t} W_{Load}(t) - Power\ supply}{\sum_{t=1}^{t} W_{Load}(t)} \quad (3.67)$$

$$Power\ supply = min\left(W_{Load}(t), W_{PV}(t)\right) + W_{CAES,dcrg}(t) + W_{B,dcrg}(t) + W_{g,per}(t)) \quad (3.68)$$

also, DL stands for the dump load, referring to the renewable power curtailment:

$$Curtailment = 1 - \frac{\sum_{t=1}^{t} min(W_{PV}(t), W_{Load}(t)) + W_{CAES,crg}(t) + W_{B,crg}(t)}{\sum_{t=1}^{8760} W_{PV}(t)} \quad (3.69)$$

where t presents the time horizon, assuming 8760 hours in the first stage (optimal sizing) and 24 hours in the second stage (optimal scheduling).

It is worth mentioning that, to achieve high resilient system within system constraints a maximum value is considered for yearly $LPSP_{max}$ as suggested in the studies in the context of optimal sizing of hybrid energy systems, especially with limited sources of energy [238,255,256]. Besides, to avoid renewable power curtailment (solar PV in this study), an upper bound is considered for curtailment (DL_{max}), which could be set according to the end-user and supplier specific requirements. Such constraints could affect the energy storage technology selection in the optimization model.

Moreover, the decision variables (X_z) included in the optimization process are the number of PV (N_{PV}), battery (N_B), compressor stage (N_c), turbine stage (N_{tr}) which are the integer variables. The continuous variables include the nominal power capacity of the compressor (W_c^r) and turbine (W_{tr}^r), energy capacity of TES (E_{TES}) and volume of AST (V_{AST}), maximum and minimum pressure of AST (P_{AST}^{max} & P_{AST}^{min}) .

3.5.1.3.2. Second stage: operation-unit commitment scope

In the second stage, the primary objective is to minimize the expected daily operational cost

while considering penalties for LPS and renewable energy curtailment. In this stage, we aim to increase resiliency and renewable penetration while reducing the dependency on the grid for day-ahead scheduling. Decisions in this stage are contingent upon the optimal size from the first stage.

$$Min\ OPEX_{daily} = \sum_{t=1}^{t=24}(C_{per}(t)\ W_{g,per}(t) - C_{sell}(t)\ W_{g,sell}(t)) + \sum_{t=1}^{t=24} C_{lps}W_{lps}(t) + \sum_{t=1}^{t=24} C_{cur}W_{cur}(t) + \sum_{t=1}^{t=24} C_{h,loss}\dot{Q}_{c,loss}(t) \quad (3.70)$$

where C_{lps} , C_{cur} and $C_{\mathrm{h,loss}}$ are the cost penalty per unit of unmet load (W_{lps}), the renewable power curtailment (W_{cur}) and heat loss ($\dot{Q}_{c,loss}$) at each time step, respectively. The objective function (Eq. 3.70) in the second stage is subject to the following constraints:

(a) Compressor and turbine train

The constraint associated with the input and output limits of the compressor and turbine train of the A-CAES system can be expressed as follows:

$$\nu_{tr}(t)\ \delta_{tr}N_{tr}W_{tr}^{r} \le W_{CAES,dcrg}\ (t) \le \nu_{tr}(t)N_{tr}W_{tr}^{r} \quad (3.71)$$

$$\nu_{c}(t)\ \delta_{c}N_{c}W_{c}^{r} \le\ W_{CAES,crg}\ (t) \le \nu_{c}(t)N_{c}W_{c}^{r} \quad (3.72)$$

$$\nu_{c}(t) + \nu_{tr}(t) + \nu_{id}(t) = 1 \qquad \nu_{c}, \nu_{tr}, \nu_{id} \in \{0,1\} \quad (3.73)$$

where $W_{CAES,crg}$ and $W_{CAES,dcrg}$ refer to the power consumption and generation by the A-CAES compressor and turbine trains, respectively, at time t. The binary variable of ν_c , ν_{tr}, ν_{id} indicate the operating status of A-CAES's compressor, turbine, and idle status, respectively; they take 1 when operating and 0 when they are inactive. It should be noted that although A-CAES's charging and discharging phases are conducted in two separate paths, A-CAES cannot charge and discharge simultaneously. Besides, in order to consider the response time of the A-CAES system and its resiliency when sudden grid disruption happens, at the initial time step (t=1), ν_{id} gets the value of one, meaning that A-CAES cannot charge and discharge immediately.

To increase the contribution of A-CAES in load demand coverage, a constraint should be defined to prioritize the PV power utilization and A-CAES discharging to avoid simultaneously discharging and curtailment or selling to the grid:

$$W_{CAES,dcrg}(t) \le \nu_{tr}(t)[W_{Load}(t) - W_{PV}\ (t)] \quad (3.74)$$

where W_{Load} and W_{PV} show the load demand and PV output power at each time step. Under the scenario of having A-CAES only for renewable integration and not load shifting, the below constraint should be defined:

$$W_{CAES,crg}\ (t) \leq \nu_c(t)[W_{PV}(t) - W_{Load}\ (t)] \quad (3.\ 75)$$

The above constraint limits the A-CAES compressor's operation only to absorb the PV panel's excess energy. In other words, it does not allow A-CAES to use the energy from the grid at off-peak hours.

(b) Compressor-turbine transition constraint

Given the involvement of mechanical systems like compressors and turbines in A-CAES technology, the time it takes to transition from the charging to the discharging phase affects the operational cost and resiliency of the hybrid system. Therefore, the constraints related to the conservative consideration of the gap time between the shutdown of a compressor and the startup of a turbine (and vice versa) in an A-CAES system could be defined as follows:

The transition from charging to discharging:

$$\nu_c(t) * \nu_t(t+1) = 0 \quad (3.\ 76)$$

The transition from discharging to charging:

$$\nu_t(t) * \nu_c(t+1) = 0 \quad (3.\ 77)$$

(c) AST of A-CAES

The constraint associated with the level of air pressure in AST (P_{AST}) can be expressed as follows:

$$P_{AST}^{min}\ \leq P_{AST}\ (t) \leq P_{AST}^{max} \quad (3.\ 78)$$

It is worth mentioning that minimum (P_{AST}^{min}) and maximum pressure (P_{AST}^{max}) of AST are achieved from the first stage as they are the design decision variables in the optimal planning-sizing stage.

(d) TES Component

The constraint associated with the state of energy in TES ($E_{TES}(t)$) is expressed as follows:

$$E_{TES}^{min} \leq\ E_{TES}(t) \leq E_{TES}^{max} \quad (3.\ 79)$$

Similarly, the E_{TES}^{max} is the TES capacity obtained in the first stage. To avoid regulating and limiting the charging mass flow rate and compressor train operation, there should be constraints associated with the thermal energy generated during the compression phase as follows:

$$\dot{Q}_{c,crg}(t) = \dot{Q}_c(t) - \dot{Q}_{c,loss}(t) \quad (3.\ 80)$$

where $\dot{Q}_c$ is the total heat generated during the compression process and $\dot{Q}_{c,loss}$ refers to the dissipated thermal energy.

(e) Battery

The constraint associated with energy capacity (E_{Batt}) of battery storage can be defined as follows:

$$(1 - dod_B)N_B W_B^r \leq E_{Batt}(t) \leq N_B W_B^r \quad (3.\ 81)$$

where W_B^r presents the rated energy capacity of the battery. $W_{B,crg}$ and $W_{B,dcrg}$ refer to the charging and discharging energy to and from the battery bank, respectively, restricted by the below constraints:

$$0 \leq W_{B,dcrg}(t) \leq \vartheta_{B,dcrg}(t)N_B W_B^r \quad (3.\ 82)$$

$$0 \leq W_{B,crg}(t) \leq \vartheta_{B,crg}(t)N_B W_B^r \quad (3.\ 83)$$

$$\vartheta_{B,crg}(t) + \vartheta_{B,dcrg}(t) + \vartheta_{B,id}(t) = 1 \qquad \vartheta_{B,crg}, \vartheta_{B,dcrg}, \vartheta_{B,id} \in \{0,1\} \quad (3.\ 84)$$

where dod_B presents the depth of discharge of the battery, and $\vartheta_{B,crg}$, $\vartheta_{B,dcrg}$,and $\vartheta_{B,id}$ are the binary variables showing the operating status of the battery bank. Eq. (3.85) and (3.86) consider the battery as a backup storage in the hybrid system. Meanwhile, Eq. (3.86) also considers batteries only for renewable integration (batteries are restricted to absorbing the extra PV power, not cheap electricity from the grid).

$$W_{B,dcrg}(t) \leq \vartheta_{B,dcrg}(t)\left[W_{Load}(t) - W_{PV}(t) - W_{CAES,dcrg}(t)\right] \quad (3.\ 85)$$

$$W_{B,crg}(t) \leq \vartheta_{B,crg}(t)[W_{PV}(t) - W_{Load}(t) - W_{CAES,crg}(t)] \quad (3.\ 86)$$

(f) The trade-off with the grid

Constraints associated with the purchase and selling from and to the grid can be expressed by Eq. (3.87) and (3.88), respectively:

$$0 \leq W_{g,per}(t) \leq \delta_{per}(t)W_{g,per}^{max} \quad (3.\ 872)$$

$$0 \leq W_{g,sell}(t) \leq \zeta_{max,s}\delta_{sell}(t)[W_{PV}(t) - W_{Load}(t) - W_{CAES,crg}(t) - W_{B,crg}(t)] \quad (3.\ 88)$$

$$\delta_{per}(t) + \delta_{sell}(t) \leq 1 \qquad \delta_{per}, \delta_{sell} \in \{0,1\} \quad (3.\ 89)$$

where δ_{per} and δ_{sell} are binary variables, indicating that the purchase and sell cannot co-occur. $W_{g,per}^{max}$ is the maximum allowable power purchased from the grid while $\zeta_{max,s}$ represent the maximum percentage of selling the surplus PV power. Eq. 3.88 shows that selling to the grid

cannot be more than surplus PV power, and if the grid does not purchase any power from the hybrid system, $\zeta_{max,s}$ considered zero.

(g) Power balance

The constraint associated with power balance at each time step could be calculated as follows:

$$W_{PV}(t) + W_{CAES,dcrg}(t) + W_{B,dcrg}(t) + W_{g,per}(t) + W_{lps}(t) = W_{Load}(t) + W_{CAES,crg}(t) + W_{B,crg}(t) + W_{g,sell}(t) + W_{cur}(t) \quad \forall t \in t \tag{3. 90}$$

(h) Resiliency constraint

To achieve a resilient system for day-ahead scheduling, the following should be met at the end of each day:

$$\sum_{t=1}^{t=24} W_{lps}(t) \leq \xi_{lpsp} \sum_{t=1}^{t=24} W_{Load}(t) \tag{3. 91}$$

where ξ_{lpsp} represent the LPSP factor.

3.5.1.4. Other performance indicators

In order to compare and evaluate the optimal configuration, in addition to the economic indicator (e.g., LCOE and LCC) defined in the previous sections, the following technical indicators are defined to investigate the performance of the entire HES in the sizing-planning stage.

$$ELMR = \frac{\sum_{t=1}^{8760} min(W_{PV}(t), W_{Load}(t)) + W_{CAES,dcrg}(t) + W_{B,dcrg}(t)}{\sum_{t=1}^{8760} W_{Load}(t)} \tag{3. 923}$$

$$SCR = \frac{\sum_{t=1}^{8760} min(W_{PV}(t), W_{Load}(t)) + W_{CAES,crg}(t) + W_{B,crg}(t)}{\sum_{t=1}^{8760} W_{PV}(t)} = 1 - Curtailment \tag{3. 93}$$

where ELMR refers to the electric load management ratio of the HES, which is the ability of the hybrid system to meet the load demand. Meanwhile, SCR stands for the self-consumption rate, which is the ability of HES to consume the generated renewable energy.

3.5.2. Case study

The same case study as considered in section 3.4.2 (paper 3) is considered for the current investigation.

3.5.2.1. Technical and economic parameters

The economic parameters of PV, battery, converter, and A-CAES sub-systems and their corresponding economic models are presented in Table 3.12 in section 3.5.2.2. The technical parameter of the studied A-CAES systems and project specifications are listed in Table 3.13 and 3.15, respectively. The characteristics of the PV panel are detailed in section 3.3. Table 3.16 presents the lower and upper bounds of design-decision variables in the first stage. The characteristics of battery are presented in Table 3.25. In addition, the penalty costs associated with LPS, and curtailment are listed in Table 3.26.

Table 3. 25. Characteristics of battery considered in this study [257]

Term (Parameter)	Value
Battery type	Lithium-ion (Li-ion)
Maximum capacity	2.1 kWh
voltage	6 V
Self-discharge rate	0.02
Charging efficiency	100%
Discharging efficiency	85%
Depth of discharge (dod_B)	80 %
Lifetime	15

Table 3. 26. Penalty costs associated with LPS and curtailment [129].

Term (Parameter)	Value ($ / kWh)
Loss of power supply penalty (C_{lps})	1
Curtailment penalty (C_{cur})	0.1
Heat loss penalty ($C_{h,loss}$)	0.01

3.5.3. Results and discussions

This study implements the whole model in Python, running on an Intel Core i7-7500U CPU @ 2.7 GHz. Moreover, the simulation is performed with a time step of 1 h and operated on data for one year. As one of the efficient hetaeristic methods in solving a sizing optimization problem, the particle swarm algorithm is employed in the first layer to obtain minimum LCOE. Detailed information regarding this method and its essential parameters can be found in section

3.5.1.6. However, the SCIP (Solving Constraint Integer Programs) solver in Python was adopted to solve the unit-commitment problem (in the second layer).

3.5.3.1. First stage: optimal configuration

Table 3.27 presents the viable and optimal configurations, organized in order of their LCOE rankings. It is important to highlight that these optimal configurations were attained under an annual $LPSP_{MAX}$ of 1% (except System #1), corresponding to an ERF of 99%, and a maximum grid importation limit of 900 kW (approximately half of the peak load demand of the building). According to the case study characteristics and components' limitations achieving a 99% resilient system with less than 900 kW grid-back up power leads to infeasible solutions. In other words, obtaining a LPSP of less than 1% (threshold) at a grid dependency level of 900 kW is not feasible.

In Table 3.27, the analysis reveals that, although the minimum LCOE of 0.103 $/kWh belongs to System #1 (solely PV), which is approximately 6.36 % lower than System #2 (PV/A-CAES), it performs less favorably in terms of ELMR and LPSP. This implies that, incorporating ESSs not only increases the renewable penetration by at least 2.3 times but also significantly reduces the LPSP of the HESs by around 41.1%.

Comparing the optimal configurations involving ESS exhibits that from a cost standpoint, System #2 (PV/A-CAES) without a battery bank exhibits the lower LCOE at 0.110 $/kWh, while System #3, incorporating a battery within the HES, demonstrates a slightly higher LCOE of 0.117 $/kWh. Notably, System #3 can satisfy 47.3% of the building's load demand. Considering load demand and solar energy management, the HES with HESS (System #3) exhibits approximately 6.3% and 6.7% higher ELMR and SCR, respectively, compared to the HES with individual A-CAES (System#2). On the other hand, the optimal number of PV panels (300W) in System #3 is only around seven units more (equivalent to approximately 2 kW), indicating a marginal difference that may not be considered significant. Hence, this underscores a direct proportionality between adding a battery to the system and increasing LCOE, ELMR, and SCR. Although the presence of battery in the system leads to an increase in the SCR (less curtailment) and ELMR (less grid dependency), it does not necessarily guarantee an improvement in annual resiliency to more than 99%. This is due to the specific conditions of the case study, where solar photovoltaic (PV) serves as the sole source of renewable energy, supplemented by limited grid power (maximum 900 kW) as backup. There are days, particularly in winter, characterized by poor solar irradiance and high end-user load demand.

Table 3. 27. Top-economic optimal configurations under a maximum grid dependency of 900 kW.

Design variable	System #1 PV	System #2 PV/ A-CAES	System #3 PV/ A-CAES/ Battery
N_{PV}	3815	7697	7704
N_B	0	0	428
N_c	0	5	4
N_{tr}	0	3	4
W_c^r (kW)	0	138.9	205.1
W_{tr}^r (kW)	0	182.6	112.3
V_{AST} (m^3)	0	300	300
E_{TES} (kWh)	0	3.26	4.74
p_{AST}^{max} (MPa)	0	14.53	16.79
p_{AST}^{min} (MPa)	0	2.5	2.5
$W_{conv.}$ (kW)	844	2309	3165
LCOE ($/kWh)	0.103	0.110	0.117
LCC (M$)	10.61	11.42	12.12
ELMR (%)	19.6	44.5	47.3
SCR (%)	95	90	96
LPSP (%)	1.696	0.999	0.997

Consequently, during such periods, the available solar power and grid power are primarily directed towards meeting the load demand to prevent power loss. As a result, storage systems such as A-CAES or batteries are left depleted after discharging their energy (if exist). Consequently, during subsequent days with similar weather conditions and high load demand, these storage systems remain unchanged, potentially leading to a loss of power supply. These dynamics may vary across different case studies and could be influenced by the addition of more renewable energy sources.

Table 3.28 presents the charging and discharging durations of ESSs in their respective optimal configurations. Notably, the charging power rated capacity of A-CAES in System #2 is

recorded at 694.5 kW, while System #3 exhibits a higher capacity of 820.4 kW, representing an 18% increase. Although the overall discharging rated capacity of A-CAES in System #2 surpasses that of System #3 (547.8 kW versus 449.2 kW, a 22% difference), the A-CAES's discharge time in System #3 is 1.5 times longer than in System #2. This disparity is attributed to the higher maximum air pressure of 16.8 MPa in the AST of System #3, signifying a greater energy capacity than System #2. In addition, the charging and discharging times exhibit an inverse relationship with the air mass flow rate in the system. In System #2, where the discharge time is 5.633 hours, the A-CAES demonstrates a higher discharging mass flow rate of 7504 kg/hr. In contrast, System #3 exhibits a lower mass flow rate of 5916 kg/hr and a longer discharge time of 8.46 hours.

Analyzing the results reported in Table 3.28, it becomes evident that in System #3, the battery and A-CAES function synergistically as short-term and long-term energy storage, complementing each other's operation. Conversely, in System #2, the individual A-CAES requires a trade-off in discharging time to function as medium-term energy storage, covering both long- and short-term operational needs.

Table 3. 28. Charging and discharging time of energy storages and AMFR of A-CAES in the corresponding optimal configuration

		Charging Time (hr)		Discharging Time (hr)		Rated AMFR of A-CAES (kg/hr)	
System	Configuration	A-CAES	Batt.	A-CAES	Batt.	Charging	Discharging
2	PV/ A-CAES	9.144	0	5.633	0	5069	7504
3	PV/ A-CAES/ Battery	9.876	1.205	8.466	1.695	4623	5916

As representative, in Fig. 3.51, the dynamic behavior of A-CAES, TES, and the battery in System #3 is depicted over a year. Notably, due to the limited solar energy potential in winter, there is a reduced availability of excess PV electricity for charging the ESSs. Consequently, the storage systems predominantly operate during the summer months. It is worth highlighting that the AST and TES in System #2 exhibit similar operational profiles. This underscores the distinct influence of seasonal variations on the utilization patterns of the energy storage components within the system.

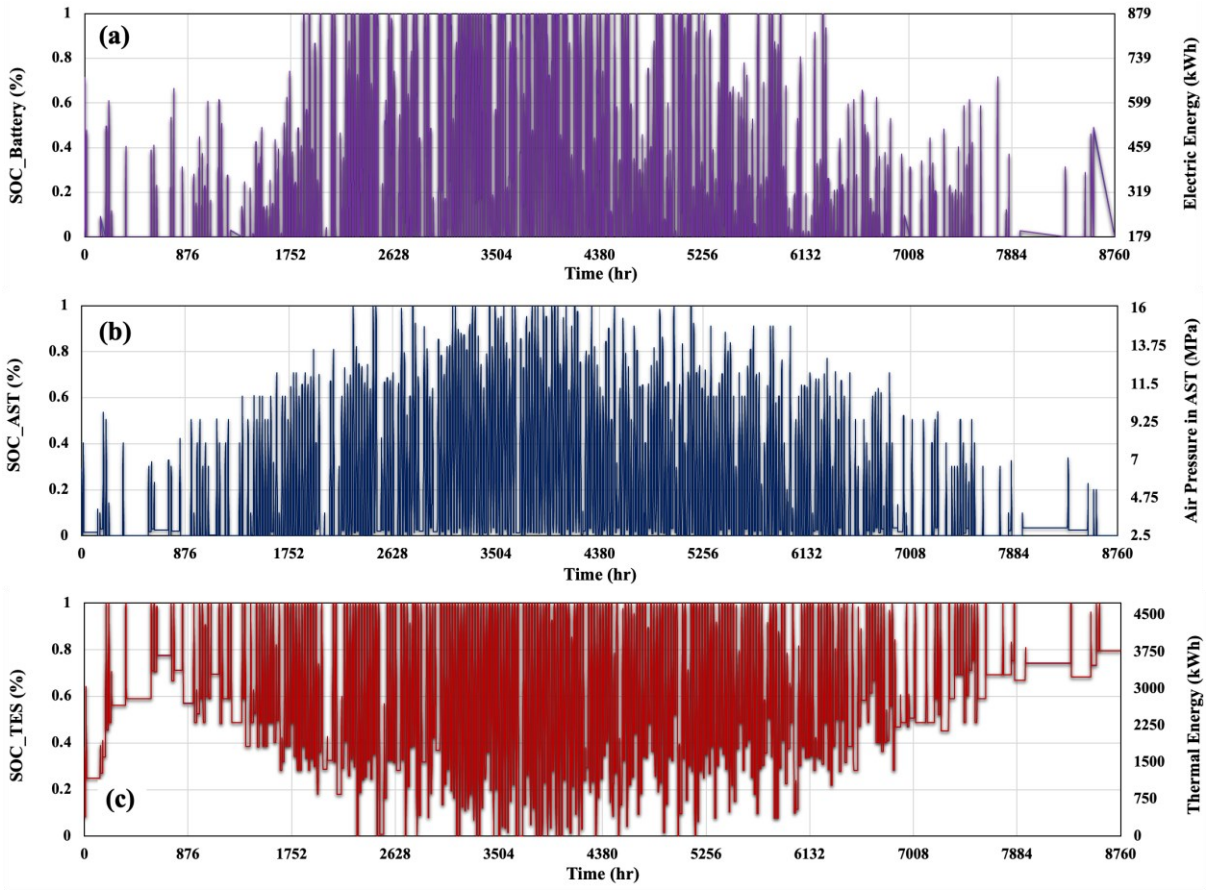

Fig. 3. 51. The dynamic behavior of a) battery bank, b) AST, and c) TES in System#3 (PV/A-CAES/Battery) over a year.

3.5.3.1.1. Resiliency analysis (long-term basis)

As previously noted, both representative optimal configurations involving ESS have attained an approximately annual 99% resiliency, equivalent to an annual LPSP of 1%. However, it is noteworthy that the curtailment in System #2, characterized by a SCR of 90%, is 6% higher than that in System #3, where the SCR is 96%, as outlined in Table 3.27. This distinction underscores the superior efficiency of System #3 in minimizing curtailment, emphasizing its enhanced capability to harness and utilize solar energy resources more effectively compared to System #2.

As a representative, Fig. 3.52 illustrates the daily LPSP of System #2 over a year. The analysis of Fig. 3.52 reveals a prominent trend wherein the majority of LPSP incidents transpire during the winter months, particularly in December. This temporal concentration of LPSP occurrences aligns with the coincidence of low solar energy potential and heightened load demand, exacerbated by limited purchasing power from the grid (maximum 900 kW). Notably, the highest LPSP is observed between the 5th and 10th of December, with the peak daily LPSP

reaching 21% on the 6th of December. This discernible pattern emphasizes the critical impact of seasonal variations on the LPSP dynamics. By monitoring such long-term behavior, designers and stakeholders can proactively identify pivotal days and hours, enabling timely interventions such as adjusting the backup power sources, implementing load shedding strategies, or adopting some energy-efficient solutions on the demand side to minimize LPSP and enhance the overall reliability and resiliency of the system.

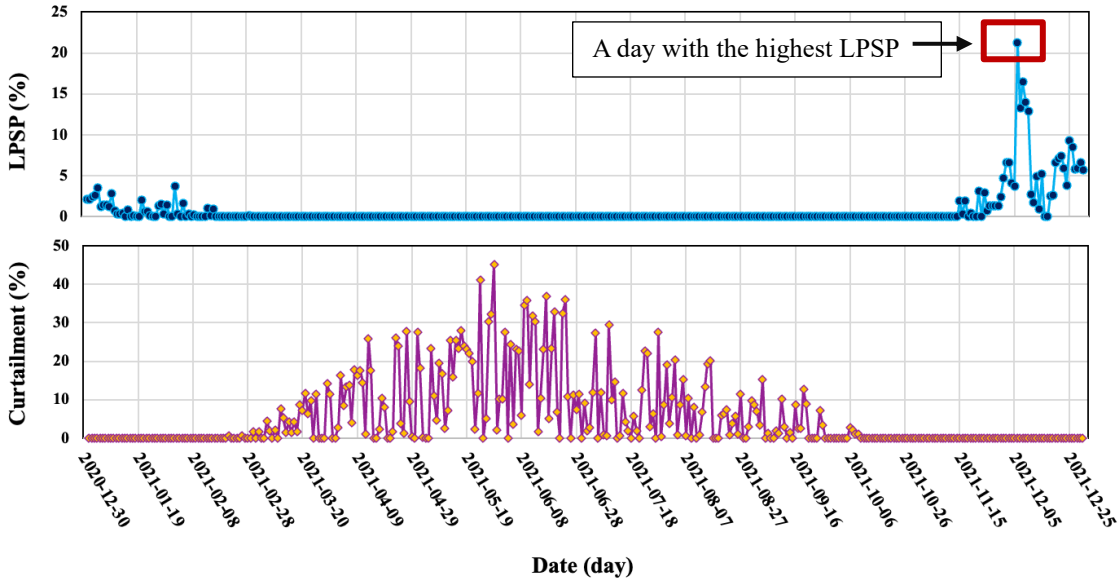

Fig. 3. 52. Daily LPSP and curtailment over a year for PV/A-CAES system (System#2).

For instance, in Fig. 3.53, the resiliency curve on the 6th of December, as a critical day in terms of power supply shortage, is presented under various quantities of backup power. The sensitivity analysis reveals that, in a worst-case scenario, a maximum of 1300 kW of backup power, obtainable from sources such as the grid or alternative electricity sources like a gas generator, is required to achieve a 100% resilient HES, where annual LPSP is reduced from 1% to 0. Furthermore, the trade-off between resiliency and level of grid dependency, as well as the corresponding impact on LCOE, is illustrated in Fig. 3.54. It is concluded that this marginal shortfall in meeting the load demand (1%) does not result in significant changes to the LCOE of the system but increases the LCC by around 1.3%.

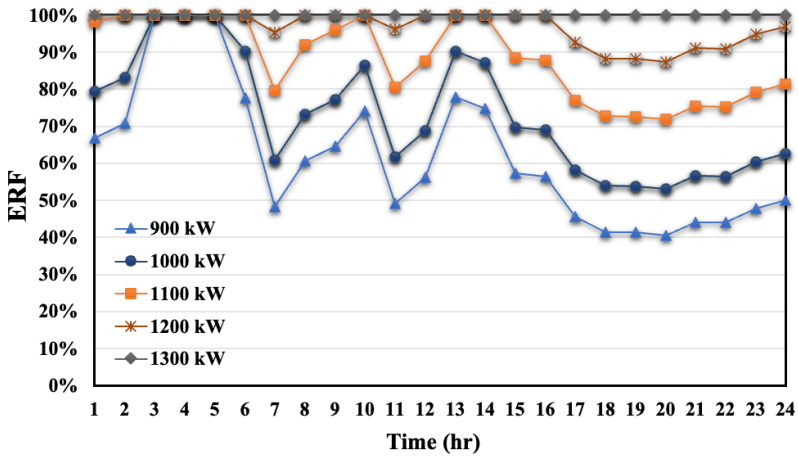

Fig. 3. 53. Resilience curve for the most critical day (6th December) under different backup power.

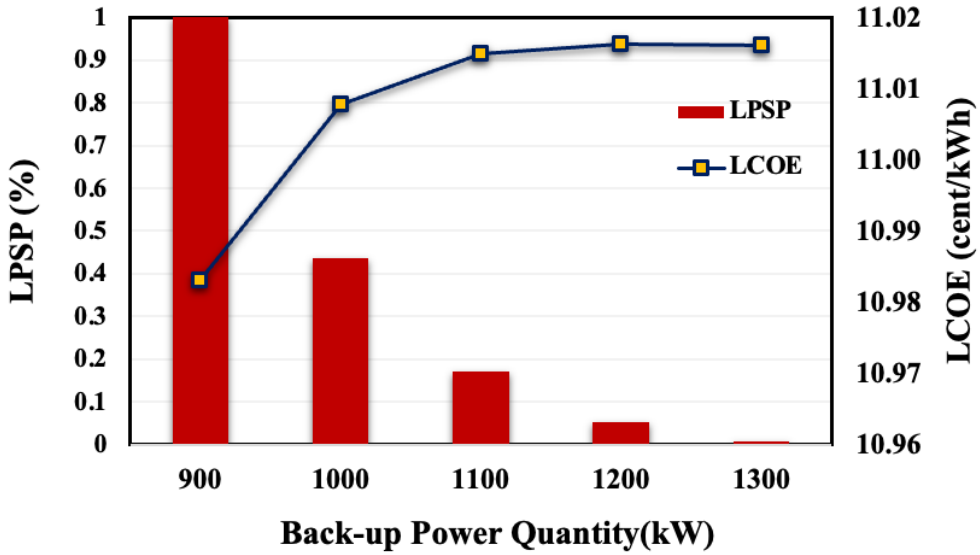

Fig. 3. 54. The LCOE and annual LPSP of System#2 under different backup power quantities.

3.5.3.2. Second stage: optimal operation-schedule

In the operational phase, the focus is on developing a unit-commitment model to schedule the storage systems effectively, with the overarching goals of enhancing the resiliency of the pre-designed HES and minimizing the LPSP. Leveraging insights gained from the long-term operational results of the optimal design phase, specific days characterized by severe LPSP, and renewable curtailment are identified for in-depth analysis. The objective is to formulate an optimal operating model to minimize operational costs and maximize system resiliency and renewable penetration.

An essential aspect of this investigation involves assessing the impact of response time and transitions among the mechanical systems within the A-CAES system. This assessment is particularly pertinent to constraints presented in Eq. 3.76 and Eq. 3.77. This exploration is crucial in understanding how these factors influence the scheduling and operational costs of the system, especially in real-world operations.

Furthermore, the subsequent stage involves comparing the results of the optimal operation with those obtained from the rule-based operation employed in the first stage. This comparative analysis aims to provide insights into the efficiency and efficacy of the developed dispatch strategy model in achieving the desired operational outcomes, explicitly focusing on minimizing costs and maximizing resiliency.

This section examines the outcomes of optimal operations through a dual lens, including economic and resilient considerations. The examination includes various conceivable scenarios, including 1) normal conditions where the grid functions as the available but limited backup power source (maximum 900 kW), and the hybrid system is tasked with meeting the entirety of the load demand, and 2) critical condition where contrastingly, there exists a disruption and disconnection from the grid. Consequently, the system is compelled to satisfy the emergency load requirements of the building. In this case, the assessment extends beyond economic considerations to include an evaluation of the system's resilience.

3.5.3.2.1. Normal scheduling (grid-connected)

The economic and resilient performance of System #2 (PV/A-CAES) is systematically assessed under various scenarios, each corresponding to distinct considerations regarding the applied PDS (rule-based or automated) and the transition time of the mechanical sub-system within the A-CAES system during the charging and discharging processes. The specific scenarios evaluated and compared are as follows:

Scenario 1. Optimal operation without considering the charging/discharging transition time of the A-CAES's mechanical systems.

Scenario 2. Optimal operation considering the charging/discharging transition time of the A-CAES's mechanical systems.

Scenario 3. Operation under a rule-based PDS without considering the charging/discharging transition time of the A-CAES's mechanical systems, offering a comparative analysis against the optimal operations.

By systematically evaluating these scenarios, the study aims to investigate the impact of transition time considerations and the type of PDS on economic and resilient performance, facilitating a comprehensive comparison and understanding of the system's behavior under various operational conditions.

By analyzing the outcomes derived from the initial stage (optimal sizing) and considering the specific characteristics of the case study, including load demand and renewable potential, a set of representative days has been chosen to assess the optimal operation of the system across defined scenarios. The details of these selected days are presented in Table 3.29. This Table compares the daily operational cost, LPSP, and PV curtailment for the PV/A-CAES/grid system (System #2) under distinct predefined scenarios.

Table 3.29 serves as a comprehensive reference for comparing the operational behaviors of the PV/A-CAES/grid system under the influence of various specified scenarios. The findings contribute to a comprehensive understanding of the system's performance on specific days, shedding light on the economic and resilient aspects under different operational conditions.

The analysis presented in Table 3.29 demonstrates that the operational cost, LPSP, and curtailment of the PV/A-CAES system under optimal dispatch strategies (Scenario 1 and Scenario 2) are generally equal to or lower than those under the rule-based dispatch strategy (Scenario 3).

The consideration of charge/discharge transition time in Scenario 2 introduces a detailed perspective, revealing that, in some instances, there is an increase in the operational cost and LPSP compared to Scenario 1. This increase is attributed to the need to purchase power from the grid to meet building load demand during the transition time from charging to the discharging process (or vice versa), leading to higher operational cost. Additionally, due to the limitation on grid purchases, there might be an increase in LPSP, especially during the period of high energy demand. While Scenario 1, which disregards A-CAES's transition time, exhibits favorable outcomes in terms of operating expense and LPSP. However, the more realistic approach in Scenario 2, adopting a more realistic approach by accounting for transition times reveals potential drawbacks or compromises in the system's performance. This shows the importance of balancing the need for accurate modeling with the associated operational costs and challenges, offering a more comprehensive understanding of the system's behavior under different operating conditions.

In the “class high demand (HD) and low PV power (LP),” primarily comprising winter days, the LPSP tends to be higher compared to other days of the year under other classes. There is

almost no renewable energy curtailment in this category due to the lower solar energy potential. For example, on December 6th, the highest LPSP of approximately 21% is observed under the rule-based PDS. Adopting the optimal dispatch model in the second stage reduces the LPSP to 19.56%, marking an around 8% reduction on the same day. Similarly, when shifting from the rule-based model to optimal operation on December 3rd and 7th, the LPSP diminishes from 6.59% and 13.27% to 0.01% and 7.8%, respectively. Additionally, on January 5th and 10th, the LPSP reaches zero under optimal operation, showcasing substantial system reliability and resiliency enhancements.

On days categorized as "class low demand (LD) and LP," the system typically exhibits almost zeroLPSP and highest SCR. Nonetheless, there could be minimal PV power curtailment, as exemplified on April 12th, where 1.13% of the PV power remains unused under both the rule-based and unit-commitment models across all scenarios.

On days falling into the category of "class HD and high PV Power (HP),” the LPSP is reduced to zero under all scenarios, indicating high system reliability. Nevertheless, there is a minor amount of PV power curtailment. Notably, under the optimal unit-commitment models (scenarios 1 and 2), this curtailment is either equivalent to or less than what is observed under the rule-based model (Scenario 3).

In "class LD and HP" days, characterized by high PV power curtailment, the highest curtailment is noted on May 29th, reaching 45% under Scenario 3 (rule-based model), while under Scenarios 1 and 2 (optimal operation), it is reduced to 43%.

These findings underscore the effectiveness of optimal dispatch strategies in minimizing LPSP and curtailment, particularly on days with challenging conditions.

It is important to note that on days where the amount of LPSP and power curtailment is identical under both Scenario 1 and Scenario 2 (unit-commitment model), the variation in operational cost is attributed to modifications in the scheduling of A-CAES sub-systems and the importation of energy from the grid. These adjustments significantly impact the overall operating cost of the system.

Table 3. 29. Typical days for power dispatching under all scenarios

		Daily Operation Cost** ($/day)			Daily LPSP (%)			Daily Curtailment (%)		
Class	*Days*	*Scen1*	*Scen2*	*Scen3*	*Scen1*	*Scen2*	*Scen3*	*Scen1*	*Scen2*	*Scen3*
HD LP	5th January	794	794	1313	0.00	0.00	3.50	0.00	0.00	0.00
	10th January	2122	2203	3024	0.00	0.00	2.83	0.00	0.00	0.00
	2nd February	1269	1325	1784	0.85	1.17	3.72	0.00	0.00	0.00
	3rd December	3550	3642	4984	0.01	0.01	6.59	0.00	0.00	0.00
	6th December	9214	9214	9584	19.56	19.56	21.27	0.00	0.00	0.00
	7th December	3149	3149	3442	7.80	7.80	13.27	0.00	0.00	0.00
LD LP	12th April	299	318	435	0.00	0.00	0.00	1.13	1.13	1.13
	25th May	216	216	266	0.00	0.00	0.00	0.00	0.00	0.00
	16th October	920	920	1141	0.00	0.00	0.00	0.00	0.00	0.00
HD HP	26th February	1633	1633	1806	0.00	0.00	0.00	0.54	0.54	0.54
	7th March	1533	1581	1562	0.00	0.00	0.00	4.42	4.42	4.42
	13th March	1119	1210	1286	0.00	0.00	0.00	5.31	5.31	5.31
	8th Jun	206	206	320	0.00	0.00	0.00	1.62	1.62	6.01
LD HP	26th May	245	245	318	0.00	0.00	0.00	4.16	4.16	5.13
	29th May	1029	1029	1034	0.00	0.00	0.00	43.05	43.05	45.15
	24th Jun	792	792	799	0.00	0.00	0.00	33.72	33.72	35.98

** Operation cost for all scenarios includes net purchase from grid and penalty associated with loss of power supply and PV power curtailment (calculated based on Eq.3.70) and heat loss

To demonstrate the influence of operational strategy and transition time on the scheduling of the A-CAES system and the resulting trade-offs with the grid, Fig. 3.55, 3.56, 3.57, and 3.58 depict the optimal power dispatch for four representative days from various classes, as presented in Table 3.29, across different scenarios.

As evident in these figures, the scheduling of A-CAES varies across scenarios, influenced not only by the PDS but also by accounting for the transition from the charging to the discharging phase in A-CAES. In many instances, particularly in Scenario 1 and Scenario 3, A-CAES initiates discharging (charging) immediately after completing the charging (discharging) phase without factoring in the transition time of the mechanical system. It becomes evident that considering this transition time is crucial for achieving a more precise schedule and optimizing the overall system operation.

Fig. 3.55 serves as an illustrative example of a typical day marked by high-power demand and low solar energy conditions, falling into the "class HD and LP." As depicted in Fig. 3.55 (a) and (b), where the PV power output is insufficient to meet the load demand, A-CAES is predominantly utilized to minimize the operational costs for load-shifting purposes. A-CAES stores energy from the grid during off-peak hours at night and periods of low solar radiation during the day. Notably, during the nighttime, when the grid is the sole source of electricity, priority is given to fulfilling the load demand before charging A-CAES, contingent upon the availability of grid-purchased energy.

Contrastingly, under the rule-based model (Scenario 3), as shown in Fig. 3.55 (c), where A-CAES is primarily planned for renewable integration and load-shifting during excess PV power, power shortages and loss of power occur due to the combination of high-load demand, low PV power, and limited grid resources (maximum 900 kW). This results in an observed LPSP of 2.83%, as indicated in Table 3.29 for the same day.

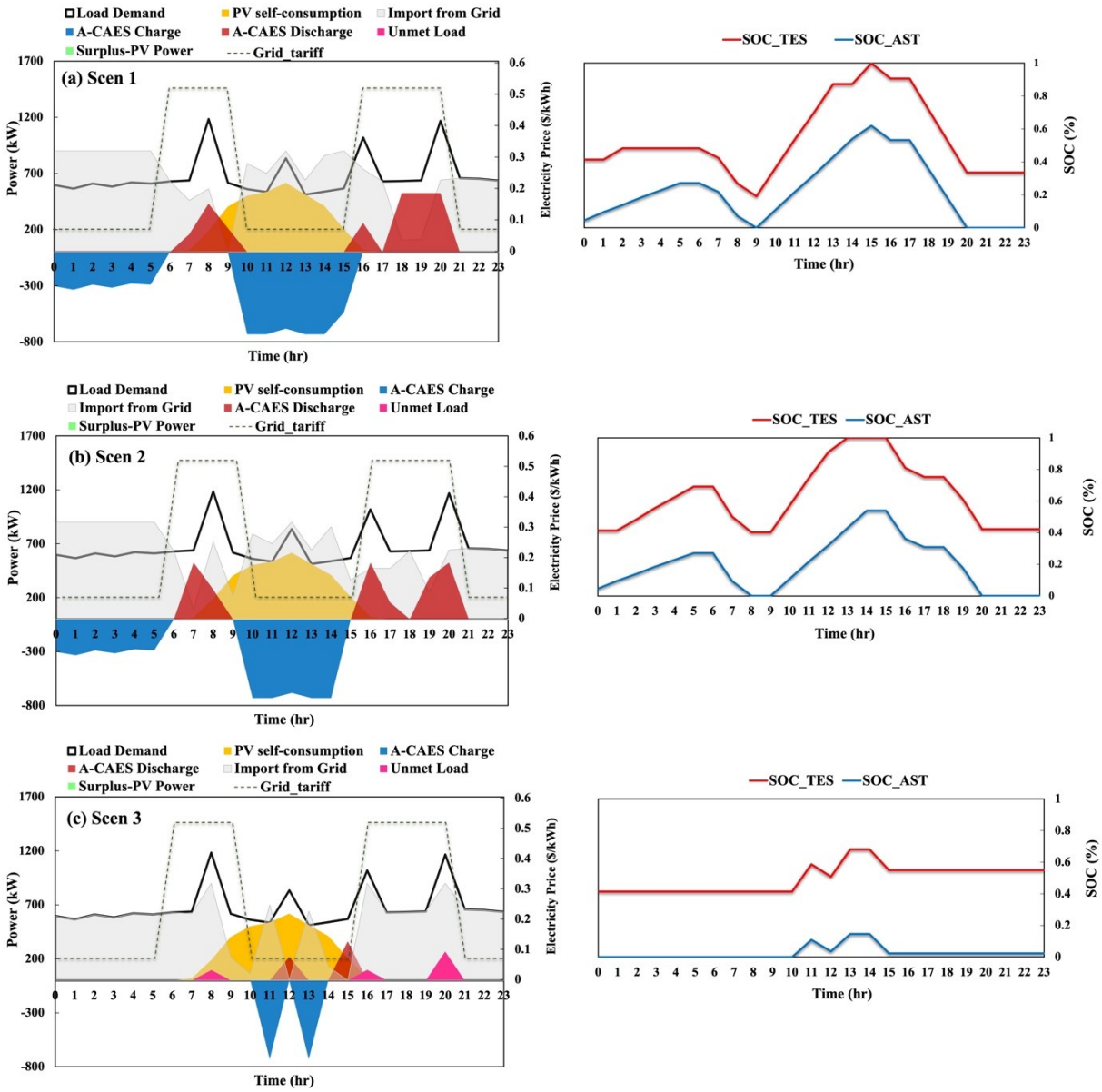

Fig. 3. 55. Power dispatch and schedule for a typical day (10th January) for class HD and LP is available under all scenarios.

Fig.3.56 provides insight into the power dispatch and schedule when power load and solar availability are at high levels (class HD and HP). In this scenario, the PV and A-CAES systems synergistically work together to fulfill the power demand while minimizing dependence on electricity imported from the grid. During nighttime, the microgrid draws power from the electricity grid, capitalizing on lower electricity prices and the inactivity of solar PV modules. In contrast, during daylight hours, the PV modules play an important role in meeting energy requirements. Excess energy generated during these hours is either used to charge the storage system or may be curtailed if the storage SOC is sufficiently high. This collaborative approach optimizes utilizing solar energy and storage resources within the HES.

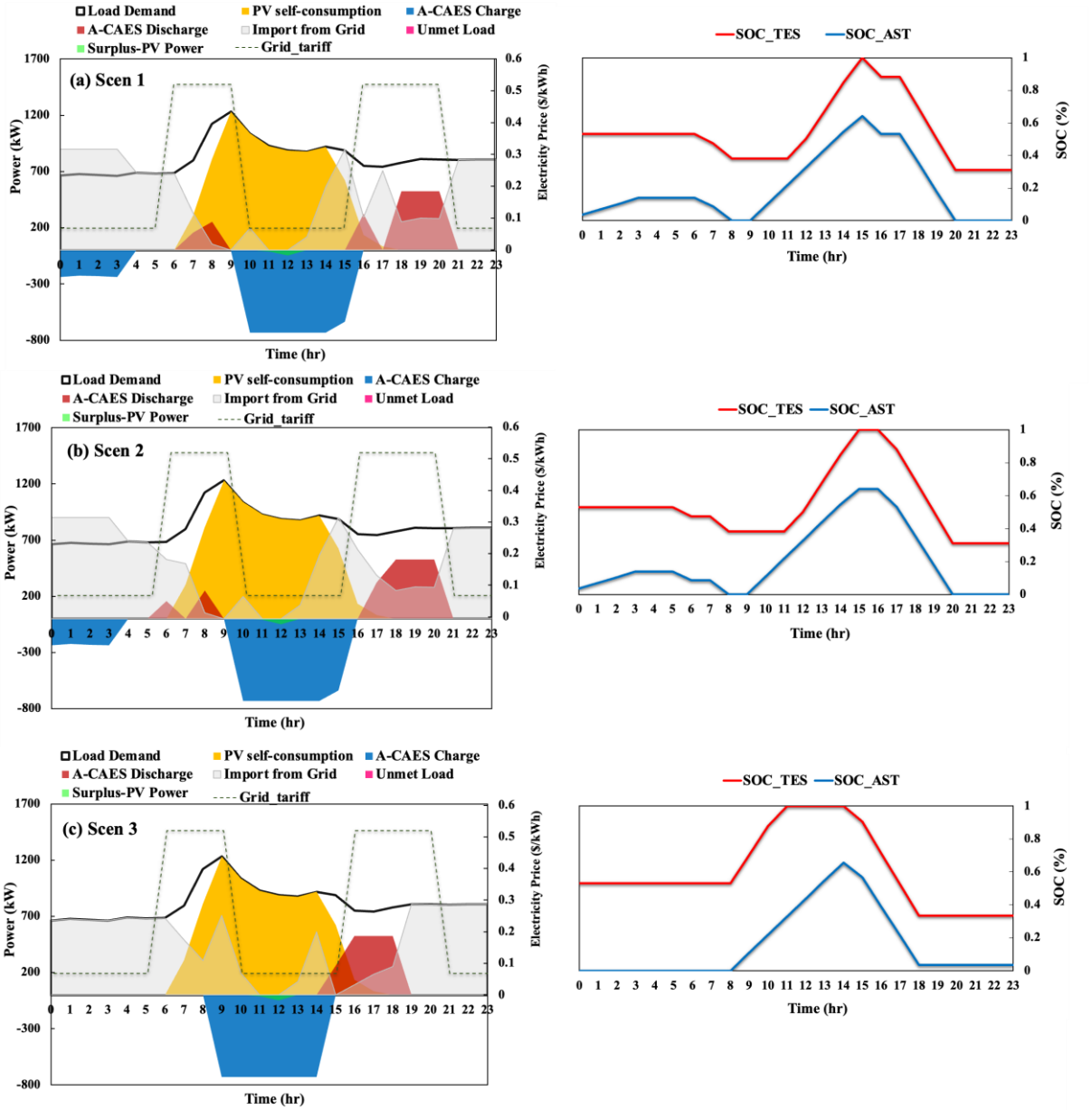

Fig. 3. 56. Power dispatch for a typical day (26th February) for class HP and HD is available under all scenarios.

In Fig. 3.57, the power dispatch for days falling into the "class LP and LD" is presented under all scenarios. In such days where the PV power output is less than the load demand, the system optimizes its operational cost by leveraging time of use (TOU) tariffs. This load-shifting strategy is implemented through the unit commitment model within the A-CAES system.

Contrastingly, under the rule-based model (Fig.3.57 (c)), when the load demand is below the maximum allowable power purchased from the grid, the grid becomes the sole source to meet the demand during periods without PV power output. This explains the observed difference in

operational cost, where Scenario 1 and Scenario 2 result in an operating cost of 920$, whereas Scenario 3 incurs a cost of 1141$, as reported in Table 3.29. Notably, LPSP and curtailment are zero under all scenarios; the variation in operational cost is attributed to the optimization of grid price utilization under optimal operation (Scenario 1 and Scenario 2) compared to rule-based operation (Scenario 3).

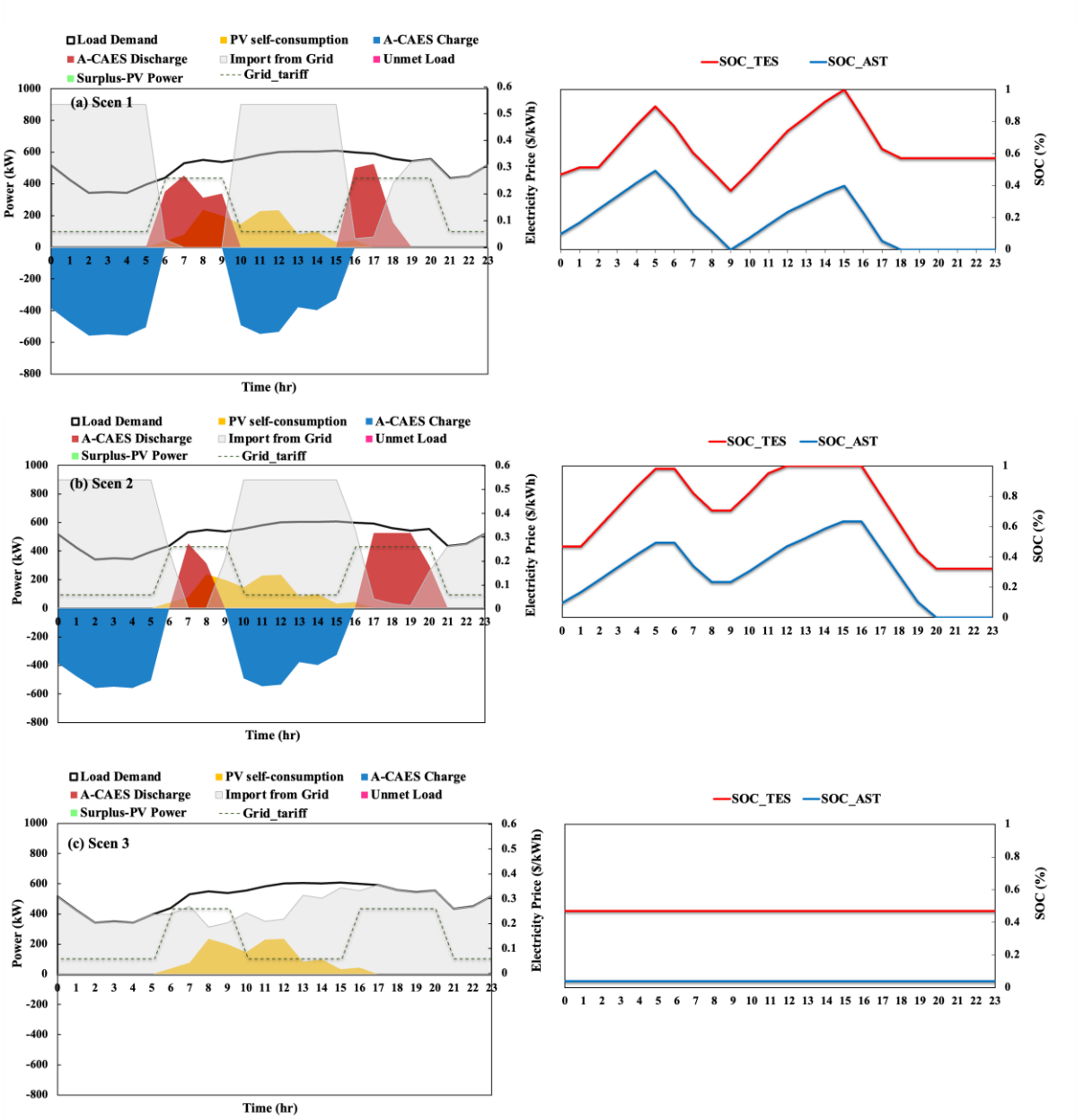

Fig. 3. 57. Power dispatch for a typical day (16th October) for class LP and LD is available under all scenarios.

In Fig. 3.58, a representative day falling into the category of HP and LD without a TOU tariff is depicted. The figure illustrates that the PV power generated is sufficient to meet the load demand throughout the day and charge the A-CAES system. PV curtailment is observed in

certain instances, amounting to around 4.16% under Scenario 1 and Scenario 2 and 5.13% under the rule-based model (Scenario 3).

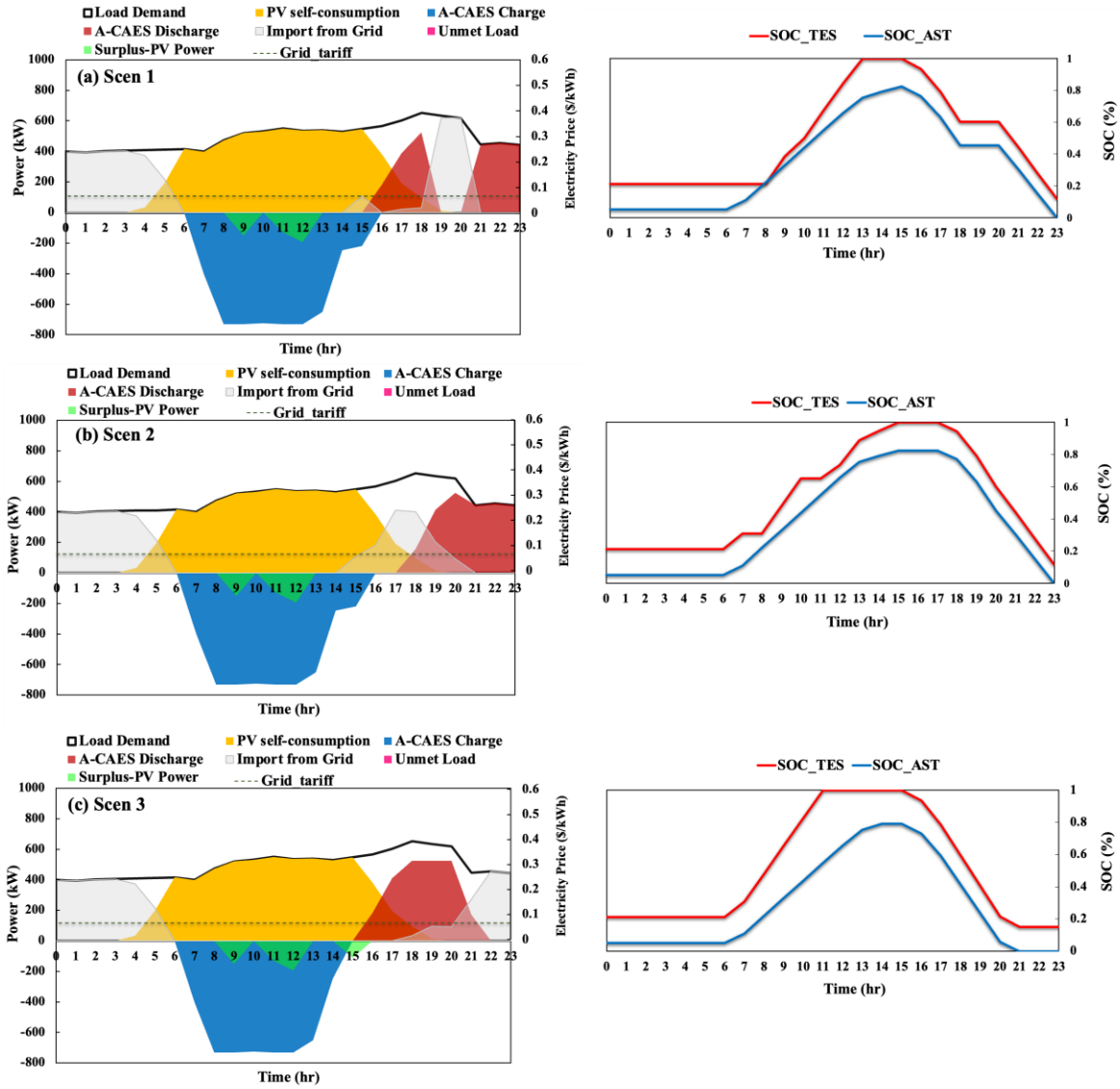

Fig. 3. 58. Power dispatch for a typical day (26th May) for class LD and HP is available under all scenarios.

3.5.3.2.2. Resilient scheduling (off-grid)

In this section, the focus is predominantly on evaluating the impact of integrating A-CAES with a battery in a PV-based energy system, explicitly examining the resiliency of the optimal HESs during grid disconnection and interruptions (shut-down). The analysis involves comparing the optimal operation and scheduling of two designed HESs (System#2 and System#3) resulting from the optimal sizing stage during off-grid modes, considering the constraints associated with the transition time of the A-CAES mechanical system (scenario 2). The assessment of resiliency is conducted from two key perspectives:1) Energy Retention

Factor (ERF), calculated as one minus the LPSP, providing insight into the system's ability to retain and supply energy during interruptions; 2) response time to measure how fast the storage systems can respond to the load demand when a sudden outage occurs.

Table 3.30 provides a comprehensive overview, showcasing the operational cost, ERF, and curtailment for both optimal hybrid systems (#2 and #3) during interruptions for selected days across different classes. This analysis aids in understanding the resiliency of the HESs under diverse scenarios, highlighting their capacity to maintain energy supply and promptly address load demands during grid disconnection events.

It's important to emphasize that the days categorized into four classes under critical conditions may not necessarily align with those identified under normal conditions. This distinction arises from considering emergency loads for the building during interruptions. This section considers an initial SOC of 40% for both storage systems, representing the best-case scenario. As highlighted in Table 3.30, the results indicate that hybridizing A-CAES with a battery enhances system resiliency, manifested by decreased LPSP, reduced curtailment, and, subsequently, lower operational costs. For instance, on certain days falling into classes LD-LP, LD-HP, and HD-HP, the hybrid storage systems enable the achievement of 100% resiliency, where LPSP drops to zero. Notably, on the most challenging day, December 6th, in the HD-LP class of hybrid system #3, an ERF of 22.5% is attained compared to 16% of system#2. This enhancement underscores the effectiveness of HESSs in strengthening the system's capability to endure interruptions and enhance overall resiliency.

Fig. 3.59 and 3.60 compare the resiliency of the PV/A-CAES system against the PV/A-CAES/Battery system for days falling into the HP-LD (best-case scenario) and HP-HD classes, respectively. The observations highlight that A-CAES, functioning primarily as a long-term energy storage, can cover the emergency load for long periods, as shown in Fig. 3.59 (a) and Fig. 3.60 (a). However, due to the transition time between the charge and discharge phases, some LPS are observed, even in situations with PV power output and significant curtailment.

Fig. 3.59 (b) and 3.60 (b) demonstrate that incorporating a battery can serve as a backup storage solution, addressing the limitations of A-CAES by providing a fast-response storage option. A-CAES, requiring time to initiate discharging, can be complemented by the battery to swiftly respond to the outage, not only reducing curtailment but also bridging the gap caused by the A-CAES discharging response time during the initial stages of a sudden interruption and the charging/discharging transition of A-CAES to cover the load.

Table 3. 30. Typical days for power dispatching where there is an outage and emergency load demand under scenario 2 for both optimal configurations with ESS.

		Daily Operation Cost** ($/day)		Daily ERF (%)		Daily Curtailment (%)	
Class	*Days*	*System 2*	*System 3*	*System 2*	*System 3*	*System 2*	*System 3*
HD LP	5th January	4453	3298	42.84	57.48	7.59	0.00
	10th January	3708	2508	50.97	66.84	0.00	0.00
	2nd February	6623	5742	36.98	45.35	0.00	0.00
	3rd December	5995	4778	45.69	56.60	0.00	0.00
	6th December	11271	10398	16.00	22.5	0.00	0.00
LD LP	12th April	980	0	88.94	100	4.09	0.00
HD HP	26th February	2684	1014	75.30	90.5	14	4.4
	13th March	1968	505	82.43	95.93	17.31	8.27
	8th Jun	644	13	94.71	100	9.23	0.00
LD HP	26th May	538	35	95.47	100	13.89	1.87
	29th May	1644	1139	93.56	100	59.91	52.37
	24th Jun	1328	761	94.64	100	44.38	37.30

** Operation cost for all scenarios includes net purchase from grid and penalty associated with loss of power supply and PV power curtailment (calculated based on Eq.3.70) and heat loss

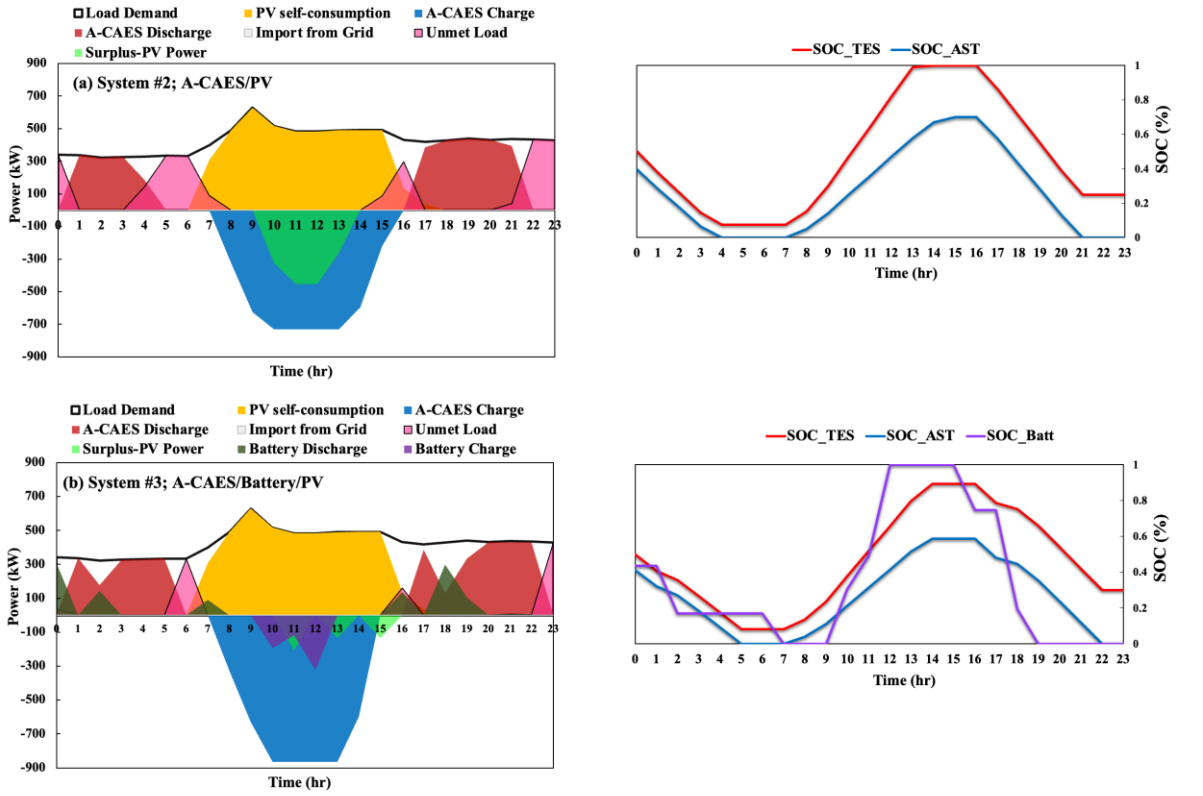

Fig. 3. 59. Power dispatch of a) A-CAES/PV system (#2), b) A-CAES/ Battery/PV system (#3) for a typical day (26th February) in class HP -HD during the grid outage.

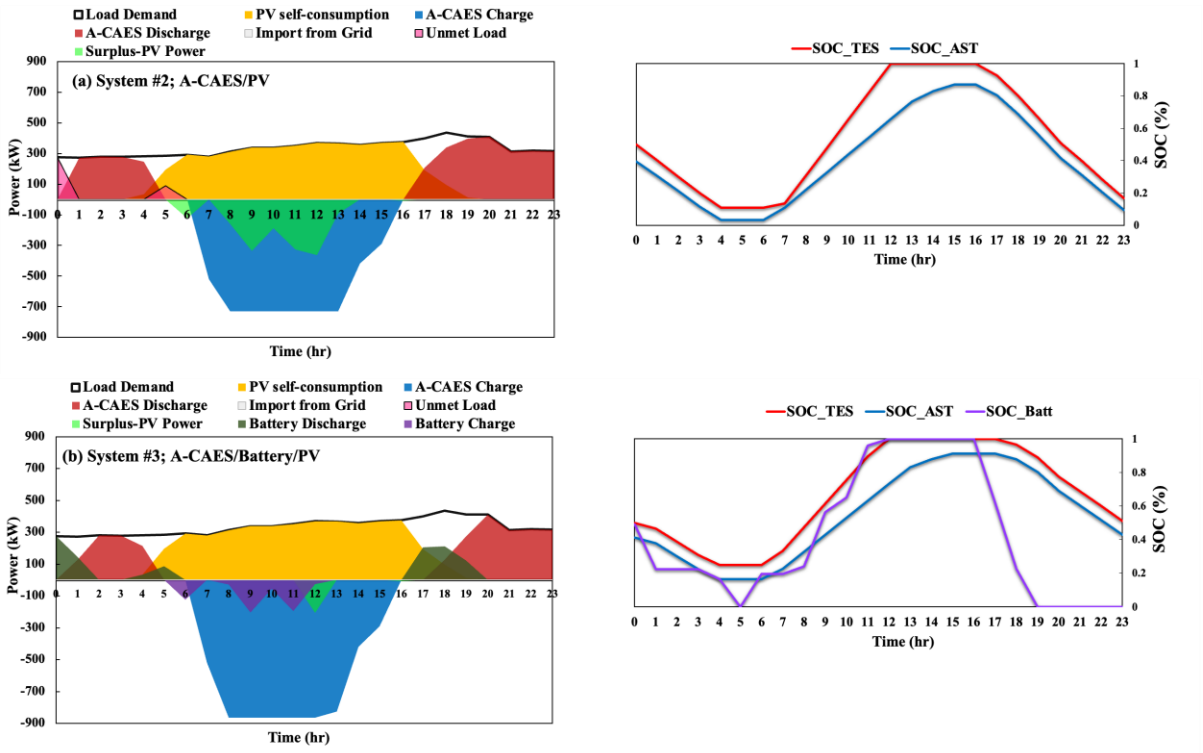

Fig. 3. 60. Power dispatch of a) A-CAES/PV system (#2), b) A-CAES/ Battery /PV system (#3) for a typical day (26th MAY) in class HP -LD during the grid outage

The results emphasize that while A-CAES can cover load demands for an extended duration, it lacks inherent resilience due to mechanical system response time and transition limitations. Hence, hybridizing it with another storage system with a fast response becomes essential to achieve a more resilient microgrid. The observed unmet load is caused by a delay in A-CAES start-up operation at the beginning of a grid failure, as well as the charging/discharging transition time during the day.

Chapter 4: Conclusions

4.1. Summary

This thesis explores the potential and significance of compressed air energy storage (CAES) in decentralized applications. Therefore, this research work begins with identifying the current research gaps and limitations pertaining to the characteristics of CAES, as well as its potential applications. This exploration is particularly focused on understanding the challenges and opportunities related to the integration, design, and scheduling of CAES systems from various perspectives. To achieve this, a comprehensive state-of-the-art literature review is conducted to thoroughly examine the existing body of knowledge in this field. Subsequently, a comprehensive multi-layer simulation and optimization framework consisting of three main modules is developed. This framework is designed to address the various barriers and challenges associated with the integration and implementation of small-scale adiabatic-CAES (A-CAES) technology in decentralized energy systems especially urban-integrated energy systems. In first module, the operation strategy of A-CAES system in terms of energy management is enhanced to develop an accurate simulation model for investigating the dynamic and long-term operation of decentralized A-CAES in energy system close to the end-users. Subsequently, second module utilized the improved operation strategy (I-EMOS) to propose several alternative PDSs according to the potential applications of A-CAES system in decentralized energy system. This enables a development of a decoupled simulation-optimization model, facilitating a comprehensive feasibility study of incorporating A-CAES systems for decentralized applications through optimal planning and sizing. Considerations include techno-economic and environmental aspects over the lifetime of the A-CAES system. Finally, the last module explores a resilience-centric procedure by integrating the planning-sizing module into an operation-scheduling optimization model. This integration aims to investigate and enhance the economic and resiliency aspects of the entire hybrid system with A-CAES technology within the scenarios involving limited grid dependency and hybrid energy storage solution. This model accounts for both long-term and short-term horizons, providing a holistic evaluation of the energy system's performance. Special attention is given to scenarios involving grid power failures, where the response time of the A-CAES' mechanical sub-systems, along with its hybridization with battery storage, is considered to ensure system reliability and resilience in operation phase.

To examine a developed methodology, a grid-connected PV-based hybrid system with A-CAES is considered as energy system to satisfy an urban building electric demand. Therefore, Concordia university located in downtown of Montreal, Canada is selected as the representative source of electrical demand.

In first module, the operation strategy of A-CAES system in terms of energy management is enhanced to develop an accurate simulation model for investigating the dynamic and long-term operation of decentralized A-CAES close to the end-users. The first step to improve the operation strategy and simulation model was integrating TES units into CAES system. The improved energy management operation strategy (I-EMOS) considered the characteristics, limitations, and the dynamic behavior, the current sates and interaction of all involved components, including power conversion units of compressor/turbine train, the air storage tank, and the thermal energy storage. Therefore, the developed simulation model of A-CAES is examined by integrating it into PV model as a primary power source and building load demand while is validated by tested and real results of existing pilot plant. The performance of A-CAES and HES under I-EMOS and the traditional operation strategy (T-EMOS) proposed in previous studies were compared to calculate the accuracy of the developed model. In addition, to verify the applicability of proposed the simulation model the effect of different influential parameters, such as the maximum pressure and volume of the AST, and TES capacity on HES's performance, was investigated. The main conclusions of first module are highlighted as follows:

- The simulation results of the proposed I-EMOS showed remarkable agreement with the tested results of the TICC-500 A-CAES pilot plant with the same characteristics.
- Adopting the limitation of power conversion units and TES in I-EMOS, in addition to the AST, caused A-CAES to have a longer charging time of 5.45 hr compared to 1 hr under T-EMOS.
- The dynamic behavior of the AST and transient operation of the compressor /turbine under I-EMOS was different from T-EMOS, which highly affects the contribution and schedule of other energy sources to answer the electric demand.
- Employing I-EMOS limited the number of A-CAES system's ramp-up /ramp-down while causing its sub-systems to work in their operating ranges to avoid compressor/turbine failure, surge, and choke, especially for decentralized applications.
- The sensitivity analysis of I-EMOS showed that there is an optimum value for the system's design parameters. Considering constant independent design parameters (power

conversion unit capacity, pressure range in AST, TES capacity), at minimum AST volume of 200 m^3, A-CAES can have the largest LCR. Subsequently, the self-sufficiency rate of building increases. The same behavior also happens for TES with an optimal volume of 8 m^3 as well as the AST's maximum pressure with values of 14 MPa.

- Also, it was indicated that the A-CAES system's integrated efficiency, LCR, SR, and ELMR rate were more sensitive to the maximum pressure of the AST than the other parameters, like the volume of the AST and TES.
- The charging and discharging times of TES raised with the increased TES volume. However, the discharging time of A-CAES had the first decrease and then a constant trend with the expanded TES volume while charging time is all constant.
- The result also indicated that dynamic operational conditions of compressor/turbine and AST stats are all affected by altering the TES rated capacity when TES is the only source of heat.
- The proposed I-EMOS offers a reliable rule-based energy management tool that presents a much more realistic operation of A-CAES in the hybrid system. Furthermore, this operation strategy allows studying other types of CAES with different characteristics for the sake of adopting TES and fuel utilization by adjusting the design parameter range of the TES unit.

The second module, proposes a systematic approach to assess the feasibility of incorporating a decentralized A-CAES system, aiming to evaluate its capabilities in renewable integration and load-shifting within urban-integrated energy system close to end-user. In doing so, a holistic simulation-optimization framework is presented to customize and optimally design an A-CAES system according to specific application requirements considering the thermodynamic, techno-economic, and environmental aspects. Therefore, a generic time-dependent mathematical model and multiple rule-based PDSs are introduced through which the A-CAES is planned for different proposes such as solar integration (A), load-shifting (B), and joint-functions (C and D). The adopted PDSs plan the A-CAES system depending on the solar energy availability, the grid's time-of-use electricity tariff, and load demand pattern. The objective is to minimize the LCOE through the project's lifetime while maximizing the A-CAES contribution in meeting the building load demand. Furthermore, several scenarios are examined as alternatives to explore the impact of managing PV-surplus power on the techno-economic viability of the proposed system. On the other hand, a sensitivity analysis (post-optimization) associated with influential input parameters (e.g., energy resource quantity and AST volume) is carried out to ensure the

model's applicability to the different case studies. The main conclusions are highlighted as follows:

- The simulation model accuracy is validated by comparing it with a real A-CAES pilot plant (TICC-500 [221]), showing an approximate 88% similarity. This ensures that the simulation accurately represents the behavior of the actual system, affirming its applicability to a variety of case studies.
- The optimal results show that the largest and smallest A-CAES systems in terms of power (compressor/turbine) and energy capacity (AST and TES) correspond to the HES planned for individual load-shifting (PDS-B) and renewable integration (PDS_A), respectively.
- Adopting A-CAES only for renewable integration is not an economically viable option unless a part of PV-surplus power is used for other applications (e.g., sold back to the grid or utilized for other usage, reducing the LCOE by a maximum of 5.7%, notably in the presence of a flexible load.
- The environmental evaluations reveal that the energy system planned for individual load-shifting results in the highest carbon emission, surpassing the primary power sources (grid) by around 25%.
- Under a worse-case scenario, when surplus PV power is curtailed, seasonally planning the A-CAES for the load-shifting joint with solar energy integration (PDS-D) emerges as the most appropriate strategy. The system designed under such a strategy exhibits superior performance in key metrics such as building ELMR (52.1%), solar self-consumption (92%), and TCER (28.3% less carbon emission) while achieving a relatively low LCOE (0.090 $/kWh).
- The electrical analysis shows that the A-CAES system’s dispatch strategy and service significantly affect the energy flow dynamics within the system. Moreover, optimal HESs designed for joint applications contribute more to grid peak shaving during peak hours compared to systems focused solely on load-shifting purposes.
- Evaluating the A-CAES operations across various strategies indicates that load demand patterns and the availability of power resources significantly influence the charging time and AMFR of A-CAES.
- Sensitivity analysis shows that the LCOE and ELMR of optimal HESs under different PDS involving solar integration decrease and increase with raised PV panel numbers.

In addition, depending on the number of installed PV panels, planning A-CAES for either seasonal (PDS-D) or yearly load-shifting (PDS-C), along with solar integration could result in the best energy solution.

- On the other hand, the level of A-CAES interaction with the grid (e.g., yearly, seasonally, or zero basis) influences the system's operational sensitivity to fluctuations in the maximum allowable power imported from the grid.
- Furthermore, increasing the upper limit of AST volume allows for the selection of larger volumes, which reduces the maximum pressure within the AST and compressor train capacity. Consequently, LCOE is reduced while efficiency is improved, leading to a modest positive variation in the ELMR and LCR under all strategies.
- From the finding it is concluded that the assessment and selection of the most suitable PDSs is a multifaceted undertaking, influenced by a multitude of factors, including cost, self-sufficiency, and carbon footprint, along with the specific characteristics of the case study.

The last module introduces a two-stage sizing-scheduling approach in presence of limited grid dependency and hybrid energy storage solution. It aims not only to minimize the LCOE over the project's lifetime while ensuring long-term resiliency, but also to achieve optimal daily scheduling in both grid-connected and off-grid scenarios under a unit-commitment operational model. This holistic approach not only obtain the optimal sizing of each component of energy system based on case study characteristics but also delves into the synergistic integration of A-CAES with battery storage, considering factors such as cost-effectiveness, energy management, and resiliency. A noteworthy aspect of this module also involves investigating the charging-discharging transition and responsiveness of the A-CAES system's mechanical units in the unit-commitment model and optimal dispatch strategy, specifically assessing its impact on operational performance and resiliency, particularly in scenarios of grid interruption. The findings of this study are highlighted as follows:

- The results derived from the sizing-planning stage reveal that, in terms of cost-effectiveness, the PV system with a LCOE of 0.103 $/kWh emerges as the most economically viable energy system compared to the PV/A-CAES and PV/A-CAES/Battery configurations with an LCOE of 0.110 $/kWh and 0.117 $/kWh, respectively. Nonetheless, adopting ESSs shows the potential to significantly enhance annual resiliency by approximately 41.1%.

- Comparing the optimal configurations incorporating ESS, despite the superior cost performance of the PV/A-CAES system, the PV-based HES featuring a hybrid A-CAES and battery storage achieves an electrical load management ratio of 47.3% and a self-consumption rate of 96%. This represents an approximately 6% improvement over the HES equipped solely with an individual A-CAES system.
- The optimal sizing analysis reveals that most power losses occur during the peak load demand and periods of low PV power availability, notably observed in December within the scope of this study. Consequently, a crucial need arises for increased backup power from the grid or alternative power sources to enhance the microgrid's reliability during these critical times.
- Upon analyzing and comparing the daily operation of a grid-connected PV/A-CAES system under the dispatch strategy of the first and second stages, it becomes evident that the operational cost, LPSP, and curtailment of the HES, when operating under the unit-commitment model (second stage), generally either align with or are lower than those observed under the rule-based dispatch strategy (first stage). This holds true even when considering the charging-discharging transition of A-CAES mechanical sub-systems in the unit-commitment model.
- During the grid interruption, even under the best-case scenario of PV power availability, a HES relying solely on individual A-CAES can fulfill the load demand by approximately 94%. This underscores the limited resilience of A-CAES as a standalone storage solution within PV-based HES. However, incorporating a fast-response battery significantly boosts resiliency to 100%, simultaneously reducing PV-power curtailment. This enhancement is noticeable during the grid interruption's beginning hour and during A-CAES's transitional phases between charging and discharging (or vice versa).

In conclusion, the proposed multi-stage simulation-optimization framework offers a reliable simulation model, sizing-planning and scheduling-operation approach for conducting a feasibility study concerning the integration of a decentralized A-CAES system into diverse services according to the specific requirements, constraints, and regulations of the individual case studies and end-users. Utilizing this model enables the identification of specific times with a higher probability of power loss, considering factors such as weather conditions and grid restrictions. This multifaceted analysis adds a unique dimension to the understanding of local energy system design, offering insights into the dynamic interplay between long-term sizing decisions and short-term operational scheduling. The adopted methodology also enables

enhanced integration of the A-CAES system with other renewable energy sources (e.g., wind, biomass) and energy storage systems (e.g., battery) either for gird-connected or stand-alone mode. The findings of this work serve as a comprehensive reference, equipping designers, and decision-makers with valuable insights to make informed choices in selecting the most suitable system, strategy, and scenario based on the importance of key performance indicators according to the unique requirements of their case study. It facilitates the exploration of a wide range of scenarios to determine the optimal configuration that balances minimal cost with high resiliency in presence of limited energy sources. It also suggests a promising avenue for further research exploring alternative sources or systems of energy within power systems. Moreover, the framework proposed in this thesis is adaptable and applicable to both smaller-scale scenarios, focusing solely on local generation, and larger-scale contexts, where regional generation is considered.

4.2. Contributions

This thesis presents a holistic user-based approach for simulation, optimal design, and optimal operation of decentralized A-CAES. The contributions made by this research work can be summarized as follows:

1) This study tthoroughly identified research gaps in the domain of integrating CAES within energy systems. A comprehensive state-of-the-art literature review highlighted gaps, particularly in optimal design and operation, including various models and methodologies in the field.
2) The research enhanced the accuracy of the simulation model for decentralized A-CAES system, considering detailed characteristics, physical limitations and interactions of different sub-systems. The developed simulation model demonstrated a long term and reliable operation of A-CAES system within the dynamic energy system environment.
3) The study proposed several alternative rule-based power dispatch strategies based on the application potentials of decentralized A-CAES within urban-integrated local energy systems.
4) A novel sizing-planning framework was developed to determine the optimal configuration of A-CAES' sub-systems, ensuring their appropriate interconnection and integration within dynamic energy system environment. This framework also provided a comprehensive feasibility assessment approach, considering techno-economic and environmental aspects throughout the system's lifetime.

4) The thesis introduced a resilience-oriented approach to co-optimize the economic and resilience of energy systems thorough two-stage optimization by adjusting the optimal value for maximum allowable loss of power supply probability across different time horizon in presence of limited power source.
5) The research enhanced the self-sufficiency, self-consumption and resilience of local energy system by hybridizing A-CAES with battery storage under both grid-connected and off-grid conditions, while considering A-CAES's longer transition and response time.
6) Collectively, this study presented the practical insights into enhancing the reliable utilization and feasibility of A-CAES in decentralized applications, particularly in the presence of limited energy sources. By considering detailed modeling of system components, their physical constraints and dynamic interrelations within the context of renewable energy systems and end-user load demands; this research unlocked A-CAES's potential for various applications, ranging from increased renewable energy integration to efficient load shifting.

4.3. Limitations and directions for future work

While this study significantly contributes to the optimal sizing and operation of CAES system in decentralized applications, certain limitations highlight areas requiring further research to enhance performance and practicality in integrated energy systems. This thesis suggests potential avenues for future research in various aspects of this PhD dissertation, including methodology, assumptions, case studies, and applications, with specific considerations for the Canadian context. The following areas are recommended for future investigation and development:

- Methodology Improvement
  1) Multigeneration integration**:** Enhance the A-CAES system model to support multigeneration by integrating heating, cooling, and electric energy demands. This will provide insights into the interactions and synergies among various energy sources, ensuring optimal operation and performance. It also enhances the feasibility and scalability of incorporating the A-CAES system for various applications.
  2) Comprehensive exergy analysis: Incorporate exergy analysis into the A-CAES system evaluation to improve performance and feasibility. This will provide deeper insights into overall efficiency, potential losses, and areas for further improvement.

Examining both energy and exergy flows can help identify optimization opportunities and enhance the performance and sustainability of decentralized energy systems.

3) Multi-objective optimization: Conduct multi-objective optimization to balance conflicting goals such as cost-effectiveness, reliability, and environmental impact for comprehensive trade-off analyses. This should include an exploration of crucial performance indicators to address system complexities and provide a detailed analysis from various perspectives.
4) Safety considerations: Enhance the reliability and safety of CAES by identifying and analyzing potential faults and hazards that could lead to unsafe conditions beyond current modeling constraints. This includes mechanical faults, electrical faults, temperature extremes, over/under pressurization, leakage, and pressure vessel ruptures. By identifying and analyzing these potential faults, safety measures can be implemented to prevent or mitigate their impact, ensuring the safe and reliable operation of the CAES system.

- Revisiting Key Assumptions
  5) Temperature variation in TES and AST units: Investigate temperature fluctuations and heat dissipation in TES and AST units for consistent and efficient energy storage, beyond the isothermal process assumed in this study.
  6) Various Pressure Operating Ranges: Explore different operating pressure ranges (sliding-constant, sliding-sliding, constant-sliding) to further improve system efficiency beyond the 'constant-constant' operating pressure assumed in this study. Addressing and resolving issues related to pressure variations during operation will contribute to further robustness of the proposed framework.
- Case Studies and Applications
  7) Integration with other energy sources in urban or remote areas: Expand the study to include the integration of CAES with alternative renewable sources (e.g., wind, biomass, hydro) and energy storage systems within power systems. This will enhance the versatility of the proposed framework for grid-connected or stand-alone applications. Investigating the synergies and challenges of combining various renewable and conventional energy sources considering specific bottlenecks such as the unique intermittency and variability patterns of renewables, availability and geographic dependence, regulatory and environmental constraints, and

compatibility between the storage system and the renewable source will contribute to a more holistic approach.

8) Hourly data-set resolution: Improve the accuracy of the proposed planning and operation framework by utilizing higher-resolution data sets to capture the precise detail of energy demand and supply fluctuations.
9) Interconnected microgrids: Extend the applicability of A-CAES in larger and more complex energy systems by exploring the simultaneous operation of multiple interconnected microgrids for power and energy sharing.

- Specific Points in the Canadian Context

10) Canadian energy landscape: Investigate factors specific to the Canadian context, such as regional energy policies, climate conditions, and market dynamics as well as studying the impact of cold climates on CAES performance, integration with hydropower, and implications of federal and provincial policies. This research will support the broader adoption and integration of CAES systems in Canada, addressing specific challenges and leveraging local opportunities.

Addressing these limitations and directions for future research will not only strengthen the current study but also pave the way for more comprehensive and applicable solutions in the domain of decentralized energy applications.

Bibliography

[1] A. Panda, U. Mishra, K.B. Aviso, Optimizing hybrid power systems with compressed air energy storage, Energy. 205 (2020) 117962. https://doi.org/10.1016/j.energy.2020.117962.

[2] J. Bai, W. Wei, L. Chen, S. Mei, Rolling-horizon dispatch of advanced adiabatic compressed air energy storage based energy hub via data-driven stochastic dynamic programming, Energy Convers. Manag. 243 (2021) 114322. https://doi.org/10.1016/j.enconman.2021.114322.

[3] C. Huang, Y. Zong, S. You, C. Træholt, Y. Zheng, J. Wang, Z. Zheng, X. Xiao, Economic and resilient operation of hydrogen-based microgrids: An improved MPC-based optimal scheduling scheme considering security constraints of hydrogen facilities, Appl. Energy. 335 (2023). https://doi.org/10.1016/j.apenergy.2023.120762.

[4] N. Shirzadi, H. Rasoulian, F. Nasiri, U. Eicker, Resilience Enhancement of an Urban Microgrid during Off-Grid Mode Operation Using Critical Load Indicators, Energies. 15 (2022). https://doi.org/10.3390/en15207669.

[5] G. Venkataramani, P. Vijayamithran, Y. Li, Y. Ding, H. Chen, V. Ramalingam, Thermodynamic analysis on compressed air energy storage augmenting power / polygeneration for roundtrip efficiency enhancement, Energy. 180 (2019) 107–120. https://doi.org/10.1016/j.energy.2019.05.038.

[6] T.M. Gür, Review of electrical energy storage technologies, materials and systems: Challenges and prospects for large-scale grid storage, Energy Environ. Sci. 11 (2018) 2696–2767. https://doi.org/10.1039/c8ee01419a.

[7] S. Zhang, S. Miao, Y. Li, B. Yin, C. Li, Regional integrated energy system dispatch strategy considering advanced adiabatic compressed air energy storage device, Int. J. Electr. Power Energy Syst. 125 (2021) 106519. https://doi.org/10.1016/j.ijepes.2020.106519.

[8] M. Amir, R.G. Deshmukh, H.M. Khalid, Z. Said, A. Raza, S.M. Muyeen, A.S. Nizami, R.M. Elavarasan, R. Saidur, K. Sopian, Energy storage technologies: An integrated survey of developments, global economical/environmental effects, optimal scheduling model, and sustainable adaption policies, J. Energy Storage. 72 (2023) 108694. https://doi.org/10.1016/j.est.2023.108694.

[9] G. Smdani, M.R. Islam, A.N. Ahmad Yahaya, S.I. Bin Safie, Performance Evaluation of Advanced Energy Storage Systems: a Review, Energy Environ. 34 (2023) 1094–1141. https://doi.org/10.1177/0958305X221074729.

[10] J.Y. Lee, A.K. Ramasamy, K.H. Ong, R. Verayiah, H. Mokhlis, M. Marsadek, Energy storage systems: A review of its progress and outlook, potential benefits, barriers and solutions within the Malaysian distribution network, J. Energy Storage. 72 (2023) 108360. https://doi.org/10.1016/j.est.2023.108360.

[11] E. Bazdar, M. Sameti, F. Nasiri, F. Haghighat, Compressed air energy storage in

integrated energy systems : A review, Renew. Sustain. Energy Rev. 167 (2022) 112701. https://doi.org/10.1016/j.rser.2022.112701.

[12] M. Heidari, D. Parra, M.K. Patel, Physical design, techno-economic analysis and optimization of distributed compressed air energy storage for renewable energy integration, J. Energy Storage. 35 (2021) 102268. https://doi.org/10.1016/j.est.2021.102268.

[13] S.O. Rey, J.A. Romero, L.T. Romero, À.F. Martínez, X.S. Roger, M.A. Qamar, J.L. Domínguez-García, L. Gevorkov, Powering the Future: A Comprehensive Review of Battery Energy Storage Systems, Energies. 16 (2023). https://doi.org/10.3390/en16176344.

[14] B. Li, Z. Liu, Y. Wu, P. Wang, R. Liu, L. Zhang, Review on photovoltaic with battery energy storage system for power supply to buildings: Challenges and opportunities, J. Energy Storage. 61 (2023) 106763. https://doi.org/https://doi.org/10.1016/j.est.2023.106763.

[15] F. Khalafian, N. Iliaee, E. Diakina, P. Parsa, M.M. Alhaider, M.H. Masali, S. Pirouzi, M. Zhu, Capabilities of compressed air energy storage in the economic design of renewable off-grid system to supply electricity and heat costumers and smart charging-based electric vehicles, J. Energy Storage. 78 (2024) 109888. https://doi.org/10.1016/j.est.2023.109888.

[16] G. Venkataramani, E. Ramakrishnan, M. Ram, A.H. Bhaskaran, P. Kumar, V. Ramalingam, J. Wang, Experimental investigation on small capacity compressed air energy storage towards e ffi cient utilization of renewable sources, 20 (2018) 364–370. https://doi.org/10.1016/j.est.2018.10.018.

[17] J. Bai, L. Chen, F. Liu, S. Mei, Interdependence of electricity and heat distribution systems coupled by an AA-CAES-based energy hub, IET Renew. Power Gener. 14 (2020) 399–407. https://doi.org/10.1049/iet-rpg.2019.0660.

[18] X. Zhang, C. (Chris) C. Qin, Y. Xu, W. Li, X. Zhou, R. Li, Y. Huang, H. Chen, Integration of small-scale compressed air energy storage with wind generation for flexible household power supply, J. Energy Storage. 37 (2021) 102430. https://doi.org/10.1016/j.est.2021.102430.

[19] Z. Tong, Z. Cheng, S. Tong, A review on the development of compressed air energy storage in China: Technical and economic challenges to commercialization, Renew. Sustain. Energy Rev. 135 (2021) 110178. https://doi.org/10.1016/j.rser.2020.110178.

[20] E. Bazdar, F. Nasiri, F. Haghighat, An improved energy management operation strategy for integrating adiabatic compressed air energy storage with renewables in decentralized applications, Energy Convers. Manag. 286 (2023) 117027. https://doi.org/10.1016/j.enconman.2023.117027.

[21] E. Bazdar, N. Fuzhan, H. Fariborz, Effect of Low-Temperature Thermal Energy Storage on the Hybrid PV-compressed Air Energy Storage Operation, in: 8th World Conf. Photovolt. Energy Convers., Milan, Italy, 2022: pp. 1609–1616.

https://doi.org/10.4229/WCPEC-82022-5DV.2.19.

[22] H. Meng, M. Wang, O. Olumayegun, X. Luo, X. Liu, Process design, operation and economic evaluation of compressed air energy storage (CAES) for wind power through modelling and simulation, Renew. Energy. 136 (2019) 923–936. https://doi.org/10.1016/j.renene.2019.01.043.

[23] R. Jiang, X. Yang, Y. Xu, M. Yang, Design/off-design performance analysis and comparison of two different storage modes for trigenerative compressed air energy storage system, Appl. Therm. Eng. 175 (2020) 115335. https://doi.org/10.1016/j.applthermaleng.2020.115335.

[24] C. Guo, Y. Xu, H. Guo, X. Zhang, X. Lin, L. Wang, Y. Zhang, H. Chen, Comprehensive exergy analysis of the dynamic process of compressed air energy storage system with low-temperature thermal energy storage, Appl. Therm. Eng. 147 (2019) 684–693. https://doi.org/10.1016/j.applthermaleng.2018.10.115.

[25] P. Zhao, Y. Dai, J. Wang, Design and thermodynamic analysis of a hybrid energy storage system based on A-CAES (adiabatic compressed air energy storage) and FESS (flywheel energy storage system) for wind power application, Energy. 70 (2014) 674–684. https://doi.org/10.1016/j.energy.2014.04.055.

[26] P. Zhao, M. Wang, J. Wang, Y. Dai, A preliminary dynamic behaviors analysis of a hybrid energy storage system based on adiabatic compressed air energy storage and flywheel energy storage system for wind power application, Energy. 84 (2015) 825–839. https://doi.org/10.1016/j.energy.2015.03.067.

[27] S.W. Mei, J.J. Wang, F. Tian, L.J. Chen, X.D. Xue, Q. Lu, Y. Zhou, X.X. Zhou, Design and engineering implementation of non-supplementary fired compressed air energy storage system: TICC-500, Sci. China Technol. Sci. 58 (2015) 600–611. https://doi.org/10.1007/s11431-015-5789-0.

[28] B. Castellani, E. Morini, B. Nastasi, A. Nicolini, F. Rossi, Small-scale compressed air energy storage application for renewable energy integration in a listed building, Energies. 11 (2018). https://doi.org/10.3390/en11071921.

[29] K. Rouindej, E. Samadani, R.A. Fraser, CAES by design: A user-centered approach to designing Compressed Air Energy Storage (CAES) systems for future electrical grid: A case study for Ontario, Sustain. Energy Technol. Assessments. 35 (2019) 58–72. https://doi.org/10.1016/j.seta.2019.05.008.

[30] E. Bazdar, F. Nasiri, F. Haghighat, Optimal planning and configuration of adiabatic-compressed air energy storage for urban buildings application : Techno-economic and environmental assessment, J. Energy Storage. 76 (2024) 109720. https://doi.org/10.1016/j.est.2023.109720.

[31] M. Adib, F. Nasiri, F. Haghighat, K. Panchabikesan, G. Venkataramani, S. Tiwari, V. Ramalingam, Integrating compressed air energy storage with wind energy system – A review, E-Prime - Adv. Electr. Eng. Electron. Energy. 5 (2023) 100194. https://doi.org/10.1016/j.prime.2023.100194.

[32] S. Sarmast, K. Rouindej, R.A. Fraser, M.B. Dusseault, Sizing-design method for compressed air energy storage (CAES) systems : A case study based on power grid in Ontario, Energy Convers. Manag. 277 (2023) 116656. https://doi.org/10.1016/j.enconman.2023.116656.

[33] I.E. Atawi, A.Q. Al-Shetwi, A.M. Magableh, O.H. Albalawi, Recent Advances in Hybrid Energy Storage System Integrated Renewable Power Generation: Configuration, Control, Applications, and Future Directions, Batteries. 9 (2023). https://doi.org/10.3390/batteries9010029.

[34] T. Xia, Y. Li, N. Zhang, C. Kang, Role of compressed air energy storage in urban integrated energy systems with increasing wind penetration, Renew. Sustain. Energy Rev. 160 (2022) 112203. https://doi.org/10.1016/j.rser.2022.112203.

[35] E.I. Come Zebra, H.J. van der Windt, G. Nhumaio, A.P.C. Faaij, A review of hybrid renewable energy systems in mini-grids for off-grid electrification in developing countries, Renew. Sustain. Energy Rev. 144 (2021). https://doi.org/10.1016/j.rser.2021.111036.

[36] C. Ammari, D. Belatrache, B. Touhami, S. Makhloufi, Sizing, optimization, control and energy management of hybrid renewable energy system—A review, Energy Built Environ. (2021). https://doi.org/10.1016/j.enbenv.2021.04.002.

[37] Our Energy Needs: World Energy Consumption & Demand | CAPP, (n.d.). https://www.capp.ca/energy/world-energy-needs/ (accessed November 27, 2020).

[38] A.Z. Arsad, M.A. Hannan, A.Q. Al-Shetwi, M. Mansur, K.M. Muttaqi, Z.Y. Dong, F. Blaabjerg, Hydrogen energy storage integrated hybrid renewable energy systems: A review analysis for future research directions, Int. J. Hydrogen Energy. (2022). https://doi.org/10.1016/j.ijhydene.2022.03.208.

[39] S.M. Dawoud, X. Lin, M.I. Okba, Hybrid renewable microgrid optimization techniques : A review, Renew. Sustain. Energy Rev. 82 (2018) 2039–2052. https://doi.org/10.1016/j.rser.2017.08.007.

[40] S. Ehsan, A. Mahmoudzadeh, M. Abdul, A review on green energy potentials in Iran, Renew. Sustain. Energy Rev. 27 (2013) 533–545. https://doi.org/10.1016/j.rser.2013.07.015.

[41] Data & Statistics - IEA, (n.d.). https://www.iea.org/data-and-statistics/data-browser/?country=WORLD&fuel=Energy supply&indicator=TPESbySource (accessed July 31, 2021).

[42] N. Shirzadi, F. Nasiri, C. El-Bayeh, U. Eicker, Optimal dispatching of renewable energy-based urban microgrids using a deep learning approach for electrical load and wind power forecasting, Int. J. Energy Res. 46 (2022) 3173–3188. https://doi.org/10.1002/er.7374.

[43] M.H. Nozari, M. Yaghoubi, K. Jafarpur, G.A. Mansoori, Development of dynamic energy storage hub concept: A comprehensive literature review of multi storage systems,

J. Energy Storage. 48 (2022) 103972. https://doi.org/10.1016/j.est.2022.103972.

[44] M. Faisal, M.A. Hannan, P.J. Ker, A. Hussain, M. Bin Mansor, F. Blaabjerg, Review of energy storage system technologies in microgrid applications: Issues and challenges, IEEE Access. 6 (2018) 35143–35164. https://doi.org/10.1109/ACCESS.2018.2841407.

[45] J. Bai, W. Wei, L. Chen, S. Mei, Modeling and dispatch of advanced adiabatic compressed air energy storage under wide operating range in distribution systems with renewable generation, Energy. 206 (2020) 118051. https://doi.org/10.1016/j.energy.2020.118051.

[46] IRENA, Electricity storage and renewables: Costs and markets to 2030. International Renewable Energy Agency, 2017.

[47] B. Zakeri, S. Syri, Electrical energy storage systems: A comparative life cycle cost analysis, Renew. Sustain. Energy Rev. 42 (2015) 569–596. https://doi.org/10.1016/j.rser.2014.10.011.

[48] M. Jafari, M. Korpås, A. Botterud, Power system decarbonization : Impacts of energy storage duration and interannual renewables variability, Renew. Energy. 156 (2020) 1171–1185. https://doi.org/10.1016/j.renene.2020.04.144.

[49] S. Koohi-Fayegh, M.A. Rosen, A review of energy storage types, applications and recent developments, J. Energy Storage. 27 (2020) 101047. https://doi.org/10.1016/j.est.2019.101047.

[50] A.G. Olabi, C. Onumaegbu, T. Wilberforce, M. Ramadan, M.A. Abdelkareem, A.H. Al – Alami, Critical review of energy storage systems, Energy. 214 (2021) 118987. https://doi.org/10.1016/j.energy.2020.118987.

[51] H. Sedighnejad, T. Iqbal, J. Quaicoe, Compressed air energy storage system control and performance assessment using energy harvested index, Electronics. 3 (2014) 1–21. https://doi.org/10.3390/electronics3010001.

[52] A.A. Khodadoost Arani, G. B. Gharehpetian, M. Abedi, Review on Energy Storage Systems Control Methods in Microgrids, Int. J. Electr. Power Energy Syst. 107 (2019) 745–757. https://doi.org/10.1016/j.ijepes.2018.12.040.

[53] X. Luo, J. Wang, M. Dooner, J. Clarke, Overview of current development in electrical energy storage technologies and the application potential in power system operation, Appl. Energy. 137 (2015) 511–536. https://doi.org/10.1016/j.apenergy.2014.09.081.

[54] F. Díaz-González, A. Sumper, O. Gomis-Bellmunt, R. Villafáfila-Robles, A review of energy storage technologies for wind power applications, Renew. Sustain. Energy Rev. 16 (2012) 2154–2171. https://doi.org/10.1016/j.rser.2012.01.029.

[55] S. Houssainy, M. Janbozorgi, P. Kavehpour, Thermodynamic performance and cost optimization of a novel hybrid thermal-compressed air energy storage system design, J. Energy Storage. 18 (2018) 206–217. https://doi.org/10.1016/j.est.2018.05.004.

[56] A.R. Razmi, S.M. Alirahmi, M.H. Nabat, E. Assareh, M. Shahbakhti, A green hydrogen

energy storage concept based on parabolic trough collector and proton exchange membrane electrolyzer/fuel cell: Thermodynamic and exergoeconomic analyses with multi-objective optimization, Int. J. Hydrogen Energy. (2022) 1–22. https://doi.org/10.1016/j.ijhydene.2022.03.021.

[57] M. Dooner, J. Wang, 14 - Compressed-Air Energy Storage, Elsevier Ltd, 2020. https://doi.org/10.1016/B978-0-08-102886-5.00014-1.

[58] K.T. Møller, T.R. Jensen, E. Akiba, H. wen Li, Hydrogen - A sustainable energy carrier, Prog. Nat. Sci. Mater. Int. 27 (2017) 34–40. https://doi.org/10.1016/j.pnsc.2016.12.014.

[59] A.G. Olabi, T. Wilberforce, M. Ramadan, M.A. Abdelkareem, A.H. Alami, Compressed air energy storage systems: Components and operating parameters – A review, J. Energy Storage. (2020) 102000. https://doi.org/10.1016/j.est.2020.102000.

[60] E. Fertig, J. Apt, Economics of compressed air energy storage to integrate wind power: A case study in ERCOT, Energy Policy. 39 (2011) 2330–2342. https://doi.org/10.1016/j.enpol.2011.01.049.

[61] F.A. Tiano, G. Rizzo, Use of an Under-Water Compressed Air Energy Storage (UWCAES) to Fully Power the Sicily Region (Italy) With Renewable Energy: A Case Study, Front. Mech. Eng. 7 (2021) 1–16. https://doi.org/10.3389/fmech.2021.641995.

[62] S. Graham, M. Momen, A. Abu-heiba, K. Gluesenkamp, O. Abdelaziz, R.K. Jackson, C. Daniel, S. Graham, THERMAL ANALYSIS OF NEAR-ISOTHERMAL COMPRESSED GAS ENERGY Keywords : energy storage , compressed air , micro pumped-hydro storage , near-isothermal expansion / compression , waste-heat utilization , Stirling cycle Nomenclature : Symbols m c temperature [, (n.d.).

[63] P. Zhao, W. Xu, S. Zhang, J. Wang, Y. Dai, Technical feasibility assessment of a standalone photovoltaic/wind/adiabatic compressed air energy storage based hybrid energy supply system for rural mobile base station, Energy Convers. Manag. 206 (2020) 112486. https://doi.org/10.1016/j.enconman.2020.112486.

[64] M. Budt, D. Wolf, R. Span, J. Yan, A review on compressed air energy storage: Basic principles, past milestones and recent developments, Appl. Energy. 170 (2016) 250–268. https://doi.org/10.1016/j.apenergy.2016.02.108.

[65] L. Chen, T. Zheng, S. Mei, X. Xue, B. Liu, Q. Lu, Review and prospect of compressed air energy storage system, J. Mod. Power Syst. Clean Energy. 4 (2016) 529–541. https://doi.org/10.1007/s40565-016-0240-5.

[66] Q. Zhou, D. Du, C. Lu, Q. He, W. Liu, A review of thermal energy storage in compressed air energy storage system, Energy. 188 (2019) 115993. https://doi.org/10.1016/j.energy.2019.115993.

[67] F. Crotogino, K.B.B. Gmbh, K. Mohmeyer, R. Scharf, E.O.N.K. Bremen, Huntorf CAES : More than 20 Years of Successful Operation by, (2001).

[68] G. Venkataramani, P. Parankusam, V. Ramalingam, J. Wang, A review on compressed

air energy storage – A pathway for smart grid and polygeneration, Renew. Sustain. Energy Rev. 62 (2016) 895–907. https://doi.org/10.1016/j.rser.2016.05.002.

[69] W. He, J. Wang, Optimal selection of air expansion machine in Compressed Air Energy Storage: A review, Renew. Sustain. Energy Rev. 87 (2018) 77–95. https://doi.org/10.1016/j.rser.2018.01.013.

[70] A. Vecchi, Y. Li, Y. Ding, P. Mancarella, A. Sciacovelli, Liquid air energy storage (LAES): A review on technology state-of-the-art, integration pathways and future perspectives, Adv. Appl. Energy. 3 (2021) 100047. https://doi.org/10.1016/j.adapen.2021.100047.

[71] C.D. Botha, M.J. Kamper, Capability study of dry gravity energy storage, J. Energy Storage. 23 (2019) 159–174. https://doi.org/10.1016/j.est.2019.03.015.

[72] A.C. Ruoso, N.R. Caetano, L.A.O. Rocha, Storage gravitational energy for small scale industrial and residential applications, Inventions. 4 (2019) 1–13. https://doi.org/10.3390/inventions4040064.

[73] J. Wang, K. Lu, L. Ma, J. Wang, J. Li, D. Wang, S.- Min, E. Com, E. Com, Overview of Compressed Air Energy Storage and Technology Development, (n.d.). https://doi.org/10.3390/en10070991.

[74] J.J. Wang, L. Ma, K. Lu, S. Miao, D. Wang, J.J. Wang, Current research and development trend of compressed air energy storage, Syst. Sci. Control Eng. 5 (2017) 434–448. https://doi.org/10.1080/21642583.2017.1377645.

[75] L. Li, W. Liang, H. Lian, J. Yang, Advances in Geo-Energy Research Compressed air energy storage : characteristics , basic principles , and geological considerations, (2018). https://doi.org/10.26804/ager.2018.02.03.

[76] M. King, A. Jain, R. Bhakar, J. Mathur, J. Wang, Overview of current compressed air energy storage projects and analysis of the potential underground storage capacity in India and the UK, Renew. Sustain. Energy Rev. 139 (2021) 110705. https://doi.org/10.1016/j.rser.2021.110705.

[77] Y. Fang, Y. Lu, A.P. Roskilly, X. Yu, A review of compressed air energy systems in vehicle transport, Energy Strateg. Rev. 33 (2021) 100583. https://doi.org/10.1016/j.esr.2020.100583.

[78] Y. Shi, F. Li, M. Cai, Q. Yu, Literature review: Present state and future trends of air-powered vehicles, J. Renew. Sustain. Energy. 8 (2016). https://doi.org/10.1063/1.4944970.

[79] F.S. Vieira, J.A.P. Balestieri, J.A. Matelli, Applications of compressed air energy storage in cogeneration systems, Energy. 214 (2021). https://doi.org/10.1016/j.energy.2020.118904.

[80] R. Li, L. Chen, T. Yuan, C. Li, Optimal dispatch of zero-carbon-emission micro Energy Internet integrated with non-supplementary fired compressed air energy storage system,

J. Mod. Power Syst. Clean Energy. 4 (2016) 566–580. https://doi.org/10.1007/s40565-016-0241-4.

[81] Y. Li, J. Wang, Y. Han, Q. Zhao, X. Fang, Z. Cao, Robust and opportunistic scheduling of district integrated natural gas and power system with high wind power penetration considering demand flexibility and compressed air energy storage, J. Clean. Prod. 256 (2020) 120456. https://doi.org/10.1016/j.jclepro.2020.120456.

[82] B. Huang, X. Qiu, W. Wang, H. Li, W. Zhou, Overview of research situation and progress on compressed air energy storage technology, IOP Conf. Ser. Earth Environ. Sci. 295 (2019). https://doi.org/10.1088/1755-1315/295/2/012020.

[83] X. Luo, J. Wang, M. Dooner, J. Clarke, C. Krupke, Overview of current development in compressed air energy storage technology, Energy Procedia. 62 (2014) 603–611. https://doi.org/10.1016/j.egypro.2014.12.423.

[84] G. Dib, P. Haberschill, R. Rullière, Q. Perroit, S. Davies, R. Revellin, Thermodynamic simulation of a micro advanced adiabatic compressed air energy storage for building application, Appl. Energy. 260 (2020) 114248. https://doi.org/10.1016/j.apenergy.2019.114248.

[85] Z. Wang, D.S.K. Ting, R. Carriveau, W. Xiong, Z. Wang, Design and thermodynamic analysis of a multi-level underwater compressed air energy storage system, J. Energy Storage. 5 (2016) 203–211. https://doi.org/10.1016/j.est.2016.01.002.

[86] O.O. Callaghan, P. Donnellan, Liquid air energy storage systems : A review, Renew. Sustain. Energy Rev. 146 (2021) 111113. https://doi.org/10.1016/j.rser.2021.111113.

[87] M.H. Nabat, S. Sharifi, A.R. Razmi, Thermodynamic and economic analyses of a novel liquid air energy storage (LAES) coupled with thermoelectric generator and Kalina cycle, J. Energy Storage. 45 (2022) 103711. https://doi.org/10.1016/j.est.2021.103711.

[88] S. Bashiri Mousavi, M.H. Nabat, A.R. Razmi, P. Ahmadi, A comprehensive study and multi-criteria optimization of a novel sub-critical liquid air energy storage (SC-LAES), Energy Convers. Manag. 258 (2022) 115549. https://doi.org/10.1016/j.enconman.2022.115549.

[89] A.J. Pimm, S.D. Garvey, M. de Jong, Design and testing of Energy Bags for underwater compressed air energy storage, Energy. 66 (2014) 496–508. https://doi.org/10.1016/j.energy.2013.12.010.

[90] S. Nojavan, A. Najafi-Ghalelou, M. Majidi, K. Zare, Optimal bidding and offering strategies of merchant compressed air energy storage in deregulated electricity market using robust optimization approach, Energy. 142 (2018) 250–257. https://doi.org/10.1016/j.energy.2017.10.028.

[91] S. Shafiee, H. Zareipour, A.M. Knight, N. Amjady, B. Mohammadi-Ivatloo, Risk-Constrained Bidding and Offering Strategy for a Merchant Compressed Air Energy Storage Plant, IEEE Trans. Power Syst. 32 (2017) 946–957. https://doi.org/10.1109/TPWRS.2016.2565467.

[92] J. Zhang, S. Zhou, S. Li, W. Song, Z. Feng, Performance analysis of diabatic compressed air energy storage (D-CAES) system, Energy Procedia. 158 (2019) 4369–4374. https://doi.org/10.1016/j.egypro.2019.01.782.

[93] G. Venkataramani, V. Ramalingam, Performance analysis of a small capacity compressed air energy storage system for renewable energy generation using TRNSYS, J. Renew. Sustain. Energy. 9 (2017). https://doi.org/10.1063/1.5000287.

[94] G. Venkataramani, V. Ramalingam, K. Viswanathan, Harnessing Free Energy From Nature For Efficient Operation of Compressed Air Energy Storage System and Unlocking the Potential of Renewable Power Generation, (2018) 1–11. https://doi.org/10.1038/s41598-018-28025-5.

[95] H. Chen, Y. Peng, Y. Wang, J. Zhang, Thermodynamic analysis of an open type isothermal compressed air energy storage system based on hydraulic pump / turbine and spray cooling, Energy Convers. Manag. 204 (2020) 112293. https://doi.org/10.1016/j.enconman.2019.112293.

[96] J.L. Liu, J.H. Wang, A comparative research of two adiabatic compressed air energy storage systems, Energy Convers. Manag. 108 (2016) 566–578. https://doi.org/10.1016/j.enconman.2015.11.049.

[97] L. Szablowski, P. Krawczyk, K. Badyda, S. Karellas, E. Kakaras, W. Bujalski, Energy and exergy analysis of adiabatic compressed air energy storage system, Energy. 138 (2017) 12–18. https://doi.org/10.1016/j.energy.2017.07.055.

[98] F. Jabari, S. Nojavan, B. Mohammadi Ivatloo, Designing and optimizing a novel advanced adiabatic compressed air energy storage and air source heat pump based μ-Combined Cooling, heating and power system, Energy. 116 (2016) 64–77. https://doi.org/10.1016/j.energy.2016.09.106.

[99] N. Hartmann, O. Vöhringer, C. Kruck, L. Eltrop, Simulation and analysis of different adiabatic Compressed Air Energy Storage plant configurations, Appl. Energy. 93 (2012) 541–548. https://doi.org/10.1016/j.apenergy.2011.12.007.

[100] T. Ren, W. Xu, M. Cai, X. Wang, M. Li, Experiments on Air Compression with an Isothermal Piston for Energy Storage, (2019). https://doi.org/10.3390/en12193730.

[101] V.C. Patil, P. Acharya, P.I. Ro, Experimental investigation of water spray injection in liquid piston for near- isothermal compression, Appl. Energy. (2019) 114182. https://doi.org/10.1016/j.apenergy.2019.114182.

[102] P.Y. Li, DSCC2015-9957 COMBINED OPTIMAL DESIGN AND CONTROL OF A NEAR ISOTHERMAL LIQUID PISTON AIR COMPRESSOR / EXPANDER FOR A COMPRESSED AIR ENERGY, (2015).

[103] A. Odukomaiya, E. Kokou, Z. Hussein, A. Abu-Heiba, S. Graham, A.M. Momen, Near-isothermal-isobaric compressed gas energy storage, J. Energy Storage. 12 (2017) 276–287. https://doi.org/10.1016/j.est.2017.05.014.

[104] M. Cheayb, M. Marin Gallego, M. Tazerout, S. Poncet, Modelling and experimental validation of a small-scale trigenerative compressed air energy storage system, Appl. Energy. 239 (2019) 1371–1384. https://doi.org/10.1016/j.apenergy.2019.01.222.

[105] R. Jiang, F.G.F. Qin, B. Chen, X. Yang, H. Yin, Y. Xu, Thermodynamic performance analysis, assessment and comparison of an advanced trigenerative compressed air energy storage system under different operation strategies, Energy. 186 (2019) 115862. https://doi.org/10.1016/j.energy.2019.115862.

[106] M. Cheayb, M. Marin Gallego, S. Poncet, M. Tazerout, Micro-scale trigenerative compressed air energy storage system: Modeling and parametric optimization study, J. Energy Storage. 26 (2019) 100944. https://doi.org/10.1016/j.est.2019.100944.

[107] A. Arabkoohsar, M. Dremark-Larsen, R. Lorentzen, G.B. Andresen, Subcooled compressed air energy storage system for coproduction of heat, cooling and electricity, Appl. Energy. 205 (2017) 602–614. https://doi.org/10.1016/j.apenergy.2017.08.006.

[108] S. Lv, W. He, A. Zhang, G. Li, B. Luo, X. Liu, Modelling and analysis of a novel compressed air energy storage system for trigeneration based on electrical energy peak load shifting, Energy Convers. Manag. 135 (2017) 394–401. https://doi.org/10.1016/j.enconman.2016.12.089.

[109] A.L. Facci, D. Sánchez, E. Jannelli, S. Ubertini, Trigenerative micro compressed air energy storage: Concept and thermodynamic assessment, Appl. Energy. 158 (2015) 243–254. https://doi.org/10.1016/j.apenergy.2015.08.026.

[110] J.L. Liu, J.H. Wang, Thermodynamic analysis of a novel tri-generation system based on compressed air energy storage and pneumatic motor, Energy. 91 (2015) 420–429. https://doi.org/10.1016/j.energy.2015.08.055.

[111] Y. Li, X. Wang, D. Li, Y. Ding, A trigeneration system based on compressed air and thermal energy storage, Appl. Energy. 99 (2012) 316–323. https://doi.org/10.1016/j.apenergy.2012.04.048.

[112] X.D. Xue, S.X. Wang, X.L. Zhang, C. Cui, L.B. Chen, Y. Zhou, J.J. Wang, Thermodynamic analysis of a novel liquid air energy storage system, Phys. Procedia. 67 (2015) 733–738. https://doi.org/10.1016/j.phpro.2015.06.124.

[113] R. Morgan, S. Nelmes, E. Gibson, G. Brett, Liquid air energy storage – Analysis and first results from a pilot scale demonstration plant q, Appl. Energy. 137 (2015) 845–853. https://doi.org/10.1016/j.apenergy.2014.07.109.

[114] B. Ameel, C.T. Joen, K. De Kerpel, P. De Jaeger, H. Huisseune, M. Van Belleghem, M. De Paepe, Thermodynamic analysis of energy storage with a liquid air Rankine cycle, Appl. Therm. Eng. 52 (2013) 130–140. https://doi.org/10.1016/j.applthermaleng.2012.11.037.

[115] H. Guo, Y. Xu, H. Chen, C. Guo, W. Qin, Thermodynamic analytical solution and exergy analysis for supercritical compressed air energy storage system, Appl. Energy. 199 (2017) 96–106. https://doi.org/10.1016/j.apenergy.2017.04.068.

[116] H. Guo, Y. Xu, X. Zhang, Q. Liang, S. Wang, H. Chen, Dynamic characteristics and control of supercritical compressed air energy storage systems, Appl. Energy. 283 (2021) 116294. https://doi.org/10.1016/j.apenergy.2020.116294.

[117] Z. Liao, H. Zhong, C. Xu, X. Ju, F. Ye, X. Du, Investigation of a packed bed cold thermal storage in supercritical compressed air energy storage systems, Appl. Energy. 269 (2020) 115132. https://doi.org/10.1016/j.apenergy.2020.115132.

[118] M. Jae, T. Seop, Feasibility study on the in fl uence of steam injection in the compressed air energy storage system, Energy. 141 (2017) 239–249. https://doi.org/10.1016/j.energy.2017.09.078.

[119] A. Pimm, S.D. Garvey, Underwater Compressed Air Energy Storage, Elsevier Inc., 2016. https://doi.org/10.1016/B978-0-12-803440-8/00007-5.

[120] S.D. Lim, A.P. Mazzoleni, J. Park, P.I. Ro, B. Quinlan, N. Carolina, Conceptual design of ocean compressed air energy storage system, (2012).

[121] B. Cheung, N. Cao, R. Carriveau, D.S. Ting, B. Cheung, N. Cao, R. Carriveau, D.S. Ting, B. Cheung, N. Cao, R. Carriveau, D.S. Ting, Distensible air accumulators as a means of adiabatic underwater compressed air energy storage Distensible air accumulators as a means of adiabatic underwater compressed air energy storage, 7233 (2012). https://doi.org/10.1080/00207233.2012.699360.

[122] Y.M. Kim, D.G. Shin, D. Favrat, Operating characteristics of constant-pressure compressed air energy storage (CAES) system combined with pumped hydro storage based on energy and exergy analysis, Energy. 36 (2011) 6220–6233. https://doi.org/10.1016/j.energy.2011.07.040.

[123] Z. Wang, W. Xiong, H. Wang, A review on underwater compressed air energy storage, Energy Storage Sci. Technol. 4 (2015) 282–296.

[124] A. Pimm, S. Garvey, Analysis of flexible fabric structures for large-scale subsea compressed air energy storage, J. Phys. Conf. Ser. 181 (2009). https://doi.org/10.1088/1742-6596/181/1/012049.

[125] D. Fiaschi, G. Manfrida, R. Secchi, D. Tempesti, A versatile system for offshore energy conversion including diversified storage, Energy. 48 (2012) 566–576. https://doi.org/10.1016/j.energy.2012.10.006.

[126] A.H. Slocum, G.E. Fennell, G. Dündar, B.G. Hodder, J.D.C. Meredith, M.A. Sager, Ocean renewable energy storage (ORES) system: Analysis of an undersea energy storage concept, Proc. IEEE. 101 (2013) 906–924. https://doi.org/10.1109/JPROC.2013.2242411.

[127] A. Hutagalung, STUDY ON UNDERGROUND GAS STORAGE IN EUROPE AND CENTRAL ASIA, Angew. Chemie Int. Ed. 6(11), 951–952. (1967) 5–24.

[128] M. Lutyński, An overview of potential benefits and limitations of Compressed Air Energy Storage in abandoned coal mines, IOP Conf. Ser. Mater. Sci. Eng. 268 (2017).

https://doi.org/10.1088/1757-899X/268/1/012006.

[129] X. Xu, W. Hu, D. Cao, Q. Huang, W. Liu, Z. Liu, Z. Chen, H. Lund, Designing a standalone wind-diesel-CAES hybrid energy system by using a scenario-based bi-level programming method, Energy Convers. Manag. 211 (2020) 112759. https://doi.org/10.1016/j.enconman.2020.112759.

[130] J. Zhang, K.J. Li, M. Wang, W.J. Lee, H. Gao, C. Zhang, K. Li, A Bi-Level Program for the Planning of an Islanded Microgrid Including CAES, IEEE Trans. Ind. Appl. 52 (2016) 2768–2777. https://doi.org/10.1109/TIA.2016.2539246.

[131] S. Sadeghi, I.B. Askari, Prefeasibility techno-economic assessment of a hybrid power plant with photovoltaic, fuel cell and Compressed Air Energy Storage (CAES), Energy. 168 (2019) 409–424. https://doi.org/10.1016/j.energy.2018.11.108.

[132] S. Simpore, F. Garde, M. David, O. Marc, J. Castaing-Lasvignottes, Sensitivity analysis and optimization of a compressed air energy storage (CAES) system powered by a photovoltaic plant to supply a building, Procedia Manuf. 35 (2019) 137–142. https://doi.org/10.1016/j.promfg.2019.05.016.

[133] D. Wolf, M. Budt, LTA-CAES - A low-temperature approach to adiabatic compressed air energy storage, Appl. Energy. 125 (2014) 158–164. https://doi.org/10.1016/j.apenergy.2014.03.013.

[134] S. Houssainy, M. Janbozorgi, P. Ip, P. Kavehpour, Thermodynamic analysis of a high temperature hybrid compressed air energy storage (HTH-CAES) system, Renew. Energy. 115 (2018) 1043–1054. https://doi.org/10.1016/j.renene.2017.09.038.

[135] B. Llamas, M.F. Ortega, G. Barthelemy, I. De Godos, F.G. Acién, Development of an e ffi cient and sustainable energy storage system by hybridization of compressed air and biogas technologies (BIO-CAES), Energy Convers. Manag. 210 (2020) 112695. https://doi.org/10.1016/j.enconman.2020.112695.

[136] M. Soltani, M.H. Nabat, A.R. Razmi, M.B. Dusseault, J. Nathwani, A comparative study between ORC and Kalina based waste heat recovery cycles applied to a green compressed air energy storage (CAES) system, Energy Convers. Manag. 222 (2020) 113203. https://doi.org/10.1016/j.enconman.2020.113203.

[137] A. Razmi, M. Soltani, M. Torabi, 19)mirreza, M. Soltani, M. Torabi, Investigation of an efficient and environmentally-friendly CCHP system based on CAES, ORC and compression-absorption refrigeration cycle: Energy and exergy analysis, Energy Convers. Manag. 195 (2019) 1199–1211. https://doi.org/10.1016/j.enconman.2019.05.065.

[138] A. Razmi, M. Soltani, C. Aghanajafi, M. Torabi, Thermodynamic and economic investigation of a novel integration of the absorption-recompression refrigeration system with compressed air energy storage (CAES), Energy Convers. Manag. 187 (2019) 262–273. https://doi.org/10.1016/j.enconman.2019.03.010.

[139] A. Razmi, M. Soltani, M. Tayefeh, M. Torabi, M.B. Dusseault, Thermodynamic analysis

of compressed air energy storage (CAES) hybridized with a multi-e ff ect desalination (MED) system, Energy Convers. Manag. 199 (2019) 112047. https://doi.org/10.1016/j.enconman.2019.112047.

[140] M. Zeynalian, A.H. Hajialirezaei, A.R. Razmi, M. Torabi, Carbon Dioxide Capture from Compressed Air Energy Storage System, Appl. Therm. Eng. 178 (2020) 115593. https://doi.org/10.1016/j.applthermaleng.2020.115593.

[141] M. Javidmehr, F. Joda, A. Mohammadi, Thermodynamic and economic analyses and optimization of a multi- generation system composed by a compressed air storage , solar dish collector , micro gas turbine , organic Rankine cycle , and desalination system, Energy Convers. Manag. 168 (2018) 467–481. https://doi.org/10.1016/j.enconman.2018.05.019.

[142] S. Mojtaba, S. Bashiri, A. Reza, P. Ahmadi, A comprehensive techno-economic analysis and multi-criteria optimization of a compressed air energy storage (CAES) hybridized with solar and desalination units, Energy Convers. Manag. 236 (2021) 114053. https://doi.org/10.1016/j.enconman.2021.114053.

[143] X. Xue, J. Li, J. Liu, Y. Wu, H. Chen, G. Xu, T. Liu, Performance evaluation of a conceptual compressed air energy storage system coupled with a biomass integrated gasification combined cycle, Energy. 247 (2022) 123442. https://doi.org/10.1016/j.energy.2022.123442.

[144] A. Reza, H. Heydari, A. Pourahmadiyan, M. Torabi, A.R. Razmi, H. Heydari Afshar, A. Pourahmadiyan, M. Torabi, Investigation of a combined heat and power (CHP) system based on biomass and compressed air energy storage (CAES), Sustain. Energy Technol. Assessments. 46 (2021) 101253. https://doi.org/10.1016/j.seta.2021.101253.

[145] R. Roushenas, A.R. Razmi, M. Soltani, M. Torabi, M.B. Dusseault, J. Nathwani, Thermo-environmental analysis of a novel cogeneration system based on solid oxide fuel cell (SOFC) and compressed air energy storage (CAES) coupled with turbocharger, Appl. Therm. Eng. 181 (2020) 115978. https://doi.org/10.1016/j.applthermaleng.2020.115978.

[146] B. Ghorbani, M. Mehrpooya, A. Ardehali, Energy and exergy analysis of wind farm integrated with compressed air energy storage using multi-stage phase change material, J. Clean. Prod. 259 (2020) 120906. https://doi.org/10.1016/j.jclepro.2020.120906.

[147] F. Musharavati, S. Khanmohammadi, M. Rahmani, S. Khanmohammadi, Thermodynamic modeling and comparative analysis of a compressed air energy storage system boosted with thermoelectric unit, J. Energy Storage. 33 (2021) 101888. https://doi.org/10.1016/j.est.2020.101888.

[148] S.B. Mousavi, P. Ahmadi, A. Pourahmadiyan, P. Hanafizadeh, A comprehensive techno-economic assessment of a novel compressed air energy storage (CAES) integrated with geothermal and solar energy, Sustain. Energy Technol. Assessments. 47 (2021) 101418. https://doi.org/10.1016/j.seta.2021.101418.

[149] H. Fu, Q. He, J. Song, X. Shi, Y. Hao, D. Du, W. Liu, Thermodynamic of a novel

advanced adiabatic compressed air energy storage system with variable pressure ratio coupled organic rankine cycle, Energy. 227 (2021) 120411. https://doi.org/10.1016/j.energy.2021.120411.

[150] A. Karapekmez, I. Dincer, N. Javani, Development of a new integrated energy system with compressed air and heat storage options, J. Energy Storage. 32 (2020) 101955. https://doi.org/10.1016/j.est.2020.101955.

[151] C. Diyoke, C. Wu, Thermodynamic analysis of hybrid adiabatic compressed air energy storage system and biomass gasification storage (A-CAES + BMGS) power system, Fuel. 271 (2020) 117572. https://doi.org/10.1016/j.fuel.2020.117572.

[152] X. Zhang, R. Zeng, Q. Deng, X. Gu, H. Liu, Y. He, K. Mu, X. Liu, H. Tian, H. Li, Energy, exergy and economic analysis of biomass and geothermal energy based CCHP system integrated with compressed air energy storage (CAES), Energy Convers. Manag. 199 (2019) 111953. https://doi.org/10.1016/j.enconman.2019.111953.

[153] A. Sadreddini, M. Fani, M. Ashjari Aghdam, A. Mohammadi, Exergy analysis and optimization of a CCHP system composed of compressed air energy storage system and ORC cycle, Energy Convers. Manag. 157 (2018) 111–122. https://doi.org/10.1016/j.enconman.2017.11.055.

[154] A.R. Razmi, M. Janbaz, Exergoeconomic assessment with reliability consideration of a green cogeneration system based on compressed air energy storage (CAES), Energy Convers. Manag. 204 (2020) 112320. https://doi.org/10.1016/j.enconman.2019.112320.

[155] F. Lashgari, S.M. Babaei, M.Z. Pedram, A. Arabkoohsar, Comprehensive analysis of a novel integration of a biomass-driven combined heat and power plant with a compressed air energy storage (CAES), Energy Convers. Manag. 255 (2022) 115333. https://doi.org/10.1016/j.enconman.2022.115333.

[156] C. Diyoke, M. Aneke, M. Wang, C. Wu, Techno-economic analysis of wind power integrated with both compressed air energy storage (CAES) and biomass gasification energy storage (BGES) for power generation, RSC Adv. 8 (2018) 22004–22022. https://doi.org/10.1039/c8ra03128b.

[157] A. Mohammadi, M. Mehrpooya, Exergy analysis and optimization of an integrated micro gas turbine , compressed air energy storage and solar dish collector process, J. Clean. Prod. 139 (2016) 372–383. https://doi.org/10.1016/j.jclepro.2016.08.057.

[158] X. Wang, C. Yang, M. Huang, X. Ma, Multi-objective optimization of a gas turbine-based CCHP combined with solar and compressed air energy storage system, Energy Convers. Manag. 164 (2018) 93–101. https://doi.org/10.1016/j.enconman.2018.02.081.

[159] L. Zhong, E. Yao, Y. Hu, C. Zhao, H. Zou, G. Xi, Thermo-economic analysis of a novel system integrating compressed air and thermochemical energy storage with solid oxide fuel cell-gas turbine, Energy Convers. Manag. 252 (2022) 115114. https://doi.org/10.1016/j.enconman.2021.115114.

[160] T. Zhang, H. Zhao, H. Du, H. Wang, Thermodynamic performance study of a novel

cogeneration system combining solid oxide fuel cell, gas turbine, organic Rankine cycle with compressed air energy storage, Energy Convers. Manag. 249 (2021) 114837. https://doi.org/10.1016/j.enconman.2021.114837.

[161] R. Roushenas, E. Zarei, M. Torabi, A novel trigeneration system based on solid oxide fuel cell-gas turbine integrated with compressed air and thermal energy storage concepts: Energy, exergy, and life cycle approaches, Sustain. Cities Soc. 66 (2021) 102667. https://doi.org/10.1016/j.scs.2020.102667.

[162] P. Jienkulsawad, Y. Patcharavorachot, Y.S. Chen, A. Arpornwichanop, Energy and exergy analyses of a hybrid system containing solid oxide and molten carbonate fuel cells, a gas turbine, and a compressed air energy storage unit, Int. J. Hydrogen Energy. 46 (2021) 34883–34895. https://doi.org/10.1016/j.ijhydene.2021.08.038.

[163] P. Jienkulsawad, D. Saebea, Y. Patcharavorachot, A. Arpornwichanop, Performance assessment of a hybrid solid oxide and molten carbonate fuel cell system with compressed air energy storage under different power demands, Int. J. Hydrogen Energy. 45 (2020) 835–848. https://doi.org/10.1016/j.ijhydene.2019.09.245.

[164] S. Khanmohammadi, M. Rahmani, F. Musharavati, S. Khanmohammadi, Q.V. Bach, Thermal modeling and triple objective optimization of a new compressed air energy storage system integrated with Rankine cycle, PEM fuel cell, and thermoelectric unit, Sustain. Energy Technol. Assessments. 43 (2021) 100810. https://doi.org/10.1016/j.seta.2020.100810.

[165] E. Hammann, R. Madlener, C. Hilgers, Economic Feasibility of a Compressed Air Energy Storage System under Market Uncertainty: A Real Options Approach, Energy Procedia. 105 (2017) 3798–3805. https://doi.org/10.1016/j.egypro.2017.03.888.

[166] C. Mohamad, M.G. Mylène, T. Mohand, P. Sébastien, A techno-economic analysis of small-scale Trigenerative Compressed Air Energy Storage system, Energy. (2021) 121842. https://doi.org/10.1016/j.energy.2021.121842.

[167] R. Li, H. Zhang, H. Chen, Y. Zhang, Z. Li, J. Zhao, X. Wang, H. Wang, Hybrid techno-economic and environmental assessment of adiabatic compressed air energy storage system in China-Situation, Appl. Therm. Eng. 186 (2021) 116443. https://doi.org/10.1016/j.applthermaleng.2020.116443.

[168] Y. Zhang, Y. Xu, X. Zhou, H. Guo, X. Zhang, H. Chen, Compressed air energy storage system with variable configuration for wind power generation, Energy Procedia. 142 (2017) 3356–3362. https://doi.org/10.1016/j.egypro.2017.12.470.

[169] A. Setiawan, A. Priyadi, M. Pujiantara, M.H. Purnomo, Sizing compressed-air energy storage tanks for solar home systems, 2015 IEEE Int. Conf. Comput. Intell. Virtual Environ. Meas. Syst. Appl. CIVEMSA 2015. (2015) 1–4. https://doi.org/10.1109/CIVEMSA.2015.7158620.

[170] E. Jannelli, M. Minutillo, A. Lubrano Lavadera, G. Falcucci, A small-scale CAES (compressed air energy storage) system for stand-alone renewable energy power plant for a radio base station: A sizing-design methodology, Energy. 78 (2014) 313–322.

https://doi.org/10.1016/j.energy.2014.10.016.

[171] M. Minutillo, A. Lubrano Lavadera, E. Jannelli, Assessment of design and operating parameters for a small compressed air energy storage system integrated with a stand-alone renewable power plant, J. Energy Storage. 4 (2015) 135–1 44. https://doi.org/10.1016/j.est.2015.10.002.

[172] S.Y. Wang, J.L. Yu, Optimal sizing of the CAES system in a power system with high wind power penetration, Int. J. Electr. Power Energy Syst. 37 (2012) 117–125. https://doi.org/10.1016/j.ijepes.2011.12.015.

[173] C.C. Anierobi, K. Bhattacharya, C.A. Canizares, Behind-the-meter compressed air energy storage feasibility and applications, Electr. Power Syst. Res. 189 (2020) 106630. https://doi.org/10.1016/j.epsr.2020.106630.

[174] A. Daneshvar Garmroodi, F. Nasiri, F. Haghighat, Optimal dispatch of an energy hub with compressed air energy storage: A safe reinforcement learning approach, J. Energy Storage. (2022) 106147. https://doi.org/10.1016/j.est.2022.106147.

[175] G. Aruta, F. Ascione, N. Bianco, G.M. Mauro, Optimization of a diabatic compressed air energy storage coupled with photovoltaics for buildings: CO2-eq emissions vs payback time, Energy Reports. 8 (2022) 12686–12698. https://doi.org/10.1016/j.egyr.2022.09.112.

[176] P. Lv, F. Zlwk, R. Vlplodu, F. Khdw, D.Q.G. Srzhu, J. V Vwhp, F. Ri, $ %L Ohyho 3Urjudp Iru Wkh 3Odqqlqj Ri Dq ,Vodqghg 0Lfurjulg ,Qfoxglqj &$(6, (2016) 1–8.

[177] Y. Yan, C. Zhang, K. Li, Z. Wang, An integrated design for hybrid combined cooling, heating and power system with compressed air energy storage, n.d. https://doi.org/10.1016/j.apenergy.2017.07.005.

[178] M. Adib, F. Nasiri, F. Haghighat, Integrating wind energy and compressed air energy storage for remote communities : A bi-level programming approach, J. Energy Storage. 72 (2023) 108496. https://doi.org/10.1016/j.est.2023.108496.

[179] Y. Yan, C. Zhang, K. Li, Z. Wang, An integrated design for hybrid combined cooling, heating and power system with compressed air energy storage, Appl. Energy. 210 (2018) 1151–1166. https://doi.org/10.1016/j.apenergy.2017.07.005.

[180] H. Ibrahim, R. Younès, A. Ilinca, M. Dimitrova, J. Perron, Study and design of a hybrid wind-diesel-compressed air energy storage system for remote areas, Appl. Energy. 87 (2010) 1749–1762. https://doi.org/10.1016/j.apenergy.2009.10.017.

[181] H. Ibrahim, K. Belmokhtar, M. Ghandour, Investigation of usage of compressed air energy storage for power generation system improving - Application in a microgrid integrating wind energy, Energy Procedia. 73 (2015) 305–316. https://doi.org/10.1016/j.egypro.2015.07.694.

[182] H. Sun, X. Luo, J. Wang, Feasibility study of a hybrid wind turbine system - Integration with compressed air energy storage, Appl. Energy. 137 (2015) 617–628.

https://doi.org/10.1016/j.apenergy.2014.06.083.

[183] R. Madlener, J. Latz, Economics of centralized and decentralized compressed air energy storage for enhanced grid integration of wind power, Appl. Energy. 101 (2013) 299–309. https://doi.org/10.1016/j.apenergy.2011.09.033.

[184] I. Arsie, V. Marano, G. Rizzo, M. Moran, Integration of wind turbines with Compressed Air Energy Storage, AIP Conf. Proc. 1159 (2009) 11–18. https://doi.org/10.1063/1.3223915.

[185] Y. Huang, A. Rolfe, I. Vorushylo, P. Keatley, R. Byrne, P. MacArtain, D. Flynn, and N. Hewitt, Integration of compressed air energy storage with wind generation into the electricity grid, (2018).

[186] A.R. Razmi, M. Soltani, A. Ardehali, K. Gharali, M.B. Dusseault, J. Nathwani, Design, thermodynamic, and wind assessments of a compressed air energy storage (CAES) integrated with two adjacent wind farms: A case study at Abhar and Kahak sites, Iran, Energy. 221 (2021) 119902. https://doi.org/10.1016/j.energy.2021.119902.

[187] J. Chen, W. Liu, D. Jiang, J. Zhang, S. Ren, L. Li, X. Li, X. Shi, Preliminary investigation on the feasibility of a clean CAES system coupled with wind and solar energy in China, Energy. 127 (2017) 462–478. https://doi.org/10.1016/j.energy.2017.03.088.

[188] W. He, M. Dooner, M. King, D. Li, S. Guo, J. Wang, Techno-economic analysis of bulk-scale compressed air energy storage in power system decarbonisation, Appl. Energy. 282 (2021) 116097. https://doi.org/10.1016/j.apenergy.2020.116097.

[189] S. Simpore, F. Garde, M. David, O.M. Marc, J. Castaing-Lasvignottes, Design and Dynamic Simulation of a Compressed Air Energy Storage System (CAES) Coupled with a Building, an Electric Grid and Photovoltaic Power Plant, CLIMA 2016, 12th REHVA World Congr. (2016). https://hal.archives-ouvertes.fr/hal-01467204.

[190] R. Cazzaniga, M. Cicu, M. Rosa-Clot, P. Rosa-Clot, G.M. Tina, C. Ventura, Compressed air energy storage integrated with floating photovoltaic plant, J. Energy Storage. 13 (2017) 48–57. https://doi.org/10.1016/j.est.2017.06.006.

[191] P.M. Congedo, C. Baglivo, L. Carrieri, Application of an unconventional thermal and mechanical energy storage coupled with the air conditioning and domestic hot water systems of a residential building, Energy Build. 224 (2020) 110234. https://doi.org/10.1016/j.enbuild.2020.110234.

[192] A. Tallini, A. Vallati, L. Cedola, Applications of micro-CAES systems: Energy and economic analysis, Energy Procedia. 82 (2015) 797–804. https://doi.org/10.1016/j.egypro.2015.11.815.

[193] L. Bagherzadeh, H. Shahinzadeh, H. Shayeghi, G.B. Gharehpetian, A short-term energy management of microgrids considering renewable energy resources, micro-compressed air energy storage and DRPs, Int. J. Renew. Energy Res. 9 (2019) 1712–1723.

[194] M. Jalili, M. Sedighizadeh, A.S. Fini, Stochastic optimal operation of a microgrid based

on energy hub including a solar-powered compressed air energy storage system and an ice storage conditioner, J. Energy Storage. 33 (2021) 102089. https://doi.org/10.1016/j.est.2020.102089.

[195] V. Marano, G. Rizzo, F.A. Tiano, Application of dynamic programming to the optimal management of a hybrid power plant with wind turbines, photovoltaic panels and compressed air energy storage, Appl. Energy. 97 (2012) 849–859. https://doi.org/10.1016/j.apenergy.2011.12.086.

[196] J. Gao, J.J. Chen, B.X. Qi, Y.L. Zhao, K. Peng, X.H. Zhang, A cost-effective two-stage optimization model for microgrid planning and scheduling with compressed air energy storage and preventive maintenance, Int. J. Electr. Power Energy Syst. 125 (2021). https://doi.org/10.1016/j.ijepes.2020.106547.

[197] S. Haghifam, A. Najafi-Ghalelou, K. Zare, M. Shafie-khah, A. Arefi, Stochastic bi-level coordination of active distribution network and renewable-based microgrid considering eco-friendly Compressed Air Energy Storage system and Intelligent Parking Lot, J. Clean. Prod. 278 (2021). https://doi.org/10.1016/j.jclepro.2020.122808.

[198] H. Daneshi, A.K. Srivastava, Security-constrained unit commitment with wind generation and compressed air energy storage, IET Gener. Transm. Distrib. 6 (2012) 167–175. https://doi.org/10.1049/iet-gtd.2010.0763.

[199] M. Ghaljehei, A. Ahmadian, M.A. Golkar, T. Amraee, A. Elkamel, Stochastic SCUC considering compressed air energy storage and wind power generation: A techno-economic approach with static voltage stability analysis, Int. J. Electr. Power Energy Syst. 100 (2018) 489–507. https://doi.org/10.1016/j.ijepes.2018.02.046.

[200] P.P. Gupta, P. Jain, K.C. Sharma, R. Bhakar, Stochastic scheduling of compressed air energy storage in DC SCUC framework for high wind penetration, IET Gener. Transm. Distrib. 13 (2019) 2747–2760. https://doi.org/10.1049/iet-gtd.2019.0330.

[201] M. Sedighizadeh, M. Esmaili, S.M. Mousavi-Taghiabadi, Optimal joint energy and reserve scheduling considering frequency dynamics, compressed air energy storage, and wind turbines in an electrical power system, J. Energy Storage. 23 (2019) 220–233. https://doi.org/10.1016/j.est.2019.03.019.

[202] Y. Li, S. Miao, S. Zhang, B. Yin, X. Luo, M. Dooner, J. Wang, A reserve capacity model of AA-CAES for power system optimal joint energy and reserve scheduling, Int. J. Electr. Power Energy Syst. 104 (2019) 279–290. https://doi.org/10.1016/j.ijepes.2018.07.012.

[203] W. Cai, R. Mohammaditab, G. Fathi, K. Wakil, A.G. Ebadi, N. Ghadimi, Optimal bidding and offering strategies of compressed air energy storage: A hybrid robust-stochastic approach, Renew. Energy. 143 (2019) 1–8. https://doi.org/10.1016/j.renene.2019.05.008.

[204] D. Xie, Q. Guo, X. Liang, K. Jermsittiparsert, Risk-based bidding and offering strategies of the compressed air energy storage using downside risk constraints, J. Clean. Prod. 302 (2021) 127032. https://doi.org/10.1016/j.jclepro.2021.127032.

[205] E. Akbari, R.A. Hooshmand, M. Gholipour, M. Parastegari, Stochastic programming-based optimal bidding of compressed air energy storage with wind and thermal generation units in energy and reserve markets, Energy. 171 (2019) 535–546. https://doi.org/10.1016/j.energy.2019.01.014.

[206] S. Shafiee, H. Zareipour, A.M. Knight, Developing Bidding and Offering Curves of a Price-Maker Energy Storage Facility Based on Robust Optimization, IEEE Trans. Smart Grid. 10 (2019) 650–660. https://doi.org/10.1109/TSG.2017.2749437.

[207] S. Nojavan, A. Akbari-Dibavar, K. Zare, Optimal energy management of compressed air energy storage in day-ahead and real-time energy markets, IET Gener. Transm. Distrib. 13 (2019) 3673–3679. https://doi.org/10.1049/iet-gtd.2018.7022.

[208] S. Narayan Dash, R. Krushna Padhi, T. Dora, A. Surendar, K. Cristan, A robust optimization method for bidding strategy by considering the compressed air energy storage, Sustain. Cities Soc. 48 (2019) 101564. https://doi.org/10.1016/j.scs.2019.101564.

[209] E. Drury, P. Denholm, R. Sioshansi, The value of compressed air energy storage in energy and reserve markets, Energy. 36 (2011) 4959–4973. https://doi.org/10.1016/j.energy.2011.05.041.

[210] S. Shafiee, H. Zareipour, A.M. Knight, Considering Thermodynamic Characteristics of a CAES Facility in Self-Scheduling in Energy and Reserve Markets, IEEE Trans. Smart Grid. 9 (2018) 3476–3485. https://doi.org/10.1109/TSG.2016.2633280.

[211] R. Khatami, K. Oikonomou, M. Parvania, Optimal Participation of Compressed Air Energy Storage in Energy and Ancillary Service Markets, Proc. IEEE Power Eng. Soc. Transm. Distrib. Conf. 2018-April (2018) 1–5. https://doi.org/10.1109/TDC.2018.8440450.

[212] A. Attarha, N. Amjady, S. Dehghan, B. Vatani, Adaptive Robust Self-Scheduling for a Wind Producer with Compressed Air Energy Storage, IEEE Trans. Sustain. Energy. 9 (2018) 1659–1671. https://doi.org/10.1109/TSTE.2018.2806444.

[213] Y. Li, S. Miao, X. Luo, J. Wang, Optimization model for the power system scheduling with wind generation and compressed air energy storage combination, 2016 22nd Int. Conf. Autom. Comput. ICAC 2016 Tackling New Challenges Autom. Comput. 973 (2016) 300–305. https://doi.org/10.1109/IConAC.2016.7604936.

[214] J. Moradi, H. Shahinzadeh, A. Khandan, M. Moazzami, A profitability investigation into the collaborative operation of wind and underwater compressed air energy storage units in the spot market, Energy. 141 (2017) 1779–1794. https://doi.org/10.1016/j.energy.2017.11.088.

[215] Y. Li, S. Miao, B. Yin, J. Liu, W. Yang, S. Zhang, Research on optimal self-scheduling horizon for the wind power and large-scale CAES combined system, IET Gener. Transm. Distrib. 13 (2019) 5197–5206. https://doi.org/10.1049/iet-gtd.2018.7081.

[216] M. Abbaspour, M. Satkin, B. Mohammadi-Ivatloo, F. Hoseinzadeh Lotfi, Y. Noorollahi,

Optimal operation scheduling of wind power integrated with compressed air energy storage (CAES), Renew. Energy. 51 (2013) 53–59. https://doi.org/10.1016/j.renene.2012.09.007.

[217] A.N. Ghalelou, A.P. Fakhri, S. Nojavan, M. Majidi, H. Hatami, A stochastic self-scheduling program for compressed air energy storage (CAES) of renewable energy sources (RESs) based on a demand response mechanism, Energy Convers. Manag. 120 (2016) 388–396. https://doi.org/10.1016/j.enconman.2016.04.082.

[218] P. Aliasghari, M. Zamani-Gargari, B. Mohammadi-Ivatloo, Look-ahead risk-constrained scheduling of wind power integrated system with compressed air energy storage (CAES) plant, Energy. 160 (2018) 668–677. https://doi.org/10.1016/j.energy.2018.06.215.

[219] Y. Zhang, Y. Xu, H. Guo, X. Zhang, C. Guo, H. Chen, A hybrid energy storage system with optimized operating strategy for mitigating wind power fluctuations, Renew. Energy. 125 (2018) 121–132. https://doi.org/10.1016/j.renene.2018.02.058.

[220] S. Hajiaghasi, A. Salemnia, M. Hamzeh, Hybrid energy storage system for microgrids applications: A review, J. Energy Storage. 21 (2019) 543–570. https://doi.org/10.1016/j.est.2018.12.017.

[221] S. Wang, X. Zhang, L. Yang, Y. Zhou, J. Wang, Experimental study of compressed air energy storage system with thermal energy storage, Energy. 103 (2016) 182–191. https://doi.org/10.1016/j.energy.2016.02.125.

[222] X. Xu, W. Hu, D. Cao, Q. Huang, W. Liu, Z. Liu, Z. Chen, H. Lund, Designing a standalone wind−diesel−CAES hybrid energy system by using a scenario−based bi−level programming method, Energy Convers. Manag. 211 (2020) 112759. https://doi.org/10.1016/j.enconman.2020.112759.

[223] Y. Li, S. Miao, B. Yin, J. Han, S. Zhang, J. Wang, X. Luo, Combined Heat and Power dispatch considering Advanced Adiabatic Compressed Air Energy Storage for wind power accommodation, Energy Convers. Manag. 200 (2019) 112091. https://doi.org/10.1016/j.enconman.2019.112091.

[224] X. Luo, J. Wang, C. Krupke, Y. Wang, Y. Sheng, J. Li, Y. Xu, D. Wang, S. Miao, H. Chen, Modelling study, efficiency analysis and optimisation of large-scale Adiabatic Compressed Air Energy Storage systems with low-temperature thermal storage, Appl. Energy. 162 (2016) 589–600. https://doi.org/10.1016/j.apenergy.2015.10.091.

[225] T. Ma, Y. Zhang, W. Gu, G. Xiao, H. Yang, S. Wang, Strategy comparison and techno-economic evaluation of a grid-connected photovoltaic-battery system, Renew. Energy. 197 (2022) 1049–1060. https://doi.org/10.1016/j.renene.2022.07.114.

[226] NASA Langley - POWER, (n.d.). https://power.larc.nasa.gov/common/php/SSE_ExSummary.php (accessed May 21, 2019).

[227] Data Download for Montréal, (n.d.). https://montreal.weatherstats.ca/download.html (accessed July 26, 2021).

[228] N. Shirzadi, F. Nasiri, U. Eicker, Optimal Configuration and Sizing of an Integrated Renewable Energy System for Isolated and Grid-Connected Microgrids: The Case of an Urban University Campus, Energies. 13 (2020) 3527. https://doi.org/10.3390/en13143527.

[229] X. Luo, M. Dooner, W. He, J. Wang, Y. Li, D. Li, O. Kiselychnyk, Feasibility study of a simulation software tool development for dynamic modelling and transient control of adiabatic compressed air energy storage with its electrical power system applications, Appl. Energy. 228 (2018) 1198–1219. https://doi.org/10.1016/j.apenergy.2018.06.068.

[230] R2022b - Updates to the MATLAB and Simulink product families - MATLAB & Simulink, (n.d.). https://www.mathworks.com/products/new_products/latest_features.html (accessed October 25, 2022).

[231] Integrated Optimization of Location , Design , and Operation of Renewable Energy Systems for Urban Microgrids Navid Shirzadi A Thesis in the Department of Building Civil and Environmental Engineering (BCEE) Presented in Partial Fulfillment of the Requir, (2023).

[232] Z. Han, S. Guo, Investigation of operation strategy of combined cooling, heating and power(CCHP) system based on advanced adiabatic compressed air energy storage, Energy. 160 (2018) 290–308. https://doi.org/10.1016/j.energy.2018.07.033.

[233] T. Korakianitis, D.G. Wilson, Models for predicting the performance of brayton-cycle engines, ASME 1992 Int. Gas Turbine Aeroengine Congr. Expo. GT 1992. 2 (1992). https://doi.org/10.1115/92-GT-361.

[234] R. Velraj, V. Gayathri, A. Thenmozhi, Performance evaluation of compressed air energy storage using TRNSYS, J. Electron. Sci. Technol. 13 (2015) 361–366. https://doi.org/10.11989/JEST.1674-862X.505252.

[235] J. Lian, Y. Zhang, C. Ma, Y. Yang, E. Chaima, A review on recent sizing methodologies of hybrid renewable energy systems, Energy Convers. Manag. 199 (2019) 112027. https://doi.org/10.1016/j.enconman.2019.112027.

[236] M. Bagheri, N. Shirzadi, E. Bazdar, C.A. Kennedy, Optimal planning of hybrid renewable energy infrastructure for urban sustainability: Green Vancouver, Renew. Sustain. Energy Rev. 95 (2018) 254–264. https://doi.org/10.1016/j.rser.2018.07.037.

[237] S. Barakat, H. Ibrahim, A.A. Elbaset, Multi-objective optimization of grid-connected PV-wind hybrid system considering reliability, cost, and environmental aspects, Sustain. Cities Soc. 60 (2020) 102178. https://doi.org/10.1016/j.scs.2020.102178.

[238] A. Maleki, F. Pourfayaz, Optimal sizing of autonomous hybrid photovoltaic/wind/battery power system with LPSP technology by using evolutionary algorithms, Sol. Energy. 115 (2015) 471–483. https://doi.org/10.1016/j.solener.2015.03.004.

[239] S. Singh, M. Singh, S.C. Kaushik, A review on optimization techniques for sizing of

solar-wind hybrid energy systems, Int. J. Green Energy. 13 (2016) 1564–1578. https://doi.org/10.1080/15435075.2016.1207079.

[240] S. Singh, M. Singh, S.C. Kaushik, Feasibility study of an islanded microgrid in rural area consisting of PV, wind, biomass and battery energy storage system, Energy Convers. Manag. 128 (2016) 178–190. https://doi.org/10.1016/j.enconman.2016.09.046.

[241] Hydro-Québec, Electricity Rates Effective April 1, 2016., (2016). https://www.hydroquebec.com/data/documents-donnees/pdf/electricity-rates-2022.pdf.

[242] M. Nasser, T.F. Megahed, S. Ookawara, H. Hassan, Techno-economic assessment of clean hydrogen production and storage using hybrid renewable energy system of PV/Wind under different climatic conditions, Sustain. Energy Technol. Assessments. 52 (2022) 102195. https://doi.org/10.1016/j.seta.2022.102195.

[243] R. Kumar, H.K. Channi, A PV-Biomass off-grid hybrid renewable energy system (HRES) for rural electrification: Design, optimization and techno-economic-environmental analysis, J. Clean. Prod. 349 (2022) 131347. https://doi.org/10.1016/j.jclepro.2022.131347.

[244] A. Maleki, Z.E. Filabi, M.A. Nazari, Techno-Economic Analysis and Optimization of an Off-Grid Hybrid Photovoltaic–Diesel–Battery System: Effect of Solar Tracker, Sustain. 14 (2022). https://doi.org/10.3390/su14127296.

[245] M. Chennaif, M. Maaouane, H. Zahboune, M. Elhafyani, S. Zouggar, Tri-objective techno-economic sizing optimization of Off-grid and On-grid renewable energy systems using Electric system Cascade Extended analysis and system Advisor Model, Appl. Energy. 305 (2022) 117844. https://doi.org/10.1016/j.apenergy.2021.117844.

[246] FAQ – Hydrostor, (n.d.). https://www.hydrostor.ca/faq/ (accessed November 7, 2022).

[247] R.P. Team, Advanced Compressed Air Energy Storage : Technical Inputs Summary, (n.d.). https://irp.nspower.ca/files/key-documents/assumptions-and-analysis-plan/20200214-JFS_Hydrostor-comments-on-draft-assumptions.pdf.

[248] B. Wang, X. Yu, J. Chang, R. Huang, Z. Li, H. Wang, Techno-economic analysis and optimization of a novel hybrid solar-wind-bioethanol hydrogen production system via membrane reactor, Energy Convers. Manag. 252 (2022) 115088. https://doi.org/10.1016/j.enconman.2021.115088.

[249] T. Sokhansefat, D. Mohammadi, A. Kasaeian, A.R. Mahmoudi, Simulation and parametric study of a 5-ton solar absorption cooling system in Tehran, Energy Convers. Manag. 148 (2017) 339–351. https://doi.org/10.1016/j.enconman.2017.05.070.

[250] Canada Interest Rate - 2023 Data - 1990-2022 Historical - 2024 Forecast - Calendar, (n.d.). https://tradingeconomics.com/canada/interest-rate (accessed January 6, 2023).

[251] Canada Inflation Rate | Inflation Rate and Consumer Price Index, (n.d.). https://www.rateinflation.com/inflation-rate/canada-inflation-rate/ (accessed January 6, 2023).

[252] M. Hossein Jahangir, E. Bazdar, A. Kargarzadeh, Techno-economic and environmental assessment of low carbon hybrid renewable electric systems for urban energy planning: Tehran-Iran, City Environ. Interact. 16 (2022) 100085. https://doi.org/10.1016/j.cacint.2022.100085.

[253] E. Bazdar, F. Nasiri, F. Haghighat, Resilience-centered optimal sizing and scheduling of a building-integrated PV-based energy system with hybrid adiabatic-compressed air energy storage and battery systems, 308 (2024) 132836.

[254] J.H. Cho, M.G. Chun, W.P. Hong, Structure optimization of stand-alone renewable power systems based on multi object function, Energies. 9 (2016) 1–19. https://doi.org/10.3390/en9080649.

[255] H. Yang, W. Zhou, L. Lu, Z. Fang, Optimal sizing method for stand-alone hybrid solar-wind system with LPSP technology by using genetic algorithm, Sol. Energy. 82 (2008) 354–367. https://doi.org/10.1016/j.solener.2007.08.005.

[256] Z. Shi, R. Wang, T. Zhang, Multi-objective optimal design of hybrid renewable energy systems using preference-inspired coevolutionary approach, Sol. Energy. 118 (2015) 96–106. https://doi.org/10.1016/j.solener.2015.03.052.

[257] A. Maleki, F. Pourfayaz, Sizing of stand-alone photovoltaic/wind/diesel system with battery and fuel cell storage devices by harmony search algorithm, J. Energy Storage. 2 (2015) 30–42. https://doi.org/10.1016/j.est.2015.05.006.